國立臺灣大學工學院土木工程學系

博士論文

Department of Civil Engineering

College of Engineering

National Taiwan University

Doctoral Dissertation

楔形函數配點法及其在工程問題應用之研究

Study of Spline Collocation Method and its Application on

Engineering Problems

黃旭輝

Hsu-Hui Huang

指導教授：吳賴雲 教授

Advisor: Lai-Yun Wu, Ph.D.

中華民國 98 年 1 月

January, 2009

# Acknowledgement

This thesis could not be finished without the help and support of many people who are gratefully acknowledged here.

At the very first, I'm honored to express my deepest gratitude to my dedicated supervisor, Prof. Lai-Yun Wu, with whose able guidance I could have worked out this thesis. He has offered me valuable ideas, suggestions and criticisms with his profound knowledge in forensic linguistics and rich research experience. His patience and kindness are greatly appreciated. Besides, he always puts high priority on our dissertation writing and is willing to discuss with me anytime he is available. I have learnt from him a lot not only about dissertation writing, but also the professional ethics. I'm very much obliged to his efforts of helping me complete the dissertation.

I'm also extremely grateful to my adjunct professor, Dr. Lap-Loi Chung, whose patient and meticulous guidance and invaluable suggestions are indispensable to the completion of this thesis. He even discussed with me when he was out for his job. I cannot make it without his support and encouragement.

I owe special thanks to Prof. Yung-Hsiang Chen, Prof. Deh-Shiu Hsu, Prof. Chung-Yue Wang, Prof. Shen-Haw Ju for their priceless comments on this study.

Thanks are also due to my postgraduate friends, who never failed to give me great encouragement and suggestions. Special thanks should go to Dr. Sheng-Fu Tsai, Dr. Kuo-Lun Huang, Mr. Yao-Sheng Yang, Mr. Cho-Yan Yang, and Mr. Kuan-Hua Lien for their brainstorming with me when I failed coming up with ideas.

At last but not least, I would like to thank my family and friend M.L. Pei-I Tsau for their support all the way from the very beginning of my postgraduate study. I am thankful to all my family members for their thoughtfulness and encouragement

<div align="right">Hsu-Hui Haung 2009.1.1</div>

# 摘要

楔形函數配點法是以楔形函數作為基底函數所構成之近似函數，搭配配點法以獲取最佳之近似函數，具有基本理論與計算步驟簡單，計算速度與收斂速度快…等優點，早期被應用於曲線擬合，後期乃因工程問題所對應之控制方程式與邊界條件趨於複雜，很難甚至無法推導其解析解，因而採用楔形函數配點法分析工程問題以求其近似解，但目前僅有少數文獻採用楔形函數配點法進行工程問題分析之研究。

本文研究採用楔形函數配點法與延伸發展之徑向楔形函數配點法與楔形函數配點元素法，針對連續梁、幾何非線性梁與矩形薄板等問題進行彈性分析、頻率分析與挫屈荷載分析，並與解析解與其他數值方法(例如：有限元素法)進行比較。分析結果顯示，楔形函數配點法應用於工程問題之數值分析時，不輸於其他數值方法，值得繼續發展楔形函數配點法分析更複雜的工程問題。

**關鍵字**：楔形函數配點法、徑向楔形函數配點法、楔形函數配點元素法。

# ABSTRACT

In this thesis, we study the spline collocation method (SCM), radial spline collocation method (RSCM) and spline collocation element method (SCEM) for solving engineering problems: beam, beam-column, frame, and plate problem. The popularity of the collocation method is in part due to their conceptual simplicity, wide applicability, and ease of implementation. In comparison to finite element difference methods, the CM provides approximations to the solution and its spatial derivatives at mesh point of the domain of problems. The obvious advantage of collocation method over Galerkin methods is that the calculation of the coefficients in the system of algebraic equations determining the approximate solution is very fast since no integrals need to be evaluated or approximated. Moreover, numerical experiments illustrate that the collocation method provide high order accuracy and super-convergence feature for a wide range of physical and engineering problems.

**Keyword** : collocation method, spline collocation method (SCM), radial spline collocation method (RSCM), spline collocation element method (SCEM)

# CONTENTS

# LIST OF FIGURES

# LIST OF TABLES

# Chapter 1 Preliminaries

## 1.1 Introduction

In this thesis, we study the spline collocation method (SCM), radial spline collocation method (RSCM) and spline collocation element method (SCEM) for solving engineering problems: beam, beam-column, frame, and plate problem. The popularity of the collocation method is in part due to their conceptual simplicity, wide applicability, and ease of implementation. In comparison to finite element difference methods, the CM provides approximations to the solution and its spatial derivatives at mesh point of the domain of problems. The obvious advantage of collocation method over Galerkin methods is that the calculation of the coefficients in the system of algebraic equations determining the approximate solution is very fast since no integrals need to be evaluated or approximated. Moreover, numerical experiments illustrate that the collocation method provide high order accuracy and super-convergence feature for a wide range of physical and engineering problems.

B-spline functions were initially adopted for data fitting, curve fitting, surface fitting and interpolation. They were then extended for approximate solutions of differential equations and structural analyses (Schoenberg, 1946; Bert and Sheu, 1996; Prenter, 1975). Spline functions possess higher smoothness than piecewise Lagrange interpolation and Hermite interpolation. The stability of spline functions was proven by Prenter (1975).

Commonly, this incorporates the use of cubic B-splines which were presented by Mizusawa *et al.* (1979) for investigation of vibration of skew plates, Shen and Wang (1987) for linear static analysis of cylindrical shells, Gupta *et al.* (1991) for linear finite element analysis of axi-symmetric shells and others. Weller (1993a, b) employed B-splines to study post-buckling behavior of infinite length cylindrical panels subjected to combined thermal and mechanical loading, and they were incorporated into collocation method for the same analysis problem.

When spline functions are combined with collocation method which can significantly simplify the solution procedure of differential equations, it is called spline collocation method (SCM)

(Prenter, 1975). Recently, researches have been developed, such as Bert and Sheu (1996) for linear static analysis of beam and plates, Wu and Chen (2003a, b) for linear static analysis of continuous beam and frame.

The use of OCM in the engineering literature can be traced back at least to Lanczos (1938, 1956). In their research, Tchebycheff polynomials collocating at Gaussian knots were used to approximate solution to initial value problems. Chemists (Horvay and Spiess, 1954; Wright, 1964; Villadsen and Stewart, 1967; Ferguson and Finlayson, 1970; Finlayson, 1971; Ferguson, 1971) used OCM extensively to solve one and two dimensional initial and boundary value problems arising in reactor dynamic and other systems. Boor and Schwartz (1973) proved the uniqueness of solution. They also showed the errors of one dimensional OCM using splines was better than using full polynomials (Prenter, 1975).

## 1.2 Outline

A brief outline of this thesis is as follows. In Chapter 2, we introduce basis functions and some formulas of spline collocation method (SCM) for solving beam, beam-column, 2D-frame, plate problems. In Chapter 3, we introduce basis functions and some formulas of radial spline collocation method (RSCM) for solving beam problem. Finally, in Chapter 4, we introduce basis functions and some formulas of spline collocation element method (SCEM) for solving 2D-frame problem.
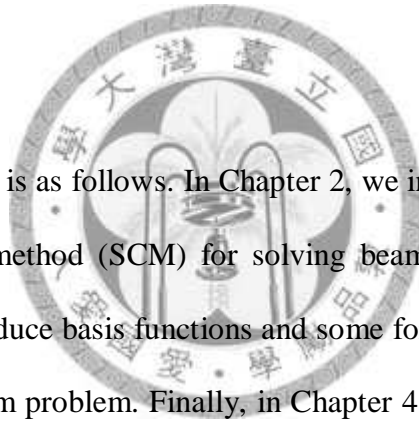
# Chapter 2 Spline collocation method

## 2.1 Spline collocation method

### 2.1.1 Introduction

By the finite difference method (FDM) or the finite element method (FEM), a large number of discretized points in the computational domain have to be manipulated in order to obtain solutions withhigh accuracy. The computational effect may be alleviated by using the differential quadrature method (DQM), which was first introduced by Bellman and Casti (1971). Solutions with reasonable accuracy can be obtained in an economical and time-saving way by DQM where the governing equations are used directly without the necessity of energy formulation (Bert *et al.*, 1993; Chen, 1997). However, when this method is applied to the problems of structural mechanics, some weak points are found in DQM (Striz *et al.*, 1994; Bert and Sheu, 1996). Loss of efficiency and simplicity arise from mapping the physical domain onto the computational domain and it is difficult to model discontinuous loads by using continuous basis functions. One boundary condition is applied at the exact boundary while the other boundary condition is applied at a small distance $\delta$ from the boundary in the solutions of systems of fourth-order or higher order differential equations. Because of $\delta$ at the boundary, the solution matrix become ill-conditioned and oscillation of the solutions is induced due to numerical instability (Bert and Sheu, 1996).

B-spline functions were initially adopted for data fitting, curve fitting, surface fitting and interpolation. They were then extended for approximate solutions of differential equations and structural analyses (Bert and Sheu, 1996; Prenter, 1975). Spline functions possess higher smoothness than piecewise Lagrange interpolation and Hermite interpolation. The stability of spline functions was proven by Prenter (1975).

The spline collocation method (SCM) basically is an interpolation method in which the solution of the governing differential equation can be approximated in terms of spline functions multiplied by the corresponding weighting coefficients. The spline functions can be derived systematically from FDM no matter whether forward, backward or central finite difference is used. In general, the spline functions should be at least one order higher than that of the governing differential equation so that accuracy and smoothness of the approximate solution can be guaranteed. Since the governing equation of a generalized beam is a fourth-order ordinary differential equation (ODE), the solution of the governing ODE is approximated by the spline function with polynomial of at least fifth degree. A quintic B-spline function is a piecewise fifth degree polynomial which is four-time continuously differentiable and an exact solution can be achieved by using this approximation method for piece-wise linearly distributed loading. A B-quintic spline function is a polynomial of degree five so that the sixth order forward difference with evenly spaced knots will be equal to zero. Therefore, the interpolatory function (B-spline function) is nonzero only within the considered interval of seven consecutive knots. As a whole, at least sixth-order forward difference expression is needed for the derivation of spline function (Prenter, 1975). Since the exact boundary conditions are directly used in the SCM without the necessity of using a small distance $\delta$ from the boundary, the problem of singularity does not exist. Moreover, not only structures under distributed loads can be solved by the SCM but also those under patch and point loads. The latter have not been analyzed successfully by using the conventional DQM. No matter how simple or complicated the problem is, higher accuracy can be achieved by the SCM through using more nodal points in the domain without encountering numerical instability while the DQM fails to do so (Bert and Sheu, 1996).

## 2.1.2 Theory

The collocation method is a method for the numerical solution of ordinary differential equation, partial differential equations and integral equations. The idea is to choose a approximate function and a number of knots in the domain (called collocation points), and to select that solution which satisfies the given equation at the collocation points.

According to spline collocation method (SCM), the approximate function and its derivatives are represented by a linear combination of B-spline functions as

$$\text{For 1D} \quad w(x) = \sum_i a_i B_i(x), \quad \frac{d^n}{dx^n} w(x) = \sum_j a_j \frac{d^n}{dx^n} B_j(x) \tag{2.1.1a}$$

$$\text{For 2D} \quad w(x,y) = \sum_i \sum_j a_{ij} B_i(x) B_j(y), \quad \frac{d^{n+m}}{dx^n dy^m} w(x,y) = \sum_k \sum_j a_{jk} \frac{d}{dx^n} B_j(x) \frac{d}{dy^m} B_k(y) \tag{2.1.1b}$$

where $a_i$ s and $a_{ij}$ s are the coefficients to be determined and $B_i(x)$, $B_j(y)$ is B-spline function. A B-spline of order $k$ is made up of a polynomial of order $k$ and has a compact support consisting of $k+2$ knots.

## 2.1.3 Cubic B-spline function

The cubic B-spline function is a cubic polynomial and $C^2$ continuous, define as (Prenter, 1975)

$$B_i(\xi) = \frac{1}{h^3} \begin{cases} (\xi - \xi_{i+2})^3, & \xi_{i+1} \leq \xi \leq \xi_{i+2} \\ (\xi - \xi_{i+2})^3 - 4(\xi - \xi_{i+1})^3, & \xi_i \leq \xi \leq \xi_{i+1} \\ (\xi - \xi_{i+2})^3 - 4(\xi - \xi_{i+1})^3 + 6(\xi - \xi_i)^3, & \xi_{i-1} \leq \xi \leq \xi_i \\ (\xi - \xi_{i+2})^3 - 4(\xi - \xi_{i+1})^3 + 6(\xi - \xi_i)^3 - 4(\xi - \xi_{i-1})^3, & \xi_{i-2} \leq \xi \leq \xi_{i-1} \\ 0, & \text{otherwise} \end{cases} \tag{2.1.2}$$

We can see that the values of cubic B-spline function vanish outside the interval $[\xi_{i-2}, \xi_{i+2}]$. Note that $B_i(\xi)$ and $B_i''(\xi)$ are symmetric functions, $B_i'(\xi)$ is anti-symmetric functions as shown in Figure 2.1.1. The values of cubic B-spline

function and and its derivatives are listed in Table 2.1.1.



(a) Cubic B-spline function.



(b) First order derivate of Cubic B-spline function



(c) Second order derivate of Cubic B-spline function
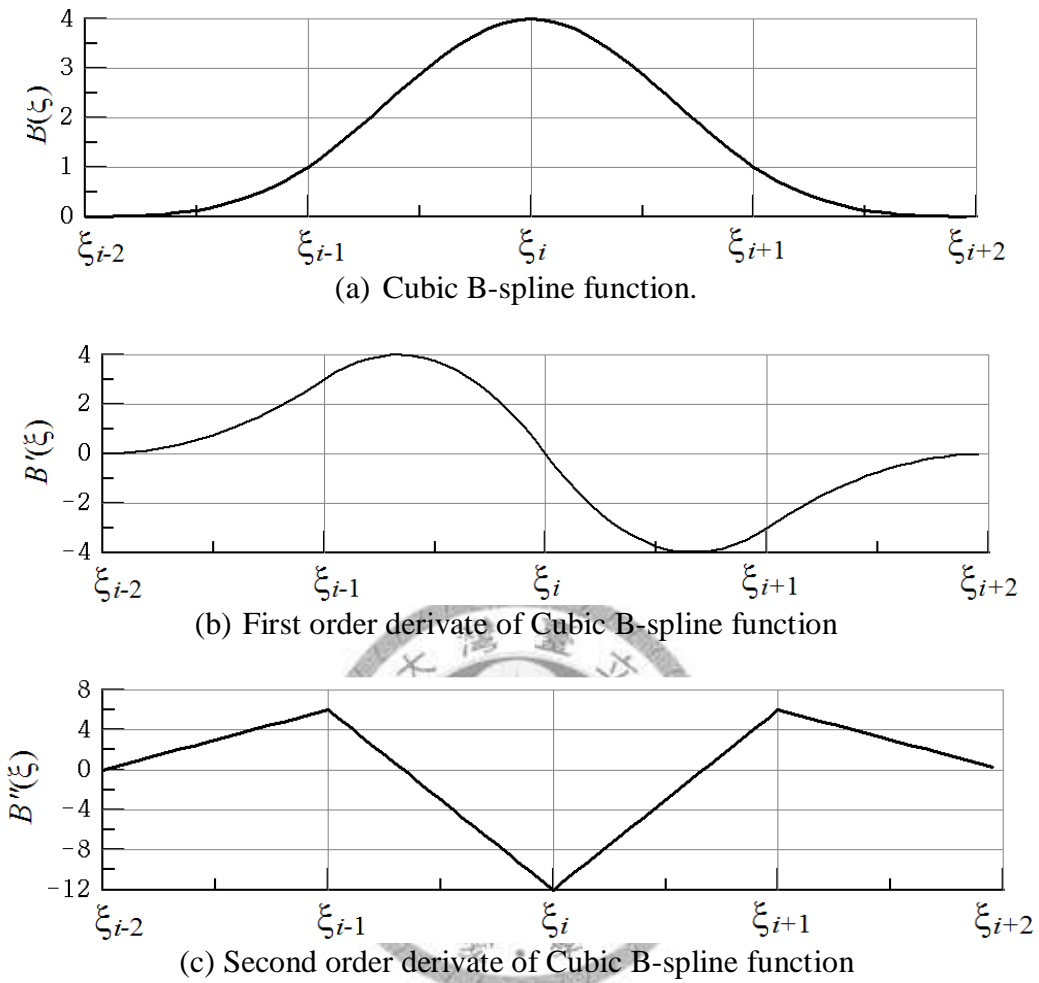
**Figure 2.1.1 The Cubic B-splines function ($h = 1$).**

**Table 2.1.1 Cubic spline values at knots**

| $\xi_j$ | $\xi_{i-2}$ | $\xi_{i-1}$ | $\xi_i$ | $\xi_{i+1}$ | $\xi_{i+2}$ |
|---|---|---|---|---|---|
| $B_i(\xi_j)$ | 0 | 1 | 4 | 1 | 0 |
| $B_i'(\xi_j)$ | 0 | $\dfrac{3}{h}$ | 0 | $-\dfrac{3}{h}$ | 0 |
| $B_i''(\xi_j)$ | 0 | $\dfrac{6}{h^2}$ | $-\dfrac{12}{h^2}$ | $\dfrac{6}{h^2}$ | 0 |

## 2.1.4 Quintic B-spline function

The quintic B-spline function is a quintic polynomial and $C^4$ continuous, define as (Bert and Sheu, 1996)

$$B_i(\xi)=\frac{1}{h^5}\begin{cases}(\xi-\xi_{i+3})^5, & \xi_{i+2}\leq\xi\leq\xi_{i+3}\\ (\xi-\xi_{i+3})^5-6(\xi-\xi_{i+2})^5, & \xi_{i+1}\leq\xi\leq\xi_{i+2}\\ (\xi-\xi_{i+3})^5-6(\xi-\xi_{i+2})^5+15(\xi-\xi_{i+1})^5, & \xi_i\leq\xi\leq\xi_{i+1}\\ (\xi-\xi_{i+3})^5-6(\xi-\xi_{i+2})^5+15(\xi-\xi_{i+1})^5-20(\xi-\xi_i)^5, & \xi_{i-1}\leq\xi\leq\xi_i\\ (\xi-\xi_{i+3})^5-6(\xi-\xi_{i+2})^5+15(\xi-\xi_{i+1})^5-20(\xi-\xi_i)^5+15(\xi-\xi_{i-1})^5, & \xi_{i-2}\leq\xi\leq\xi_{i-1}\\ (\xi-\xi_{i+3})^5-6(\xi-\xi_{i+2})^5+15(\xi-\xi_{i+1})^5-20(\xi-\xi_i)^5+15(\xi-\xi_{i-1})^5-6(\xi-\xi_{i-2})^5, & \xi_{i-3}\leq\xi\leq\xi_{i-2}\\ 0, & \text{otherwise}\end{cases} \qquad (2.1.3)$$

We can see that the values of quintic B-spline function vanish outside the interval $[\xi_{i-3},\xi_{i+3}]$. Note that $B_i(\xi)$, $B_i''(\xi)$ and $B_i^{(4)}(\xi)$ are symmetric functions, $B_i'(\xi)$ and $B_i'''(\xi)$ are anti-symmetric functions as shown in Figure 2.1.2. The values of quintic B-spline function and and its derivatives are listed in Table 2.1.2.



(a) Quintic B-spline function.



(b) First order derivate of quintic B-spline function

7
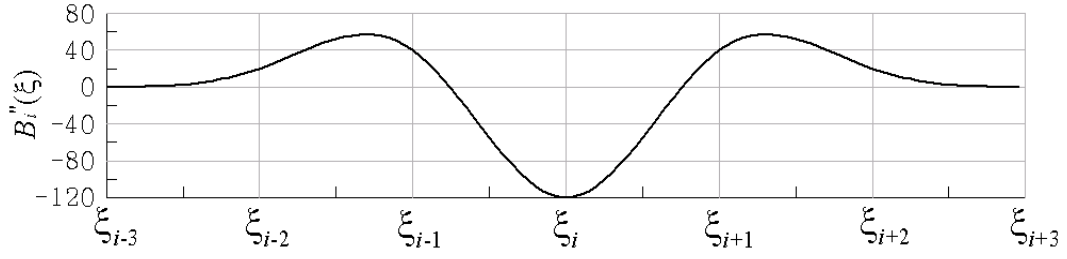
(c) Second order derivate of quintic B-spline function



(d) Third order derivate of quintic B-spline function
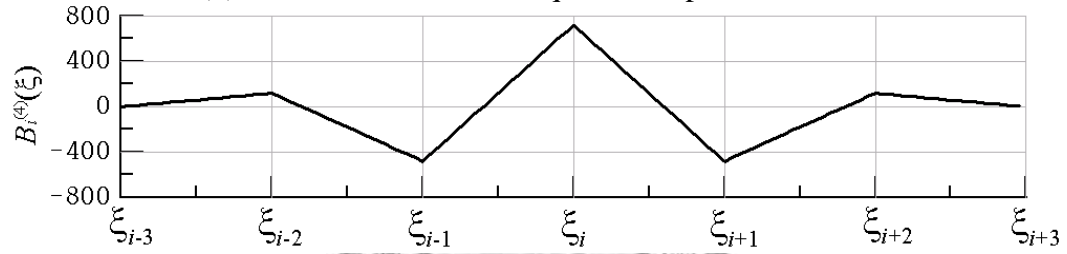


(e) Fourth order derivate of quintic B-spline function

**Figure 2.1.2 The quintic B-splines function ($h = 1$).**

**Table 2.1.2 Quintic spline values at knots**

| $\xi_j$ | $\xi_{i-3}$ | $\xi_{i-2}$ | $\xi_{i-1}$ | $\xi_i$ | $\xi_{i+1}$ | $\xi_{i+2}$ | $\xi_{i+3}$ |
|---|---|---|---|---|---|---|---|
| $B_i(\xi_j)$ | 0 | 1 | 26 | 66 | 26 | 1 | 0 |
| $B_i'(\xi_j)$ | 0 | $\dfrac{5}{h}$ | $\dfrac{50}{h}$ | 0 | $-\dfrac{50}{h}$ | $-\dfrac{5}{h}$ | 0 |
| $B_i''(\xi_j)$ | 0 | $\dfrac{20}{h^2}$ | $\dfrac{40}{h^2}$ | $-\dfrac{120}{h^2}$ | $\dfrac{40}{h^2}$ | $\dfrac{20}{h^2}$ | 0 |
| $B_i'''(\xi_j)$ | 0 | $\dfrac{60}{h^3}$ | $-\dfrac{120}{h^3}$ | 0 | $\dfrac{120}{h^3}$ | $-\dfrac{60}{h^3}$ | 0 |
| $B_i^{(4)}(\xi_j)$ | 0 | $\dfrac{120}{h^4}$ | $-\dfrac{480}{h^4}$ | $\dfrac{720}{h^4}$ | $-\dfrac{480}{h^4}$ | $\dfrac{120}{h^4}$ | 0 |

## 2.2 Flexural Vibration Analysis of a Geometrically Nonlinear Beam

### 2.2.1 Introduction

Large amplitude of vibrating beams is nonlinear systems so the small deflection theory is no longer applicable in nonlinear problems. The geometric non-linear or large-amplitude vibrations of beams had been studied by many scholars using the approximately analytical and numerical methods such as finite difference and finite element method *etc*. A comprehensive survey of such works had been presented by Sathyamoorthy (1982). Woinowsky-Krieger (1950) investigated the problem of simply supported beams with immovable ends using elliptic integrals. Evensen (1968) studied the non-linear vibrations of beams for different boundary conditions using a perturbation method. Srinivasan (1965) used a Ritz-Galerkin technique to obtain the non-linear free vibration response of simply supported beams and plates with immovable ends/edges. The non-linear vibratory behavior of beam with pinned ends was presented by Ray and Bert (1969) with test results. A wealth of information on non-linear systems and non-linear vibrations had been provided by Nayfeh and Mook (1979) and Chia (1980). The non-linear free vibration response of beam had been studied by Mei (1973), using a finite element method.

### 2.2.2 Formulation

A Bernoulli–Euler beam oscillating with large amplitude on immovable ends is considered here. The governing equation for non-linear vibrations of beams can be described as (Bhashyam and Prathap, 1980)

$$EI\frac{\partial^4 w}{\partial x^4} - N\frac{\partial^2 w}{\partial x^2} + m\ddot{w} = 0 \tag{2.2.1}$$

where $w$, $E$, $I$, $A$, and $m$ are the deflection, Young's modulus, moment of inertia of the cross-section, area of the cross-section, and the mass per unit length, respectively.

Assuming that the ends are axially immovable, i.e., $u(0,t) = u(L,t) = 0$, it is evident that the axial force $N$ is independent of x and thus depends only on time (Bhashyam and Prathap, 1980),

$$N(x,t) = EA\left[\frac{\partial u}{\partial x} + \frac{1}{2}\left(\frac{\partial w}{\partial x}\right)^2\right] = N(t) = \frac{EA}{2L}\int_0^L \left(\frac{\partial w}{\partial x}\right)^2 dx \qquad (2.2.2)$$

For a simply supported beam, it is reasonable to assume that (Sarma, 1983)

$$w(x,t) = av(x)\cos\omega t \qquad (2.2.3)$$

The governing equation for simply supported beams can be developed using the Ritz–Galerkin technique (Singh, et. al), i.e.,

$$EI\frac{d^4v}{dx^4} - \frac{3}{4}\left[\frac{EAa^2}{2L^2}\int_0^L \left(\frac{dv}{dx}\right)^2 dx\right]\frac{d^2v}{dx^2} = \omega^2 mv \qquad (2.2.4)$$

Its dimensionless form is

$$\frac{d^4v}{d\xi^4} - \frac{3}{4}\left[\frac{1}{2}\frac{a^2}{r^2}\int_0^1 \left(\frac{dv}{d\xi}\right)^2 d\xi\right]\frac{d^2v}{d\xi^2} = \left(\omega^*\right)^2 v \qquad (2.2.5)$$

where

$$\xi = \frac{x}{L}, \quad (\omega^*)^2 = \omega^2\frac{mL^4}{EI}, \quad r^2 = \frac{I}{A} \qquad (2.2.6)$$

For a simply supported beam, the boundary conditions can be written as

$$v = 0 \quad \text{and} \quad \frac{d^2v}{d\xi^2} = 0 \quad \text{at} \quad \xi = 0, 1 \qquad (2.2.7)$$

As noted by some researchers (Evensen, 1968; Mei, 1972; Raju et al., 1976), on the framework of the moderately large bending theory, the non-linear vibration of simply supported beams would admit a variable-separable solution, but the beams with clamped-clamped end or hinged-clamped end would not. For beam with a clamped end, it is usually assumed (Raju et al., 1976) that maximum amplitude of each point on the beam exists during the vibration and that is also its point of reversal of motion. Assume

10

that the maximum amplitude of each point on vibrating beam is reached, the configuration of the beam is represented by $\overline{w}$ and there exists (Raju *et al.*, 1976)

$$\ddot{\overline{w}} = -\omega^2 \overline{w}, \quad \dot{\overline{w}} = 0 \tag{2.2.8}$$

Substituting the above expression into governing equation (2.2.1) results in the differential equation

$$\frac{d^4 \overline{w}}{d\xi^4} - \left[ \frac{1}{2} \frac{a^2}{r^2} \int_0^1 \left( \frac{d\overline{w}}{d\xi} \right)^2 d\xi \right] \frac{d^2 \overline{w}}{d\xi^2} = \left( \omega^* \right)^2 \overline{w} \tag{2.2.9}$$

where $\xi$, $(\omega^*)^2$ are given in Eq. (2.2.6).

The corresponding dimensionless boundary conditions are

clamped-clamped :

$$\overline{w} = 0 \quad \text{at} \quad \xi = 0, \ 1 \tag{2.2.10a}$$

$$\frac{d\overline{w}}{d\xi} = 0 \quad \text{at} \quad \xi = 0, \ 1 \tag{2.2.10b}$$

hinged-clamped :

$$\overline{w} = 0 \quad \text{at} \quad \xi = 0, \ 1 \tag{2.2.11a}$$

$$\frac{d^2 \overline{w}}{d\xi^2} = 0 \quad \text{at} \quad \xi = 0 \tag{2.2.11b}$$

$$\frac{d\overline{w}}{d\xi} = 0 \quad \text{at} \quad \xi = 1 \tag{2.2.11c}$$

## 2.2.3 Approach by spline collocation method

Considering a set of equi-spaced knots is selected in a normalized interval $\xi \in [0,1]$, i.e.,

$$\xi_0 = 0, \quad \xi_n = 1, \quad \xi_{j+1} - \xi_j = h, \quad j = 0, \dots, n-1 \tag{2.2.12}$$

where $h$ is distance of equi-spaced knots. In order to apply the SCM (Prenter, 1975; Bert and Sheu, 1996), one needs to extend two added knots (fictitious) $\xi_{-2}$, $\xi_{-1}$ and

$\xi_{n+1}$, $\xi_{n+2}$ at each end of beam, respectively (shown in Figure 2.2.1).
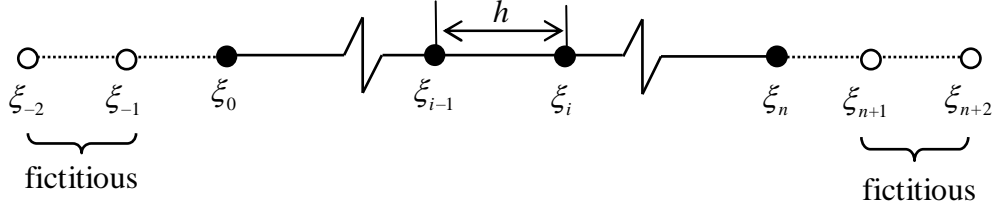


**Figure 2.2.1 Partitions of beam.**

Then the nonlinear normal mode of a geometrically nonlinear beam with simply supported ends and a clamped end, respectively, for flexural vibration can be approximated by using the quintic B-spline function (QSF) (Prenter, 1975; Bert and Sheu, 1996) as follows

$$v(\xi) = \sum_{i=-2}^{n+2} c_i B_i(\xi) \quad \text{or} \quad \bar{w}(\xi) = \sum_{i=-2}^{n+2} c_i B_i(\xi) \tag{2.2.13}$$

where $c_i$ s are the coefficients to be determined and $B_i(\xi)$ is QSF.

Substituting the approximations of nonlinear normal mode of a beam, that are Eq. (2.2.13), into the governing equations in Eq. (2.2.5) and Eq. (2.2.9) can obtain

$$\sum_{i=-2}^{n+2} c_i \left[ B_i^{(4)}(\xi) - \frac{3}{4} N(\xi) B_i''(\xi) \right] = \left( \omega^* \right)^2 \sum_{i=-2}^{n+2} c_i B_i(\xi) \tag{2.2.14}$$

$$\sum_{i=-2}^{n+2} c_i \left[ B_i^{(4)}(\xi) - N(\xi) B_i''(\xi) \right] = \left( \omega^* \right)^2 \sum_{i=-2}^{n+2} c_i B_i(\xi) \tag{2.2.15}$$

where

$$N(\xi) = \frac{a^2}{2r^2} \int_0^1 \left[ \sum_{i=-1}^{n+2} c_i B_i'(\xi) \right]^2 d\xi \tag{2.2.16}$$

Note that $N(\xi)$ can be evaluated by Gauss integration method.

Similarly, the boundary conditions in Eq. (2.2.7), Eq. (2.2.10) and Eq. (2.2.11) can obtain,

clamped-clamped :

$$v(\xi_0) = \sum_{i=-2}^{n+2} c_i B_i(\xi_0) = 0 \tag{2.2.17a}$$

$$v(\xi_n) = \sum_{i=-2}^{n+2} c_i B_i(\xi_n) = 0 \tag{2.3.17b}$$

$$\frac{dv(\xi_0)}{d\xi} = \sum_{i=-2}^{n+2} c_i B_i'(\xi_0) = 0 \tag{2.2.17c}$$

$$\frac{dv(\xi_n)}{d\xi} = \sum_{i=-2}^{n+2} c_i B_i'(\xi_n) = 0 \tag{2.2.17d}$$

hinged- hinged :

$$v(\xi_0) = \sum_{i=-2}^{n+2} c_i B_i(\xi_0) = 0 \tag{2.2.18a}$$

$$v(\xi_n) = \sum_{i=-2}^{n+2} c_i B_i(\xi_n) = 0 \tag{2.2.18b}$$

$$\frac{d^2 v(\xi_0)}{d\xi^2} = \sum_{i=-2}^{n+2} c_i B_i''(\xi_0) = 0 \tag{2.2.18c}$$

$$\frac{d^2 v(\xi_n)}{d\xi^2} = \sum_{i=-2}^{n+2} c_i B_i''(\xi_n) = 0 \tag{2.2.18d}$$

hinged-clamped :

$$v(\xi_0) = \sum_{i=-2}^{n+2} c_i B_i(\xi_0) = 0 \tag{2.2.19a}$$

$$v(\xi_n) = \sum_{i=-2}^{n+2} c_i B_i(\xi_n) = 0 \tag{2.2.19b}$$

$$\frac{d^2 v(\xi_0)}{d\xi^2} = \sum_{i=-2}^{n+2} c_i B_i''(\xi_0) = 0 \tag{2.2.19c}$$

$$\frac{dv(\xi_n)}{d\xi} = \sum_{i=-2}^{n+2} c_i B_i'(\xi_n) = 0 \tag{2.2.19d}$$

In general, after substituting the coordinates of the $n+1$ knots, $\xi_i$, $i = 0, 1, \ldots, n$,

13

into the governing equation in Eq. (2.2.14) or Eq. (2.2.15), and coupling the four given

boundary conditions in Eq. (2.2.17) to Eq. (2.2.19) at the ends, $\xi_0$ and $\xi_n$, one obtains

the following simultaneous equations.

$$
\begin{bmatrix}
\text{1st B.C. at } \xi_0 \\
\text{2nd B.C. at } \xi_0 \\
\text{1st B.C. at } \xi_n \\
\text{2nd B.C. at } \xi_n \\
\sum_{i=-2}^{n+2} c_i \left[ B_i^{(4)}(\xi_0) - \dfrac{3}{4} N(\xi) B_i''(\xi_0) \right] \\
\sum_{i=-2}^{n+2} c_i \left[ B_i^{(4)}(\xi_1) - \dfrac{3}{4} N(\xi) B_i''(\xi_1) \right] \\
\vdots \\
\sum_{i=-2}^{n+2} c_i \left[ B_i^{(4)}(\xi_n) - \dfrac{3}{4} N(\xi) B_i''(\xi_n) \right]
\end{bmatrix}
=
\begin{bmatrix}
0 \\
0 \\
0 \\
0 \\
(\omega^*)^2 \sum_{i=-2}^{n+2} c_i B_i(\xi_0) \\
(\omega^*)^2 \sum_{i=-2}^{n+2} c_i B_i(\xi_1) \\
\vdots \\
(\omega^*)^2 \sum_{i=-2}^{n+2} c_i B_i(\xi_n)
\end{bmatrix}
\tag{2.2.20}
$$

$$
\begin{bmatrix}
\text{1st B.C. at } \xi_0 \\
\text{2nd B.C. at } \xi_0 \\
\text{1st B.C. at } \xi_n \\
\text{2nd B.C. at } \xi_n \\
\sum_{i=-2}^{n+2} c_i \left[ B_i^{(4)}(\xi_0) - N(\xi) B_i''(\xi_0) \right] \\
\sum_{i=-2}^{n+2} c_i \left[ B_i^{(4)}(\xi_1) - N(\xi) B_i''(\xi_1) \right] \\
\vdots \\
\sum_{i=-2}^{n+2} c_i \left[ B_i^{(4)}(\xi_n) - N(\xi) B_i''(\xi_n) \right]
\end{bmatrix}
=
\begin{bmatrix}
0 \\
0 \\
0 \\
0 \\
(\omega^*)^2 \sum_{i=-2}^{n+2} c_i B_i(\xi_0) \\
(\omega^*)^2 \sum_{i=-2}^{n+2} c_i B_i(\xi_1) \\
\vdots \\
(\omega^*)^2 \sum_{i=-2}^{n+2} c_i B_i(\xi_n)
\end{bmatrix}
\tag{2.2.21}
$$

Matrix Eq. (2.2.20) and Eq. (2.2.21) are eigen-value problem of the following form

$$
\begin{bmatrix}
\mathbf{S}_{bb} & \mathbf{S}_{bd} \\
\mathbf{S}_{db} & \mathbf{S}_{db}
\end{bmatrix}
\begin{Bmatrix}
\mathbf{c}_b \\
\mathbf{c}_d
\end{Bmatrix}
= (\omega^*)^2
\begin{bmatrix}
\mathbf{0} & \mathbf{0} \\
\mathbf{M}_{db} & \mathbf{M}_{dd}
\end{bmatrix}
\begin{Bmatrix}
\mathbf{c}_b \\
\mathbf{c}_d
\end{Bmatrix}
\tag{2.2.22}
$$

where $\mathbf{c}_b^{\mathrm{T}} = \{ c_{-2} \quad c_{-1} \quad c_{n+1} \quad c_{n+2} \} \in R^4$, $\mathbf{c}_d^{\mathrm{T}} = \{ c_0 \quad c_1 \quad \cdots \quad c_n \} \in R^{n+1}$, $R^{n+1}$ denotes

$n+1$ dimensional vector space, etc., subscripts b and d denote the two fictitious knots

at each end and all internal knots, respectively. From the right hand side of Eq. (2.2.22)

the $\mathbf{S}_{db}$ and $\mathbf{S}_{dd}$ can be decomposed into the linear part and nonlinear part as

14

$$\mathbf{S}_{db} = \left(\mathbf{S}_{db}\right)_{L} - N\left(\xi\right)\left(\mathbf{S}_{db}\right)_{N} \tag{2.2.23a}$$

$$\mathbf{S}_{dd} = \left(\mathbf{S}_{dd}\right)_{L} - N\left(\xi\right)\left(\mathbf{S}_{dd}\right)_{N} \tag{2.2.23b}$$

where subscripts  L  and  N  denote the linear part and nonlinear part.

Multiplying out Eq. (2.2.22), obtains

$$\mathbf{S}_{bb}\mathbf{c}_{b} + \mathbf{S}_{bd}\mathbf{c}_{d} = \mathbf{0} \tag{2.2.24a}$$

$$\mathbf{S}_{db}\mathbf{c}_{b} + \mathbf{S}_{dd}\mathbf{c}_{d} = \left(\omega^{*}\right)^{2}\left(\mathbf{M}_{db}\mathbf{c}_{b} + \mathbf{M}_{dd}\mathbf{c}_{d}\right) \tag{2.2.24b}$$

From Eq. (2.2.24a),

$$\mathbf{c}_{b} = -\mathbf{S}_{bb}^{-1}\mathbf{S}_{bd}\mathbf{c}_{d} \tag{2.2.25}$$

Substituting Eq. (2.2.25) into the Eq. (2.2.24b), yields

$$\bar{\mathbf{S}}\mathbf{c}_{d} = \left(\omega^{*}\right)^{2}\bar{\mathbf{M}}\mathbf{c}_{d} \tag{2.2.26}$$

where

$$\bar{\mathbf{S}} = \left[\left(\mathbf{S}_{dd}\right)_{L} - N\left(\xi\right)\left(\mathbf{S}_{dd}\right)_{N}\right] - \left[\left(\mathbf{S}_{db}\right)_{L} - N\left(\xi\right)\left(\mathbf{S}_{db}\right)_{N}\right]\mathbf{S}_{bb}^{-1}\mathbf{S}_{bd} \tag{2.2.27a}$$

$$\bar{\mathbf{M}} = -\mathbf{M}_{db}\mathbf{S}_{bb}^{-1}\mathbf{S}_{bd} + \mathbf{M}_{dd} \tag{2.2.27b}$$

The Eq. (2.2.26) is a generalized eigen-value nonlinear problem. In order to solve the fundamental dimensionless frequency $\omega_{1}^{*}$ of nonlinear vibrating beam, an iterative scheme can be applied and described by the following procedure.

Given the initial value of dimensionless stretching force $N^{(0)}(\xi)$ is zero into Eq. (2.2.27a) firstly, it means that the corresponding linear problem of vibrating beam is considered, then the eigen-value problem equation in Eq. (2.2.26) can be solved for eigen-value $(\omega^{*})^{(0)}$ and eigen-vector $\mathbf{c}_{d}^{(0)}$. Consequently, the initial linear mode $v^{(0)}$ or $\bar{w}^{(0)}$ can be determined. Further, the value of dimensionless stretching force $N^{(1)}(\xi)$ can be computed by using Eq. (2.2.16) .

In place of the initial value of dimensionless stretching force $N^{(0)}(\xi)$ by $N^{(1)}(\xi)$, and this process is repeated till convergence is achieved to the required accuracy for the fundamental dimensionless frequency of nonlinear vibrating beam $(\omega^*)$ and nonlinear mode shapes $v$ or $\bar{w}$. (See flow chart Figure 2.2.2)
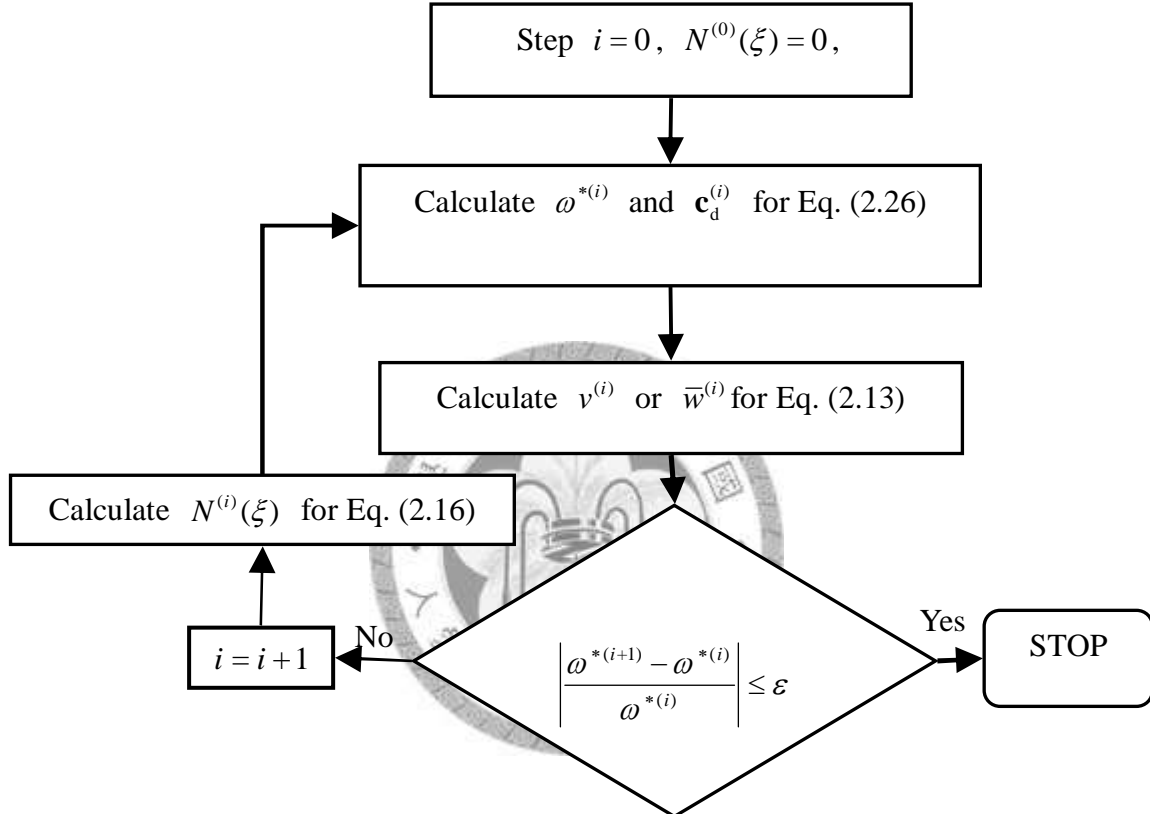


**Figure 2.2.2 Flow-chart of iterative scheme.**

## 2.2.4 Numerical Results

The numerical examples including linear and nonlinear vibrating beam, three types of boundary conditions: clamped-clamped, hinged-hinged and clamped-hinged end of beam, the amplitude of vibration $a/r = 0.1, 0.2, 0.4, 0.6, 0.8, 1.0, 1.5, 2.0$ for nonlinear cases.

From the numerical examples for linear vibrating beam, the dimensionless fundamental natural frequency $\left(\omega_1^*\right)_L$ is shown in Table 2.2.1. The convergence analysis of using SCM can be shown in Figure 2.2.3 based on Table 2.2.1, and the order

16

of convergence $\left| \omega_{\text{exact}}^* - \omega^* \right| = O(h^q)$ for clamped-clamped, hinged-hinged and clamped-hinged of linear vibrating beam are $q = 2.01$ , $q = 1.85$ , $q = 1.97$ , respectively.

**Table 2.2.1 Fundamental natural frequencies $\left( \omega_1^* \right)_{\text{L}}$ for linear vibrating beams.**

| No. of knots ($n$) | Boundary conditions | | |
|---|---|---|---|
| | hinged-hinged | clamped-clamped | hinged-clamped |
| 3 | 10.9545 | 23.4216 | 17.0238 |
| 6 | 10.0338 | 22.8167 | 15.7135 |
| 11 | 9.9103 | 22.4872 | 15.4922 |
| 21 | 9.8798 | 22.4019 | 15.4367 |
| 51 | 9.8712 | 22.3778 | 15.4212 |
| 101 | 9.8700 | 22.3744 | 15.4189 |
| 201 | 9.8697 | 22.3736 | 15.4184 |
| Exact[*] | 9.8696 | 22.3733 | 15.4182 |

\* Woinowsky-Krieger (1950)



(a) hinged-hinged

(b) clamped-clamped

(c) hinged -clamped
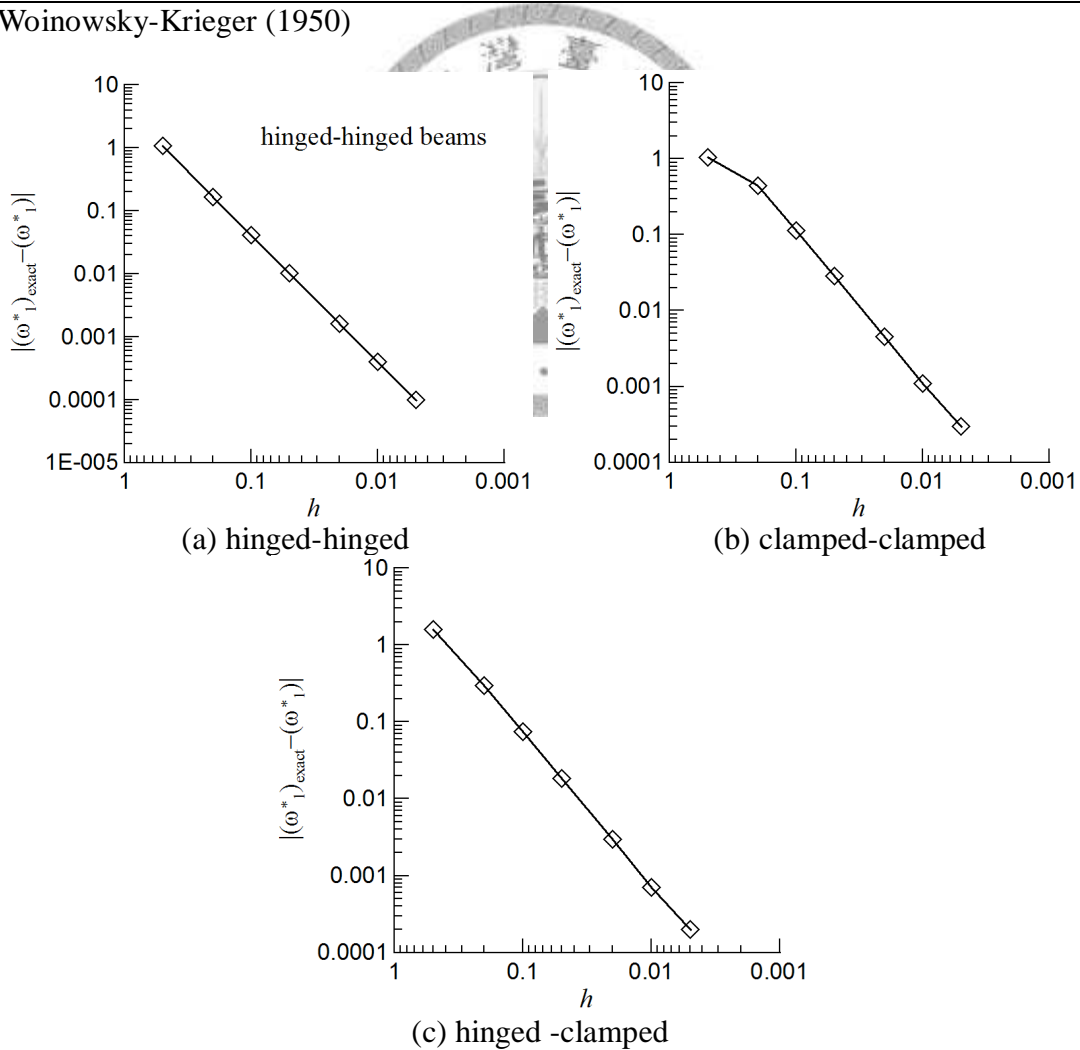
**Figure 2.2.3 Convergence analyses for linear vibrating beams.**

Figure 2.2.4 shows that four numerical methods, SCM, SDQM (Guo and Zhong, 2004), DQM (Feng and Bert, 1992), and FEM (Mei, 1972), all can reach appropriate high accurate results for non-linear frequency ratio $\omega_1^* / (\omega_1^*)_L$ of hinged-hinged beam, however, Table 2.2.2 shows that the most accurate results is SCM.
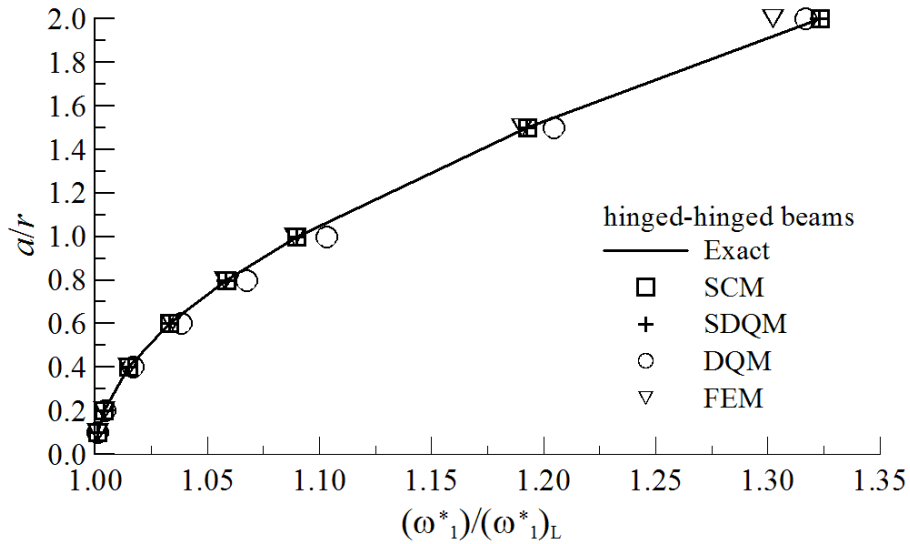


**Figure 2.2.4 Dimensionless amplitude-frequency curves of hinged-hinged beam.**

**Table 2.2.2 Fundamental natural frequency ratio $\omega_1^* / (\omega_1^*)_L$ for hinged-hinged beams.**

| $a/r$ | Exact | SCM | SDQM | DQM | FEM |
|-------|-------|-------|-------|-------|-------|
| 0.1 | 1.0009 | 1.0009 | 1.0009 | 1.0010 | 1.0009 |
| 0.2 | 1.0037 | 1.0038 | 1.0037 | 1.0043 | 1.0037 |
| 0.4 | 1.0149 | 1.0149 | 1.0149 | 1.0170 | 1.0148 |
| 0.6 | 1.0332 | 1.0332 | 1.0332 | 1.0384 | 1.0339 |
| 0.8 | 1.0583 | 1.0584 | 1.0583 | 1.0673 | 1.0578 |
| 1.0 | 1.0897 | 1.0898 | 1.0897 | 1.1030 | 1.0889 |
| 1.5 | 1.1924 | 1.1926 | 1.1924 | 1.2045 | 1.1902 |
| 2.0 | 1.3229 | 1.3232 | 1.3229 | 1.3170 | 1.3022 |

Figure 2.2.5 shows that five numerical methods, GFEM (Bhashyam and Prathap, 1980), SCM, SDQM (Guo and Zhong, 2004) , FEM, and ASM (Evensen, 1968) all approach to the same results for non-linear frequency ratio $\omega_1^* / (\omega_1^*)_L$ of clamped-clamped beam, but only DQM has slight deviation of results which increasing with $a/r$, are listed in Table 2.2.3.
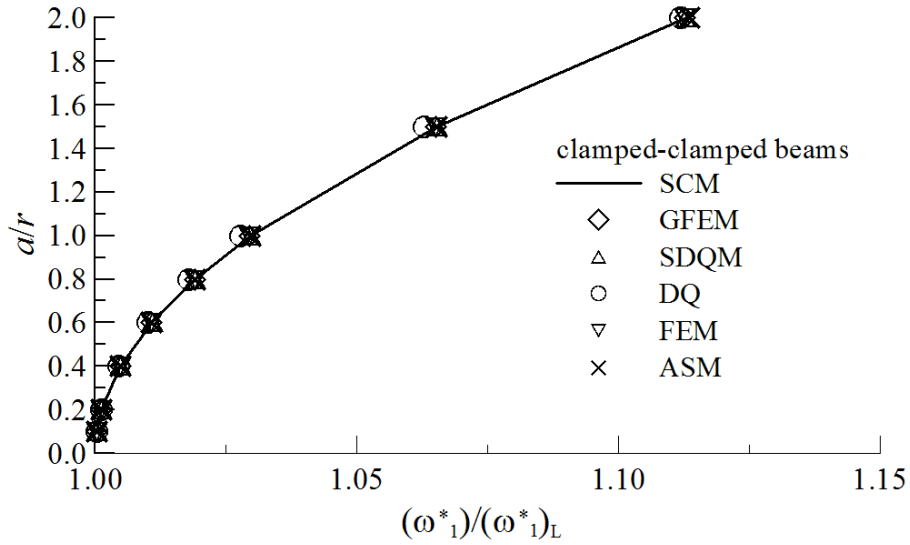
**Figure 2.2.5 Dimensionless amplitude-frequency curves of clamped-clamped beam.**

**Table 2.2.3 Fundamental natural frequency ratio $\omega_1^*\big/\left(\omega_1^*\right)_L$ for clamped-clamped beams.**

| $a/r$ | GFEM | SCM | SDQM | DQM | FEM | ASM |
|-------|--------|--------|--------|--------|--------|--------|
| 0.1 | 1.0003 | 1.0003 | 1.0003 | 1.0003 | 1.0003 | 1.0003 |
| 0.2 | 1.0012 | 1.0012 | 1.0012 | 1.0011 | 1.0012 | 1.0012 |
| 0.4 | 1.0048 | 1.0048 | 1.0048 | 1.0044 | 1.0048 | 1.0048 |
| 0.6 | 1.0107 | 1.0108 | 1.0108 | 1.0100 | 1.0107 | 1.0107 |
| 0.8 | 1.0190 | 1.0190 | 1.0190 | 1.0178 | 1.0190 | 1.0190 |
| 1.0 | 1.0295 | 1.0296 | 1.0296 | 1.0278 | 1.0295 | 1.0296 |
| 1.5 | 1.0650 | 1.0652 | 1.0652 | 1.0628 | 1.0650 | 1.0653 |
| 2.0 | 1.1127 | 1.1129 | 1.1129 | 1.1119 | 1.1127 | 1.1135 |

Figure 2.2.6 shows that four numerical methods, GFEM, SCM, FEM, and ASM all approach to the same result for non-linear frequency ratio $\omega_1^*\big/\left(\omega_1^*\right)_L$ of hinged-clamped beam, but only SDQM has slight deviation of result which increasing with $a/r$, are listed in Table 2.2.4.

19
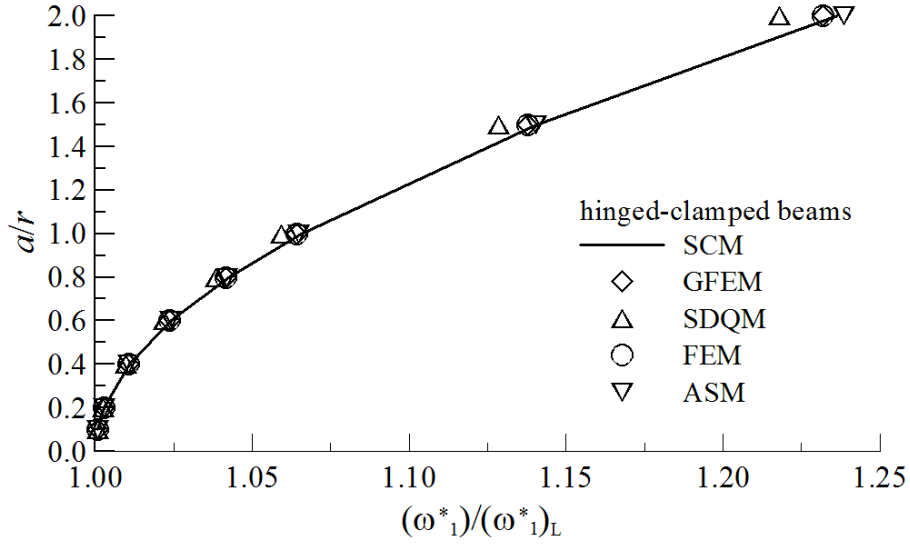
**Figure 2.2.6 Dimensionless amplitude-frequency curves of hinged-clamped beam.**

**Table 2.2.4 Fundamental natural frequency ratio $\omega_1^*/(\omega_1^*)_L$ for hinged-clamped beams.**

| $a/r$ | GFEM | SCM | SDQM | FEM | ASM |
|-------|--------|--------|--------|--------|--------|
| 0.1 | 1.0006 | 1.0007 | 1.0006 | 1.0006 | 1.0006 |
| 0.2 | 1.0026 | 1.0027 | 1.0024 | 1.0026 | 1.0026 |
| 0.4 | 1.0106 | 1.0109 | 1.0097 | 1.0106 | 1.0106 |
| 0.6 | 1.0237 | 1.0242 | 1.0218 | 1.0237 | 1.0238 |
| 0.8 | 1.0416 | 1.0425 | 1.0383 | 1.0416 | 1.0418 |
| 1.0 | 1.0641 | 1.0655 | 1.0592 | 1.0641 | 1.0647 |
| 1.5 | 1.1378 | 1.1406 | 1.1284 | 1.1378 | 1.1404 |
| 2.0 | 1.2318 | 1.2361 | 1.2179 | 1.2319 | 1.2385 |

Figure 2.2.7 shows that SCM result for non-linear frequency ratio $\omega_1^*/(\omega_1^*)_L$ of three types of boundary conditions: hinged-hinged, clamped-clamped, and hinged-clamped ends of beam, the physical characteristics are :

1.  The more amplitude of vibration $a/r$, the larger non-linear frequency ratio $\omega_1^*/(\omega_1^*)_L$ for each type of boundary condition of beam.

2.  For the same amplitude of vibration $a/r$, the order of amplitude of non-linear frequency ratio $\omega_1^*/(\omega_1^*)_L$ is hinged-hinged, hinged-clamped, and clamped-clamped ends of beam.

3.  The more amplitude of vibration $a/r$, the larger the non-linear frequency

ratio $\omega_1^* / (\omega_1^*)_L$ change for each type of boundary condition of beam.
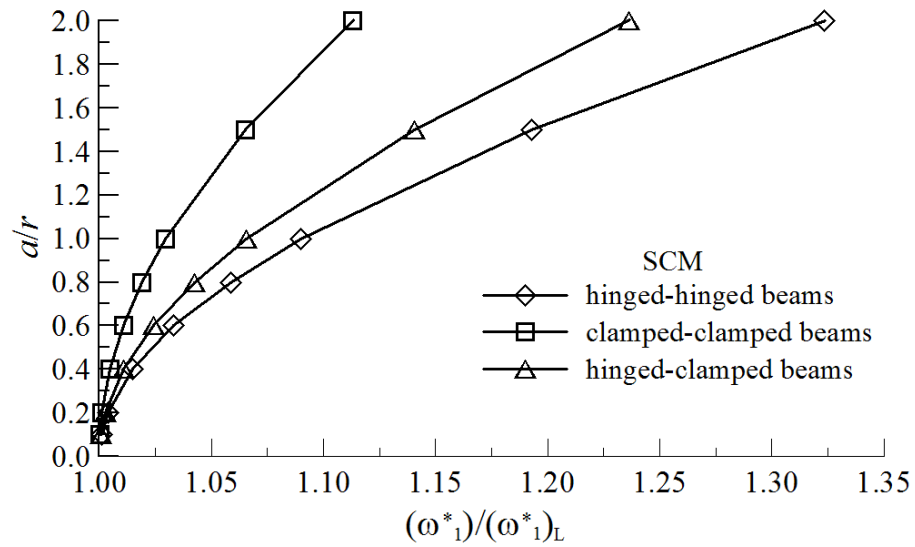


**Figure 2.2.7 Dimensionless amplitude-frequency curves with different boundary conditions.**

Figure 2.2.8 shows that the fist three normal mode shapes of three types of boundary conditions: hinged-hinged, clamped-clamped, and hinged-clamped ends of beam.
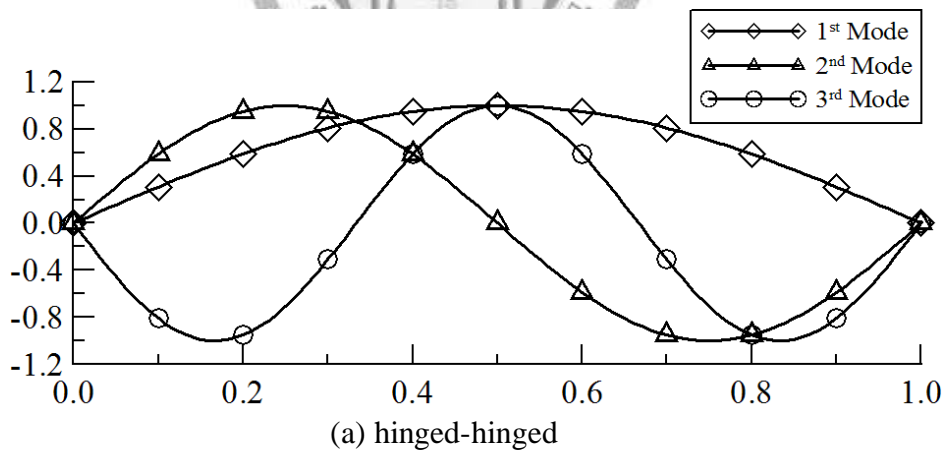


(a) hinged-hinged
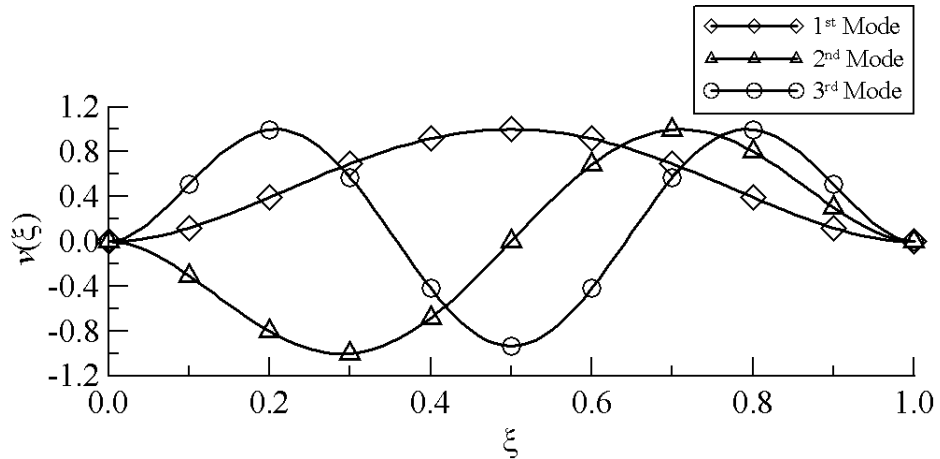
(b) clamped-clamped
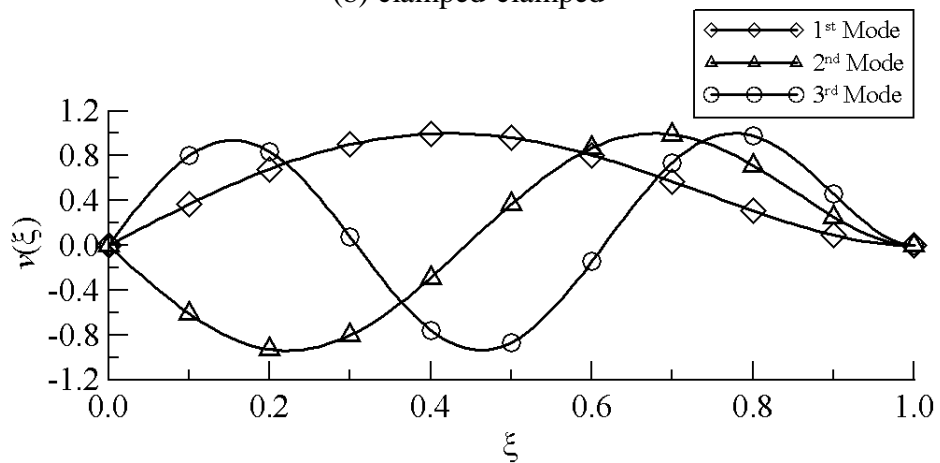


(c) hinged -clamped

**Figure 2.2.8 Fist three normal mode shapes by SCM ( $a/r = 2.0$ ).**

## 2.2.5 Nomenclature

| | |
|---|---|
| $A$ | area of the cross-section |
| $B_i(\xi)$ | quintic B-spline function |
| $c_i$ | coefficient to be determined |
| $E$ | Young's modulus |
| $h$ | distance of equi-spaced knots |
| $I$ | moment of inertia of the cross-section |
| $m$ | mass per unit length |
| $N(\xi)$ | dimensionless stretching force |
| $q$ | order of convergence |

$$r = \sqrt{\dfrac{I}{A}}$$

$v$             nonlinear mode shapes

$w$            deflection

$\bar{w}$           nonlinear mode shapes

$x$            coordinate system

$\xi = \dfrac{x}{L}$       dimensionless coordinate system

$\omega$           fundamental frequency of nonlinear vibrating beam

$\omega^{*} = \omega \sqrt{\dfrac{mL^4}{EI}}$   fundamental dimensionless frequency of nonlinear vibrating beam

$\left(\omega_1^{*}\right)_L$      dimensionless fundamental natural frequency of linear vibrating beam

$a/r$          amplitude of vibration

## 2.3 Elastic Analysis of Rectangular Thin Plates

### 2.3.1 Introduction

Spline functions, introduced by Schoenberg (Schoenberg, 1946) for approximation purposes, were extended to solve differential equations. Commonly, this incorporates the use of cubic B-splines which were presented by Mizusawa *et al*. (1979) for investigation of vibration of skew plates, Shen and Wang (1987) for linear static analysis of cylindrical shells, Gupta *et al*. (1991) for linear finite element analysis of axi-symmetric shells and others. Weller employed B-splines to study post-buckling behavior of infinite length cylindrical panels subjected to combined thermal and mechanical loading (Weller and Patlashenko,1993), and they were incorporated into collocation method for same analysis problem (Weller and Patlashenko,1993).

The SCM is proposed to analyze thin plate problems. The transverse deflection of the plate is expressed in term of spline functions. A set of algebraic equations is established to solve the coefficients for spline functions from the governing equations and boundary conditions. The feasibility of SCM to plate analysis is studied by considering different plate problems with various boundary conditions and loading patterns. Moreover, the rapid convergence properties and accuracy of the SCM are demonstrated through comparison of the numerical results with the corresponding exact solutions.

### 2.3.2 Formulation

An rectangular plate with dimensions $c \times d$ is considered as shown in Figure 2.3.1. The governing equations of a uniform thin plate subjected to a distributed loading can be derived as (Timoshenko and Woinowsky-Krieger, 1959) :

$$D\left(\frac{\partial^4 w}{\partial x^4} + 2\frac{\partial^4 w}{\partial^2 x \partial^2 y} + \frac{\partial^4 w}{\partial y^4}\right) = q(x, y) \qquad (2.3.1)$$

where $w$ is the transverse deflection; $D = Eh^3/[12(1-\nu^2)]$, $E$ and $\nu$ are the plate flexural rigidity, Young's modulus and Poisson's ratio, respectively; $q$ is the surface load intensity.
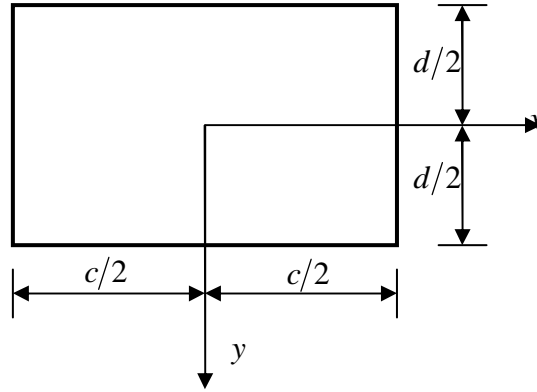


**Figure 2.3.1 Configuration of thin plate.**

The moments and shear forces are expressed as:

$$M_x = -D\left(\frac{\partial^2 w}{\partial x^2} + \nu\frac{\partial^2 w}{\partial y^2}\right) \tag{2.3.2a}$$

$$M_y = -D\left(\frac{\partial^2 w}{\partial y^2} + \nu\frac{\partial^2 w}{\partial x^2}\right) \tag{2.3.2b}$$

$$M_{xy} = -M_{yx} = D(1-\nu)\frac{\partial^2 w}{\partial x\partial y} \tag{2.3.2c}$$

$$Q_x = -D\frac{\partial}{\partial x}\left(\frac{\partial^2 w}{\partial x^2} + \frac{\partial^2 w}{\partial y^2}\right) \tag{2.3.2d}$$

$$Q_y = -D\frac{\partial}{\partial y}\left(\frac{\partial^2 w}{\partial x^2} + \frac{\partial^2 w}{\partial y^2}\right) \tag{2.3.2e}$$

The boundary conditions considered herein are divided into three kinds. For example, for an edge with $x = c/2$, they are:

(a) Built-in edge (B) :

$$w = 0; \quad \frac{\partial w}{\partial x} = 0, \tag{2.3.3}$$

(b) Simply-supported edge (S) :

$$w = 0; \quad \frac{\partial^2 w}{\partial x^2} + \nu \frac{\partial^2 w}{\partial y^2} = 0, \tag{2.3.4}$$

(c) Free edge (F) :

$$\frac{\partial^3 w}{\partial x^3} + (2-\nu)\frac{\partial^3 w}{\partial x \partial y^2} = 0; \frac{\partial^2 w}{\partial x^2} + \nu \frac{\partial^2 w}{\partial y^2} = 0. \tag{2.3.5}$$

## 2.3.3 Approach by spline collocation method

The analyzed domain is taken $(N_x + 1) \times (N_y + 1)$ knots in the $x$ and $y$ directions as shown in Figure 2.3.2, respectively. Extend SCM theory (Prenter, 1975) to two dimension problem, the transverse deflection is approximated as :

$$w(x, y) = \sum_{i=-2}^{N_x+2} \sum_{j=-2}^{N_y+2} B_i(x)B_j(y)a_{ij} \tag{2.3.6}$$

where $B_i(x)$ 's and $B_j(y)$ 's are quintic spline functions, $a_{ij}$ 's are coefficients to be determined.



● knot    ○ fictitious knot
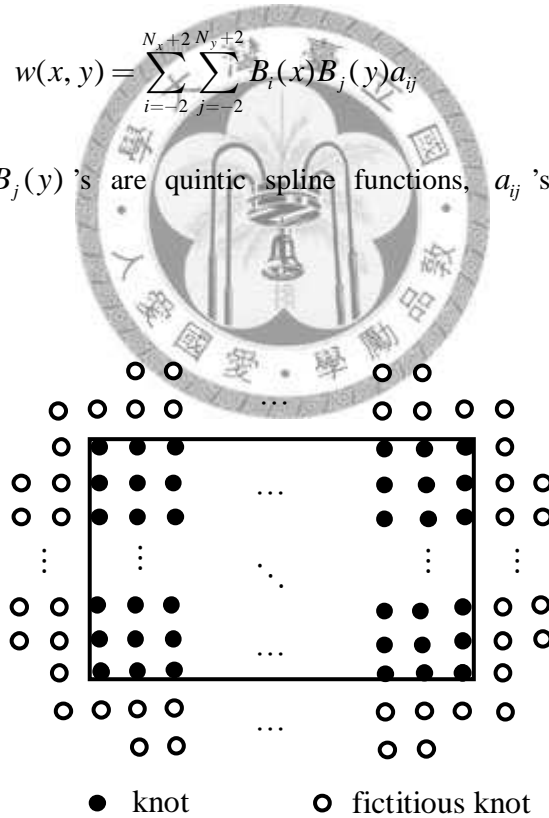
**Figure 2.3.2 Distribution knots of thin plate.**

The discrete governing equation takes the following discrete form:

$$D\sum_{i=-2}^{N_x+2} \sum_{j=-2}^{N_y+2} \left[ B_i^{(4)}(x)B_j(y) + 2B_i^{(2)}(x)B_j^{(2)}(y) + B_i(x)B_j^{(4)}(y) \right]a_{ij} = q(x, y) \tag{2.3.7}$$

Similarly, the moments and shear forces can be discretized as:

$$M_x = -D \sum_{i=-2}^{N_x+2} \sum_{j=-2}^{N_y+2} \left[ B_i^{(2)}(x)B_j(y) + \nu B_i(x)B_j^{(2)}(y) \right] a_{ij}$$
(2.3.8a)

$$M_y = -D \sum_{i=-2}^{N_x+2} \sum_{j=-2}^{N_y+2} \left[ \nu B_i^{(2)}(x)B_j(y) + B_i(x)B_j^{(2)}(y) \right] a_{ij}$$
(2.3.8b)

$$M_{xy} = -M_{yx} = D(1-\nu) \sum_{i=-2}^{N_x+2} \sum_{j=-2}^{N_y+2} \left[ B_i^{(1)}(x)B_j^{(1)}(y) \right] a_{ij}$$
(2.3.8c)

$$Q_x = -D \sum_{i=-2}^{N_x+2} \sum_{j=-2}^{N_y+2} \left[ B_i^{(3)}(x)B_j(y) + B_i^{(1)}(x)B_j^{(2)}(y) \right] a_{ij}$$
(2.3.8d)

$$Q_y = -D \sum_{i=-2}^{N_x+2} \sum_{j=-2}^{N_y+2} \left[ B_i^{(2)}(x)B_j^{(1)}(y) + B_i(x)B_j^{(3)}(y) \right] a_{ij}$$
(2.3.8e)

Taking the edge $x = c/2$ as an example, the three kinds of boundary conditions can be discretized into the following forms:

(B) $\quad \sum_{i=-2}^{N_x+2} \sum_{j=-2}^{N_y+2} \left[ B_i(c/2)B_j(y) \right] a_{ij} \neq 0 ,$
(2.3.9a)

$$\sum_{i=-2}^{N_x+2} \sum_{j=-2}^{N_y+2} \left[ B_i^{(1)}(c/2)B_j(y) \right] a_{ij} = 0$$
(2.3.9b)

(S) $\quad \sum_{i=-2}^{N_x+2} \sum_{j=-2}^{N_y+2} \left[ B_i(c/2)B_j(y) \right] a_{ij} = 0 ,$
(2.3.10a)

$$\sum_{i=-2}^{N_x+2} \sum_{j=-2}^{N_y+2} \left[ B_i^{(2)}(c/2)B_j(y) + \nu B_i(c/2)B_j^{(2)}(y) \right] a_{ij} = 0$$
(2.3.10b)

(F) $\quad \sum_{i=-2}^{N_x+2} \sum_{j=-2}^{N_y+2} \left[ B_i^{(3)}(c/2)B_j(y) + (2-\nu)B_i^{(1)}(c/2)B_j^{(2)}(y) \right] a_{ij} = 0 ,$
(2.3.11a)

$$\sum_{i=-2}^{N_x+2} \sum_{j=-2}^{N_y+2} \left[ B_i^{(2)}(c/2)B_j(y) + \nu B_i(c/2)B_j^{(2)}(y) \right] a_{ij} = 0$$
(2.3.11b)

Since both the discretized governing equations and the discretized boundary conditions are written out on a spline function basis, the discretized governing equations and the

discretized boundary conditions should be satisfied simultaneously. In order to get solutions for the problems, virtual knots are assigned beyond the analyzed domain to satisfy the boundary conditions (Figure 2.3.2). Thus, solutions of the problems are acquired by solving a set of linear algebraic equations, which consist of $(N_x + 1) \times (N_y + 1)$ governing equations at all the knots, and $4(N_x + 1) + 4(N_y + 1) - 4$ boundary conditions at the edge knots. It have to notice, there using three virtual knots for four corners to resolve singular matrix problem (Bert and Sheu, 1996).

## 2.3.4 Numerical Results

To investigate the applicability, convergence and accuracy of the SCM for plate problems, plates with different combinations of free (F), simply supported (S) and fixed (B) boundaries are calculated. The rectangular plates subjected to linearly distributed load and cosine distributed load are shown in Figure 2.3.3.The boundary conditions of the plates are denoted by four *letter symbols*, the first symbol relates to the $x = -c/2$ edge, the second symbol relates to the $x = c/2$ edge, the third symbol relates to the $y = -d/2$ edge and the fourth symbol relates to the $y = d/2$ edge. The Poisson ratio $\nu$ is taken to be $0.30$ for all cases.

$$q(x, y) = q_0(1/2 + x/c) \qquad\qquad q(x, y) = q_0 \cos(x\pi/c)$$

(a) line distributed load        (b) cosine distributed load
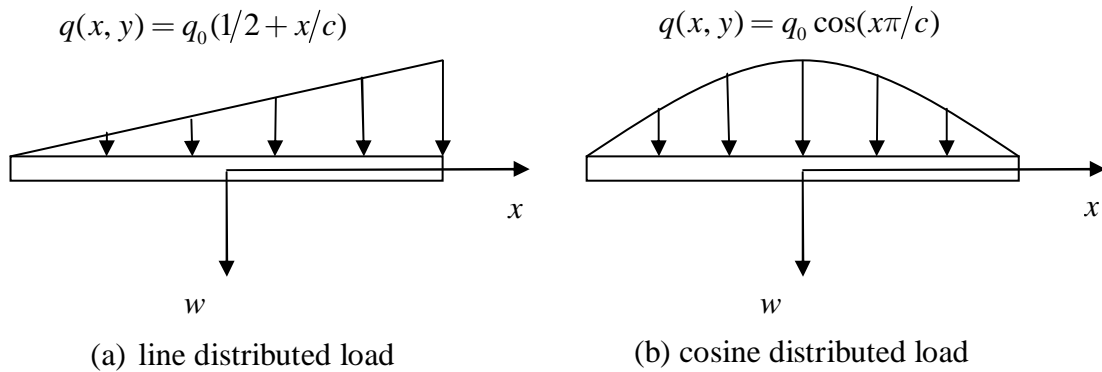
**Figure 2.3.3 Loading pattern of thin plate.**

In order to investigate the convergence pattern of the different plates, deflections for plates with various length-to-width ratio $(d/c)$ subjected to various combinations of boundary conditions are presented. Table 2.3.1 to Table 2.3.3 present results of deflections of plates

28

subjected to linearly distributed load with $d/c = 0.5, 1.0, 2.0$. Table 2.3.4 to Table 2.3.6

present results of deflections of plates subjected to cosine distributed load with

$d/c = 0.5, 1.0, 2.0$. The proposed method provides rapid converged and good accurate results

for all the cases as the number of knots increases.

**Table 2.3.1 Center deflection** $w^*$ **in rectangular plates subjected to line distributed load.** ($w^* = wD/q_0 d^4$, $d/c = 0.5$)

| knots | $9 \times 5$ | $21 \times 11$ | $41 \times 21$ | $61 \times 31$ | EXACT |
|---|---|---|---|---|---|
| B-B-B-B | 0.13091E-02 | 0.12735E-02 | 0.12683E-02 | 0.12673E-02 | 0.128E-02 |
| B-B-B-S | 0.23417E-02 | 0.22599 E-02 | 0.22484 E-02 | 0.22462E-02 | - |
| B-B-B-F | 0.71620E-02 | 0.68274 E-02 | 0.67551 E-02 | 0.67380E-02 | - |
| B-B-F-F | 0.22011E-01 | 0.21185 E-01 | 0.21026 E-01 | 0.2988 E-01 | - |
| S-S-B-B | 0.13281E-02 | 0.13096 E-02 | 0.13065 E-02 | 0.13059E-02 | - |
| S-B-S-S | 0.46409E-02 | 0.44912 E-02 | 0.44699 E-02 | 0.44659E-02 | 0.45E-02 |
| S-S-S-S | 0.52041E-02 | 0.50865 E-02 | 0.50698 E-02 | 0.50668E-02 | - |

**Table 2.3.2 Center deflection** $w^*$ **in rectangular plates subjected to line distributed load.** ($w^* = wD/q_0 c^4$, $d/c = 1.0$)

| knots | $5 \times 5$ | $11 \times 11$ | $21 \times 21$ | $31 \times 31$ | EXACT |
|---|---|---|---|---|---|
| B-B-B-B | 0.74093E-03 | 0.64766E-03 | 0.63634E-03 | 0.63429E-03 | 0.63E-03 |
| B-B-B-S | 0.89840E-03 | 0.80181E-03 | 0.78933E-03 | 0.78705E-03 | - |
| B-B-B-F | 0.10257E-02 | 0.95994E-03 | 0.94917E-03 | 0.94682E-03 | - |
| B-B-F-F | 0.13237E-02 | 0.12902E-02 | 0.12831E-02 | 0.12811E-02 | - |
| S-S-B-B | 0.10692E-02 | 0.97597E-03 | 0.96290E-03 | 0.96049E-03 | - |
| S-B-S-S | 0.14140E-02 | 0.13045E-02 | 0.12893E-02 | 0.12865E-02 | 0.13E-02 |
| S-S-S-S | 0.21969E-02 | 0.20560E-02 | 0.20373E-02 | 0.20338E-02 | - |

**Table 2.3.3 Center deflection** $w^*$ **in rectangular plates subjected to line distributed load.** ( $w^* = wD/q_0c^4$ , $d/c = 2.0$ )

| knots | $5\times9$ | $11\times21$ | $21\times41$ | $31\times61$ | EXACT |
|---|---|---|---|---|---|
| B-B-B-B | 0.13091E-02 | 0.12735E-02 | 0.12683E-02 | 0.12673E-02 | - |
| B-B-B-S | 0.13186E-02 | 0.12916E-02 | 0.12874E-02 | 0.12866E-02 | - |
| B-B-B-F | 0.13010E-02 | 0.12837E-02 | 0.12814E-02 | 0.12811E-02 | - |
| B-B-F-F | 0.12918E-02 | 0.12939E-02 | 0.12946E-02 | 0.12948E-02 | - |
| S-S-B-B | 0.44233E-02 | 0.42546E-02 | 0.42305E-02 | 0.42261E-02 | - |
| S-B-S-S | 0.22583E-02 | 0.22135E-02 | 0.22068E-02 | 0.22055E-02 | 0.23E-02 |
| S-S-S-S | 0.52041E-02 | 0.50865E-02 | 0.50698E-02 | 0.50668E-02 | - |

**Table 2.3.4 Center deflection** $w^*$ **in rectangular plates subjected to cosine distributed load.** ( $w^* = wD/q_0d^4$ , $d/c = 0.5$ )

| knots | $9\times5$ | $21\times11$ | $41\times21$ | $61\times31$ |
|---|---|---|---|---|
| B-B-B-B | 0.23305E-02 | 0.22653E-02 | 0.22563E-02 | 0.22547E-02 |
| B-B-B-S | 0.40435E-02 | 0.39224E-02 | 0.39060E-02 | 0.39029E-02 |
| B-B-B-F | 0.12058E-01 | 0.11608E-01 | 0.11506E-01 | 0.11481E-01 |
| B-B-F-F | 0.36737E-01 | 0.35767E-01 | 0.35562E-01 | 0.35512E-01 |
| S-S-B-B | 0.23486E-02 | 0.23019E-02 | 0.22955E-02 | 0.22943E-02 |
| S-B-S-S | 0.79695E-02 | 0.77867E-02 | 0.77616E-02 | 0.77570E-02 |
| S-S-S-S | 0.84746E-02 | 0.83422E-02 | 0.83241E-02 | 0.83207E-02 |

**Table 2.3.5 Center deflection** $w^*$ **in rectangular plates subjected to cosine distributed load.** ( $w^* = wD/q_0c^4$ , $d/c = 1.0$ )

| knots | $5\times5$ | $11\times11$ | $21\times21$ | $31\times31$ |
|---|---|---|---|---|
| B-B-B-B | 0.12081E-02 | 0.10916E-02 | 0.10790E-02 | 0.10768E-02 |
| B-B-B-S | 0.14558E-02 | 0.13474E-02 | 0.13345E-02 | 0.13322E-02 |
| B-B-B-F | 0.16566E-02 | 0.16133E-02 | 0.16050E-02 | 0.16029E-02 |
| B-B-F-F | 0.21270E-02 | 0.21654E-02 | 0.21669E-02 | 0.21660E-02 |
| S-S-B-B | 0.16501E-02 | 0.15565E-02 | 0.15447E-02 | 0.15426E-02 |
| S-B-S-S | 0.23832E-02 | 0.22877E-02 | 0.22751E-02 | 0.22728E-02 |
| S-S-S-S | 0.33192E-02 | 0.32408E-02 | 0.32308E-02 | 0.32290E-02 |

**Table 2.3.6 Center deflection** $w^*$ **in rectangular plates subjected to cosine distributed load.** ( $w^* = wD/q_0 c^4$ , $d/c = 2.0$ )

| knots | 5×9 | 11×21 | 21×41 | 31×61 |
|---|---|---|---|---|
| B-B-B-B | 0.21039E-02 | 0.21368E-02 | 0.21411E-02 | 0.21419E-02 |
| B-B-B-S | 0.21190E-02 | 0.21668E-02 | 0.21731E-02 | 0.21743E-02 |
| B-B-B-F | 0.20912E-02 | 0.21542E-02 | 0.21636E-02 | 0.21654E-02 |
| B-B-F-F | 0.20767E-02 | 0.21715E-02 | 0.21860E-02 | 0.21889E-02 |
| S-S-B-B | 0.66476E-02 | 0.66676E-02 | 0.66709E-02 | 0.66716E-02 |
| S-B-S-S | 0.38522E-02 | 0.39387E-02 | 0.39507E-02 | 0.39529E-02 |
| S-S-S-S | 0.78048E-02 | 0.79639E-02 | 0.79868E-02 | 0.79910E-02 |

## 2.3.5 Nomenclature

| | |
|---|---|
| $a_{ij}$ | coefficients to be determined |
| $B_i(x)$ , $B_j(y)$ | quintic spline functions |
| $D = Eh^3 / \left[ 12(1 - \nu^2) \right]$ | plate flexural rigidity |
| $E$ | Young's modulus |
| $N_x + 1$ | knots in the $x$ directions |
| $N_y + 1$ | knots in the $y$ directions |
| $q$ | surface load intensity |
| $w$ | transverse deflection |
| $w^* = wD/q_0 c^4$ | dimensionless transverse deflection |
| $\nu$ | Poisson's ratio |

## 2.4 Shear Buckling of Rectangular Thin Plates

### 2.4.1 Introduction

The critical shear buckling load of a thin elastic rectangular plate is an important design factor for applications in aeronautical, civil, mechanical, and marine structures. It is essential for the critical shear buckling load of a thin plate to be large enough to endure a safe design. This paper uses the classical Kirchhoff thin plate theory to analyze the critical shear buckling load of a thin rectangular plate. Although the same problem was analyzed previously by numerous researchers, their solutions were limited to relatively few cases of boundary conditions (Timoshenko and Gere, 1961; Roark and Young, 1975; Japan, 1971). Conventionally, the letters C, S, and F have been used to denote the clamped, simply supported, and free boundary conditions, respectively, of each edge of the plate. Research on this topic was carried out by NASA (Stein and Neff, 1947; Batdorf and Stein, 1947; Budiansky and Connor, 1948) in the late 1940's, but only approximate results for simply supported (SSSS) and clamped (CCCC) plates were mentioned. The upper and lower bounds of the critical pure shear buckling loads of clamped plates were approximated by NASA (Budiansky and Connor, 1948) using the Lagrangian multiplier method (LMM). The shear buckling loads for SSSS plates of several aspect ratios were analyzed by Smith (1995) using the finite element method (FEM). The critical shear buckling loads of thin plates were solved for various boundary conditions (CCCC, CSCS, SSSS, CCFF, and CFCF) by researchers using the extended Kantorovich method (EKM) (Yuan and Jin, 1998; Eisenberger and Alexandrov, 2003; Shufrin and Eisenberger, 2005; Shufrin and Eisenberger, 2007).

The main objective of this paper is to present highly accurate solutions for a thin elastic rectangular plate with various combinations of boundary conditions (CCCC, CSCS, SSSS, CCFF, and CFCF), aspect ratios, uni- and bi-directional

compressive/tensile loadings. The results obtained will be compared with the published results by FEM, LMM, EKM, etc.

## 2.4.2 Formulation

Elastic shear buckling of a rectangular thin plate with in-plane normal forces $N_x$, $N_y$ and shear force $N_{xy}$ are considered, as shown in Figure 2.4.1.
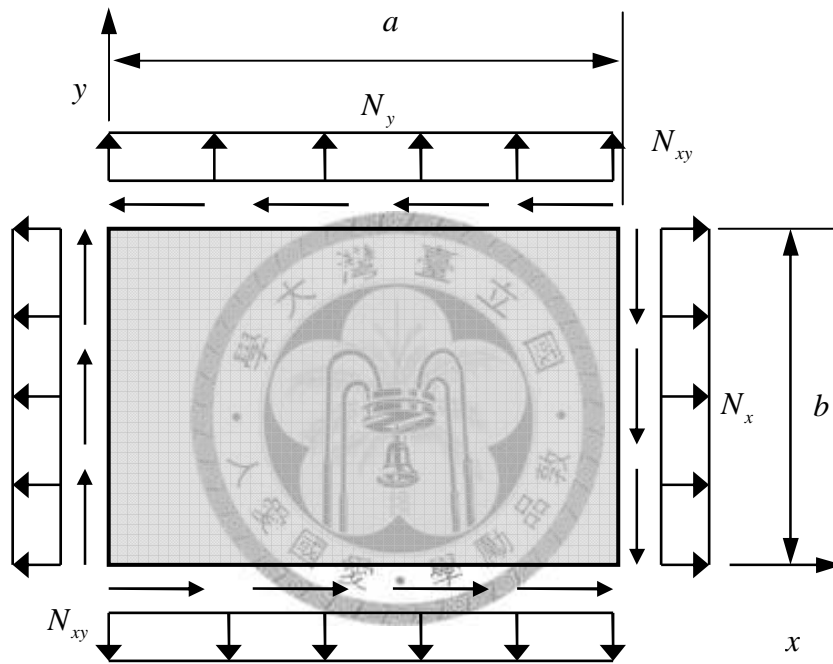


**Figure 2.4.1 System coordinates of rectangular thin plate.**

According to the classical Kirchhoff thin plate theory, the governing equation of the plate under in-plane forces is (Reddy, 1999)

$$D\left[\frac{\partial^4 w}{\partial x^4} + 2\frac{\partial^4 w}{\partial x^2 \partial y^2} + \frac{\partial^4 w}{\partial y^4}\right] = N_x\frac{\partial^2 w}{\partial x^2} + N_y\frac{\partial^2 w}{\partial y^2} + 2N_{xy}\frac{\partial^2 w}{\partial x \partial y} \qquad (2.4.1)$$

where $w(x, y)$ is the elastic lateral buckling displacement, and $D$ is the flexural rigidity of the plate given by

$$D = \frac{Et^3}{12\left(1 - v^2\right)} \qquad (2.4.2)$$

Here, $E$ is Young's modulus, $t$ is the thickness, and $\nu$ is Poisson's ratio of the plate.

For the purpose of description, notations will be adopted as follows. Any edge of the plate can have one of the three boundary conditions: clamped (C), simply supported (S), and free (F). The symbolism SCSF will denote the plate boundary conditions with the edges $x = 0$, $x = a$, $y = 0$, $y = b$ having simply supported, clamped, simply supported, and free boundary conditions, respectively, etc. The clamped, simply supported, and free boundary conditions at edge $x = 0$ or $a$ can be sequentially given as follows:

$$w = 0, \quad \frac{\partial w}{\partial x} = 0 \tag{2.4.3}$$

$$w = 0, \quad \frac{\partial^2 w}{\partial x^2} + \nu \frac{\partial^2 w}{\partial y^2} = 0 \tag{2.4.4}$$

$$\frac{\partial^2 w}{\partial x^2} + \nu \frac{\partial^2 w}{\partial y^2} = 0, \quad \frac{\partial^3 w}{\partial x^3} + (2 - \nu) \frac{\partial^3 w}{\partial x \partial y^2} = 0 \tag{2.4.5}$$

Similarly, the clamped, simply supported, and free boundary conditions at edge $y = 0$ or $b$ can be sequentially given as follows:

$$w = 0, \quad \frac{\partial w}{\partial y} = 0 \tag{2.4.6}$$

$$w = 0, \quad \frac{\partial^2 w}{\partial y^2} + \nu \frac{\partial^2 w}{\partial x^2} = 0 \tag{2.4.7}$$

$$\frac{\partial^2 w}{\partial y^2} + \nu \frac{\partial^2 w}{\partial x^2} = 0, \quad \frac{\partial^3 w}{\partial y^3} + (2 - \nu) \frac{\partial^3 w}{\partial^2 x \partial y} = 0 \tag{2.4.8}$$

For a corner point of a rectangular plate with both neighboring edges clamped, or simply supported, or free, the boundary conditions can be sequentially expressed as follows:

$$w = 0, \quad \frac{\partial w}{\partial x} = 0, \quad \frac{\partial w}{\partial y} = 0 \tag{2.4.9}$$

$$w = 0, \quad \frac{\partial^2 w}{\partial x^2} = 0, \quad \frac{\partial^2 w}{\partial y^2} = 0 \tag{2.4.10}$$

$$\frac{\partial^2 w}{\partial x \partial y} = 0, \quad \frac{\partial^2 w}{\partial x^2} + \nu \frac{\partial^2 w}{\partial y^2} = 0, \quad \nu \frac{\partial^2 w}{\partial x^2} + \frac{\partial^2 w}{\partial y^2} = 0 \tag{2.4.11}$$

When a plate is simply supported edge at $x = 0$ or $a$, the boundary conditions of the two corner points, $(x, y) = (0, 0), (0, b)$ or $(x, y) = (a, 0), (a, b)$, can be given as

$$w = 0, \quad \frac{\partial^2 w}{\partial x^2} = 0, \quad \frac{\partial w}{\partial y} = 0 \tag{2.4.12}$$

From Eq. (2.4.12), we can obtain $\partial^2 w / \partial y^2 = 0$, $\partial^3 w / \partial x^3 = 0$, and $\partial^3 w / \partial x \partial y^2 = 0$. Therefore, if Eq. (2.4.12) is satisfied then Eqs. (2.4.4) and (2.4.5) are satisfied automatically. Consequently, Eq. (2.4.12) holds regardless of the types of boundary conditions at edges $y = 0$ and $b$ whenever the edge at $x = 0$ or $a$ is simply supported.

Similarly, when a plate is simply-supported edge at $y = 0$ or $b$, the boundary conditions of the two corner points, $(x, y) = (0, 0), (a, 0)$ or $(x, y) = (0, b), (a, b)$, are

$$w = 0, \quad \frac{\partial w}{\partial x} = 0, \quad \frac{\partial^2 w}{\partial y^2} = 0. \tag{2.4.13}$$

### 2.4.3 Approach by spline collocation method

A rectangular thin plate with size $a \times b$ has been assigned $n_x$ and $n_y$ inner knots with equal-space $h_x$ and $h_y$ in the $x$- and $y$- directions, respectively, as shown in Figure 2.4.2. The serial numbers of the inner knots are defined as

$$x_3 = 0, \quad x_{n_x+2} = a, \quad x_{j+1} - x_j = h_x = a/(n_x - 1), \quad j = 3, \ldots, n_x + 1. \tag{2.4.14}$$

$$y_3 = 0, \quad y_{n_y+2} = b, \quad y_{j+1} - y_j = h_y = b/(n_y - 1), \quad j = 3, \ldots, n_y + 1. \tag{2.4.15}$$

The total number of inner knots is $n_x n_y$. The governing equation in Eq. (2.4.1) must be satisfied for each inner knot of the plate.

Fictitious knots are needed in order to satisfy the boundary conditions of physical problem. One needs two fictitious knots outside the plate to satisfy two boundary conditions of one set equations of Eq. (2.4.3) to Eq. (2.4.8) for each boundary knot of the plate, except the four corner knots $(x_3, y_3)$, $(x_3, y_{n_y+2})$, $(x_{n_x+2}, y_3)$, and $(x_{n_x+2}, y_{n_y+2})$. Therefore, the total number of fictitious knots for the boundary knots, excluding the four corner knots, is $4\left[(n_x - 2) + (n_y - 2)\right]$. Each corner knot has three boundary conditions, which are regarded as one set of Eq. (2.4.9) to Eq. (2.4.13). Thus, the total number of fictitious knots for four corners is 12. Consequently, the total number of boundary fictitious knots for the plate is $4(n_x + n_y) - 4$, which is exactly equal to the total number of boundary conditions of the problem. The total number of knots including fictitious knots for the whole plate is $n_x n_y + 4(n_x + n_y) - 4$, as shown in Figure 2.4.2.

The elastic lateral buckling displacement $w(x, y)$ of a rectangular thin plate subjected to in-plane forces can be approximated by using the QSFs as follows:

$$w(x, y) = \sum_{i=1}^{n_x+4} \sum_{j=1}^{n_y+4} B_i(x) B_j(y) a_{ij} \tag{2.4.16}$$

where $a_{ij}$s are the coefficients to be determined, noting that $a_{ij} = 0$ exists for no knots when $i = 1, n_x + 4$, $j = 1, 2, 3, n_y + 2, n_y + 3, n_y + 4$ and $i = 2, 3, n_x + 2, n_x + 3$, $j = 1, , n_y + 4$.
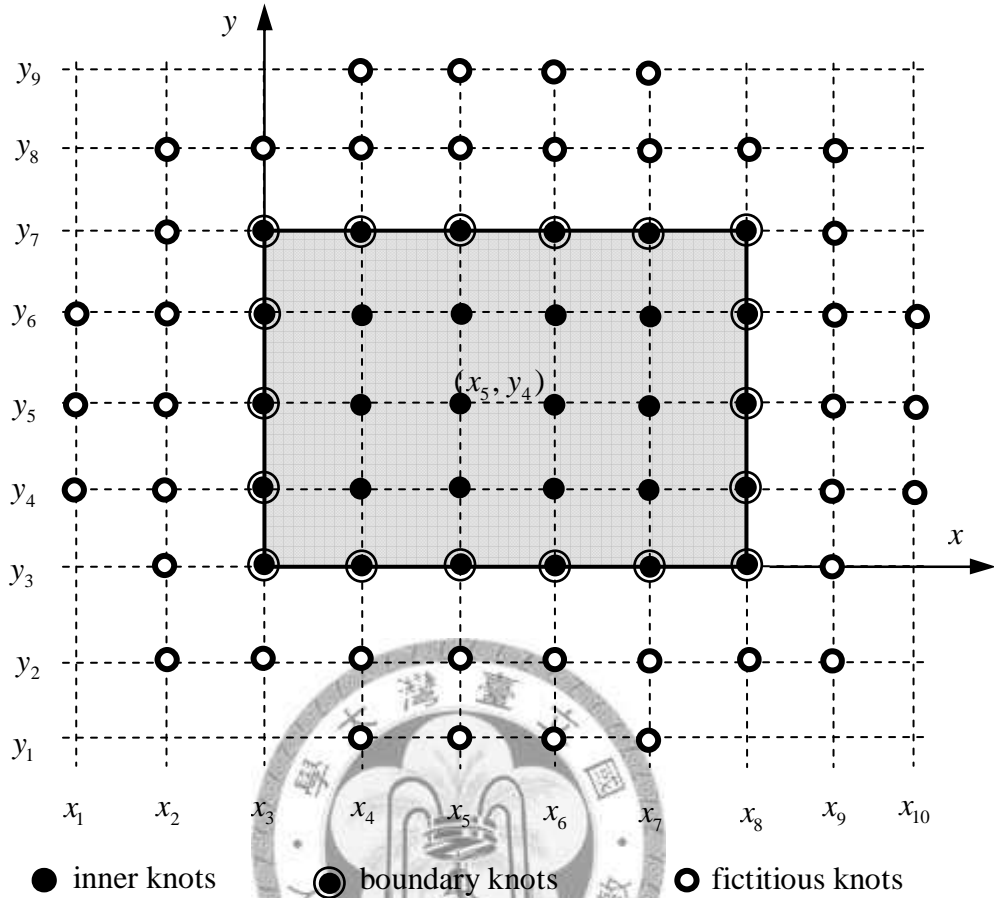
**Figure 2.4.2 Distribution of knots of the plate ($n_x = 6$, $n_y = 5$).**

The partial derivatives for $w(x, y)$ can be given as

$$\frac{\partial w^r(x, y)}{\partial x^r} = \sum_{i=1}^{n_x+4} \sum_{j=1}^{n_y+4} B_i^{(r)}(x)B_j(y)a_{ij} \tag{2.4.17}$$

$$\frac{\partial w^s(x, y)}{\partial y^s} = \sum_{i=1}^{n_x+4} \sum_{j=1}^{n_y+4} B_i(x)B_j^{(s)}(y)a_{ij} \tag{2.4.18}$$

$$\frac{\partial w^{(r+s)}(x, y)}{\partial x^r \partial y^s} = \sum_{i=1}^{n_x+4} \sum_{j=1}^{n_y+4} B_i^{(r)}(x)B_j^{(s)}(y)a_{ij} \tag{2.4.19}$$

Substituting the displacement of thin rectangular plate and its partial derivatives in Eq. (2.4.16) to Eq. (2.4.19) into the governing equation in Eq. (2.4.1), one can obtain the field equation as:

37

$$D \sum_{i=1}^{n_x+4} \sum_{j=1}^{n_y+4} \left[ B_i^{(4)}(x)B_j(y) + 2B_i''(x)B_j''(y) + B_i(x)B_j^{(4)}(y) \right] a_{ij}$$

$$= \sum_{i=1}^{n_x+4} \sum_{j=1}^{n_y+4} \left[ N_x B_i''(x)B_j(y) + N_y B_i(x)B_j''(y) + 2N_{xy} B_i'(x)B_j'(y) \right] a_{ij}$$

(2.4.20)

Similarly, the boundary conditions in Eq. (2.4.3) to Eq. (2.4.13) can be discretized and reduced as the same way.

Clamped boundary conditions at edge $x = 0$ or $a$:

$$w = \sum_{i=1}^{n_x+4} \sum_{j=1}^{n_y+4} B_i(x)B_j(y)a_{ij} = 0 \tag{2.4.21a}$$

$$\frac{\partial w}{\partial x} = \sum_{i=1}^{n_x+4} \sum_{j=1}^{n_y+4} B_i'(x)B_j(y)a_{ij} = 0 \tag{2.4.21b}$$

Simply supported boundary conditions at edge $x = 0$ or $a$:

$$w = \sum_{i=1}^{n_x+4} \sum_{j=1}^{n_y+4} B_i(x)B_j(y)a_{ij} = 0 \tag{2.4.22a}$$

$$\frac{\partial^2 w}{\partial x^2} + \nu \frac{\partial^2 w}{\partial y^2} = \sum_{i=1}^{n_x+4} \sum_{j=1}^{n_y+4} \left[ B_i''(x)B_j(y) + \nu B_i(x)B_j''(y) \right] a_{ij} = 0 \tag{2.4.22b}$$

Free boundary conditions at edge $x = 0$ or $a$:

$$\frac{\partial^2 w}{\partial x^2} + \nu \frac{\partial^2 w}{\partial y^2} = \sum_{i=1}^{n_x+4} \sum_{j=1}^{n_y+4} \left[ B_i''(x)B_j(y) + \nu B_i(x)B_j''(y) \right] a_{ij} = 0 \tag{2.4.23a}$$

$$\frac{\partial^3 w}{\partial x^3} + (2-\nu)\frac{\partial^3 w}{\partial x \partial y^2} = \sum_{i=1}^{n_x+4} \sum_{j=1}^{n_y+4} \left[ B_i'''(x)B_j(y) + (2-\nu)B_i'(x)B_j''(y) \right] a_{ij} = 0 \tag{2.4.23b}$$

Clamped boundary conditions at edge $y = 0$ or $b$:

$$w = \sum_{i=1}^{n_x+4} \sum_{j=1}^{n_y+4} B_i(x)B_j(y)a_{ij} = 0 , \tag{2.4.24a}$$

$$\frac{\partial w}{\partial y} = \sum_{i=1}^{n_x+4} \sum_{j=1}^{n_y+4} B_i(x)B_j'(y)a_{ij} = 0 \tag{2.4.24b}$$

Simply supported conditions at edge $y = 0$ or $b$:

$$w = \sum_{i=1}^{n_x+4} \sum_{j=1}^{n_y+4} B_i(x)B_j(y)a_{ij} = 0 \qquad (2.4.25a)$$

$$\frac{\partial^2 w}{\partial y^2} + \nu \frac{\partial^2 w}{\partial x^2} = \sum_{i=1}^{n_x+4} \sum_{j=1}^{n_y+4} \left[ B_i(x)B_j''(y) + \nu B_i''(x)B_j(y) \right] a_{ij} = 0 \qquad (2.4.25b)$$

Free boundary conditions at edge $y = 0$ or $b$:

$$\frac{\partial^2 w}{\partial y^2} + \nu \frac{\partial^2 w}{\partial x^2} = \sum_{i=1}^{n_x+4} \sum_{j=1}^{n_y+4} \left[ B_i(x)B_j''(y) + \nu B_i''(x)B_j(y) \right] a_{ij} = 0 \qquad (2.4.26a)$$

$$\frac{\partial^3 w}{\partial y^3} + (2-\nu)\frac{\partial^3 w}{\partial^2 x \partial y} = \sum_{i=1}^{n_x+4} \sum_{j=1}^{n_y+4} \left[ B_i(x)B_j'''(y) + (2-\nu)B_i''(x)B_j'(y) \right] a_{ij} = 0 \qquad (2.4.26b)$$

Boundary conditions of a corner point of a rectangular plate with both neighboring edges clamped:

$$w = \sum_{i=1}^{n_x+4} \sum_{j=1}^{n_y+4} B_i(x)B_j(y)a_{ij} = 0 \qquad (2.4.27a)$$

$$\frac{\partial w}{\partial x} = \sum_{i=1}^{n_x+4} \sum_{j=1}^{n_y+4} B_i'(x)B_j(y)a_{ij} = 0 \qquad (2.4.27b)$$

$$\frac{\partial w}{\partial y} = \sum_{i=1}^{n_x+4} \sum_{j=1}^{n_y+4} B_i(x)B_j'(y)a_{ij} = 0 \qquad (2.4.27c)$$

Boundary conditions of a corner point of a rectangular plate with both neighboring edges simply supported:

$$w = \sum_{i=1}^{n_x+4} \sum_{j=1}^{n_y+4} B_i(x)B_j(y)a_{ij} = 0 \qquad (2.4.28a)$$

$$\frac{\partial^2 w}{\partial x^2} = \sum_{i=1}^{n_x+4} \sum_{j=1}^{n_y+4} B_i''(x)B_j(y)a_{ij} = 0 \qquad (2.4.28b)$$

$$\frac{\partial^2 w}{\partial y^2} = \sum_{i=1}^{n_x+4} \sum_{j=1}^{n_y+4} B_i(x)B_j''(y)a_{ij} = 0 \qquad (2.4.28c)$$

Boundary conditions of a corner point of a rectangular plate with both

neighboring edges free:

$$\frac{\partial^2 w}{\partial x \partial y} = \sum_{i=1}^{n_x+4} \sum_{j=1}^{n_y+4} B_i'(x)B_j'(y)a_{ij} = 0 \tag{2.4.29a}$$

$$\frac{\partial^2 w}{\partial x^2} + \nu \frac{\partial^2 w}{\partial y^2} = \sum_{i=1}^{n_x+4} \sum_{j=1}^{n_y+4} \left[ B_i''(x)B_j(y) + \nu B_i(x)B_j''(y) \right] a_{ij} = 0 \tag{2.4.29b}$$

$$\frac{\partial^2 w}{\partial y^2} + \nu \frac{\partial^2 w}{\partial x^2} = \sum_{i=1}^{n_x+4} \sum_{j=1}^{n_y+4} \left[ B_i(x)B_j''(y) + \nu B_i''(x)B_j(y) \right] a_{ij} = 0 \tag{2.4.29c}$$

Boundary conditions of two associated corner points, $(x,y) = (0,0),(0,b)$ or $(x,y) = (a,0),(a,b)$, and simply supported edge at $x = 0$ or $a$:

$$w = \sum_{i=1}^{n_x+4} \sum_{j=1}^{n_y+4} B_i(x)B_j(y)a_{ij} = 0 \tag{2.4.30a}$$

$$\frac{\partial^2 w}{\partial x^2} = \sum_{i=1}^{n_x+4} \sum_{j=1}^{n_y+4} B_i''(x)B_j(y)a_{ij} = 0 \tag{2.4.30b}$$

$$\frac{\partial w}{\partial y} = \sum_{i=1}^{n_x+4} \sum_{j=1}^{n_y+4} B_i(x)B_j'(y)a_{ij} = 0 \tag{2.4.30c}$$

Boundary conditions of two associated corner points, $(x,y) = (0,0),(a,0)$ or $(x,y) = (0,b),(a,b)$, and simply-supported edge at $y = 0$ or $b$:

$$w = \sum_{i=1}^{n_x+4} \sum_{j=1}^{n_y+4} B_i(x)B_j(y)a_{ij} = 0 \tag{2.4.31a}$$

$$\frac{\partial w}{\partial x} = \sum_{i=1}^{n_x+4} \sum_{j=1}^{n_y+4} B_i'(x)B_j(y)a_{ij} = 0 \tag{2.4.31b}$$

$$\frac{\partial^2 w}{\partial y^2} = \sum_{i=1}^{n_x+4} \sum_{j=1}^{n_y+4} B_i(x)B_j''(y)a_{ij} = 0 \tag{2.4.31c}$$

By substituting the coordinates of the all inner knots with a total number of $n_x n_y$ into the field equation in Eq. (2.4.20), and those of the boundary knots with a total number of $4(n_x + n_y) - 4$ into the boundary conditions in Eq. (2.4.21) to Eq. (2.4.31),

then a well defined linear system of ordinary differential equations in the matrix form $\mathbf{Ax} = \lambda \mathbf{Bx}$ can be obtained, which is referred to as the eigen-value problem. More details will be given below.

From the field equation in Eq. (2.4.20), the following can be derived:

$$\mathbf{B}_{db}\mathbf{a}_b + \mathbf{B}_{dd}\mathbf{a}_d = \left[ N_x(\mathbf{B}_{N_x})_{db} + N_y(\mathbf{B}_{N_y})_{db} + N_{xy}(\mathbf{B}_{N_{xy}})_{db} \right]\mathbf{a}_b$$
$$+ \left[ N_x(\mathbf{B}_{N_x})_{dd} + N_y(\mathbf{B}_{N_y})_{dd} + N_{xy}(\mathbf{B}_{N_{xy}})_{dd} \right]\mathbf{a}_d \quad , \qquad (2.4.32)$$

where $\mathbf{a}_b$ and $\mathbf{a}_d$ are column vectors of the undetermined coefficients matrix $[a_{ij}] = \{\mathbf{a}_b \quad \mathbf{a}_d\}^T$, with subscripts b and d denoting the fictitious knots and all inner knots, respectively.

Also, from the boundary conditions in Eq. (2.4.21) to Eq.(2.4.31), the following can be derived:

$$\mathbf{B}_{bb}\mathbf{a}_b + \mathbf{B}_{bd}\mathbf{a}_d = \mathbf{0} \qquad (2.4.33)$$

where the first 12 equations are obtained from Eq. (2.4.27) to Eq. (2.4.31), and the remaining $4\left[(n_x - 2) + (n_y - 2)\right]$ equations from Eq. (2.4.21) to Eq. (2.4.26). It can be seen that Eqs. (2.4.32) and (2.4.33) form a simultaneous matrix equation with unknown matrices $\mathbf{a}_b$ and $\mathbf{a}_d$.

From Eq. (2.4.33), the following can be solved:

$$\mathbf{a}_b = -\mathbf{B}_{bb}^{-1}\mathbf{B}_{bd}\mathbf{a}_d . \qquad (2.4.34)$$

Substituting Eq. (2.4.34) into Eq. (2.4.32) yields a generalized eigen-value problem $\mathbf{Ax} = \lambda \mathbf{Bx}$ as follows:

$$\overline{\mathbf{B}}\mathbf{a}_d = N_{xy}\overline{\mathbf{B}}_{N_{xy}}\mathbf{a}_d . \qquad (2.4.35)$$

where $N_{xy}$, $\mathbf{a}_d$ are the required eigen-values and eigen-vectors, respectively. The $\overline{\mathbf{B}}$ and $\overline{\mathbf{B}}_{N_{xy}}$ matrices are defined as

$$\overline{\mathbf{B}} = -\left[ \mathbf{B}_{db} - N_x (\mathbf{B}_{N_x})_{db} - N_y (\mathbf{B}_{N_y})_{db} \right] \mathbf{B}_{bb}^{-1} \mathbf{B}_{bd}$$
$$+ \left[ \mathbf{B}_{dd} - N_x (\mathbf{B}_{N_x})_{dd} - N_y (\mathbf{B}_{N_y})_{dd} \right], \tag{2.4.36a}$$

$$\overline{\mathbf{B}}_{N_{xy}} = -(\mathbf{B}_{N_{xy}})_{db} \mathbf{B}_{bb}^{-1} \mathbf{B}_{bd} + (\mathbf{B}_{N_{xy}})_{dd}. \tag{2.4.36b}$$

Consequently, the eigen-values $N_{xy}$ and eigen-vectors $\mathbf{a}_d$, can be determined by solving the eigen-value problem in Eq. (2.4.35) for given matrices $\overline{\mathbf{B}}$ and $\overline{\mathbf{B}}_{N_{xy}}$. The value $N_{xy}$ is exactly the shear buckling load of the thin plate. Then, $\mathbf{a}_b$ can be determined from Eq. (2.4.34). Finally, the shear buckling mode shapes can be obtained by Eq. (2.4.16), where it is noted that $[a_{ij}] = \{\mathbf{a}_b \quad \mathbf{a}_d\}^T$.

## 2.4.4 Numerical Results

### 2.4.4.1 Definition of Parameters

The stability of rectangular thin plates with different in-plane loads are studied here using the extended SCM. In the following numerical examples, Poisson's ratio $\nu$ is taken as 0.3, the plate aspect ratio $\gamma$, the ratio of applied force to buckling load $\alpha$, and dimensionless critical shear buckling load $P_{xy}$ are defined as

$$\gamma = \frac{a}{b} \tag{2.4.37}$$

$$\alpha = \frac{N_x}{N_{cr,x}} \text{ or } \alpha = \frac{N_y}{N_{cr,y}} \tag{2.4.38}$$

$$P_{xy} = \frac{N_{xy}\pi^2}{Db^2} \tag{2.4.39}$$

where $N_{cr,x}$ and $N_{cr,y}$ indicate that the critical buckling loads of the plate with the same boundary conditions due to the compressive loading in the $x$- and $y$-direction, respectively; $N_{cr,xy}$ indicates the critical shear buckling load of the plate with the same boundary conditions, but due to pure shear loads $N_{xy}$ ($N_x = N_y = 0$).

### 2.4.4.2 Convergence Study

The convergence characteristics of the dimensionless critical shear buckling loads $P_{xy}$ of the square plates ($\gamma = 1$) for five types of boundary conditions, CCCC, CSCS, SSSS, CCFF, and CFCF, are shown in Table 2.4.1. Clearly, the convergence characteristics by SCM are very good. In addition, one observes that using $60 \times 60$ inner knots are enough to obtain stable and accurate results.

**Table 2.4.1 Convergence of the dimensionless shear buckling load $P_{xy}$.**

| Inner knots $(n_x \times n_y)$ | CCCC | CSCS | SSSS | CCFF | CFCF |
|---|---|---|---|---|---|
| $10 \times 10$ | 14.9513 | 11.9370 | 9.4852 | 7.5744 | 0.6340 |
| $20 \times 20$ | 14.6866 | 11.7731 | 9.3647 | 7.5385 | 0.6328 |
| $30 \times 30$ | 14.6774 | 11.7437 | 9.3423 | 7.5104 | 0.6319 |
| $40 \times 40$ | 14.6620 | 11.7331 | 9.3345 | 7.4994 | 0.6308 |
| $50 \times 50$ | 14.6548 | 11.7282 | 9.3309 | 7.4952 | 0.6303 |
| $60 \times 60$ | 14.6509 | 11.7256 | 9.3290 | 7.4922 | 0.6300 |

### 2.4.4.3 Uni-directional Forces Acting on a Plate

A SSSS plate subjected to constant uniform uni-directional compressive/tensile forces $N_x$ in the $x$-direction and shear force $N_{xy}$ is shown in Figure 2.4.3. The magnitude of the applied constant uniform force $N_x$ is taken as $\alpha N_{cr,x}$, where $N_{cr,xy}$ is the critical shear buckling force of the plate. Based on Eq. (2.4.35) and Eq. (2.4.36), one can find the solution of the eigen-value $N_{xy}$ and eigen-vector $\mathbf{a}$ for the case with $N_y = 0$. Consequently, the uni-directional compressive/tensile forces $N_x$ acting on a plate can be solved. In Table 2.4.2, the dimensionless critical shear buckling loads $P_{xy}$ for the SSSS plates are presented and compared with existing ones for several aspect ratios $\gamma (= 1.0, 1.2, 1.4, 2.0, 4.0)$, and load factors $\alpha (= 0.0, \pm 0.5)$. The values of $P_{xy}$ solved by the SCM are slightly lower than the others, except the one by EKM.
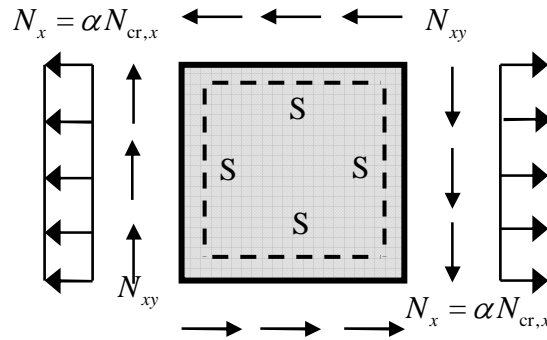
**Figure 2.4.3 Square plates with uni-directional in-plane loading for SSSS.**

**Table 2.4.2 Dimensionless critical shear buckling loads $P_{xy}$ for SSSS plates.**

| $\gamma(=a/b)$ | 1.0 | 1.2 | 1.4 | 2.0 | 1.0 | 1.0 | 2.0 | 2.0 | 4.0 | 4.0 |
|---|---|---|---|---|---|---|---|---|---|---|
| $\alpha(=N_x/N_{cr,x})$ | 0.0 | 0.0 | 0.0 | 0.0 | -0.5 | 0.5 | -0.5 | 0.5 | -0.5 | 0.5 |
| * | 9.40 | 8.40 | 7.30 | 6.60 | — | — | — | — | 4.63 | 7.75 |
| ** | 9.35 | 8.00 | — | 6.59 | — | — | — | — | — | — |
| *** | — | — | — | — | 6.62 | 11.56 | 4.66 | 7.89 | 4.10 | — |
| EKM | 9.32 | 7.98 | 7.29 | 6.55 | 6.59 | 11.56 | 4.63 | 7.78 | 4.07 | 6.88 |
| SCM | 9.33 | 7.99 | 7.29 | 6.55 | 6.58 | 11.50 | 4.62 | 7.79 | 4.07 | 6.89 |

*Column Research Committee of Japan, 1971; **Stein and Neff, 1947
*** Batdorf and Stein, 1947

Similarly, a CCCC plate subjected to constant uniform uni-directional compressive/tensile forces $N_x$ in the $x$-direction and shear force $N_{xy}$ is shown in Figure 2.4.4. Table 2.4.3 shows the dimensionless critical shear buckling loads $P_{xy}$ for the CCCC plates with constant uniform forces $N_x(=\alpha N_{cr,x})$ in the $x$-direction. As can be seen, the $P_{xy}$ values approach to each other for the SCM and EKM solutions in most cases.
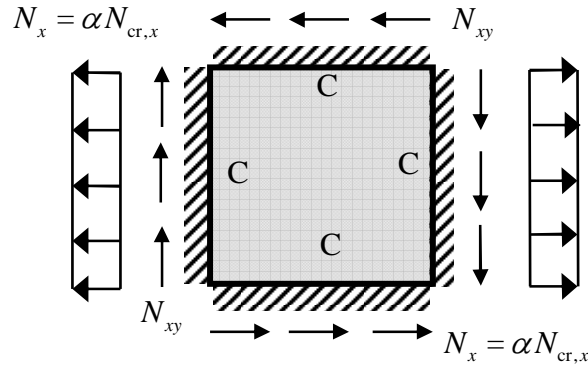
**Figure 2.4.4 Square plates with uni-directional in-plane loading for CCCC.**

**Table 2.4.3 Dimensionless critical shear buckling loads $P_{xy}$ for CCCC plates.**

| $\alpha(=N_x/N_{cr,x})$ | $\alpha = 0.5$ | | $\alpha = 0.0$ | | $\alpha = -0.5$ | |
|---|---|---|---|---|---|---|
| $\gamma(=a/b)$ | SCM | EKM | SCM | EKM | SCM | EKM |
| 2.0 | 12.74 | 12.71 | 10.26 | 10.25 | 7.23 | 7.22 |
| 3.0 | 11.75 | 11.71 | 9.55 | 9.53 | 6.80 | 6.78 |
| 4.0 | 11.42 | 11.39 | 9.32 | 9.30 | 6.58 | 6.56 |
| 6.0 | 11.19 | 11.16 | 9.14 | 9.12 | 6.47 | 6.46 |
| 10.0 | 11.09 | 11.06 | 9.06 | 9.03 | 6.41 | 6.39 |

Comparisons with results by the other methods are given in Table 2.4.4 for the plates with four types of boundary conditions, SSSS, CCCC, CCSF, and CCFF, and several aspect ratios $\gamma$ $(=1.0 \sim 2.0)$. Here one can see that except for the EKM results, the solutions given by SCM for the dimensionless critical shear buckling loads $P_{xy}$ are slightly lower than the other ones. Evidently, the results obtained by the, SCM are quite accurate.

**Table 2.4.4 Dimensionless pure critical shear buckling load** $P_{xy}$ **for plates with various boundary conditions.**

|  | $\gamma(=a/b)$ | SCM | EKM | FEM | EKM | Timoshenko |
|---|---|---|---|---|---|---|
| SSSS | 1.0 | 9.3290 | 9.3245 | 9.3250 | 9.3257 | 9.3400 |
|  | 1.5 | 7.0763 | 7.0700 | 7.0700 | — | 7.1000 |
|  | 2.0 | 6.5531 | 6.5460 | 6.5460 | — | 6.6000 |
|  | 3.0 | 5.8479 | 5.8402 | 5.8400 | — | 5.9000 |
| CCCC | 1.0 | 14.6509 | 14.6420 | 14.6400 | 14.6428 | 14.7100 |
|  | 1.5 | 11.4722 | 11.4583 | 11.4600 | — | 11.5000 |
|  | 2.0 | 10.2604 | 10.2480 | 10.2500 | — | 10.3400 |
| CCSF | 1.0 | 8.4402 | 8.4289 | 8.4330 | — | — |
|  | 2.0 | 2.3678 | 2.3501 | 2.3510 | — | — |
| CCFF | 1.0 | 7.5002 | 7.4869 | 7.4920 | — | — |
|  | 2.0 | 2.7827 | 1.7703 | 1.7720 | — | — |

## 2.4.4.4 Aspect Ratio Effects of Thin Plates

The variations of the dimensionless critical shear buckling loads $P_{xy}$ for three aspect ratios ($\gamma = 1.0, 2.0, 4.0$) of a SSSS plate are shown in Table 2.4.5 and Figure 2.4.5. Note that all the dimensionless critical shear buckling loads $P_{xy} = P_{xy}(\alpha) = P_{xy\alpha}$ are normalized with respect to the one for pure shear loading only, i.e., $P_{xy0}$. The results of analyses indicate that the larger the aspect ratio $\gamma$ is, the smaller the dimensionless critical shear buckling load $P_{xy}$. One can also see that for three plate aspect ratios ($\gamma = 1.0, 2.0, 4.0$), the same behaviors can be observed, namely, a nearly linear relation exists in the range $-0.4 < \alpha \le 1.0$, and a sharp drop occurs as the compressive force $N_x (= \alpha N_{cr,x})$ in the $x$-direction approaches the critical buckling load $N_{cr,x}$ (i.e. $\alpha \to -1.0$).

**Table 2.4.5 Dimensionless critical shear loading $P_{xy}$ for three aspect ratios $\gamma$.**

| $\alpha(= N_x/N_{cr,x})$ | SSSS plates | | |
|:---:|:---:|:---:|:---:|
| | $\gamma = 1.0$ | $\gamma = 2.0$ | $\gamma = 4.0$ |
| 1.0 | 22.071 | 14.889 | 13.239 |
| 0.8 | 20.713 | 14.051 | 12.545 |
| 0.6 | 19.303 | 13.177 | 11.813 |
| 0.4 | 17.833 | 12.260 | 11.039 |
| 0.2 | 16.289 | 11.293 | 10.215 |
| 0.0 | 14.655 | 10.261 | 9.326 |
| -0.2 | 12.901 | 9.144 | 8.350 |
| -0.4 | 10.980 | 7.907 | 7.219 |
| -0.6 | 8.795 | 6.483 | 5.883 |
| -0.8 | 6.088 | 4.703 | 4.162 |
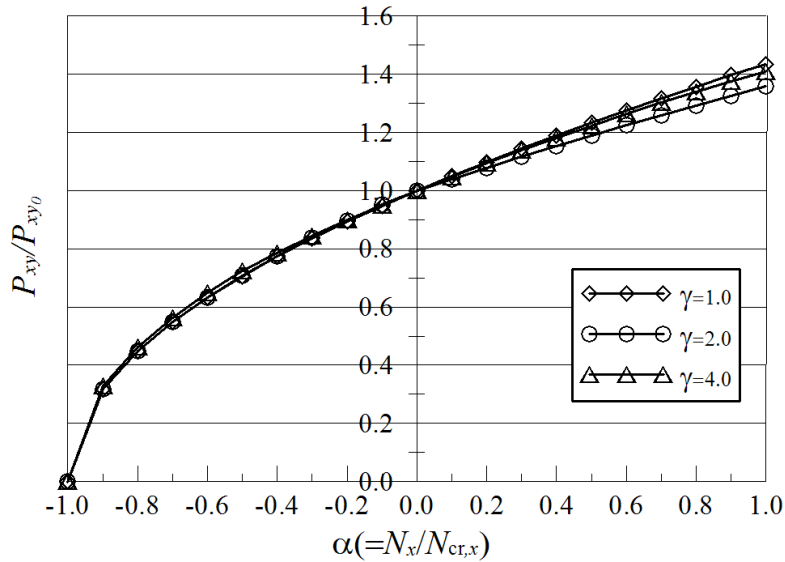


**Figure 2.4.5 Normalized dimensionless critical shear loadings versus different $\alpha$ for three plate aspect ratios $\gamma$.**

The critical buckling modes of SSSS plates for five constant uniform uni-directional loads $N_x (= \alpha N_{cr,x})$, $\alpha = 1.0, 0.5, 0.0, -0.5, -1.0$, and three aspect ratios $(\gamma = 1.0, 2.0, 4.0)$ are shown in Figure 2.4.6. It is seen that as the force changes from tension to compression, the number of waves in the shape increases.
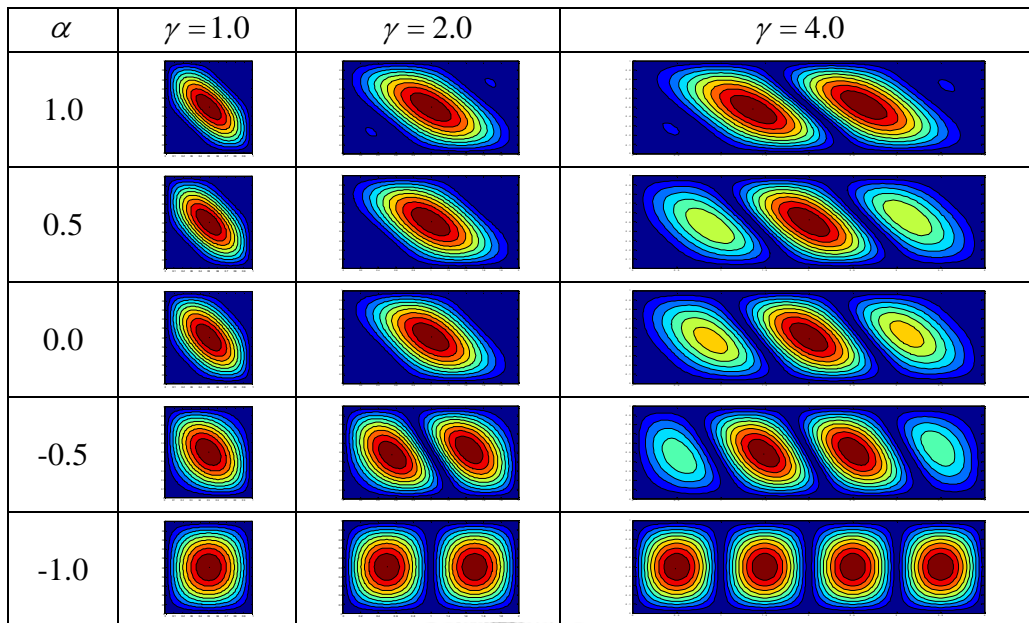
| $\alpha$ | $\gamma = 1.0$ | $\gamma = 2.0$ | $\gamma = 4.0$ |
|---|---|---|---|
| 1.0 | | | |
| 0.5 | | | |
| 0.0 | | | |
| -0.5 | | | |
| -1.0 | | | |

**Figure 2.4.6 Critical buckling modes for SSSS plates with variable uni-directional loading.**

For a CCCC plate, the variations of the constant uniform uni-directional loading $N_x (= \alpha N_{cr,x})$ of the thin plates for three aspect ratios ($\gamma = 1.0, 2.0, 4.0$) are shown in Table 2.4.6 and Figure 2.4.7.

**Table 2.4.6 Dimensionless critical shear loading $P_{xy}$ for three aspect ratios $\gamma$.**

| | CCCC plates | | |
|---|---|---|---|
| $\alpha (= N_x / N_{cr,x})$ | $\gamma = 1.0$ | $\gamma = 2.0$ | $\gamma = 4.0$ |
| 1.0 | 13.389 | 8.913 | 7.948 |
| 0.8 | 12.659 | 8.476 | 7.555 |
| 0.6 | 11.896 | 8.025 | 7.125 |
| 0.4 | 11.095 | 7.557 | 6.661 |
| 0.2 | 10.244 | 7.069 | 6.168 |
| 0.0 | 9.331 | 6.556 | 5.640 |
| -0.2 | 8.333 | 5.873 | 5.066 |
| -0.4 | 7.212 | 5.078 | 4.429 |
| -0.6 | 5.893 | 4.145 | 3.656 |
| -0.8 | 4.177 | 2.937 | 2.603 |
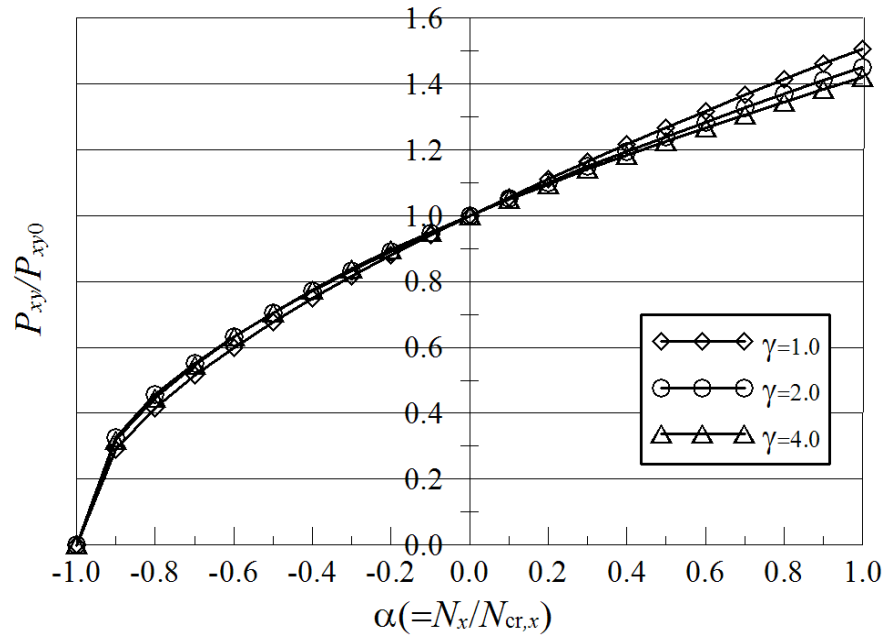
**Figure 2.4.7 Normalized dimensionless critical shear loadings versus different** $\alpha$
**for three plate aspect ratios** $\gamma$ .

The critical buckling modes of CCCC plates for five constant uniform uni-directional loads $N_x (= \alpha N_{cr,x})$ , $\alpha = 1.0, 0.5, 0.0, -0.5, -1.0$ , and aspect ratios $(\gamma = 1.0, 2.0, 4.0)$ are shown in Figure 2.4.8. As for the CCCC plate, it is seen that as the force changes from tension to compression, the number of waves in the shape increases. The variation of the critical shear forces is similar to that of the simply supported plates, which need not be repeated here.

| $\alpha$ | $\gamma = 1.0$ | $\gamma = 2.0$ | $\gamma = 4.0$ |
|:---:|:---:|:---:|:---:|
| 1.0 | | | |
| 0.5 | | | |
| 0.0 | | | |
| -0.5 | | | |
| -1.0 | | | |
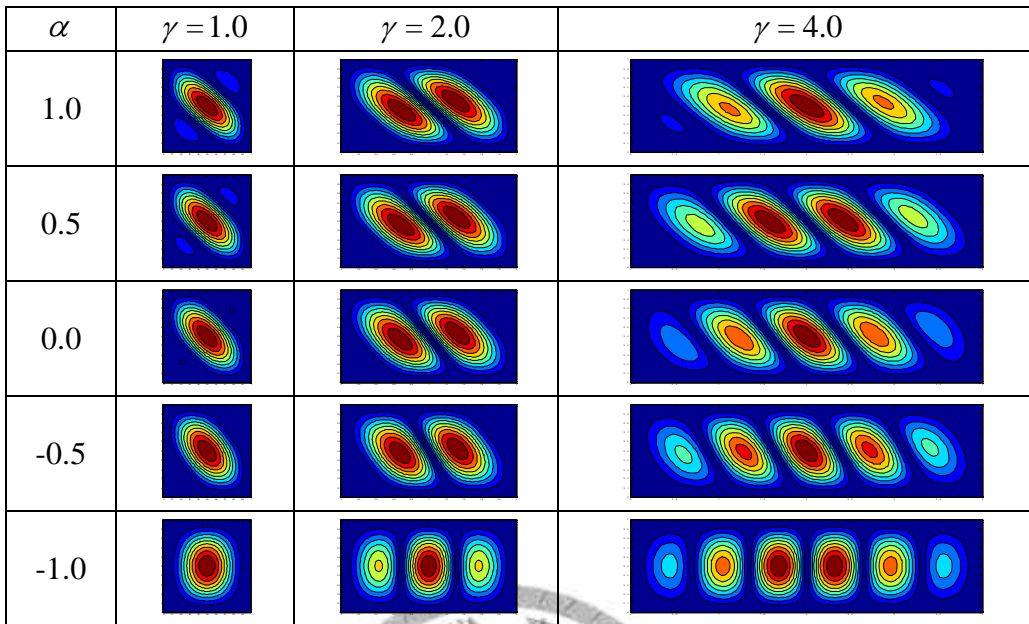
**Figure 2.4.8 Critical buckling modes for CCCC plates with variable uni-directional loading.**

Square plates ($\gamma = 1.0$) with four combinations of boundary conditions, CFCF, CSCS, FFCC, and FFFC, are also solved by SCM (see Figures 2.4.9). In Table 2.4.7, the results for the dimensionless critical shear loadings $P_{xy}$ of the square plate with different levels of constant uniform compressive/tensile loadings $N_x (= \alpha N_{cr,x})$ are presented. It is sufficient to mention that the dimensionless critical shear buckling loads determined by the SCM are very close to the EKM results.



50
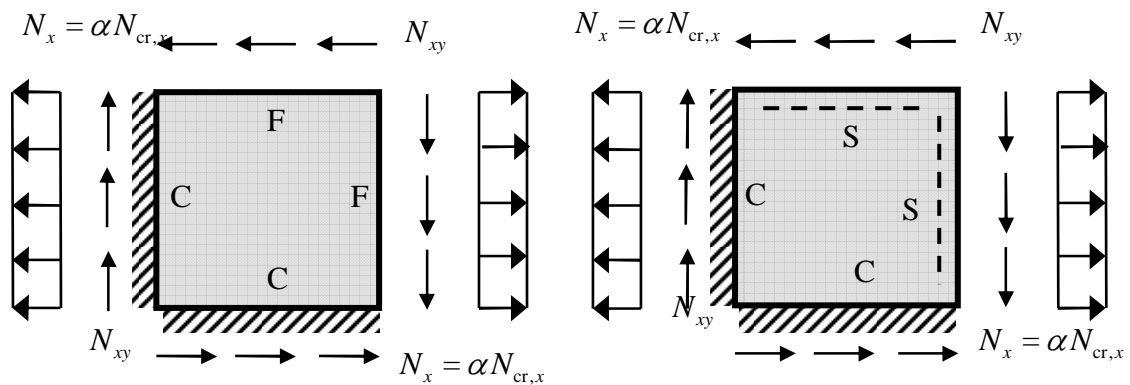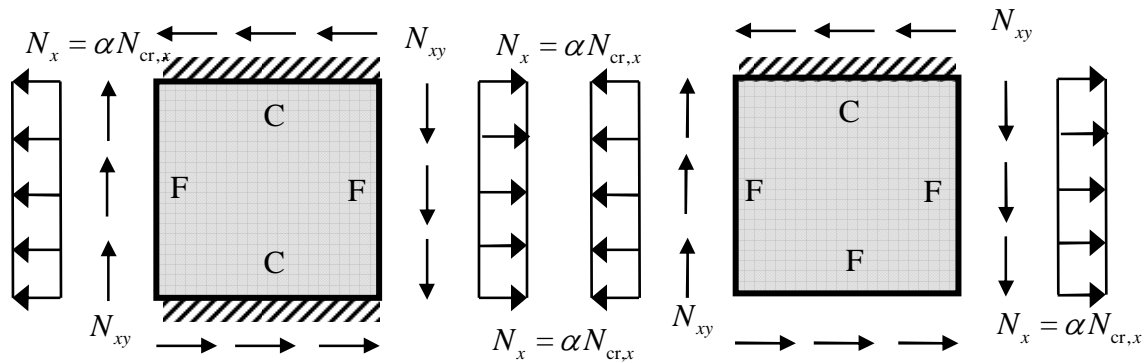
**Figure 2.4.9 Square plates with uni-directional in-plane loading and with different boundary conditions.**

**Table 2.4.7 Dimensionless critical shear buckling loads** $P_{xy}$ **for square plates.**

| $\alpha$ | CFCF | | CSCS | | FFCC | | FFFC | |
|---|---|---|---|---|---|---|---|---|
| $(= N_x / N_{cr,x})$ | SCM | EKM | SCM | EKM | SCM | EKM | SCM | EKM |
| 1.0 | 1.1145 | 1.1023 | 17.1201 | 17.1015 | 9.8283 | 9.8184 | 0.5528 | 0.5561 |
| 0.8 | 1.0133 | 1.0143 | 16.1310 | 16.1257 | 9.3915 | 9.3848 | 0.5283 | 0.5275 |
| 0.6 | 0.9282 | 0.9235 | 15.1238 | 15.1095 | 8.9528 | 8.9382 | 0.4985 | 0.4973 |
| 0.4 | 0.8315 | 0.8295 | 14.1613 | 14.0450 | 8.4923 | 8.4765 | 0.4679 | 0.4652 |
| 0.2 | 0.7346 | 0.7318 | 12.9414 | 12.9207 | 8.0101 | 7.9964 | 0.4382 | 0.4307 |
| 0.0 | 0.6308 | 0.6298 | 11.7256 | 11.7197 | 7.5083 | 7.4927 | 0.3969 | 0.3932 |
| -0.2 | 0.5238 | 0.5226 | 10.4322 | 10.4146 | 6.5639 | 6.9566 | 0.3583 | 0.3517 |
| -0.4 | 0.4093 | 0.4087 | 8.9723 | 8.9579 | 6.3901 | 6.3712 | 0.3081 | 0.3045 |
| -0.6 | 0.2894 | 0.2866 | 7.2688 | 7.2532 | 5.7205 | 5.7005 | 0.2498 | 0.2486 |
| -0.8 | 0.1573 | 0.1520 | 5.0618 | 5.0478 | 4.3914 | 4.3726 | 0.1738 | 0.1758 |
| -1.0 | 0.0801 | 0.0794 | 3.5006 | 3.4885 | 3.1419 | 3.1298 | 0.1282 | 0.1243 |

## 2.4.4.5 Bi-directional Forces Acting on a Plate

Thin plates with two types of boundary conditions SSSS/CCCC subjected to constant uniform bi-directional compressive/tensile forces $N_x$, $N_y$, and shear force $N_{xy}$ are shown in Figure 2.4.10.

The values of the dimensionless critical shear buckling loads of the SSSS and CCCC plate with variable bi-directional loads $N_x (= \alpha N_{cr,x}) / N_y (= \alpha N_{cr,y})$ and three aspect ratios $(\gamma = 1.0, 2.0, 4.0)$ obtained by the SCM are listed sin Table 2.4.8 and Table 2.4.9, respectively. We like to point out that the critical shear buckling loads obtained by the SCM are very close to that by the EKM.
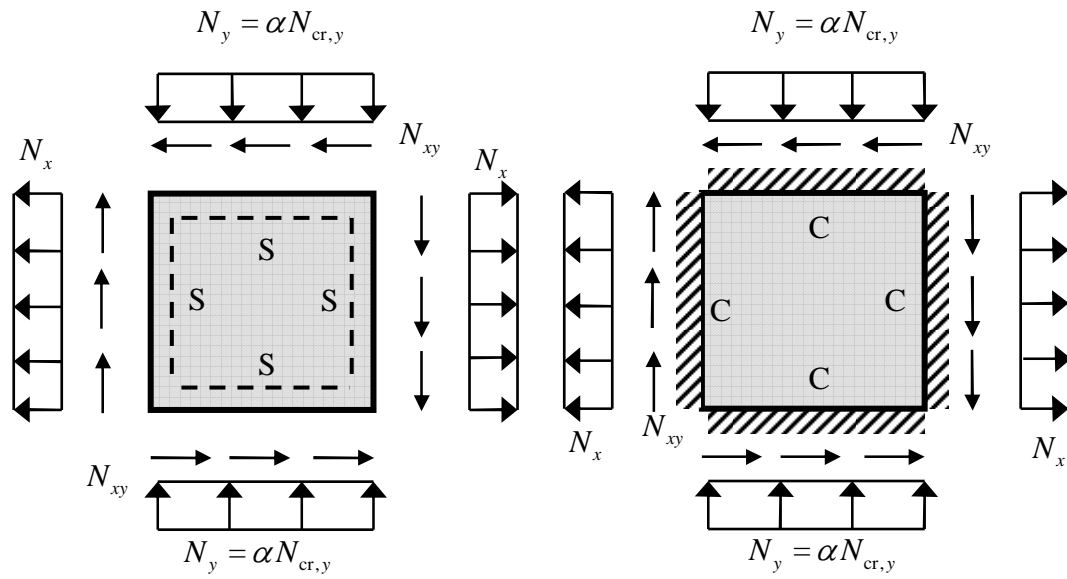
**Figure 2.4.10 Plates with bi-directional in-plane loads.**

**Table 2.4.8 Dimensionless critical shear buckling loads $P_{xy}$ for SSSS plates.**

| $\gamma = a/b$ | | 1.0 | 2.0 | 4.0 | 1.0 | 2.0 | 4.0 |
|---|---|---|---|---|---|---|---|
| $N_{cr,xy}$ (pure shear) | | 92.031 | 64.607 | 55.512 | 92.031 | 64.607 | 55.512 |
| $N_x/\pi^2$ | | -2.000 | -2.000 | -2.000 | 2.000 | 2.000 | 2.000 |
| $N_{cr,y}/\pi^2$ | | 2.000 | 1.063 | 1.004 | 6.000 | 2.063 | 1.254 |
| | 1.00 | 9.309 | 5.979 | 5.318 | 16.811 | 10.193 | 8.465 |
| | 0.75 | 8.704 | 5.661 | 5.027 | 15.595 | 9.697 | 8.099 |
| | 0.50 | 8.058 | 5.332 | 4.725 | 14.317 | 9.188 | 7.716 |
| | 0.25 | 7.358 | 4.990 | 4.410 | 12.961 | 8.572 | 7.316 |
| $\alpha(=\dfrac{N_y}{N_{cr,y}})$ | 0.00 | 6.585 | 4.633 | 4.079 | 11.501 | 7.790 | 6.896 |
| | -0.25 | 5.709 | 4.260 | 3.647 | 9.892 | 6.859 | 6.405 |
| | -0.50 | 4.670 | 3.865 | 3.157 | 8.041 | 5.697 | 5.799 |
| | -0.75 | 3.311 | 2.871 | 2.583 | 5.688 | 4.099 | 4.918 |

**Table 2.4.9 Dimensionless critical shear buckling loads $P_{xy}$ for CCCC plates.**

| $\gamma(=a/b)$ | | 1.0 | 2.0 | 4.0 | 1.0 | 2.0 | 4.0 |
|---|---|---|---|---|---|---|---|
| $N_{cr,xy}$ (pure shear) | | 144.513 | 101.145 | 91.740 | 144.513 | 101.145 | 91.740 |
| $N_x/\pi^2$ | | -5.037 | -3.934 | -3.604 | 5.037 | 3.934 | 3.604 |
| $N_{cr,y}/\pi^2$ | | 5.569 | 3.921 | 3.891 | 12.772 | 5.656 | 4.338 |
| | 1.00 | 14.628 | 10.344 | 9.602 | 27.641 | 17.383 | 15.127 |
| | 0.75 | 13.558 | 9.673 | 8.916 | 25.546 | 16.299 | 14.282 |
| | 0.50 | 12.430 | 8.946 | 8.180 | 23.352 | 15.150 | 13.392 |
| $\alpha(=\dfrac{N_y}{N_{cr,y}})$ | 0.25 | 11.230 | 8.115 | 7.404 | 21.039 | 13.964 | 12.438 |
| | 0.00 | 9.934 | 7.227 | 6.585 | 18.574 | 12.723 | 11.431 |
| | -0.25 | 8.504 | 6.268 | 5.708 | 15.901 | 11.382 | 10.351 |
| | -0.50 | 6.858 | 5.215 | 4.674 | 12.915 | 9.433 | 9.087 |
| | -0.75 | 4.790 | 4.019 | 3.430 | 9.353 | 6.748 | 7.582 |

## 2.4.5 Nomenclature

$\mathbf{a}_b, \mathbf{a}_d$          column vectors of the undetermined coefficients matrix

$a_{ij}$          coefficients to be determined

$B_i(x), B_j(y)$          quintic spline functions

$D = \dfrac{Et^3}{12(1-v^2)}$          flexural rigidity

$E$          Young's modulus

$h_x$          equal-space in the $x$ directions

$h_y$          equal-space in the $y$ directions

$n_x$          inner knots in the $x$ directions

$n_y$          inner knots in the $y$ directions

$P_{xy}$          dimensionless critical shear buckling load

$t$          thickness of the plate

$N_{cr,xy}$          critical shear buckling load of the plate

$N_x$ in-plane normal forces in the $x$ directions

$N_y$ in-plane normal forces in the $y$ directions

$N_{xy}$ shear force

$w(x, y)$ elastic lateral buckling displacement

$\alpha = \dfrac{N_x}{N_{cr,x}}$ , $\alpha = \dfrac{N_y}{N_{cr,y}}$ ratio of applied force to buckling load

$\gamma = \dfrac{a}{b}$ plate aspect ratio

$\nu$ Poisson's ratio

## 2.5 Buckling Analysis of Rectangular Thin Plates

### 2.5.1 Introduction

The buckling problem of a thin rectangular elastic plate subjected to in-plane compressive and/or shear loading is important in the aircraft and automotive industries. Bert and Devarakonda (2003) gave a brief historical review recently on this subject . As is noticed that there have been very few previous solutions for the case of nonlinearly distributed edge loadings. The possible reason is perhaps due to the additional complexity of having to first solve a problem in plane-stress elasticity for obtaining the in-plane stress distributions, then to solve the buckling problem. The first work in this field was due to van der Neut (1958). A uniaxial compressive loading with a half-sine distribution was considered. Later, Benoy (1969) considered a uniaxial compressive loading with a parabolic distribution and obtained a solution by using the energy method. It is pointed out, however, that both works suffered several serious deficiencies (Bert and Devarakonda, 2003). Recently, Bert and Devarakonda (2003) presented an analytical solution for in-plane stresses for the case of a half-sine load distribution on two opposite sides. As can be seen that the in-plane stress distributions are more realistic, showing a decrease (diffusion) in axial stress as the distance from the loaded edges is increased. The buckling loads are then calculated using Galerkin method. Much more accurate buckling load is obtained for a rectangular plate simply supported along all edges. Xinwei (2006) used differential quadrature method (DQM) to analysis buckling loads of thin rectangular plates under non-uniform distributed in-plane loadings. It indicates that the DQM can be employed for obtaining buckling loads of plates with other combinations of boundary conditions subjected to non-uniform distributed loadings.

SCM is used herein for the first time for buckling analysis of thin rectangular

plates subjected to non- uniform distributed in-plane loadings. Formulations and procedures are worked out in detail and two non-uniform in-plane loading cases are studied. SCM results are well compared with existing analytical solutions DQM and finite element method (FEM). Some conclusions are drawn based on the results presented herein.

## 2.5.2 Formulation

Consider a problem of in-plane elasticity, an isotropic rectangular thin plate with length $a$ and width $b$ subjected to a uniaxial non-uniform distributed in-plane edge load as shown in Figure 2.5.1.



(a) $\sigma_x = -\sigma_0(1 - 2y/3)$



(b) $\sigma_x = -\sigma_0 \cos(\pi y/b)$
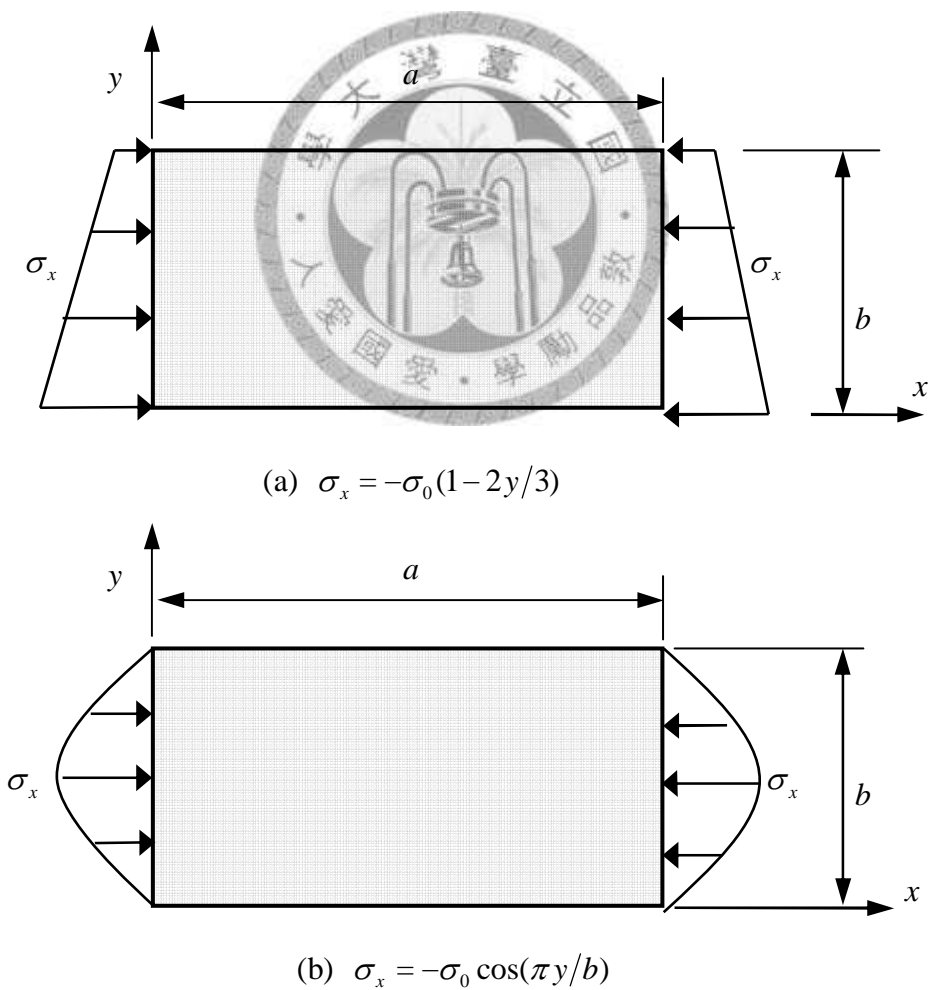
**Figure 2.5.1 Rectangular plates under uni-axial edge compressions.**

The governing differential equation can be expressed as

$$D\left[\frac{\partial^4 w(x,y)}{\partial x^4} + 2\frac{\partial^4 w(x,y)}{\partial x^2 \partial y^2} + \frac{\partial^4 w(x,y)}{\partial y^4}\right] = \sigma_x h \frac{\partial^2 w(x,y)}{\partial x^2} \tag{2.5.1}$$

where $w(x,y)$ is the normal deflection, $D$ is the flexural rigidity of the plate given by

$$D = \frac{Eh^3}{12\left(1-v^2\right)} \tag{2.5.2}$$

in which $E$ is the Young's modulus, $h$ is the plate thickness and $v$ is Poisson's ratio. The internal forces of plate are given by

$$M_x(x,y) = -D\left[\frac{\partial^2 w(x,y)}{\partial x^2} + v\frac{\partial^2 w(x,y)}{\partial y^2}\right] \tag{2.5.3}$$

$$M_y(x,y) = -D\left[v\frac{\partial^2 w(x,y)}{\partial x^2} + \frac{\partial^2 w(x,y)}{\partial y^2}\right] \tag{2.5.4}$$

$$V_x(x,y) = -D\left[\frac{\partial^3 w(x,y)}{\partial x^3} + (2-v)\frac{\partial^3 w(x,y)}{\partial x \partial y^2}\right] \tag{2.5.5}$$

$$V_y(x,y) = -D\left[\frac{\partial^3 w(x,y)}{\partial y^3} + (2-v)\frac{\partial^3 w(x,y)}{\partial y \partial x^2}\right] \tag{2.5.6}$$

$$F_c(x,y) = -2D(1-v)\frac{\partial^2 w(x,y)}{\partial x \partial y} \tag{2.5.7}$$

where $M_x(x,y)$, $V_x(x,y)$, $F_c(x,y)$ are bending moment, effective transverse force per length, and concentrated force produced at each corner, respectively, etc.

Two types of boundary conditions (BCs) are considered as follow :

(1) simply supported (SSSS) BC :

$$w(x,y) = M_x(x,y) = 0 \quad \text{at edge} \quad x = 0, a \tag{2.5.8a}$$

$$w(x,y) = M_y(x,y) = 0 \quad \text{at edge} \quad y = 0, b \tag{2.5.8b}$$

(2) clamped (CCCC) BC :

$$w(x, y) = \frac{\partial w(x, y)}{\partial x} = 0 \quad \text{at edge} \quad x = 0, a \qquad (2.5.9a)$$

$$w(x, y) = \frac{\partial w(x, y)}{\partial y} = 0 \quad \text{at edge} \quad y = 0, b \qquad (2.5.9b)$$

Note that corner conditions are automatically satisfied for both BCs.

Each corner point of a thin rectangular plate has three degrees-of-freedom (DOFs), namely, $w$, $\partial w/\partial x$, $\partial w/\partial y$. Each point of the remaining boundaries has two DOFs, $w$, $\partial w/\partial x$ at edges parallel to the $y$-axis, and $w$, $\partial w/\partial y$ at edges parallel to the $x$-axis, respectively. Each inner point of plate has only one DOF $w$.

## 2.5.3 Approach by spline collocation method

A rectangular thin plate with size $a \times b$ has been assigned $n_x$ and $n_y$ inner knots with equal-space $h_x$ and $h_y$ in the $x$- and $y$- directions, respectively, as shown in Figure 2.3.1. The serial numbers of the inner knots are defined as

$$x_3 = 0, \quad x_{n_x+2} = a, \quad x_{j+1} - x_j = h_x = a/(n_x - 1), \quad j = 3, \ldots, n_x + 1. \qquad (2.5.10)$$

$$y_3 = 0, \quad y_{n_y+2} = b, \quad y_{j+1} - y_j = h_y = b/(n_y - 1), \quad j = 3, \ldots, n_y + 1. \qquad (2.5.11)$$

The total number of inner knots is $n_x n_y$. The governing equation in Eq. (2.5.1) must be satisfied for each inner knot of the plate.

The fictitious knots should be based on, and required to satisfy the BCs. One needs two fictitious knots outside the plate to satisfy two BCs for each boundary knot of the plate except for four corner knots. Therefore, the total number of fictitious knots for boundary knots, excluding four corner knots, is $4\left[(n_x - 2) + (n_y - 2)\right]$. Each corner knot has three BCs. Thus, the total number of fictitious knots for four corners is 12. Consequently, the total number of boundary fictitious knots for the plate are

$4(n_x + n_y) - 4$, which exactly equal to the total number of BCs. The total number of knots including fictitious knots for the whole plate is $n_x n_y + 4(n_x + n_y) - 4$, as shown in Figure 2.4.2.

The displacement $w(x, y)$ of a rectangular thin plate subjected to in-plane forces can be approximated by using the QSF as follows

$$w(x, y) = \sum_{i=1}^{n_x+4} \sum_{j=1}^{n_y+4} B_i(x) B_j(y) \overline{w}_{ij} \qquad (2.5.12)$$

where $\overline{w}_{ij}$ s are coefficients to be determined, note that $\overline{w}_{ij} = 0$ for no knots $i = 1, n_x + 4$, $j = 1, 2, 3, n_y + 2, n_y + 3, n_y + 4$ and $i = 2, 3, n_x + 2, n_x + 3$, $j = 1,, n_y + 4$.

Therefore, the partial derivatives for $w(x, y)$ given as

$$\frac{\partial w^{(r+s)}(x, y)}{\partial x^r \partial y^s} = \sum_{i=1}^{n_x+4} \sum_{j=1}^{n_y+4} B_i^{(r)}(x) B_j^{(s)}(y) \overline{w}_{ij} \qquad (2.5.13)$$

Substituting Eq. (2.5.12) and Eq. (2.5.13) into governing equation in Eq. (2.5.1), generalized forces in Eq. (2.5.3) to Eq. (2.5.7), and BCs in Eqs. (2.5.8) and Eqs.(2.5.9), respectively, can obtain.

Governing equation:

$$\frac{D}{h} \sum_{i=1}^{n_x+4} \sum_{j=1}^{n_y+4} \left[ B_i^{(4)}(x) B_j(y) + 2 B_i''(x) B_j''(y) + B_i(x) B_j^{(4)}(y) \right] \overline{w}_{ij} =$$
$$\sigma_x \sum_{i=1}^{n_x+4} \sum_{j=1}^{n_y+4} B_i''(x) B_j(y) \overline{w}_{ij} \qquad (2.5.14)$$

Generalized forces:

$$M_x(x, y) = -D \sum_{i=1}^{n_x+4} \sum_{j=1}^{n_y+4} \left[ B_i''(x) B_j(y) + \nu B_i(x) B_j''(y) \right] \overline{w}_{ij} \qquad (2.5.15)$$

$$M_y(x, y) = -D \sum_{i=1}^{n_x+4} \sum_{j=1}^{n_y+4} \left[ \nu B_i''(x) B_j(y) + B_i(x) B_j''(y) \right] \overline{w}_{ij} \qquad (2.5.16)$$

$$V_x(x,y) = -D \sum_{i=1}^{n_x+4} \sum_{j=1}^{n_y+4} \left[ \nu B_i'''(x)B_j(y) + (2-\nu)B_i'(x)B_j''(y) \right] \overline{w}_{ij} \qquad (2.5.17)$$

$$V_y(x,y) = -D \sum_{i=1}^{n_x+4} \sum_{j=1}^{n_y+4} \left[ \nu B_i(x)B_j'''(y) + (2-\nu)B_i''(x)B_j'(y) \right] \overline{w}_{ij} \qquad (2.5.18)$$

$$F_c(x,y) = -2D(1-\nu) \sum_{i=1}^{n_x+4} \sum_{j=1}^{n_y+4} B_i'(x)B_j'(y)\overline{w}_{ij} \qquad (2.5.19)$$

Boundary conditions:

(1) SSSS BC:

$$w(x,y) = \sum_{i=1}^{n_x+4} \sum_{j=1}^{n_y+4} B_i(x)B_j(y)\overline{w}_{ij} = 0 \quad \text{at edge} \quad x = 0, a \qquad (2.5.20a)$$

$$M_x(x,y) = -D \sum_{i=1}^{n_x+4} \sum_{j=1}^{n_y+4} \left[ B_i''(x)B_j(y) + \nu B_i(x)B_j''(y) \right] \overline{w}_{ij} = 0 \quad \text{at edge} \quad x = 0, a \qquad (2.5.20b)$$

$$w(x,y) = \sum_{i=1}^{n_x+4} \sum_{j=1}^{n_y+4} B_i(x)B_j(y)\overline{w}_{ij} = 0 \quad \text{at edge} \quad y = 0, b \qquad (2.5.20c)$$

$$M_y(x,y) = -D \sum_{i=1}^{n_x+4} \sum_{j=1}^{n_y+4} \left[ \nu B_i''(x)B_j(y) + B_i(x)B_j''(y) \right] \overline{w}_{ij} = 0 \quad \text{at edge} \quad y = 0, b \qquad (2.5.20d)$$

(2) CCCC BC:

$$w(x,y) = \sum_{i=1}^{n_x+4} \sum_{j=1}^{n_y+4} B_i(x)B_j(y)\overline{w}_{ij} = 0 \quad \text{at edge} \quad x = 0, a \qquad (2.5.21a)$$

$$\frac{\partial w(x,y)}{\partial x} = \sum_{i=1}^{n_x+4} \sum_{j=1}^{n_y+4} B_i'(x)B_j(y)\overline{w}_{ij} = 0 \quad \text{at edge} \quad x = 0, a \qquad (2.5.21b)$$

$$w(x,y) = \sum_{i=1}^{n_x+4} \sum_{j=1}^{n_y+4} B_i(x)B_j(y)\overline{w}_{ij} = 0 \quad \text{at edge} \quad y = 0, b \qquad (2.5.21c)$$

$$\frac{\partial w(x,y)}{\partial y} = \sum_{i=1}^{n_x+4} \sum_{j=1}^{n_y+4} B_i(x)B_j'(y)\overline{w}_{ij} = 0 \quad \text{at edge} \quad y = 0, b \qquad (2.5.21d)$$

In general, after substituting the coordinates of the all inner knots into the governing equation in Eq. (2.5.14), and boundary knots into the BCs in Eqs. (2.5.20) or

Eqs.(2.5.21), then a well determined linear eigen-value system of matrix form can be obtained, and expressed as

$$\frac{D}{h}\begin{bmatrix} \mathbf{B}_{db} & \mathbf{B}_{dd} \\ \mathbf{B}_{bb} & \mathbf{B}_{bd} \end{bmatrix}\begin{Bmatrix} \bar{\mathbf{w}}_{b} \\ \bar{\mathbf{w}}_{d} \end{Bmatrix} = \sigma_x \begin{bmatrix} \mathbf{B}_{db}^* & \mathbf{B}_{dd}^* \\ \mathbf{0} & \mathbf{0} \end{bmatrix}\begin{Bmatrix} \bar{\mathbf{w}}_{b} \\ \bar{\mathbf{w}}_{d} \end{Bmatrix}$$ (2.5.22)

where $\bar{\mathbf{w}}_{b}$ and $\bar{\mathbf{w}}_{d}$ are column vectors of undetermined coefficients, subscripts b and d denote the fictitious knots and all inner knots, respectively. The first $n_x n_y$ equations are obtained from governing equation in Eq. (2.5.14) and the remaining equations are obtained from BCs in Eqs. (2.5.20) or Eqs.(2.5.21). From Eq. (2.5.22) can obtained as

$$\bar{\mathbf{w}}_{b} = -\mathbf{B}_{bb}^{-1}\mathbf{B}_{bd}\bar{\mathbf{w}}_{d}.$$ (2.5.23)

Substituting Eq. (2.5.23) into the Eq. (2.5.22), obtained an generalized eigen-value problem as follow

$$\bar{\mathbf{B}}\bar{\mathbf{w}}_{d} = \frac{\sigma_x h}{D}\bar{\mathbf{B}}^*\bar{\mathbf{w}}_{d}.$$ (2.5.24)

where $\sigma_x h/D$, $\bar{\mathbf{w}}_{d}$ are the required eigen-values and eigen-vectors, respectively, $\bar{\mathbf{B}}$ and $\bar{\mathbf{B}}^*$ defined as follow

$$\bar{\mathbf{B}} = -\mathbf{B}_{db}\mathbf{B}_{bb}^{-1}\mathbf{B}_{bd} + \mathbf{B}_{dd}, \quad \bar{\mathbf{B}}^* = -\mathbf{B}_{db}^*\mathbf{B}_{bb}^{-1}\mathbf{B}_{bd} + \mathbf{B}_{dd}^*$$ (2.5.25a,b)

Consequently, eigen-values $\sigma_x$ and eigen-vectors $\bar{\mathbf{w}}_{d}$ can be found easily from solving the Eq. (2.5.12).

## 2.5.4 Numerical Examples and Discussions

In following numerical examples, Poisson's ratio $\nu$ is taken as 0.3, the plate aspect ratio $\gamma$ and buckling coefficient $k$ are defined, respectively, as

$$\gamma = \frac{a}{b}$$ (2.5.26)

$$k = \frac{\sigma_0 h b^2}{\pi^2 D}$$ (2.5.27)

where $\sigma_0$ is maximum stress for uniaxial non-uniform distributed in-plane edge load. In this paper, two non-uniform distributed loading cases are studied.

## 2.5.4.1 Linearly Varying Distributed Load

Consider a rectangular plate under linearly varying distributed compressive load, $\sigma_x = -2\sigma_0/3(1-y/b)$, shown in Figure 2.5.1(a). Since $\sigma_x = -2\sigma_0/3(1-y/b)$ and $\sigma_y = \tau_{xy} = 0$ everywhere in the plate, solutions for buckling loads are available for designers (Aircraft design manual, 2001; Young and Budynas, 2002). This example serves as a check of both the formulations as well as the computer program.

Two boundary conditions, i.e., all edges are simply supported or clamped and denoted by SSSS or CCCC, are considered. Table 2.5.1 shows the convergence study for the buckling load with $a/b = 1$. As can be seen that converged results can be obtained with $N = 11$. Table 2.5.2 shows the SCM results for various aspect ratios. It is found that differences are observed between the data obtained by SCM, DQM (Wang *et al*., 2006), FEM (Wang *et al*., 2006) and cited from manual (Aircraft design manual, 2001). Consequently, SCM can obtain good accurate solutions.

**Table 2.5.1 Convergence for square thin plates under linearly varying compressive load.**

| B.C. | $n_x \times n_y$ | | | |
|------|------------------|------------------|------------------|------------------|
|      | $10 \times 10$ | $20 \times 20$ | $30 \times 30$ | $40 \times 40$ |
| SSSS | 5.9842 | 5.9685 | 5.9657 | 5.9647 |
| CCCC | 15.2477 | 15.0349 | 14.9953 | 14.9811 |

**Table 2.5.2 Buckling load k of simply supported rectangular thin plates under linearly varying compressive load.**

| $\gamma = a/b$ | 0.4 | 0.6 | 0.75 | 0.8 | 1.0 | 1.5 |
|----------------|-------|------|------|------|------|------|
| SCM | 12.24 | 7.60 | 6.45 | 6.25 | 5.96 | 6.45 |
| DQM | 12.24 | 7.60 | 6.45 | 6.25 | 5.96 | 6.45 |
| FEM | 12.23 | 7.59 | 6.44 | 6.25 | 5.96 | 6.45 |
| Manual | 10.80 | 7.10 | 6.10 | 6.00 | 5.90 | 6.10 |

## 2.5.4.1 Non-uniformly Distributed Load

Consider a rectangular plate under non-uniformly distributed compressive load, $X = -\sigma_0 \cos(\pi y/b)$, shown in Figure 2.5.1(b). For this loading case, $\sigma_x \neq -\sigma_0 \cos(\pi y/b)$, $\sigma_y \neq 0$ and $\tau_{xy} \neq 0$ within the plate. This makes analytical solutions be difficult to be obtained if not impossible. Relatively accurate buckling loads are only available recently for plates with all edges simply supported (Bert and Devarakonda, 2003).

Table 2.5.3 shows the convergence study for the buckling load of rectangular plates with three different aspect ratios. As can be seen that converged results are obtained. Table 2.5.4 shows the SCM results with $N = 15$ for three different aspect ratios. It is found that differences are observed between the data obtained by SCM and results cited from literatures (Bert and Devarakonda, 2003; Van der Neut, 1958; Benoy, 1969). To check the data, finite element analyses are also performed by MSC-NASTRAN. There are difference between SCM data and solutions by Galerkin method in (Bert and Devarakonda, 2003). The possible reasons to cause the discrepancy are that a minor error exists in their derivations and the stress boundary conditions are not satisfied to obtain their inplane stress solutions. Data in (Van der Neut, 1958; Benoy, 1969) are obviously too small and are not accurate, as are pointed out by Bert and Devarakonda (2003).

**Table 2.5.3 Convergence for rectangular thin plates under half-cosine compressive load.**

| B.C. | $\gamma = a/b$ | $n_x \times n_y$ | | | |
|------|------|------|------|------|------|
| | | $10 \times 10$ | $20 \times 20$ | $30 \times 30$ | $40 \times 40$ |
| SSSS | 0.5 | 7.3539 | 7.3244 | 7.3189 | 7.3170 |
| | 1.0 | 4.7205 | 4.7087 | 4.7064 | 4.7056 |
| | 3.0 | 4.7986 | 4.7280 | 4.7150 | 4.7104 |
| CCCC | 0.5 | 22.2457 | 21.8098 | 21.7289 | 21.7007 |
| | 1.0 | 11.5205 | 11.3467 | 11.3143 | 11.3029 |
| | 3.0 | 10.8380 | 10.3469 | 10.0615 | 9.9622 |

**Table 2.5.4 Buckling load k of simply supported rectangular thin plates under half-cosine distributed compressive load.**

| $\gamma = a/b$ | SCM | DQM | FEM | Bert (2003) | Benoy (1969) | Van Der Neut (1958) |
|---|---|---|---|---|---|---|
| 0.5 | 7.317 | 7.452 | 7.409 | 7.841 | 7.08 | |
| 1.0 | 4.706 | 5.419 | 5.383 | 5.146 | 4.59 | 4.68 |
| 3.0 | 4.710 | 5.849 | 5.818 | 5.748 | 4.53 | |

## 2.5.5 Nomenclature

$a$ — length of rectangular thin plate

$b$ — width of rectangular thin plate

$D = \dfrac{Eh^3}{12(1-v^2)}$ — flexural rigidity of the plate

$E$ — Young's modulus

$F_c(x, y)$ — concentrated force

$h$ — plate thickness

$h_x$ — equal-space in the $x$ directions

$h_y$ — equal-space in the $y$ directions

$M_x(x, y)$ — bending moment

$V_x(x, y)$ — effective transverse force per length

$n_x$ — inner knots in the $x$ directions

$n_y$ — inner knots in the $y$ directions

$w(x, y)$ — normal deflection

$\bar{\mathbf{w}}_b,\ \bar{\mathbf{w}}_d$ — column vectors of undetermined coefficients

$\bar{w}_{ij}$ — is coefficients to be determined

$v$ — Poisson's ratio

$\gamma = \dfrac{a}{b}$ — plate aspect ratio
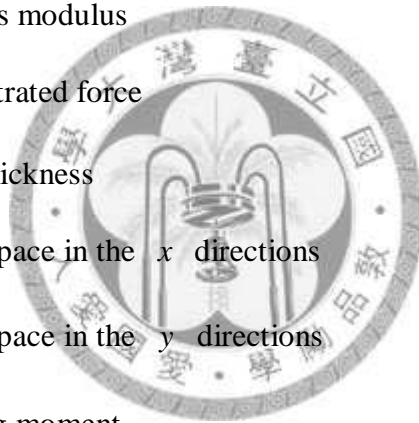
$$k = \frac{\sigma_0 h b^2}{\pi^2 D}$$    buckling coefficient

$\sigma_0$    maximum stress

## 2.6 Vibration Analysis of Beams on Pasternak Elastic Foundation

### 2.6.1 Introduction

The initial stress in a structural member can significantly affect its dynamic behaviour. Vibration characteristics of beams on Pasternak elastic foundation without initial stress were studied by Franciosi and Masi (1993). However, a study of the effect of initial stress on the dynamic behaviour of beams on Pasternak elastic foundation is not available in literature. The purpose of the present note is to study the vibration characteristics of beams on Pasternak elastic foundation under initial stress using the spline collocation method.

### 2.6.2 Formulation

The elastic foundation, in a simplified form, can be represented as a continuous layer of independent linear elastic springs (Winkler, 1867). The relation between the pressure and the deflection of the foundation is

$$p(x) = Kw(x) \tag{2.6.1}$$

where $K$ is the foundation modulus, known as the Winkler foundation parameter and $x$ is the axial coordinate of the beam.

As this foundation model cannot represent the continuous elastic medium, the following pressure displacement relationship is used for the present study:

$$p(x) = Kw(x) - K_1 \frac{d^2 w(x)}{dx^2} \tag{2.6.2}$$

where the second parameter $K_1$, represents the stiffness of the shearing layer (Figure 2.6.1) connecting the top of the Winkler springs. This physical model with constants $K$ and $K_1$, is known as the Pasternak model (Pasternak, 1954).
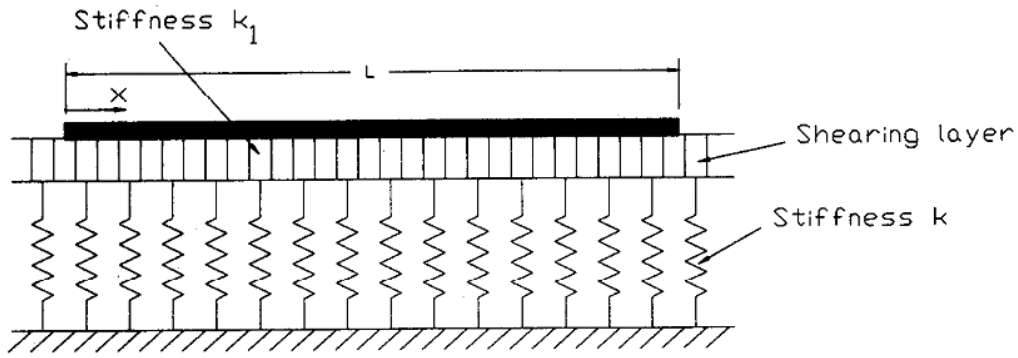
**Figure 2.6.1. Pasternak elastic foundation.**

For a uniform beam of length $L$, moment of inertia $I$, Young's modulus $E$ subjected to an end concentrated load $P$ and executing harmonic oscillations resting on an elastic foundation characterized by Eq. (2.6.2), the governing equation is given by

$$\frac{d^4 w(x)}{dx^4} + K w(x) - K_1 \frac{d^2 w(x)}{dx^2} + \lambda \frac{d^2 w(x)}{dx^2} - \lambda_f w(x) = 0 \qquad (2.6.3)$$

Nondimensionalizing all the length quantities in Eq. (2.6.3) by the length of the column $L$, we get

$$\frac{d^4 W(X)}{dX^4} + \bar{K} W(X) - \bar{K}_1 \frac{d^2 W(X)}{dX^2} + \lambda \frac{d^2 W(X)}{dX^2} - \lambda_f W(X) = 0 \qquad (2.6.4)$$

where

$$W(X) = \frac{w(x)}{L}, \quad X = \frac{x}{L}, \quad \bar{K} = \frac{KL^4}{EI}, \quad \bar{K}_1 = \frac{K_1 L^2}{\pi^2 EI},$$

$$\lambda = \frac{PL^2}{EI}, \quad \lambda_f = \left[ \frac{mL^4 \omega^2}{EI} \right]^{1/4} \qquad (2.6.5)$$

The deflection slope, bending moment and shear force are

$$\theta(X) = \frac{dW(X)}{dX} \qquad (2.6.6)$$

$$M(X) = EI \frac{d^2 W(X)}{dX^2} \qquad (2.6.7)$$

67

$$V(X) = -EI \frac{d^3 W(X)}{dX^3} \tag{2.6.8}$$

The boundary conditions can be divided into the following two kinds:

clamped (C):

$$W = 0, \quad \theta = 0 \tag{2.6.9}$$

Hinged (H):

$$W = 0, \quad M = 0 \tag{2.6.10}$$

at the extremity $X = 0,1$.

## 2.6.3 Approach by spline collocation method

Since the governing equation of a uniform beams on Pasternak elastic foundation is a fourth-order ordinary differential equation (ODE), the solution of the governing ODE can be approximated by the spline functions with polynomial at least fifth degree. A quintic spline functions (QSFs) is a piecewise fifth degree polynomial which is belonging to $C^4$.

Considering a set of equi-spaced knots is selected in a normalized interval $X \in [0,1]$, i.e.,

$$X_0 = 0, \quad X_n = 1, \quad X_{j+1} - X_j = h, \quad j = 0, \ldots, n-1 \tag{2.6.11}$$

where $h$ is distance of equi-spaced knots. In order to apply the SCM, one needs to extend two added knots (fictitious) $X_{-2}$, $X_{-1}$ and $X_{n+1}$, $X_{n+2}$ at each end of beam, respectively (Figure 2.6.2).
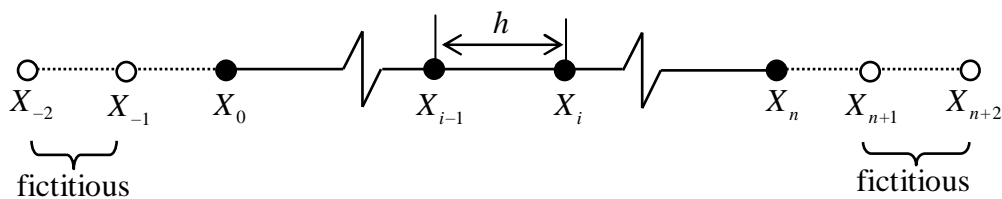


**Figure 2.6.2. Partitions of beam into $n$ sections with two added knots at each end.**

Then the uniform beams on Pasternak elastic foundation for flexural vibration can

be approximated by using the QSF (Prenter, 1975) as follows

$$W(X) = \sum_{i=-2}^{n+2} B_i(X)a_i \qquad (2.6.12)$$

where $c_i$s are the coefficients to be determined and $B_i(\xi)$ is QSF.

Substituting Eq. (2.6.12), into the governing equations in Eq. (2.6.4) can obtain

$$\sum_{i=-2}^{n+2} \left[ B_i^{(4)}(X) + \bar{K}B_i(X) - \bar{K}_1 B_i''(X) + \lambda B_i''(X) - \lambda_f B_i(X) \right] a_i = 0 \qquad (2.6.13)$$

Similarly, the two kinds of boundary conditions in Eq. (2.6.9) and Eq. (2.6.10) to Eq. (2.6.12) can obtain,

clamped (C):

$$\sum_{i=-2}^{n+2} B_i(X)a_i = 0, \qquad \sum_{i=-2}^{n+2} B_i'(X)a_i = 0 \qquad (2.6.14)$$

Hinged (H):

$$\sum_{i=-2}^{n+2} B_i(X)a_i = 0, \qquad \sum_{i=-2}^{n+2} B_i''(X)a_i = 0 \qquad (2.6.15)$$

In general, after substituting the coordinates of the $n+1$ knots, $X_i$, $i = 0,1,\ldots,n$, into the Eq. (2.6.13), and coupling the four given boundary conditions in Eq. (2.6.14) and Eq. (2.6.15) at the ends, $X_0$ and $X_n$, one obtains the following simultaneous equations.

$$\begin{bmatrix} \text{1st B.C. at } X_0 \\ \text{2nd B.C. at } X_0 \\ \text{1st B.C. at } X_n \\ \text{2nd B.C. at } X_n \\ \sum_{i=-2}^{n+2} \left[ B_i^{(4)}(X_0) + \bar{K}B_i(X_0) - \bar{K}_1 B_i''(X_0) + \lambda B_i''(X_0) - \lambda_f B_i(X_0) \right] a_i \\ \sum_{i=-2}^{n+2} \left[ B_i^{(4)}(X_1) + \bar{K}B_i(X_1) - \bar{K}_1 B_i''(X_1) + \lambda B_i''(X_1) - \lambda_f B_i(X_1) \right] a_i \\ \vdots \\ \sum_{i=-2}^{n+2} \left[ B_i^{(4)}(X_n) + \bar{K}B_i(X_n) - \bar{K}_1 B_i''(X_n) + \lambda B_i''(X_n) - \lambda_f B_i(X_n) \right] a_i \end{bmatrix} = \mathbf{0} \qquad (2.6.16)$$

Matrix equations in Eq. (2.6.16) of the following form

$$[K]\{a\} + [F]\{a\} + \lambda[G]\{a\} - \lambda_f[M]\{a\} = 0 \qquad (2.6.17)$$

where $[K]$, $[F]$ and $[G]$ are the assembled elastic stiffness matrix, foundation matrix and geometric stiffness matrix respectively. $\lambda$ is the load parameter representing the initial stress in the beam and $\lambda_f$ is the frequency parameter (eigenvalue). Eq. (2.6.17) can be solved using any standard algorithm to obtain eigen-values and eigen-vectors

## 2.6.4 Numerical Examples and Discussions

Frequency parameter $\lambda_f$ is evaluated for $\gamma = 0.0$, 0.2, 0.4, 0.6 and 0.8. $\gamma$ is defined as the ratio between the load parameter $\lambda$ and the stability parameter $\lambda_b$ ($\gamma = \lambda/\lambda_b$). Stability parameter $\lambda_b$ ($PL^2/EI$) is obtained by using Eq. (2.6.17) by neglecting the fourth term and replacing $\lambda$ by $\lambda_b$.

Convergence of the stability parameter $\lambda_b$ of beams ($\bar{K} = 0$ and $\bar{K}_f = 0$) for three types of boundary conditions, H-H, C-C, and H-C, are shown in Table 2.6.1. It is sufficiently to indicate that the convergences by SCM are very good, and observe that using inner 301 knots are enough to obtain stable and very accurate results.

**Table 2.6.1 Variation of stability parameter $\lambda_b$ ($PL^2/EI$) with $\bar{K} = 0$ and $\bar{K}_1 = 0$ for vibrating beams.**

| No. of knots ($n$) | H-H | C-C | H-C |
|---|---|---|---|
| 21 | 9.8899 | 39.8042 | 20.2758 |
| 51 | 9.8729 | 39.5304 | 20.2043 |
| 101 | 9.8704 | 39.4914 | 20.1941 |
| 201 | 9.8698 | 39.4816 | 20.1916 |
| 301 | 9.8697 | 39.4799 | 20.1911 |
| 401 | 9.8697 | 39.4792 | 20.1911 |

The above formulation is employed to obtain the frequency parameter $\lambda_f$ of a uniform beam for various values of $\bar{K}$ and $\bar{K}_f$ for the H-H, C-C, and H-C beams. The beam is idealized into 301 knots of equal length.

70

The variation of $\lambda_b$ and $\lambda_f$ is given in Table 2.6.2 to Table 2.6.4, and Table 2.6.5 to Table 2.6.7, respectively, for the values of $\bar{K}$ - 0.0, 1.0, $10^2$, $10^4$, $10^6$ and $\bar{K}_1$ = 0.0, 0.5, 1.0, 2.5 for H-H, C-C, and H-C beams.

From the numerical results presented in the Tables 2.6.6, 2.6.7, and 2.6.8, the following observations have been made:

(a) $\lambda_f$ decreases with increasing $\gamma$ for a given $\bar{K}$ and $\bar{K}_1$ ;

(b) reduction in $\lambda_f$ with increasing $\gamma$ is more for lower values of $\bar{K}$ ;

(c) reduction in $\lambda_f$ with increasing $\gamma$ is small for simply supported beam compared to clamped beam for a given $\bar{K}$ and $\bar{K}_1$ ;

(d) the values of $\lambda_f$, are almost the same for simply supported and lamped beams for stong foundation (i.e. higher values of $\bar{K}$) for a given $\bar{K}$ and $\bar{K}_1$ ;

(e) for a given $\bar{K}$ and $\gamma$, the values of $\lambda_f$ increase with increasing $\bar{K}_1$ ;

(f) the increase in $\lambda_f$, with increasing $\bar{K}_1$, is more for lower values of $\bar{K}$ ;

(g) for a given $\bar{K}_1$, and $\gamma$, the values of $\lambda_f$, increase with increasing $\bar{K}$ ;

(h) The increase in $\lambda_f$, with increasing $\bar{K}_1$ is more for lower values of $\bar{K}$.

**Table 2.6.2. Variation of stability parameter $\lambda_b$ for H-H beam.**

| $\bar{K}$ | $\bar{K}_1$ | | | |
|---|---|---|---|---|
| | 0.0 | 1.0 | 10 | $10^2$ |
| 0.0 | 9.8697 | 10.8699 | 19.8699 | 109.8698 |
| 1.0 | 9.9710 | 10.9712 | 19.9712 | 109.9712 |
| $10^2$ | 20.0039 | 21.0036 | 30.0037 | 120.0036 |
| $10^4$ | 201.4158 | 202.4140 | 211.4146 | 301.4150 |
| $10^6$ | 2001.0728 | 2002.0747 | 2011.0743 | 2101.0738 |

**Table 2.6.3 Variation of stability parameter $\lambda_b$ for C-C beam.**

| $\bar{K}$ | $\bar{K}_1$ | | | |
|---|---|---|---|---|
| | 0.0 | 1.0 | 10 | $10^2$ |
| 0.0 | 39.4799 | 40.4805 | 49.4808 | 139.4805 |
| 1.0 | 39.5567 | 40.5567 | 49.5566 | 139.5568 |
| $10^2$ | 47.0099 | 48.0104 | 57.0099 | 147.0105 |
| $10^4$ | 233.8066 | 234.8077 | 243.8067 | 333.8063 |
| $10^6$ | 2039.6859 | 2040.6860 | 2049.6861 | 2139.6860 |

**Table 2.6.4 Variation of stability parameter $\lambda_b$ for H-C beam.**

| $\bar{K}$ | $\bar{K}_1$ | | | |
|---|---|---|---|---|
| | 0.0 | 1.0 | 10 | $10^2$ |
| 0.0 | 20.2758 | 21.1918 | 30.1919 | 120.1918 |
| 1.0 | 20.2745 | 21.2745 | 30.2744 | 120.2745 |
| $10^2$ | 28.3095 | 29.3090 | 38.3092 | 128.3087 |
| $10^4$ | 208.9871 | 209.9880 | 218.9885 | 308.9884 |
| $10^6$ | 2010.6861 | 2011.6811 | 2020.6882 | 2110.6925 |

**Table 2.6.5 Variation of frequency parameter $\lambda_f$ for H-H beam.**

| $\bar{K}$ | $\gamma$ | $\bar{K}_1$ | | | |
|---|---|---|---|---|---|
| | | 0.0 | 1.0 | 10 | $10^2$ |
| 0.0 | 0.0 | 3.1416 | 3.2183 | 3.7422 | 5.7384 |
| | 0.2 | 2.9711 | 3.0437 | 3.5391 | 5.4271 |
| | 0.4 | 2.7650 | 2.8324 | 3.2935 | 5.0505 |
| | 0.6 | 2.4984 | 2.5594 | 2.9760 | 4.5636 |
| | 0.8 | 2.1009 | 2.1522 | 2.5025 | 3.8375 |
| 1.0 | 0.0 | 3.1496 | 3.2258 | 3.7469 | 5.7398 |
| | 0.2 | 2.9787 | 3.0508 | 3.5436 | 5.4283 |
| | 0.4 | 2.7720 | 2.8390 | 3.2977 | 5.0516 |
| | 0.6 | 2.5048 | 2.5654 | 2.9798 | 4.5647 |
| | 0.8 | 2.1063 | 2.1571 | 2.5057 | 3.8384 |
| $10^2$ | 0.0 | 3.7484 | 3.7944 | 4.1482 | 5.8664 |
| | 0.2 | 3.5450 | 3.5885 | 3.9231 | 5.5481 |
| | 0.4 | 3.2989 | 3.3394 | 3.6509 | 5.1631 |
| | 0.6 | 2.9809 | 3.0175 | 3.2989 | 4.6653 |
| | 0.8 | 2.5070 | 2.5372 | 2.7739 | 3.9230 |
| $10^4$ | 0.0 | 10.0243 | 10.0267 | 10.0487 | 10.2608 |
| | 0.2 | 9.9077 | 9.9261 | 9.9442 | 10.1202 |
| | 0.4 | 9.4177 | 9.5736 | 9.6341 | 9.9735 |
| | 0.6 | 8.5837 | 9.0820 | 9.1290 | 9.5643 |
| | 0.8 | 5.9770 | 7.7437 | 7.8284 | 8.5551 |
| $10^6$ | 0.0 | 31.6235 | 31.6236 | 31.6243 | 31.6313 |
| | 0.2 | 31.3160 | 31.3169 | 31.3262 | 31.4182 |
| | 0.4 | 30.2909 | 30.2929 | 30.3102 | 30.4809 |
| | 0.6 | 28.2934 | 28.2962 | 28.3213 | 28.5683 |
| | 0.8 | 24.4913 | 24.4940 | 24.5184 | 24.7589 |

**Table 2.6.6 Variation of frequency parameter $\lambda_f$ for C-C beam.**

| $\bar{K}$ | $\gamma$ | $\bar{K}_1$ 0.0 | 1.0 | 10 | $10^2$ |
|-----------|----------|-----|-----|-----|--------|
| 0.0 | 0.0 | 4.7300 | 4.7588 | 4.9957 | 6.4025 |
|     | 0.2 | 4.4803 | 4.5077 | 4.7331 | 6.0714 |
|     | 0.4 | 4.1764 | 4.2021 | 4.4132 | 5.6683 |
|     | 0.6 | 3.7808 | 3.8041 | 3.9965 | 5.1426 |
|     | 0.8 | 3.1856 | 3.2054 | 3.3688 | 4.3467 |
| 1.0 | 0.0 | 4.7324 | 4.7611 | 4.9977 | 6.4035 |
|     | 0.2 | 4.4826 | 4.5099 | 4.7350 | 6.0723 |
|     | 0.4 | 4.1785 | 4.2041 | 4.4150 | 5.6693 |
|     | 0.6 | 3.7827 | 3.8060 | 3.9981 | 5.1434 |
|     | 0.8 | 3.1872 | 3.2070 | 3.3702 | 4.3474 |
| $10^2$ | 0.0 | 4.9504 | 4.9755 | 5.1852 | 6.4957 |
|        | 0.2 | 4.6909 | 4.7148 | 4.9144 | 6.1616 |
|        | 0.4 | 4.3747 | 4.3972 | 4.5845 | 5.7548 |
|        | 0.6 | 3.9625 | 3.9829 | 4.1539 | 5.2238 |
|        | 0.8 | 3.3409 | 3.3583 | 3.5038 | 4.4191 |
| $10^4$ | 0.0 | 10.1229 | 10.1258 | 10.1522 | 10.3960 |
|        | 0.2 | 9.9757 | 9.9784 | 10.0185 | 10.2183 |
|        | 0.4 | 9.7972 | 9.7999 | 9.8640 | 10.0194 |
|        | 0.6 | 9.1510 | 9.1578 | 9.4538 | 9.7523 |
|        | 0.8 | 8.1464 | 8.1519 | 8.6765 | 8.6366 |
| $10^6$ | 0.0 | 31.6267 | 31.6268 | 31.6277 | 31.6361 |
|        | 0.2 | 31.3434 | 31.3446 | 31.3643 | 31.4560 |
|        | 0.4 | 30.3465 | 30.3486 | 30.4083 | 30.5519 |
|        | 0.6 | 28.3781 | 28.3806 | 28.5113 | 28.6242 |
|        | 0.8 | 24.6045 | 24.6072 | 24.9308 | 24.8665 |

**Table 2.6.7 Variation of frequency parameter $\lambda_f$ for H-C beam.**

| $\overline{K}$ | $\gamma$ | $\overline{K}_1$ 0.0 | 1.0 | 10 | $10^2$ |
|---|---|---|---|---|---|
| 0.0 | 0.0 | 3.9266 | 3.9733 | 4.3313 | 6.0483 |
| | 0.2 | 3.7169 | 3.7622 | 4.1022 | 5.7317 |
| | 0.4 | 3.4619 | 3.5057 | 3.8237 | 5.3476 |
| | 0.6 | 3.1298 | 3.1723 | 3.4615 | 4.8487 |
| | 0.8 | 2.6290 | 2.6719 | 2.917 | 4.0974 |
| 1.0 | 0.0 | 3.9307 | 3.9772 | 4.3344 | 6.0494 |
| | 0.2 | 3.7218 | 3.766 | 4.1051 | 5.7328 |
| | 0.4 | 3.4679 | 3.5092 | 3.8265 | 5.3487 |
| | 0.6 | 3.1380 | 3.1758 | 3.4641 | 4.8499 |
| | 0.8 | 2.6428 | 2.6746 | 2.9192 | 4.0983 |
| $10^2$ | 0.0 | 4.2869 | 4.3231 | 4.6107 | 6.1583 |
| | 0.2 | 4.0618 | 4.0961 | 4.3697 | 5.8381 |
| | 0.4 | 3.7880 | 3.8201 | 4.0774 | 5.4500 |
| | 0.6 | 3.4313 | 3.4605 | 3.6943 | 4.9459 |
| | 0.8 | 2.8936 | 2.9185 | 3.1176 | 4.1865 |
| $10^4$ | 0.0 | 10.059 | 10.062 | 10.087 | 10.319 |
| | 0.2 | 9.9298 | 9.9327 | 9.9572 | 10.163 |
| | 0.4 | 9.6418 | 9.6487 | 9.7086 | 9.9896 |
| | 0.6 | 9.0307 | 9.0379 | 9.1015 | 9.6206 |
| | 0.8 | 7.8933 | 7.9016 | 7.9743 | 8.5581 |
| $10^6$ | 0.0 | 31.625 | 31.625 | 31.626 | 31.633 |
| | 0.2 | 31.314 | 31.315 | 31.326 | 31.428 |
| | 0.4 | 30.293 | 30.295 | 30.315 | 30.498 |
| | 0.6 | 28.312 | 28.315 | 28.338 | 28.567 |
| | 0.8 | 24.521 | 24.524 | 24.548 | 24.787 |

## 2.6.5 Nomenclature

$B_i(\xi)$      quintic spline functions

$c_i$      is the coefficients to be determined

$E$      Young's modulus

$h$      distance of equi-spaced knots

$I$      moment of inertia

$K$      foundation modulus

$K_1$      second parameter

| | |
|---|---|
| $L$ | uniform beam of length |
| $M(X)$ | dimensionless bending moment |
| $P$ | concentrated load |
| $V(X)$ | dimensionless shear force |
| $x$ | axial coordinate of the beam |
| $X = \dfrac{x}{L}$ | dimensionless coordinate system |
| $\theta(X)$ | dimensionless deflection slope |
| $\lambda$ | load parameter representing the initial stress in the beam |
| $\lambda_b$ | stability parameter |
| $\lambda_f$ | frequency parameter |
| $\gamma = \dfrac{\lambda}{\lambda_b}$ | frequency ratio |

## 2.7 Vibration Analysis of Timoshenko Beam-Columns on Pasternak Elastic Foundations

### 2.7.1 Introduction

Many problems related to soil-structure interaction can be modeled by means of a beam or a beam-column on an elastic foundation. Practical examples of these are railroad tracks, highway pavements, continuously supported pipelines, and strip foundations. The free flexural vibrations of beams on continuous elastic foundations have been analyzed by a number of investigators. The effect of a partial elastic foundation on the natural frequencies of beams or piles was examined by Doyle and Pavlovic (1982), Eisenberger er al. (1985), Valsangkar and Pradhanang (1987), Laura and Cortinez (1987). The exact dynamic stiffness matrices for free vibration calculations of a uniform beam on an elastic foundation were developed by Williams and Kennedy (1987).

The problems of bending vibrations of uniform beams on nonuniform elastic foundations were solved by Pavlovic and Wylie (1983), Eisenberger and Clastornik (1987), Filipich *et al*. (1988), De Rosa (1993), Kukla (1991) and Zhou (1993). The similar problem for stepped beams on uniform elastic foundations was treated by Wang (1991). The free vibrations of nonuniform beams resting on nonuniform elastic foundation with general elastic end restraints were studied by Lee and Ke (1990). In the aforementioned studies, the elastic foundation was idealized by a Winkler model (one-parameter model) for mathematical simplicity. Although the Winkler model is quite simple, it does not represent accurately the characteristics of many practical foundations. In order to eliminate the discontinuous nature of this model, several two-parameter foundation models that are more accurate than the Winkler model and simpler than semi-infinite elastic continuum foundation models (see, Richart *et al*.

(1970)) have been reported in the literature. The vibration and buckling of beams on variable Pasternak elastic foundations were discussed by Eisenberger and Clastornik (1987). The same problems for beams on an elastic half-space or a two-parameter elastic soil were considered by Karamanlidis and Prakash (1988), and De Rosa (1989). The free vibration analysis of a beam on a two-parameter elastic soil was performed by Franciosi and Masi (1993) using a matrix displacement approach. The influences of the partial elastic foundation and the magnitude of the axial force on the natural frequencies of beam-columns lying on Pasternak models were studied by Valsangker and Pradhanang (1988). All of the foregoing work has been conducted within the framework of the elementary Euler-Bernoulli beam theory of flexural vibration, which is not applicable to moderately short and thick beams. In order to evaluate the effects of transverse shear deformation and rotatory inertia on the dynamic behavior of beams, the lateral vibrations of Timoshenko beams (see Timoshenko *et al.* (1974)) laid on Pasternak foundations (or two-parameter foundations) were analyzed by Wang and Stephens (1977), Wang and Gagnon (1978), Yokoyama (1987), Filipich and Rosales (1988). The transverse vibrations of curved Timoshenko beams on the Winkler foundations were investigated by Panayotounakos and Theocaris (1980), and Issa (1988). A transfer matrix method for the vibration and buckling analysis of an axially loaded Timoshenko beam on a Winkler foundation was developed by Djodjo (1969). The exact dynamic stiffness matrices for an axially loaded Timoshenko member embedded in the Winkler-type foundation were derived by Capron and Williams (1988). The vibration analysis of Timoshenko beam-columns on elastic media was presented by Cheng and Pantelides (1988) using the dynamic stiffness approach. In their work, the elastic media were replaced by a constant Winkler foundation and the effect of the partial elastic foundation was not taken into account.

The present paper describes a spline collocation technique for determining the free vibration characteristics of a uniform Timoshenko beam-column on Pasternak elastic foundation. The beam-column is divided lengthwise into a number of knots of equal length. The influences of axial force, foundation stiffness parameters, transverse shear deformation and rotatory inertia are incorporated into a spline collocation model. The governing matrix equation for small-amplitude, free vibrations of the beam-column on the elastic foundation is derived by application of Hamilton's principle. The numerical results for the natural frequencies and the corresponding mode shapes of the classical Euler-Bernoulli and Timoshenko beam-columns on the elastic foundations are provided and compared with the exact solutions or the available results in the published literature. The advantages and limitations associated with the technique are discussed.

## 2.7.2 Formulation

Consider a Timoshenko beam-column partially supported on an elastic foundation as depicted in Figure 2.7.1 The elastic foundation is idealized as a constant two-parameter model characterized by two module, i.e. the Winkler foundation modulus $k$ and the shear foundation modulus $k_G$. In the case $k_G = 0$ this model reduces to the usual Winkler model.
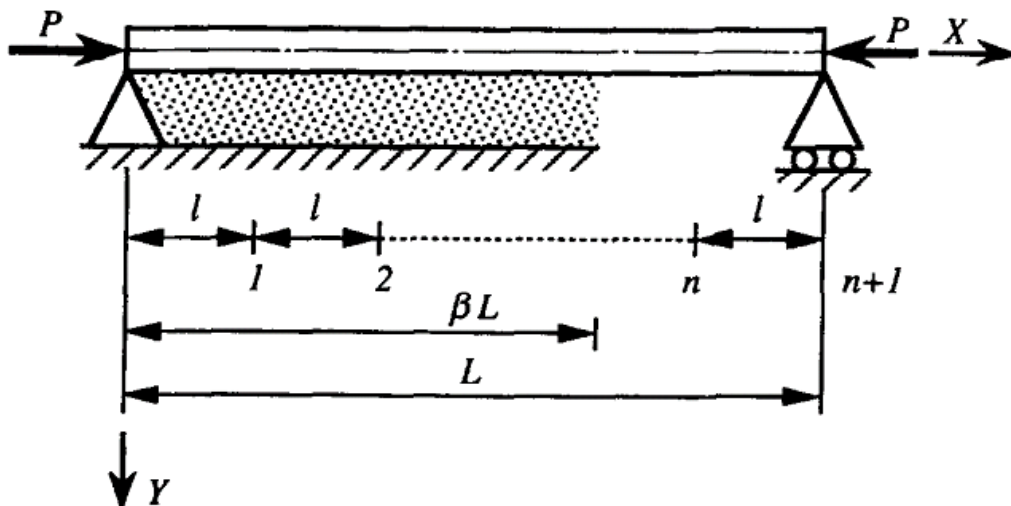


**Figure 2.7.1. A Timoshenko beam-column supported on an elastic foundation.**

Figure 2.7.2 shows a Timoshenko beam element with an axial force $P$, resting on Pasternak elastic foundation model. The beam element consists of two nodes $i$ and $j$; each node has the degrees of freedom of lateral displacement $v$ and bending rotation (or slope) $\theta$. In the present formulation, it is assumed that: (i) the beam material is isotropic, homogeneous and linearly elastic; (ii) the vibration amplitudes of the beam are sufficiently small; (iii) the cross-sections initially normal to the neutral axis of the beam remain plane, but no longer normal to that axis during bending; (iv) the normal inertia and damping of the foundation are negligible; and (v) bonding between the beam and the foundation is perfect.
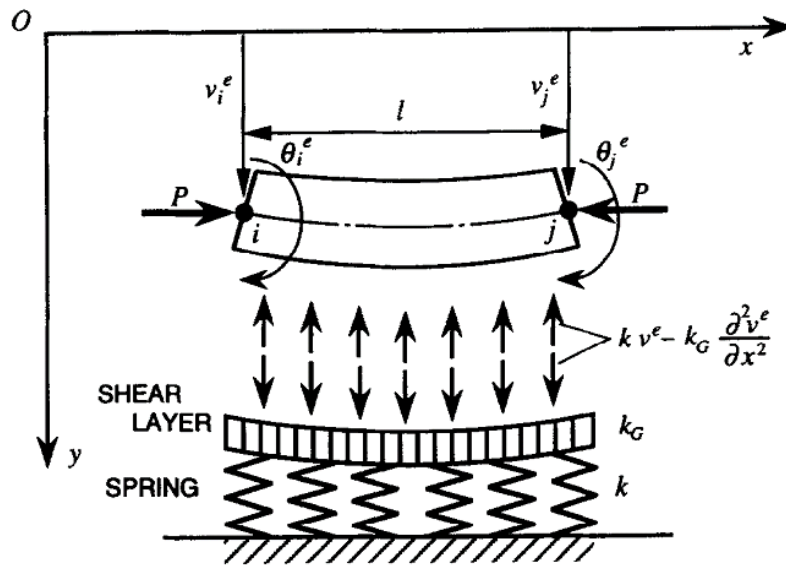


**Figure 2.7.2. Timoshenko beam element with an axial force, resting on Pasternak-type elastic foundation.**

The strain energy $U$ of the beam of length $L$ including the effects of both transverse shear deformation and elastic foundation may be written as

$$U = \frac{1}{2}\int_0^L EI\left(\frac{\partial\theta}{\partial x}\right)^2 dx + \frac{1}{2}\int_0^L \kappa'GA\left(\frac{\partial v}{\partial x}-\theta\right)^2 dx$$
$$+ \frac{1}{2}\int_0^L k(v)^2 dx + \frac{1}{2}\int_0^L k_G\left(\frac{\partial v}{\partial x}\right)^2 dx$$

(2.7.1)

where $E$ is Young's modulus; $I$ the second moment of area; $\kappa'$ the shear coefficient depending on the shape of the cross-section (see Cowper, 1996); $G$ the

shear modulus; $A$ the cross-sectional area; and $x$ the local coordinate along the axis of the beam element.

The kinetic energy $T$ of the beam allowing for the rotatory inertia effect is given by

$$U = \frac{1}{2}\int_0^L \rho A \left(\frac{\partial v}{\partial t}\right)^2 dx + \frac{1}{2}\int_0^L \rho I \left(\frac{\partial \theta}{\partial t}\right)^2 dx \qquad (2.7.2)$$

in which $\rho$ is the mass density of the beam material, and $t$ is the time.

The $W$ work done by a compressive axial force $P$ (positive in tension) can be represented as

$$W = -\frac{1}{2}P\int_0^L \left(\frac{\partial v}{\partial x}\right)^2 dx \qquad (2.7.3)$$

Summation of the individual energies and the work over the entire beam-column using Eqs. (2.7.1)-(2.7.3) gives the total potential energy is given by

$$\Pi = U - T + W \qquad (2.7.4)$$

Taking variation the governing equation for Timoshenko beam-column partially supported on Pasternak elastic foundation can be evaluated as

$$EI\frac{\partial^2\theta}{\partial x^2} - \kappa'GA\left(\theta - \frac{\partial v}{\partial x}\right) + \rho I\frac{\partial^2\theta}{\partial t^2} = 0 \qquad (2.7.5a)$$

$$\kappa'GA\left(\frac{\partial^2 v}{\partial x^2} - \frac{\partial \theta}{\partial x}\right) - kv + k_G\frac{\partial^2 v}{\partial x^2} - P\frac{\partial^2 v}{\partial x^2} + \rho A\frac{\partial^2 v}{\partial t^2} = 0 \qquad (2.7.5b)$$

If the assembled displacement assumed to be harmonic in time with circular frequency $\omega$, i.e. $v(x,t) = v(x)e^{i\omega t}$ and $\theta(x,t) = \theta(x)e^{i\omega t}$, after incorporation of the appropriate end conditions, Eqs. (2.7.5) becomes an eigenvalue problem of the form

$$EI\frac{d^2\theta}{dx^2} - \kappa'GA\left(\theta - \frac{dv}{dx}\right) + \rho I\omega^2\theta = 0 \qquad (2.7.6a)$$

$$\kappa'GA\left(\frac{d^2v}{dx^2} - \frac{d\theta}{dx}\right) - kv + k_G\frac{d^2v}{dx^2} - P\frac{d^2v}{dx^2} + \rho A\omega^2 v = 0 \qquad (2.7.6b)$$

Nondimensionalizing all the length quantities in Eqs. (2.7.6) by the length of the column $l$, and following mechanical and geometric properties of the Timoshenko beam used by Cheng and Pantelides (1988) are chosen for the analysis: Poisson's ratio: $\nu = 1/4$ (or $G/E = 2/5$), shear coefficient: $\kappa' = 2/3$ (for rectangular cross-section), slenderness ratio: $L/r_g = 10$, we get

$$\frac{d^2\theta}{dX^2} - \frac{80}{3}\left(\theta - \frac{1}{L}\frac{dV}{dX}\right) + \frac{1}{100}c^2\theta = 0 \qquad (2.7.7a)$$

$$\frac{80}{3}\left(\frac{\partial^2 V}{\partial X^2} - L\frac{\partial\theta}{\partial X}\right) - \lambda\pi^4 V + \lambda_G\pi^2\frac{\partial^2 V}{\partial X^2} - P_r\pi^2\frac{\partial^2 V}{\partial X^2} + c^2 V = 0 \qquad (2.7.7b)$$

where

$$V = \frac{v}{L}, \quad X = \frac{x}{L}, \quad \lambda = \frac{kL^4}{\pi^4 EI}, \quad \lambda_G = \frac{k_G L^2}{\pi^2 EI}, \quad P_r = \frac{PL^2}{\pi^2 EI}, \quad c^2 = \frac{\rho AL^4}{EI}\omega^2 \qquad (2.7.8)$$

The boundary conditions can be divided into the following two kinds:

clamped (C):

$$V = 0, \quad \theta = 0 \qquad (2.7.9)$$

Hinged (H):

$$V = 0, \quad \frac{d\theta}{dX} = 0 \qquad (2.7.10)$$

at the extremity $X = 0,1$.

Alternatively, when the shear deformation parameter $\phi = \partial V/\partial X$ is set equal to zero and the rotatory inertia mass $\rho I$ is neglected, the resulting model is identical to the classical Euler-Bernoulli beam-column model on Pasternak elastic foundation used by Karamandilis and Prakash (1989).

$$\frac{d^4V}{dX^4} - \lambda \pi^4 V + \lambda_G \pi^2 \frac{d^2V}{dX^2} - P_r \pi^2 \frac{d^2V}{dX^2} = -c^2 V \qquad (2.7.11)$$

## 2.7.3 Approach by spline collocation method

Since the governing equation of a Timoshenko beam-column partially supported on Pasternak elastic foundation is a second-order ordinary differential equation (ODE), the solution of the governing ODE can be approximated by the spline functions with polynomial at least fifth degree. A cubic spline functions (CSFs) is a piecewise third degree polynomial which is belonging to $C^3$.

Considering a set of equi-spaced knots is selected in a normalized interval $X \in [0,1]$, i.e.,

$$X_0 = 0, \quad X_n = 1, \quad X_{j+1} - X_j = h, \quad j = 0,\ldots,n-1 \qquad (2.7.12)$$

where $h$ is distance of equi-spaced knots. In order to apply the SCM, one needs to extend two added knots (fictitious) $X_{-1}$ and $X_{n+1}$ at each end of beam, respectively (Figure 2.7.3).
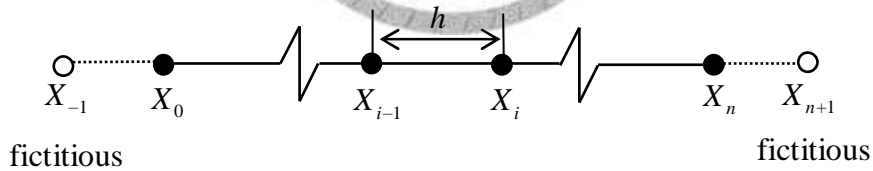


**Figure 2.7.3 Partitions of beam into $n$ sections with one added knots at each end.**

Then the uniform beams on Pasternak elastic foundation for flexural vibration can be approximated by using the CSF (Prenter, 1975) as follows

$$V(X) = \sum_{i=-1}^{n+1} B_i(X) a_i \qquad (2.7.13a)$$

$$\theta(X) = \sum_{i=n+2}^{2n+5} B_i(X) a_i \qquad (2.7.13b)$$

where $c_i$ s are the coefficients to be determined and $B_i(X)$ is QSF.

Substituting Eqs. (2.8.13), into the governing equations in Eqs. (2.8.7) can obtain

$$\frac{1}{L}\sum_{i=-1}^{n+1} B_i'(X)a_i + \sum_{i=n+2}^{2n+5}\left[ B_i''(X) - \frac{80}{3}B_i(X) + \frac{1}{100}c^2 B_i(X)\right]a_i = 0 \tag{2.7.14a}$$

$$\sum_{i=-1}^{n+1}\left[ \frac{80}{3}B_i''(X) - \lambda\pi^4 B_i(X) + \lambda_G\pi^2 B_i''(X) - P_r\,\pi^2 B_i''(X) + c^2 B_i(X)\right]a_i$$
$$-\frac{80}{3}L\sum_{i=n+2}^{2n+5} B_i(X)a_i = 0 \tag{2.7.14b}$$

Similarly, the two kinds of boundary conditions in Eq. (2.7.9) and Eq. (2.7.10) to Eqs. (2.7.13) can obtain,

clamped (C):

$$\sum_{i=-1}^{n+1} B_i(X)a_i = 0, \qquad \sum_{i=n+2}^{2n+5} B_i(X)a_i = 0 \tag{2.7.15}$$

Hinged (H):

$$\sum_{i=-1}^{n+1} B_i(X)a_i = 0, \qquad \sum_{i=n+2}^{2n+5} B_i'(X)a_i = 0 \tag{2.7.16}$$

In general, after substituting the coordinates of the $n+1$ knots, $X_i$, $i = 0,1,\ldots,n$, into the Eqs. (2.7.14), and coupling the four given boundary conditions in Eq. (2.7.15) and Eq. (2.7.16) at the ends, $X_0$ and $X_n$, one obtains the following simultaneous equations.

$$\begin{bmatrix} \text{1st B.C. at } X_0 \\ \text{2nd B.C. at } X_0 \\ \text{1st B.C. at } X_n \\ \text{2nd B.C. at } X_n \\ \frac{1}{L}\sum_{i=-1}^{n+1} B_i'(X_0)a_i + \sum_{i=n+2}^{2n+5}\left[ B_i''(X_0) - \frac{80}{3}B_i(X_0) + \frac{1}{100}c^2 B_i(X_0)\right]a_i \\ \sum_{i=-1}^{n+1}\left[ \frac{80}{3}B_i''(X_0) - \lambda\pi^4 B_i(X_0) + \lambda_G\pi^2 B_i''(X_0) - P_r\,\pi^2 B_i''(X_0) + c^2 B_i(X_0)\right]a_i - \frac{80}{3}L\sum_{i=n+2}^{2n+5} B_i(X_0)a_i \\ \vdots \\ \frac{1}{L}\sum_{i=-1}^{n+1} B_i'(X_n)a_i + \sum_{i=n+2}^{2n+5}\left[ B_i''(X_n) - \frac{80}{3}B_i(X_n) + \frac{1}{100}c^2 B_i(X_n)\right]a_i \\ \sum_{i=-1}^{n+1}\left[ \frac{80}{3}B_i''(X_n) - \lambda\pi^4 B_i(X_n) + \lambda_G\pi^2 B_i''(X_n) - P_r\,\pi^2 B_i''(X_n) + c^2 B_i(X_n)\right]a_i - \frac{80}{3}L\sum_{i=n+2}^{2n+5} B_i(X_n)a_i \end{bmatrix} = \mathbf{0} \tag{2.7.17}$$

Matrix equations in Eq. (2.7.17) of the following form

$$[K]\{a\} - \lambda\pi^4[K_{f1}]\{a\} + \lambda_G\pi^2[K_{f2}]\{a\} - P_r[K_g]\{a\} + c^2[M]\{a\} = 0 \qquad (2.7.18)$$

where $[K]$, $[K_{f1}]$, $[K_{f2}]$, $[K_g]$, and $[M]$ are the elastic stiffness matrix, first-parameter foundation stiffness matrix, second-parameter foundation stiffness matrix, geometric stiffness matrix, and consistent mass matrix respectively. $c$ is the frequency parameter (eigenvalue). Eq. (2.7.18) can be solved using any standard algorithm to obtain eigen-values and eigen-vectors

## 2.7.4 Numerical Examples and Discussions

In order to check the validity of the present technique described in the previous section, several examples of the transverse vibrations of beam-columns supported on elastic foundations were considered.

The individual parameter may be dropped when the associated effect is neglected. Consequently, the computer program developed may be widely applied to various cases of: (i) Euler-Bernoulli beam; (ii) Timoshenko beam; (iii) Euler-Bernoulli beam-column; (iv) Timoshenko beam-column; (v) Euler-Bernoulli beam-column on a Winkler foundation; (vi) Timoshenko beam-column on a Winkler foundation; (vii) Euler-Bernoulli beam-column on Pasternak elastic foundation; (viii) Timoshenko beam-column on Pasternak elastic foundation; and so on. The effect of the partial elastic foundation on the natural frequencies of the Timoshenko beam-columns, as well as the Euler-Bernoulli beam-columns, was previously examined by the author (1991). In the following, only a fully supported beam or beam-column is considered.

### 2.7.4.1 Euler-Bernoulli beam-columns

The first example is concerned with the conventional beam-columns or the classical Euler-Bernoulli beam-columns on the Winkler and Pasternak elastic foundations. Two kinds of end conditions, i.e. hinged-hinged and hinged-clamped ends are considered in

this study. The choice of the buckling load parameter $P_r$, and the Winkler foundation parameter $\lambda$, is based on Cheng and Pantelides' examples (1988). The value of the shear foundation parameter $\lambda_G$ is taken from Valsangker and Pradhanang's work (1988).

Tables 2.7.1 and 2.7.2, respectively, show a comparison between the present numerical results, finite element method (FEM) and the exact ones for the lowest three frequency parameters of the beams and beam-columns without elastic foundations.

**Table 2.7.1 Frequency parameter $c$ for Euler-Bernoulli beams without elastic foundation ($\lambda = \lambda_G = 0$, $P_r = 0.0$).**

| Mode no. | Hinged-hinged | | | Hinged-clamped | | |
|---|---|---|---|---|---|---|
| | Exact[a] | FEM[b] | SCM[c] | Exact[a] | FEM[b] | SCM[c] |
| 1 st | 9.87 | 9.87 | 9.870 | 15.42 | 15.42 | 15.418 |
| 2 nd | 39.48 | 39.49 | 39.480 | 49.96 | 49.99 | 49.967 |
| 3 rd | 88.83 | 88.94 | 88.835 | 104.25 | 104.43 | 104.26 |

[a] Timoshenko *et al.* (1974); [b] Yokoyamat (1996), 8 elements; [c] 201 knots

**Table 2.7.2 Frequency parameter $c$ for Euler-Bernoulli beams without elastic foundation ($\lambda = \lambda_G = 0$, $P_r = 0.6$).**

| Mode no. | Hinged-hinged | | | Hinged-clamped | | |
|---|---|---|---|---|---|---|
| | Exact[a] | FEM[b] | SCM[c] | Exact[a] | FEM[b] | SCM[c] |
| 1 st | 6.24 | 6.24 | 6.242 | 13.01 | 13.01 | 13.007 |
| 2 nd | 36.40 | 36.41 | 36.399 | 47.35 | 47.38 | 47.356 |
| 3 rd | 85.81 | 85.93 | 85.823 | 101.54 | 101.73 | 101.55 |

[a] Timoshenko *et al.* (1974); [b] Yokoyamat (1996), 8 elements; [c] 201 knots

In Table 2.7.2, the exact solutions for the hinged-hinged beam-column were calculated directly from the analytical closed-form expression derived by Cheng and Pantelides (1988) using their "first approach", and the exact solutions for the hinged-clamped beam-column were obtained by solving the frequency equation derived by Bokaian (1988). The eight-element solutions clearly converge from above to the exact ones. A comparison of Tables 2.7.1 and 2.7.2 reveals that, as anticipated, the compressive axial force reduces all modes of natural frequencies of the beams. The reduction in the fundamental frequency of the hinged-clamped beam is less than that of the hinged-hinged beam. This is due to the fact that the critical buckling load for the

hinge-clamped beam is given by $P_{cr} = 2.046(\pi^2 EI/L^2)$, and hence the buckling load

parameter is practically reduced to $P_r = 0.3$ (normalized with respect to $P_{cr}$) for the

hinged- clamped beam under study.

Tables 2.7.3 and 2.7.4 list the numerical results for the lowest three frequency

parameters of the beam-columns on the Winkler and Pasternak elastic foundations. In

contrast to the effect of the compressive axial forces, the presence of the elastic

foundations increases the natural frequencies, especially the fundamental frequencies of

the beam-columns. The frequency parameters for the beam-column on the Pasternak

model in Table 2.7.4 are higher than those on the Winkler model in Table 2.7.3. This is

attributed to the stiffening effect (equivalent to that of a tensile axial force in the

beam-column) caused by the shear layer of the Pasternak model.

**Table 2.7.3 Frequency parameter $c$ for Euler-Bernoulli beams on Winkler elastic foundation ($\lambda = 0.6$, $\lambda_G = 0$, $P_r = 0.6$).**

| Mode no. | Hinged-hinged | | | Hinged-clamped | | |
|---|---|---|---|---|---|---|
| | Exact[a] | FEM[b] | SCM[c] | Exact[a] | FEM[b] | SCM[c] |
| 1 st | 9.87 | 9.87 | 9.8697 | — | 15.09 | 15.087 |
| 2 nd | 37.19 | 37.20 | 37.193 | — | 47.99 | 57.969 |
| 3 rd | 86.15 | 86.27 | 86.163 | — | 102.02 | 101.84 |

[a] Timoshenko *et al.* (1974); [b] Yokoyamat (1996), 8 elements; [c] 201 knots

**Table 2.7.4 Frequency parameter $c$ for Euler-Bernoulli beams on Pasternak elastic foundation ($\lambda = 0.6$, $\lambda_G = 1$, $P_r = 0.6$).**

| Mode no. | Hinged-hinged | | | Hinged-clamped | | |
|---|---|---|---|---|---|---|
| | Exact[a] | FEM[b] | SCM[c] | Exact[a] | FEM[b] | SCM[c] |
| 1 st | — | 13.96 | 13.958 | — | 18.48 | 18.479 |
| 2 nd | — | 42.11 | 42.107 | — | 52.21 | 52.196 |
| 3 rd | — | 91.21 | 91.108 | — | 106.47 | 106.30 |

[a] Timoshenko *et al.* (1974); [b] Yokoyamat (1996), 8 elements; [c] 201 knots

Figure 2.7.4 indicates the plots of the lowest three mode shapes for the

Euler-Bernoulli beams with hinged-hinged and hinged-clamped ends given in Table

2.7.1. It is observed that the mode shapes as well as the frequency parameters are

greatly influenced by the end conditions. It should, however, be noted that, for the beam

or beam-columns with hinged-hinged ends in Tables 2.7.1-2.7.4, the $n$ th mode shape or the $n$ th eigen-function is expressed by $\sin(n\pi x/L)$ ($n = 1, 2,\ldots$) and hence, remains the same for different values of the axial load and the elastic foundation parameters. The mode shapes corresponding to the hinged-clamped beam-columns in Tables 2.7.2-2.7.4 are hardly affected by the presence of the axial forces or the elastic foundations under consideration, and are therefore not shown here.
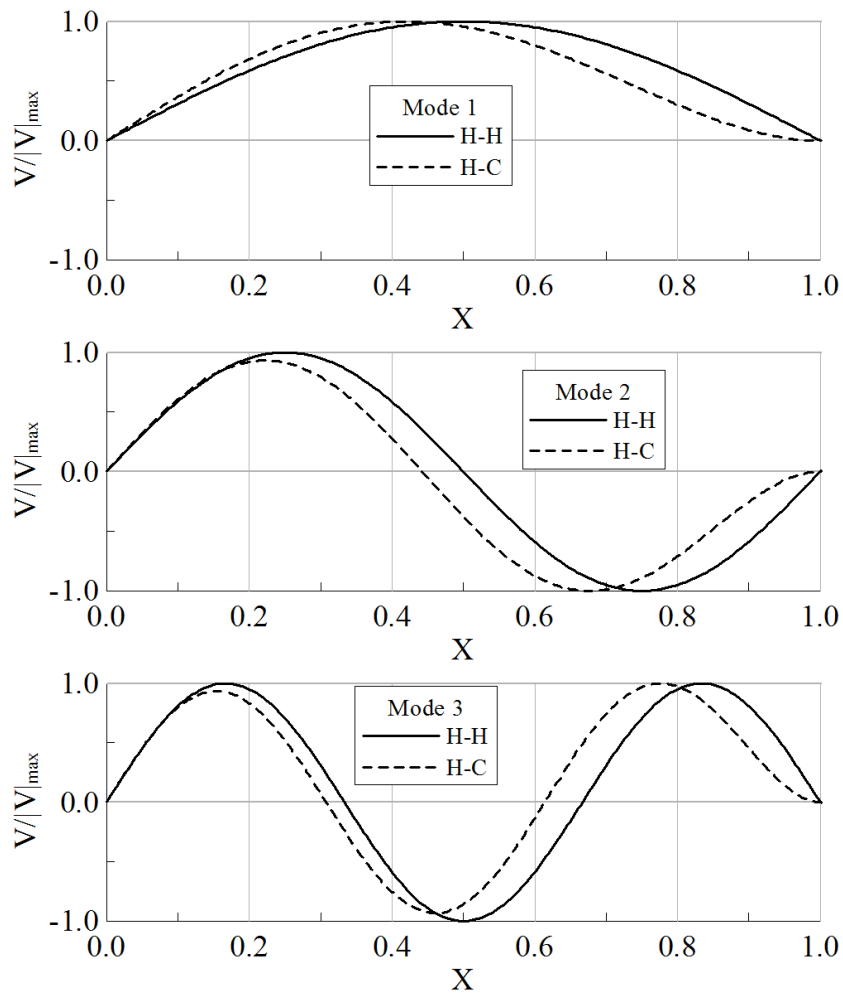


**Figure 2.7.4 Lowest three mode shapes for Euler-Bernoulli beams with hinged-hinged and hinged-clamped ends.**

## 2.7.4.2 Timoshenko beam-columns

The second example deals with the Timoshenko beam-columns having the same two end conditions, resting on the same elastic foundations. Tables 2.7.5 and 2.7.6, respectively, display a comparison between the present solutions, FEM and the exact or

available results for the lowest three frequency parameters of the Timoshenko beams and beam-columns without elastic foundations.

**Table 2.7.5 Frequency parameter $c$ for Timoshenko beams without elastic foundation ($\lambda = \lambda_G = 0$, $P_r = 0.0$).**

| Mode no. | Hinged-hinged | | | Hinged-clamped | | |
|---|---|---|---|---|---|---|
| | Exact[a] | FEM[c] | SCM[d] | Exact[b] | FEM[c] | SCM[d] |
| 1 st | 8.21 | 8.22 | 8.215 | 10.63 | 10.63 | 10.627 |
| 2 nd | 24.23 | 24.31 | 24.230 | 25.62 | 25.71 | 25.618 |
| 3 rd | 41.54 | 41.96 | 41.548 | 42.03 | 42.46 | 42.037 |

[a] Cheng and Pantelides (1988); [b] Huang (1961); [c] Yokoyamat (1996), 8 elements; [d] 201 knots

Note: $\nu = 1/4$, $\kappa' = 2/3$, $L/r_g = 10$

**Table 2.7.6 Frequency parameter $c$ for Timoshenko beams without elastic foundation ($\lambda = \lambda_G = 0$, $P_r = 0.6$).**

| Mode no. | Hinged-hinged | | | Hinged-clamped | | |
|---|---|---|---|---|---|---|
| | Exact[a] | FEM[c] | SCM[d] | Exact[b] | FEM[c] | SCM[d] |
| 1 st | 3.47 | 3.47 | 3.467 | 7.32 | 7.33 | 7.325 |
| 2 nd | 19.22 | 19.31 | 19.223 | 20.93 | 21.03 | 20.933 |
| 3 rd | 35.08 | 35.48 | 35.085 | 35.70 | 36.16 | 35.752 |

[a] Cheng and Pantelides (1988); [b] Huang (1961); [c] Yokoyamat (1996), 8 elements; [d] 201 knots

Note: $\nu = 1/4$, $\kappa' = 2/3$, $L/r_g = 10$

In Table 2.7.5, the exact solutions for the hinged-hinged Timoshenko beam were calculated directly from the analytical closed-form expression of Cheng and Pantelides (1988), whereas the exact solutions for the hinged-clamped Timoshenko beam were found by solving the frequency equation given by Huang (1961). The solutions are in excellent agreement with the exact or available results. The reduction in the fundamental frequencies of the Timoshenko beams due to the compressive axial forces is more significant than that of the Euler-Bernoulli beams. The reason for this is that, since the critical buckling loads for the Timoshenko beams are smaller than those for the Euler-Bernoulli beams, the buckling load parameter $P_r$, increases virtually for the Timoshenko beam- columns under study.

Table 2.7.7 provides a comparison between the present results and the exact or

available results for the lowest three frequency parameters of the Timoshenko beam-columns on the Winkler elastic foundation. Good agreement is obtained with increasing number of elements. Table 2.7.8 contains the numerical results for the lowest three frequency parameters of the Timoshenko beam-columns on Pasternak foundation. As in the case of the Euler-Bernoulli beam-columns, the frequency parameters of the Timoshenko beam-columns increase definitely because of the presence of Pasternak elastic foundations.

**Table 2.7.7 Frequency parameter $c$ for Timoshenko beams Winkler elastic foundation ($\lambda = 0.6$, $\lambda_G = 0$, $P_r = 0.6$).**

| Mode no. | Hinged-hinged | | | Hinged-clamped | | |
|---|---|---|---|---|---|---|
| | Exact[a] | FEM[c] | SCM[d] | Exact[b] | FEM[c] | SCM[d] |
| 1 st | 8.21 | 8.22 | 8.215 | 10.46 | 10.49 | 10.481 |
| 2 nd | 20.59 | 20.67 | 20.592 | 22.20 | 22.30 | 22.209 |
| 3 rd | 35.86 | 36.25 | 35.863 | 36.50 | 36.90 | 36.510 |

[a] Cheng and Pantelides (1988); [b] Huang (1961); [c] Yokoyamat (1996), 8 elements; [d] 201 knots
Note: $\nu = 1/4$, $\kappa' = 2/3$, $L/r_g = 10$

**Table 2.7.8 Frequency parameter $c$ for Timoshenko beams Winkler elastic foundation ($\lambda = 0.6$, $\lambda_G = 1$, $P_r = 0.6$).**

| Mode no. | Hinged-hinged | | | Hinged-clamped | | |
|---|---|---|---|---|---|---|
| | Exact | FEM[a] | SCM[b] | Exact | FEM[a] | SCM[b] |
| 1 st | — | 12.64 | 12.638 | — | 14.42 | 14.419 |
| 2 nd | — | 28.10 | 28.028 | — | 29.34 | 29.250 |
| 3 rd | — | 46.34 | 45.927 | — | 46.71 | 46.283 |

[a] Yokoyamat (1996), 8 elements; [b] 201 knots
Note: $\nu = 1/4$, $\kappa' = 2/3$, $L/r_g = 10$

A further comparison of Tables 2.7.1-2.7.4 and 2.7.5-2.7.8, respectively, indicates that the higher mode frequencies of the beams or beam-columns are reduced significantly, owing to the effects of shear deformation and rotatory inertia which make the beam less stiff, regardless of the end conditions, the axial forces and the elastic foundations.

In the following, the effects of shear deformation, rotatory inertia, compressive axial forces and elastic foundations on the mode shapes of vibrations are investigated.

Figure 2.7.5 depicts the lowest three mode shapes for the hinged-clamped Euler-Bernoulli beam in Table 2.7.1 and for the corresponding Timoshenko beam in Table 2.7.4. It is found that the differences in mode shapes due to the influences of shear deformation and rotatory inertia increase with increasing mode number.
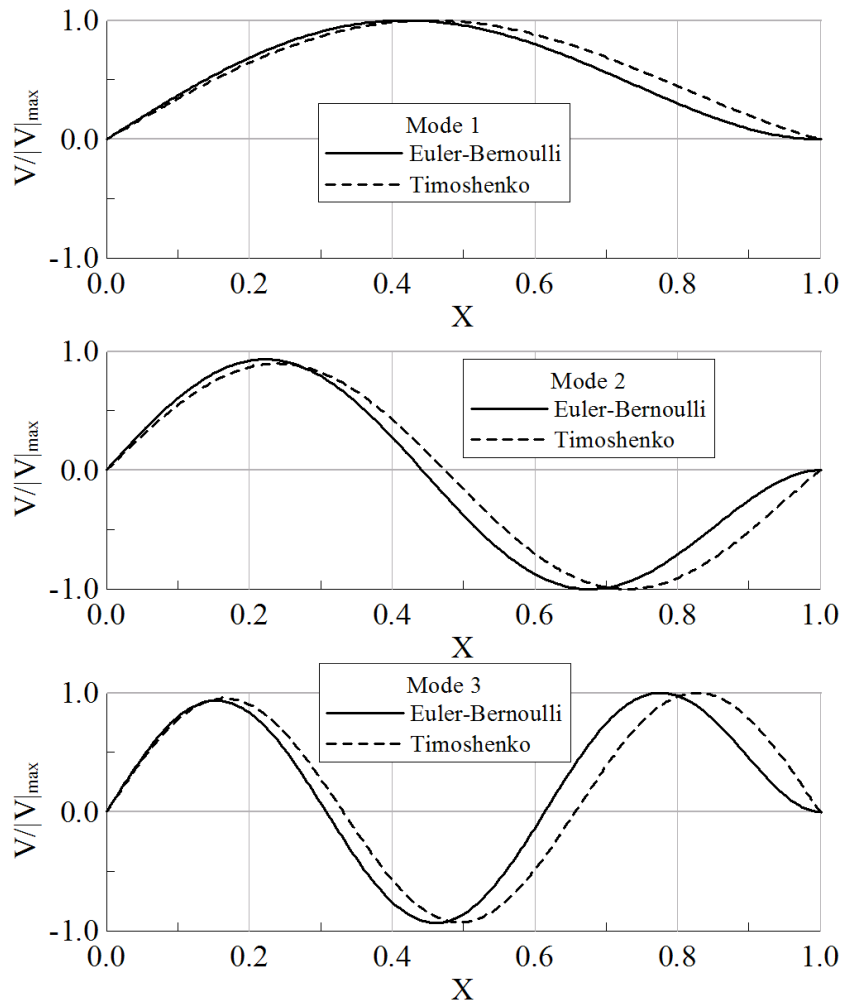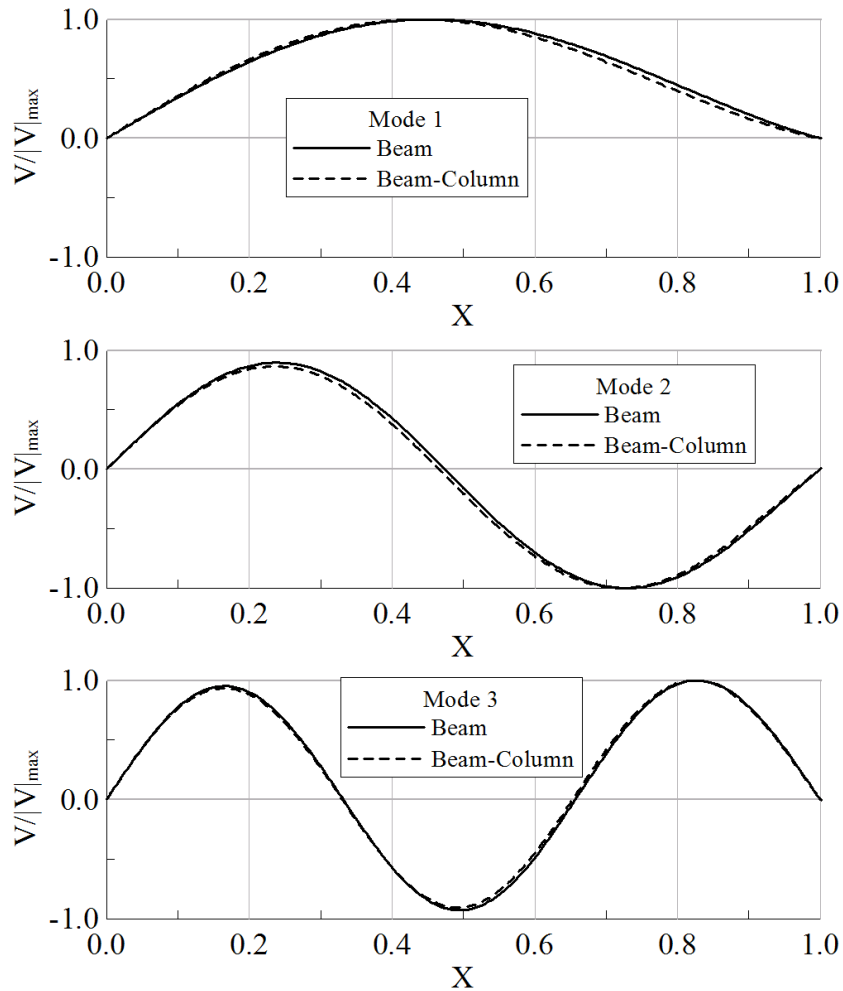


**Figure 2.7.5 Lowest three mode shapes for Euler-Bernoulli beam and Timoshenko beam with hinged-clamped ends.**

Similarly, Figure 2.7.6 represents the lowest three mode shapes for the hinged-clamped Timoshenko beam in Table 2.7.5 and for the corresponding Timoshenko beam-column in Table 2.7.6.

**Figure 2.7.6 Lowest three mode shapes for Timoshenko beam and Timoshenko beam-column with hinged-clamped ends.**

Figure 2.7.7 shows the lowest three mode shapes for the hinged-clamped Timoshenko beam-columns without and with the Pasternak elastic foundation, given in Tables 2.7.6 and 2.7.8, respectively. It can be seen that the effect of the axial forces as well as the elastic foundations on the lowest three mode shape is small, and this effect decreases as the mode number increases.
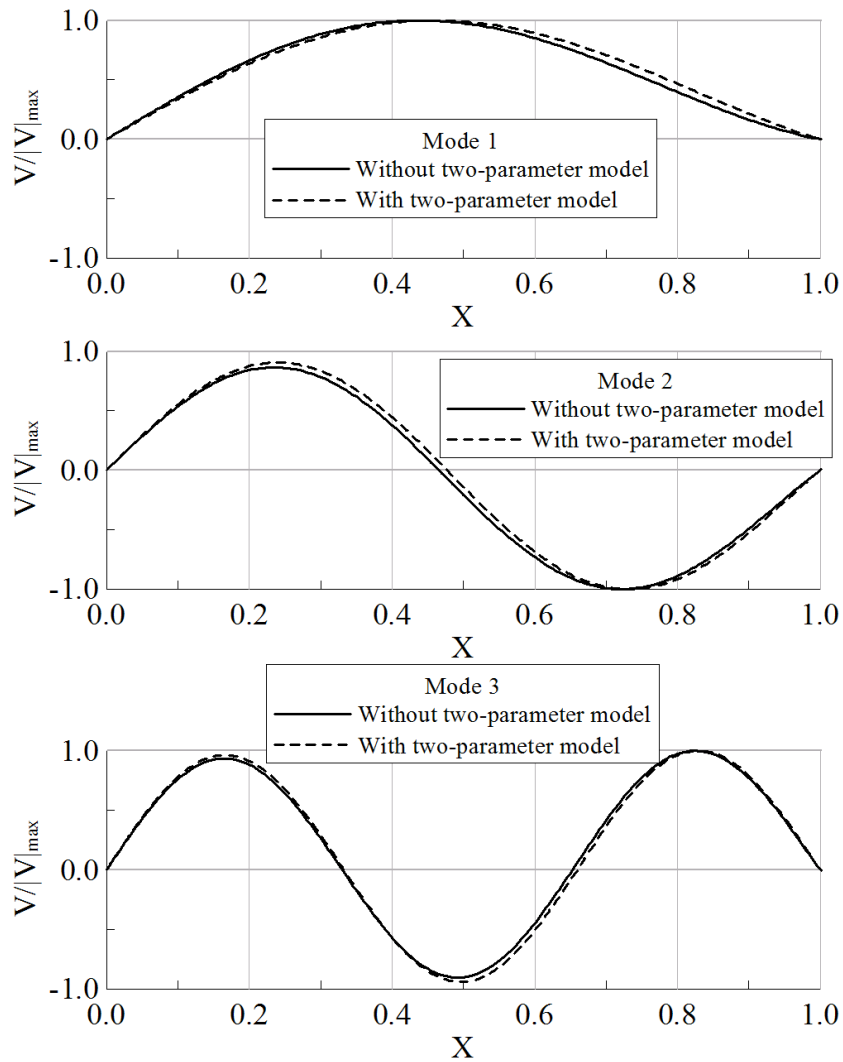
**Figure 2.7.7 Lowest three mode shapes for hinged-clamped Timoshenko beams without and with Pasternak elastic foundation.**

## 2.7.5 Nomenclature

| | |
|---|---|
| *A* | cross-sectional area |
| $B_i(X)$ | quintic spline functions |
| *c* | frequency parameter |
| $c_i$ | coefficients to be determined |
| *E* | Young's modulus |
| *G* | shear modulus |
| *I* | second moment of area |

| | |
|---|---|
| $k$ | Winkler foundation modulus |
| $k_G$ | shear foundation modulus |
| $L$ | length of the beam |
| $P$ | compressive axial force |
| $P_{cr}$ | critical buckling load |
| $P_r$ | buckling load parameter |
| $t$ | time |
| $T$ | kinetic energy |
| $U$ | strain energy of the beam |
| $v$ | lateral displacement |
| $W$ | work |
| $x$ | local coordinate along the axis of the beam element |
| $\theta$ | bending rotation (or slope) |
| $\kappa'$ | shear coefficient depending on the shape of the cross-section |
| $\rho$ | mass density of the beam material |
| $\Pi$ | total potential energy |
| $\omega$ | circular frequency |
| $\lambda$ | Winkler foundation parameter |
| $\lambda_G$ | shear foundation parameter |
| $L/r_g$ | slenderness ratio |
| $\rho I$ | rotatory inertia mass |
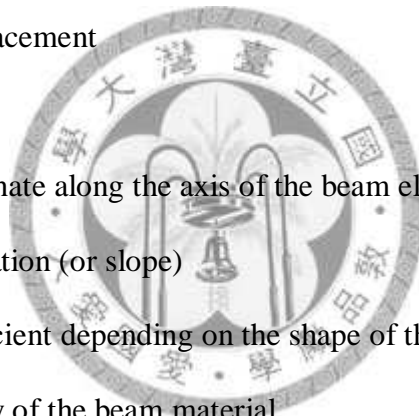
## 2.8 Conclusions

The spline functions in the spline collocation method (SCM) are re-formulated and extended compactly through finite difference approach that can be easily understood and accepted by engineers. The solution of the governing differential equation is approximated in terms of the spline functions multiplied by the corresponding weighting coefficients. The coefficient matrix for the weighting coefficients can be assembled easily by finding then in the spline function. The weighting coefficients can be obtained easily by solving the simultaneous linear algebraic equations because the inverse of the coefficient matrix always exists uniquely solution.

Therefore, the ease of using SCM has been shown. By comparing with exact solutions and other numerical method, it is shown that the analysis of

1. Flexural Vibration Analysis of a Geometrically Nonlinear Beam

2. Elastic Analysis of Rectangular Thin Plates

3. Shear Buckling of Rectangular Thin Plates

4. Buckling Analysis of Rectangular Thin Plates

5. Vibration Analysis of Beams on Pasternak Elastic Foundation

6. Vibration Analysis of Timoshenko Beam-Columns on Pasternak

by the SCM is stable and converged to the correct result. The order of convergence for SCM is approaches 2

Consequently, it is believed that SCM will have more application developed in the dynamic analysis, large deformation analysis, two-dimensional, and three-dimensional problems of engineering problems in near future.

# Chapter 3 Radial Spline Collocation Method

## 3.1 Radial Spline Collocation Method

### 3.1.1 Introduction

Finite element method (FEM) and finite difference method (FDM) are numerical methods commonly used to solve partial differential equation. In the problems of extremely large deformation, remeshing is frequently needed for mesh-based methods but this drawback is not present for the meshless methods. Therefore, many scholars worked for development of the meshless method recently, such as the Smooth Particle Hydrodynamics (SPH) (Gingold and Moraghan, 1977), the Element-Free Galerkin (EFG) method (Belytschko *et al*., 1994), the Reproducing Kernel Particle (RKP) method (Liu *et al*., 1995), the Finite Point (FP) method (Onate *et al*., 1996), the hp-clouds method (Liszka *et al*., 1996), Meshless Local Petrov-Galerkin (MLPG) (Atluri *et al*, 1998, 1999, 2000), Local Boundary Integral Equation (LBIE) (Atluri *et al*., 2000, Zhu *et al*., 1998), and several others.

Meshless methods include two major methods: collocation methods and Galerkin methods. The major difference between these two methods is the non-interpolatory character of the approximation in the Galerkin-based meshless methods. The required computational effort for the collocation methods is much less than that required for the Galerkin-based meshless methods. However, the accuracy of the collocation methods is

less than that of the Galerkin methods, so that more nodes are needed for the collocation

method than those needed for the Galerkin methods to obtain reasonable accuracy of

results.

The radial basis functions (RBFs) are ones of the basis functions in the collocation

methods. Using RBFs for a meshless collocation method to solve PDEs possesses some

advantages: (1) it is mesh-free algorithm; (2) convergence order is independent of

dimension of analyzed domain; (3) different radial basis functions have different

convergence orders for scattered data interpolation. The RBFs have been successfully

developed for interpolation. Frank (1972) compared many RBFs with interpolation

methods, and had showed that the Hardy's multiquadric (MQ) (Hardy, 1971) and

Duchon's thin-plate spline (TPS) were ranked the best in accuracy. Kansa (1999) used

RBFs with collocation to solve PDEs of hyperbolic, parabolic, and elliptic types. Kansa

(1999), and Sharan *et al.* (1997) had shown exponential convergence of Hardy's

multiquadric (MQ) scheme. Wu *et al.* (1993) and Franke *et al.* (1998) provided the

convergence proofs and error estimations in applying the RBFs for scattered data

interpolation and solution of PDEs.

Spline functions, introduced by Schoenberg (1946) for approximation purposes,

were extended to solve differential equations. Commonly, this incorporates the use of

cubic B-splines which were presented by Mizusawa *et al.* (1979) for investigation of

vibration of skew plates, Shen and Wang (1987) for linear static analysis of cylindrical shells, Gupta *et al*. (1991) for linear finite element analysis of axi-symmetric shells and others. Weller (1993) employed B-splines to study post-buckling behavior of infinite length cylindrical panels subjected to combined thermal and mechanical loading, and they were incorporated into collocation method for the same analysis problem.

When spline functions are combined with collocation method which can significantly simplify the solution procedure of differential equations, it is called spline collocation method (SCM) (Prenter, 1975). Recently, researches have been developed, such as Bert and Sheu (1996) for linear static analysis of beam and plates, Wu (2003) for linear static analysis of continuous beam and frame.

The conventional SCM uses equally spaced knots for computation of approximation. However, when load distribution, geometry, material property of structure are discontinuous, it will greatly reduce accuracy. Although it can be resolved by increasing the number of knots, efficiency will decrease and error will increase for calculation. The goal of this paper is to develop radial spline collocation method (RSCM) to improve the disadvantage of equally spaced knots.

The basis functions for governing equation with $n$-th order differential equation must satisfy $C^n$ continuous, so that the $(n+1)$-st order spline function should be derived from $(n+2)$-nd order difference equation. Utilizing the concept of RBF, spline

97

function is transformed into radial spline function (RSF). Therefore RSF can conveniently calculate the values for unequally spaced knots.

## 3.1.2 Radial radial Quintic B-spline function

In order to solve the fourth-order differential equation of beam problem, the basis functions for displacement must be at least $C^4$ continuous. The quintic spline function (QSF) is a polynomial of degree five and continuous up to fourth-order differential. It is derived from sixth-order finite difference equation and expressed as follows (Prenter, 1975)

$$B_i(x)=\frac{1}{h^5}\begin{cases}(x-x_{i-3})^5 & x_{i-3}\le x\le x_{i-2}\\(x-x_{i-3})^5-6(x-x_{i-2})^5 & x_{i-2}\le x\le x_{i-1}\\(x-x_{i-3})^5-6(x-x_{i-2})^5+15(x-x_{i-1})^5 & x_{i-1}\le x\le x_i\\(x-x_{i-3})^5-6(x-x_{i-2})^5+15(x-x_{i-1})^5-20(x-x_i)^5 & x_i\le x\le x_{i+1}\\(x-x_{i-3})^5-6(x-x_{i-2})^5+15(x-x_{i-1})^5-20(x-x_i)^5+15(x-x_{i+1})^5 & x_{i+1}\le x\le x_{i+2}\\(x-x_{i-3})^5-6(x-x_{i-2})^5+15(x-x_{i-1})^5-20(x-x_i)^5+15(x-x_{i+1})^5-6(x-x_{i+2})^5 & x_{i+2}\le x\le x_{i+3}\\0 & \text{otherwise}\end{cases}$$

(3.1.1)

where $h$ is the distance between two consecutive knots. QSF is zero beyond the range between knots $x_{i-3}$ and $x_{i+3}$. Equally spaced knots are used for conventional SCM.

Because QSF is symmetric with respect to $\xi_i$, Equation (3.1.1) can be rewritten as

$$B_i(\xi) = \frac{1}{h^5} \begin{cases} (\xi - \xi_{i-3})^5 & \xi_{i-3} \le \xi \le \xi_{i-2} \\ (\xi - \xi_{i-3})^5 - 6(\xi - \xi_{i-2})^5 & \xi_{i-2} \le \xi \le \xi_{i-1} \\ (\xi - \xi_{i-3})^5 - 6(\xi - \xi_{i-2})^5 + 15(\xi - \xi_{i-1})^5 & \xi_{i-1} \le \xi \le \xi_i \\ (\xi_{i+3} - \xi)^5 - 6(\xi_{i+2} - \xi)^5 + 15(\xi_{i+1} - \xi)^5 & \xi_i \le \xi \le \xi_{i+1} \\ (\xi_{i+3} - \xi)^5 - 6(\xi_{i+2} - \xi)^5 & \xi_{i+1} \le \xi \le \xi_{i+2} \\ (\xi_{i+3} - \xi)^5 & \xi_{i+2} \le \xi \le \xi_{i+3} \\ 0 & \text{otherwise} \end{cases} \tag{3.1.2}$$

If radius is defined as the distance form a certain position $\xi$ to the center position $\xi_i$, shown in Figure 3.1.1, QSF can be transformed into quintic radial spline function (QRSF) as shown in Figure 3.1.2(a).
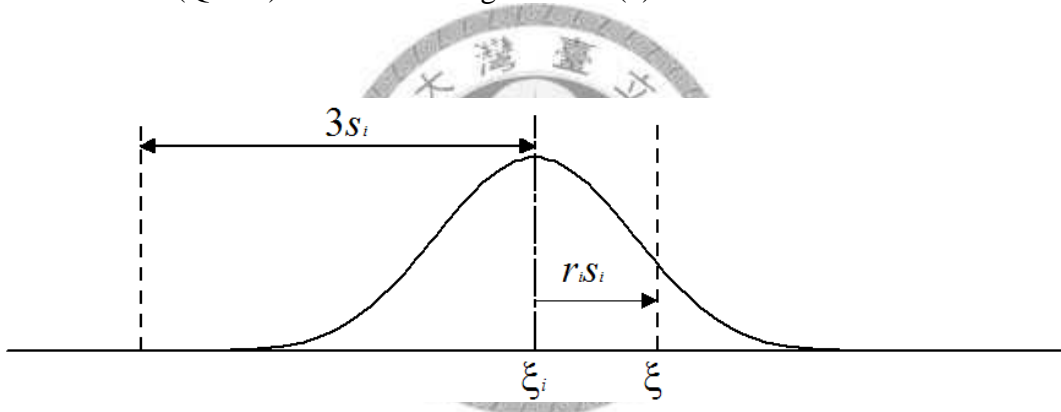


**Figure 3.1.1 Radius and radius of influence for quintic radial spline function.**

$$B_i(\xi) = \begin{cases} (3 - |r_i|)^5 - 6(2 - |r_i|)^5 + 15(1 - |r_i|)^5 & 0 \le |r_i| \le 1 \\ (3 - |r_i|)^5 - 6(2 - |r_i|)^5 & 1 \le |r_i| \le 2 \\ (3 - |r_i|)^5 & 2 \le |r_i| \le 3 \\ 0 & 3 < |r_i| \end{cases} \tag{3.1.3a}$$

$$B_i(\xi_i - \xi) = B_i(\xi - \xi_i) \tag{3.1.3b}$$

where $r_i = (\xi - \xi_i)/s_i$ is the dimensionless radius, $3s_i$ is the radius of influence domain of QRSF at the center position $\xi_i$. The values of QRSF at the knots beyond

the radius of influence domain are zero.

Define $h_i = \xi_{i+1} - \xi_i$ as the distance of knot $\xi_{i+1}$ from knot $\xi_i$. In order to cover at least two neighboring knots at each sides of the center knot $\xi_i$, the radius of influence domain of QRSF at the center position $\xi_i$ is suggested to be least $3s_i > \max(h_{i-2} + h_{i-1}, h_i + h_{i+1})$.

Analogously, the 1st, 2nd, 3rd and 4th order derivatives of QRSF are given as follows

$$B_i'(\xi) = \begin{cases} -5(3-|r_i|)^4 + 30(2-|r_i|)^4 - 75(1-|r_i|)^4 & 0 \le |r_i| \le 1 \\ -5(3-|r_i|)^4 + 30(2-|r_i|)^4 & 1 \le |r_i| \le 2 \\ -5(3-|r_i|)^4 & 2 \le |r_i| \le 3 \\ 0 & 3 < |r_i| \end{cases} \qquad (3.1.14a)$$

$$B_i'(\xi_i - \xi) = -B_i'(\xi - \xi_i) \qquad (3.1.14b)$$

$$B_i''(\xi) = \begin{cases} 20(3-|r_i|)^3 - 120(2-|r_i|)^3 + 300(1-|r_i|)^3 & 0 \le |r_i| \le 1 \\ 20(3-|r_i|)^3 - 120(2-|r_i|)^3 & 1 \le |r_i| \le 2 \\ 20(3-|r_i|)^3 & 2 \le |r_i| \le 3 \\ 0 & 3 < |r_i| \end{cases} \qquad (3.1.15a)$$

$$B_i''(\xi_i - \xi) = B_i''(\xi - \xi_i) \qquad (3.1.15b)$$

$$B_i'''(\xi) = \begin{cases} -60(3-|r_i|)^2 + 360(2-|r_i|)^2 - 900(1-|r_i|)^2 & 0 \le |r_i| \le 1 \\ -60(3-|r_i|)^2 + 360(2-|r_i|)^2 & 1 \le |r_i| \le 2 \\ -60(3-|r_i|)^2 & 2 \le |r_i| \le 3 \\ 0 & 3 < |r_i| \end{cases} \qquad (3.1.16a)$$

$$B_i'''(\xi_i - \xi) = -B_i'''(\xi - \xi_i) \qquad (3.1.16b)$$

$$B_i^{(4)}(\xi) = \begin{cases} 120(3-|r_i|) - 720(2-|r_i|) + 1800(1-|r_i|) & 0 \le |r_i| \le 1 \\ 120(3-|r_i|) - 720(2-|r_i|) & 1 \le |r_i| \le 2 \\ 120(3-|r_i|) & 2 \le |r_i| \le 3 \\ 0 & 3 < |r_i| \end{cases} \qquad (3.1.17a)$$

$$B_i^{(4)}(\xi_i - \xi) = B_i^{(4)}(\xi - \xi_i) \qquad (3.1.17b)$$

Note that $B_i'(\xi)$ and $B_i'''(\xi)$ are anti-symmetric functions, and $B_i''(\xi)$ and $B_i^{(4)}(\xi)$ are symmetric functions as shown in Figures 3.1.2.

QRSF formulas is used to calculate the value of spline function at knot $\xi_j$ where $\xi_j$ is arbitrarily point in the analyzed domain.
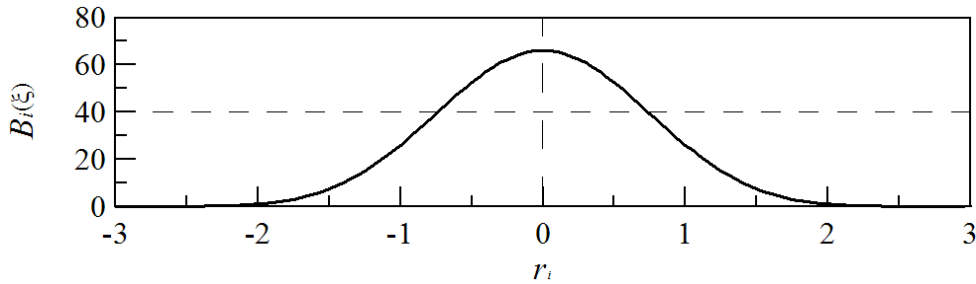


(a) Quintic radial spline function (QRSF)
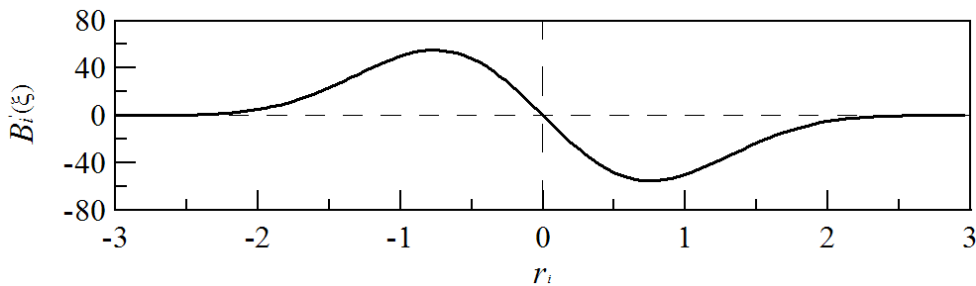


(b) First order derivative of QRSF
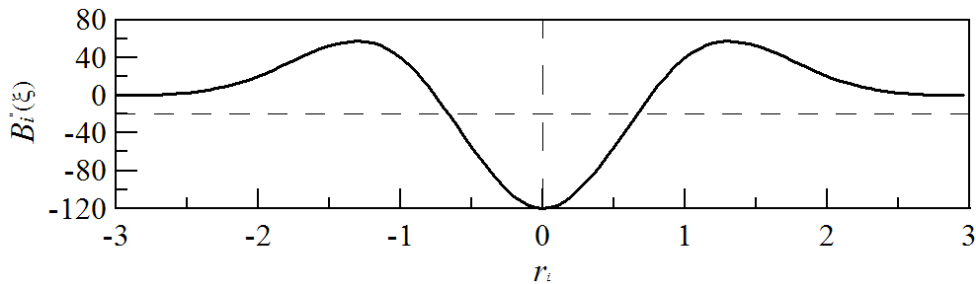


(c) Second order derivative of QRSF

101
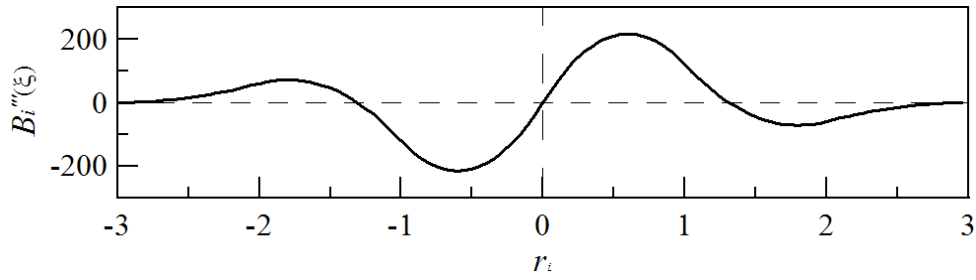
(d) Third order derivative of QRSF
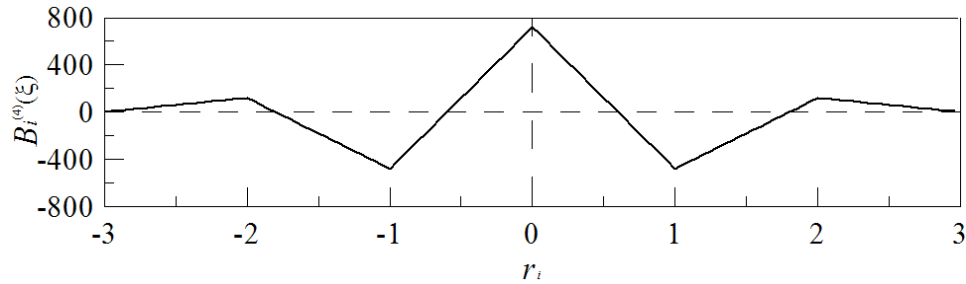


(e) Fourth order derivative of QRSF

**Figure 3.1.2 The quintic radial B-spline function.**

### 3.1.3 Radial Spline Collocation Method

According to SCM (Prenter, 1975), the approximated function by Spline Function

can be shown as

$$w(x) \cong \sum_{i=-m}^{n+m} a_i B_i(x) \qquad (3.1.18)$$

where $B_i(x)$ is Spline Function, $a_i$'s are unknown coefficients, and $m$ is the

number of virtual knots at each end outside the analyzed domain. $m$ is dependent on

the order of the governing differential equation, $m=1$ for 2nd-order and $m=2$ for

4th-order, etc. There are totally $(n+1+2m)$ knots: $(n+1)$ knots in the analyzed

domain and $2m$ virtual knots beyond the analyzed domain.

In this paper, RSF is used as basis function in stead of the spline function. It is

called as Radial Spline Collocation Method (RSCM).

102

In general, RSCM can exactly express the polynomials of any degree depending on the degree of the basis function used. For example, if quintic spline function is used as basis function, RSCM can exactly express the polynomials up to degree five.

Polynomials up to degree five are written as:

$$P_n(x) = x^n, \quad -1 \le x \le 1, \quad n = 0, 1, 2, 3, 4, 5 \tag{3.1.19a}$$

with boundary conditions

$$P_n'(\pm 1) = n(\pm 1)^{n-1}, \quad P_n''(\pm 1) = n(n-1)(\pm 1)^{n-2} \tag{3.1.19b}$$

As shown in Figure 3.1.3, only one knot is needed at each end of the analyzed domain, and two virtual knots beyond the analyzed domain at each end. Consequently, totally six knots are used to represent the polynomials. The knots are spaced unequally with $h_{-2} = h_{-1} = h_1 = h_2 = 0.25$ and $h_0 = 2.00$ where $h_i = x_{i+1} - x_i$. The polynomials are exactly represented by QRSF with six unequally spaced knots. The approximated values of $P_n(x)$ by RSCM are computed at 31 points within the analyzed domain, $-1 \le x \le 1$, using Eq. (3.1.18) and agreed exactly with the polynomials as shown in Figure 3.1.3.
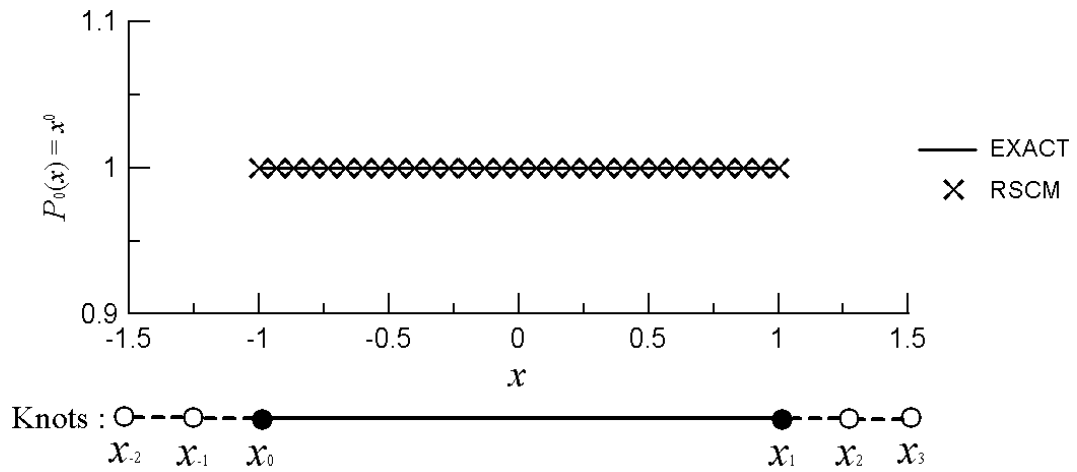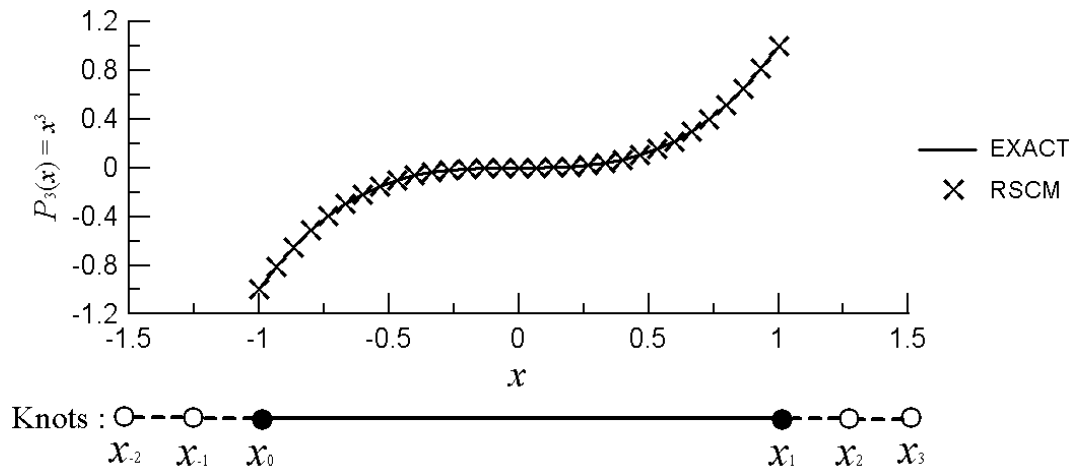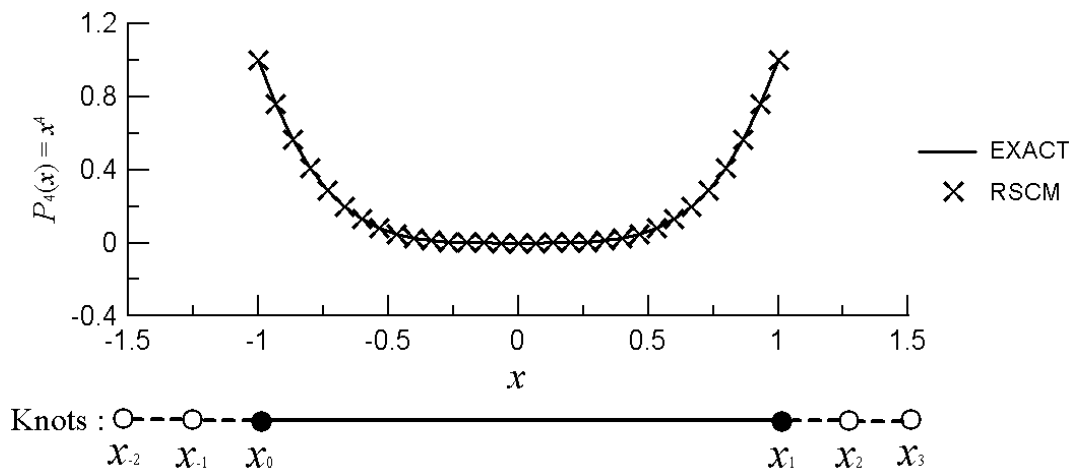
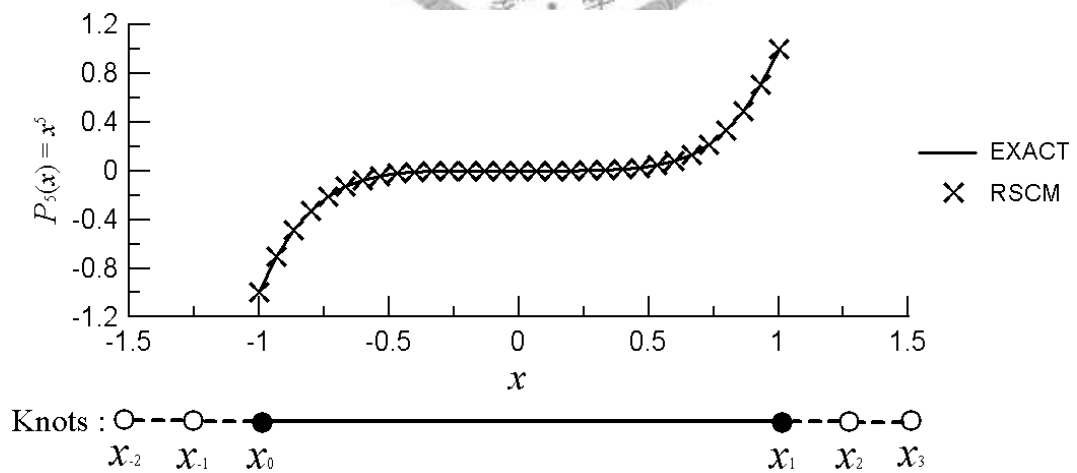(a) polynomial of degree zero
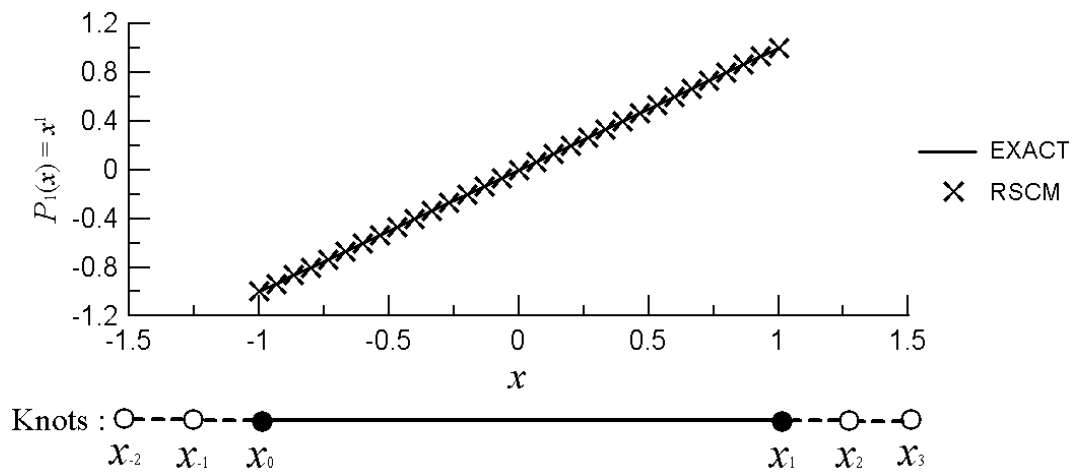


(b) polynomial of degree one
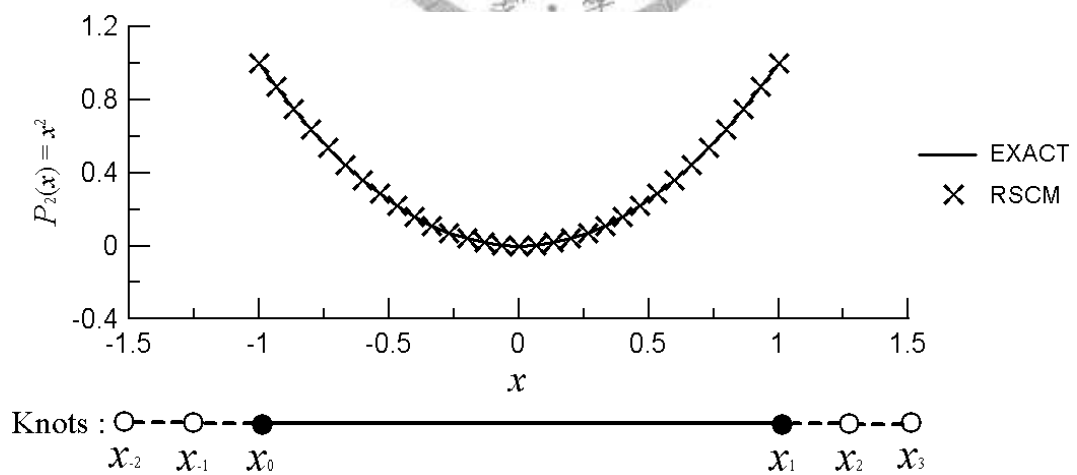


(c) polynomial of degree two

(d) polynomial of degree three



(e) polynomial of degree four



(f) polynomial of degree five

**Figure 3.1.3 Interpolated and exact values of polynomial.**

## 3.2 Static Analysis of Beams

### 3.2.1 Introduction

### 3.2.2 Approach by Radial Spline Collocation Method

The prismatic Bernoulli-Euler Beam is governed by the following fourth-order differential equation:

$$EI\frac{d^4w}{dx^4} = q \quad \text{in domain} \quad \Omega \tag{3.2.1}$$

where $w$ is the transverse deflection, $E$ is the Young's modulus, $I$ is the second moment of sectional area, and $q$ is the distributed load over the beam.

According to RSCM, the deflection of beam can be approximated by Eq. (3.1.18). Therefore, Eq. (3.2.1) can be rewritten as

$$EI\sum_{i=-2}^{n+2} a_i B_i^{(4)}(x) = q(x) \tag{3.2.2}$$

Similarly, the given boundary conditions at global boundary, $\Gamma$, are approximated as

$$w(x_0) = \sum_{i=-2}^{n+2} a_i B_i(x_0) = \overline{w} \qquad \text{on } \Gamma_w \tag{3.2.3a}$$

$$-\frac{dw(x_0)}{dx} = -\sum_{i=-2}^{n+2} a_i B_i^{'}(x_0) = \overline{\theta} \qquad \text{on } \Gamma_\theta \tag{3.2.3b}$$

$$EI\frac{d^2w(x_0)}{dx^2} = EI\sum_{i=-2}^{n+2} a_i B_i^{''}(x_0) = \overline{M} \qquad \text{on } \Gamma_M \tag{3.2.3c}$$

$$-EI\frac{d^3w(x_0)}{dx^3} = -EI\sum_{i=-2}^{n+2} a_i B_i^{'''}(x_0) = \overline{V} \qquad \text{on } \Gamma_V \qquad (3.2.3\text{d})$$

where $M$ and $V$ denote the moment and the shear force, respectively; $\Gamma_w$, $\Gamma_\theta$, $\Gamma_M$ and $\Gamma_V$ denote the boundary regions where deflection, slope, moment, and shear force are specified, respectively.

There are totally $n+5$ independent linear equations: $n+1$ field equations at $n+1$ knots and two boundary conditions at each end of the beam. On the other hand, there are $n+5$ unknown coefficients $a_i$'s to be determined. For the stable structure, unique solution will exist.

### 3.2.3 Numerical Results

Example 1: a simply supported beam with length $L$ is subjected to uniformly distributed load $q$ as shown in Figure 3.2.1.
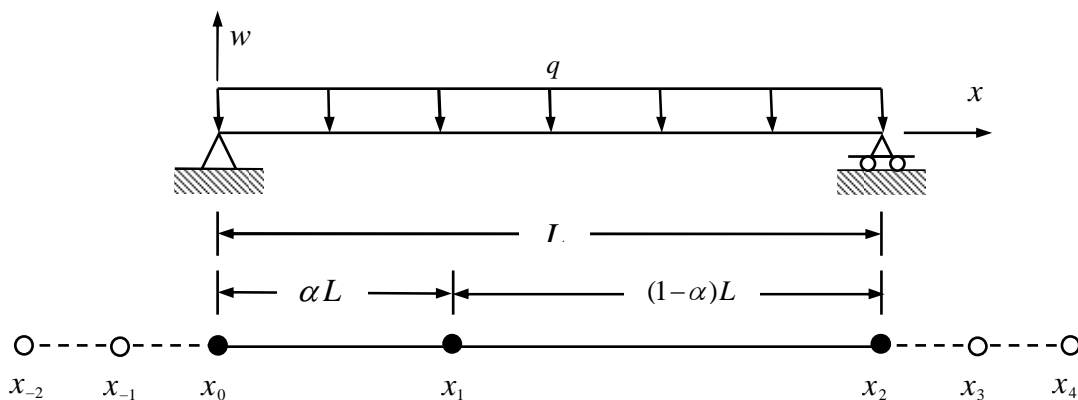


**Figure 3.2.1 Simply supported beam subjected to uniformly distributed load.**

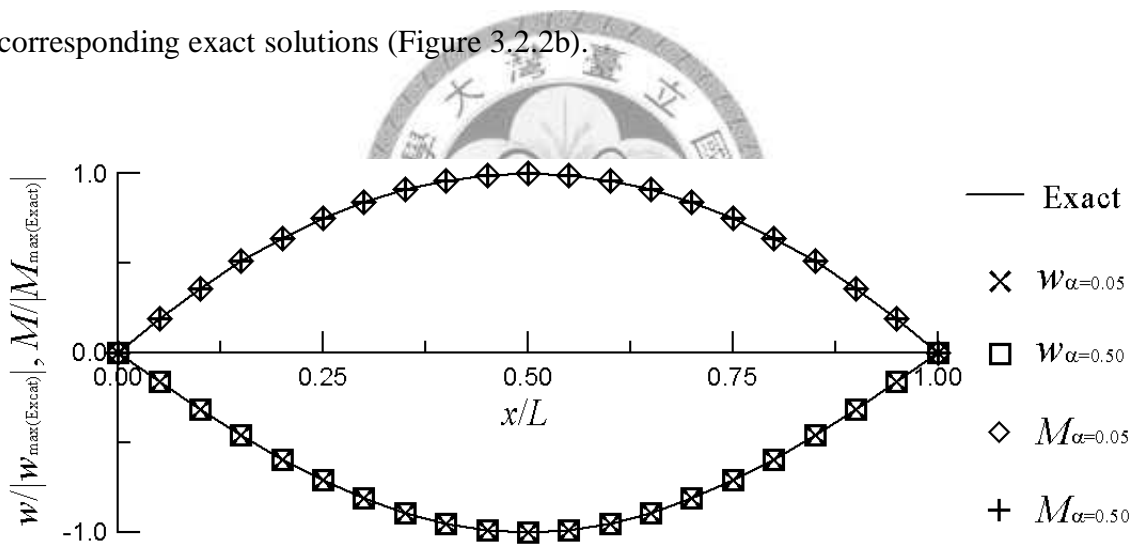The deflection of the beam is approximately represented by QRSF with seven

knots: three in the analyzed domain and four virtual ones beyond the analyzed domain.

The location of the knot $x_1$ is $x = \alpha L$, where $\alpha$ varies from $0.05$ to $0.50$ with

increment $0.05$. The spacing of virtual knots beyond the analyzed domain is $0.5L$.

When $\alpha = 0.50$, those seven knots are equally spaced to be $0.5L$. The dimensionless

deflection and moment diagrams of the beam for both $\alpha = 0.05$ and $\alpha = 0.50$ are

coincided with the corresponding exact ones (Figure 3.2.2a). No matter how $\alpha$ varies

in $(0,1)$, the maximum dimensionless moment and deflection agree with the

corresponding exact solutions (Figure 3.2.2b).



(a) dimensionless deflection and moment diagram
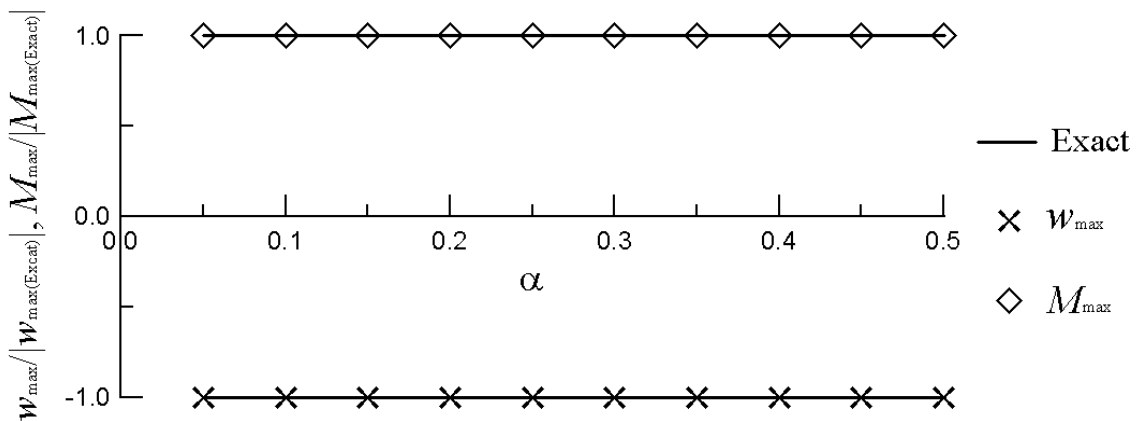


(b) maximum dimensionless deflection and moment

**Figure 3.2.2 Radial Spline Collocation Method and exact solutions.**

108

Example 2: a cantilever beam with length $L$ is subjected to a triangularly distributed load, where the maximum intensity of the distributed load $q$ is at the location $x = 0.25L$ as shown in Figure 3.2.3.
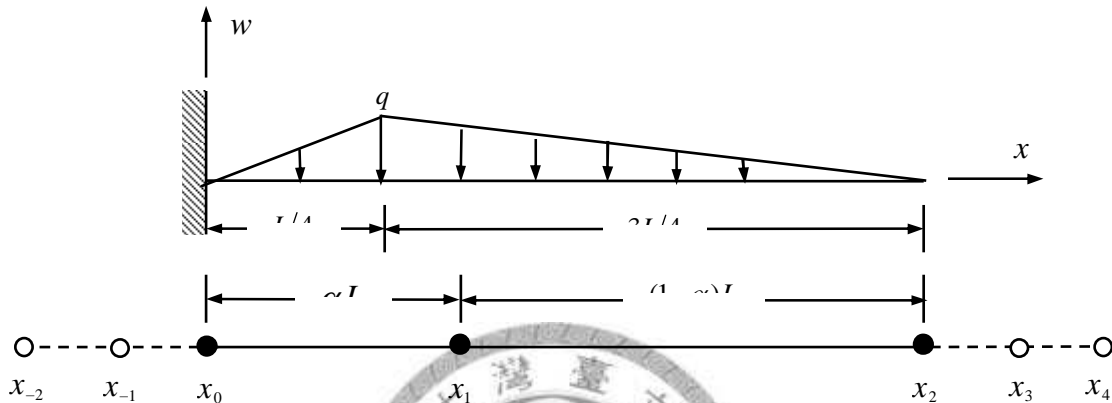


**Figure 3.2.3 Cantilever beam with triangular distributed load on portion of beam.**
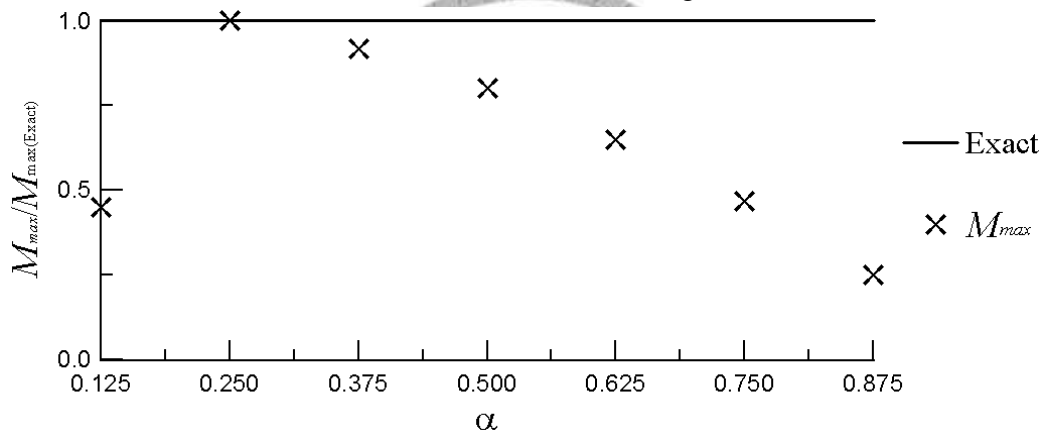
The deflection of the beam is approximately represented by QRSF with seven knots: three in the analyzed domain and four virtual ones beyond the analyzed domain. The location of the knot $x_1$ is $x = \alpha L$, where $\alpha$ varies from 0.125 to 0.875 with increment 0.125. The spacing of virtual knots beyond the analyzed domain is $0.5L$. When $\alpha = 0.5$, the seven knots are equally spaced to be $0.5L$. Comparisons of the dimensionless moment diagrams of the beam for both $\alpha = 0.25$ and $\alpha = 0.50$ are shown in Figure 3.2.4a. The maximum dimensionless moment $(M_{max} / M_{max(Exact)})$ between the RSCM and exact solutions for different values of $\alpha$ are shown in Figure 3.2.4b. When $\alpha = 0.25$ the maximum dimensionless moment is 1.00, because the variation of distributed load can be exactly described. When $\alpha \neq 0.25$, since the

distributed load cannot be described exactly so that error of maximum dimensionless

moment increases with the difference from $\alpha = 0.25$.
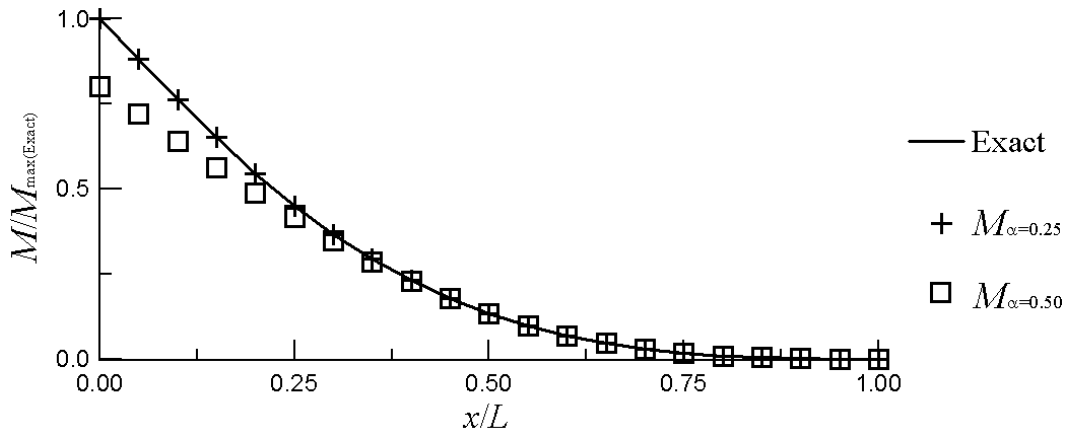


(a) dimensionless moment diagram



(b) maximum dimensionless moment

**Figure 3.2.4 Radial Spline Collocation Method and exact solutions.**

Example 3: a continuous beam of two spans, each span with length $L$, is subjected to uniformly distributed load $q$ as shown in Figure 3.2.5.
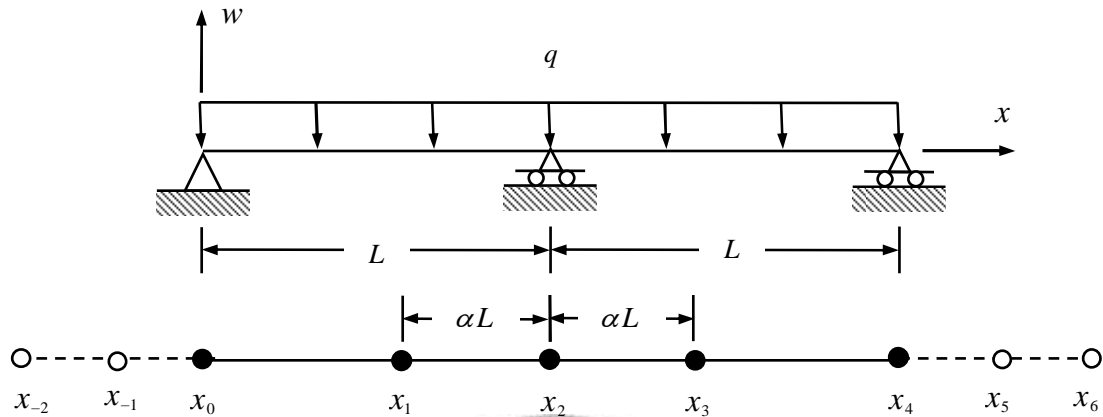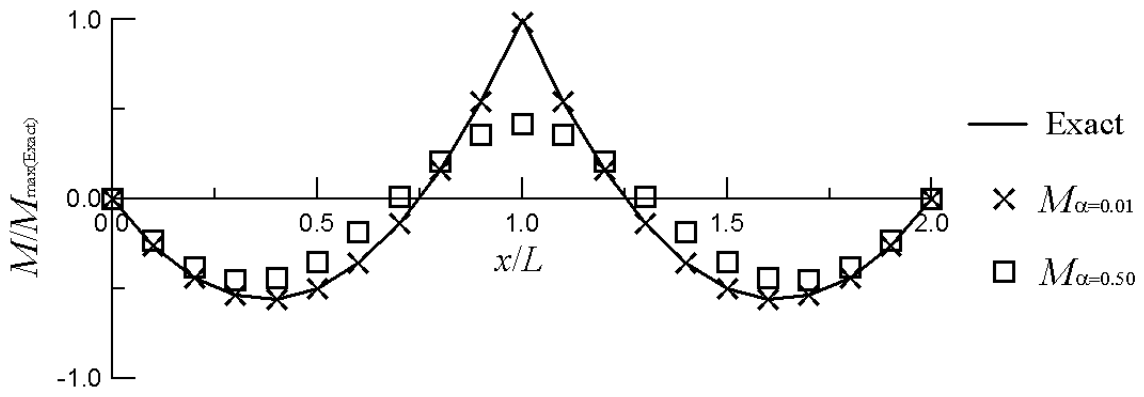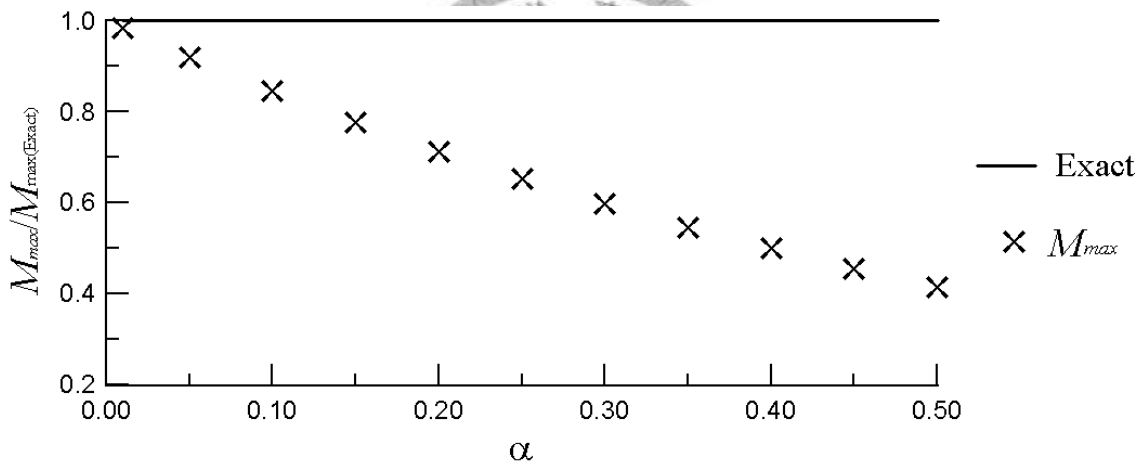


**Figure 3.2.5 Continuous beam subjected to uniformly distributed load.**

The deflection of the beam is approximately represented by QRSF with nine knots: five in the analyzed domain and four virtual ones beyond the analyzed domain. The distances of the knots $x_1$ and $x_3$ from central knot $x_2$ are taken as $\alpha L$ for convenience, where $\alpha$ varies from $0.01$ to $0.50$ with increment $0.05$. The spacing of virtual knots beyond the analyzed domain is $0.5L$. When $\alpha = 0.5$, the nine knots are equally spaced to be $0.5L$. The dimensionless moment diagrams of the beam for both $\alpha = 0.01$ and $\alpha = 0.50$ are shown in Figure 3.2.6a. The maximum dimensionless moment $(M_{max} / M_{max(Exact)})$ between the RSCM and exact solutions for different values of $\alpha$ are shown in Figure 3.2.6b. The agreement between RSCM and exact solutions becomes better and better as $\alpha$ decreases because the shear force at the central knot $x_2$ is discontinuous due to the reaction force. When $\alpha = 0.01$ and

111

$\alpha = 0.25$ , the maximum dimensionless moment are 0.9835 and 0.4150 ,

respectively.



(a) dimensionless moment diagram



(b) maximum dimensionless moment

**Figure 3.2.6 Radial Spline Collocation Method and exact solutions.**

Example 4: a simply supported beam with length $L$ is subjected to a single concentrated load $P$ at the mid-span as shown in Figure 3.2.7.
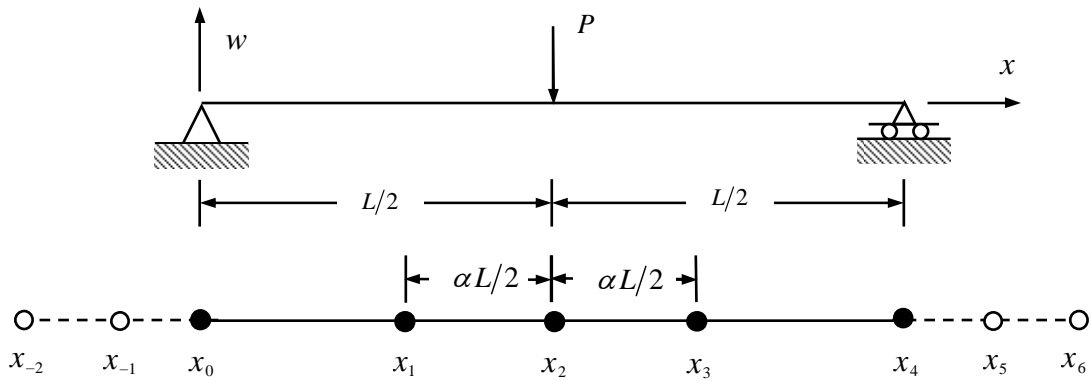


**Figure 3.2.7 Simply supported beam subjected to concentrated load.**

The deflection of the beam is approximately represented by QRSF with nine knots: five in the analyzed domain and four virtual ones beyond the analyzed domain. The distances of the knots $x_1$ and $x_3$ from central knot $x_2$ are $\alpha L/2$, where $\alpha$ varies from $0.01$ to $0.50$ with increment $0.05$. The spacing of virtual knots beyond the analyzed domain is $0.25L$. When $\alpha = 0.25$, the nine knots are equally spaced to be $0.25L$. By using equivalent load concept, the concentrated load at the knot $x_i$ is simulated by an equivalent triangular distributed load where the maximum intensity of distributed load is $q_i = P/h$ and $h_{i-1} = h_i = h$, Figure 3.2.8.
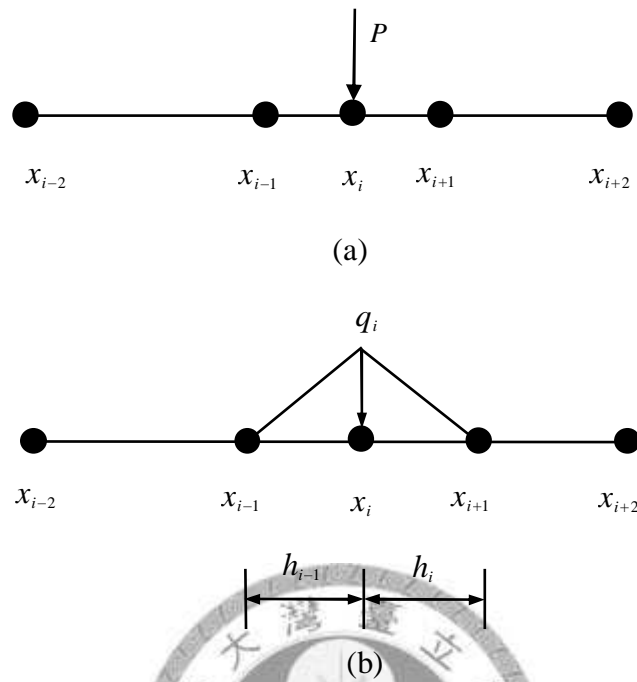
(a)



(b)

**Figure 3.2.8 Equivalent centralization load.**

The dimensionless moment diagrams of the beam for both $\alpha = 0.01$ and $\alpha = 0.25$ are shown in Figure 3.2.9a. The maximum dimensionless moment $(M_{\max} / M_{\max(Exact)})$ between the RSCM and exact solutions for different values of $\alpha$ are shown in Figure 3.2.9b. The agreement between RSCM and exact solutions becomes better as $\alpha$ is decreases, because the shear force at the central knot $x_2$ is discontinuous due to the concentrated load $P$. When $\alpha = 0.01$ and $\alpha = 0.25$ the maximum dimensionless moment are $0.9933$ and $0.8333$, respectively.
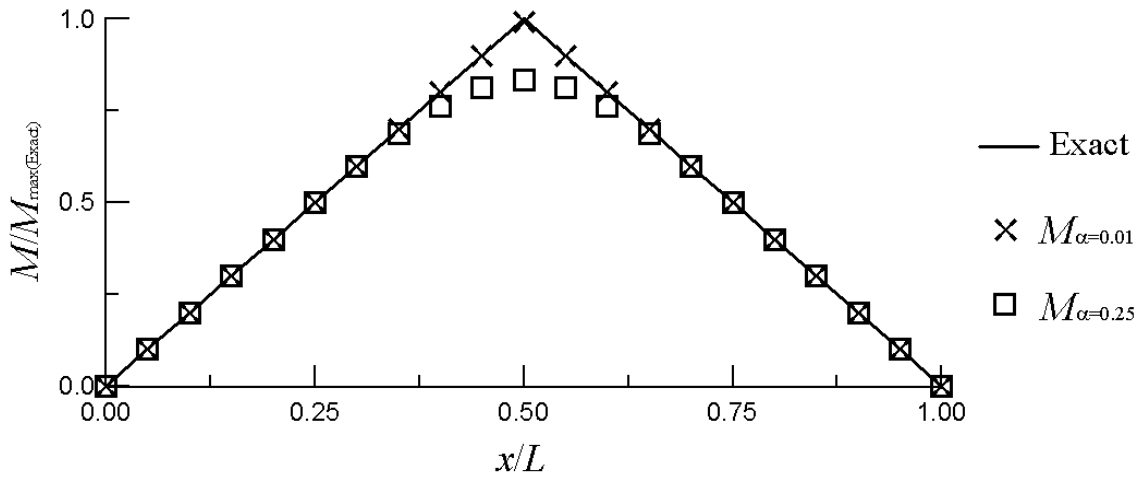
(a) dimensionless moment diagram
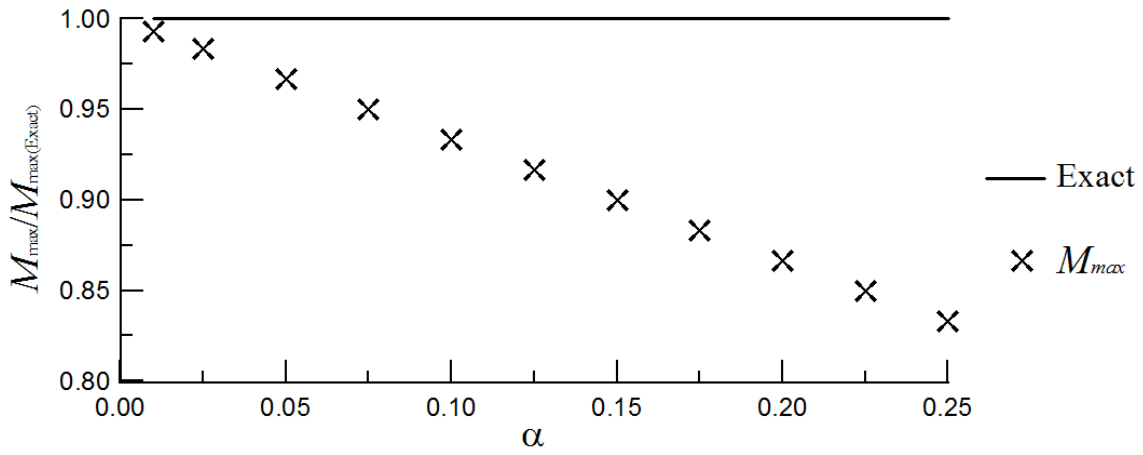


(b) maximum dimensionless moment

**Figure 3.2.9 Radial Spline Collocation Method and exact solutions.**

Example 5: a simply supported beam with length $L$ is subjected to concentrated moment $M$ at the mid-span as shown in Figure 3.2.10.
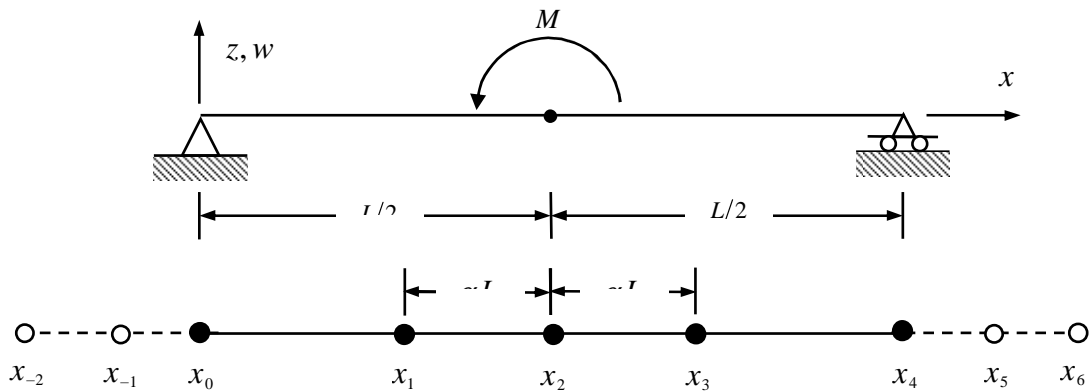


**Figure 3.2.10 Simply supported beam subjected to concentrated moment.**

The deflection of the beam is approximately represented by QRSF with nine knots: five in the analyzed domain and four virtual ones beyond the analyzed domain. The distances of the knots $x_1$ and $x_3$ from central knot $x_2$ are $\alpha L/2$, where $\alpha$ varies from $0.01$ to $0.50$ with increment $0.05$. The spacing of virtual knots beyond the analyzed domain is $0.25L$. When $\alpha = 0.25$, the nine knots are equally spaced to be $0.25L$. The dimensionless moment diagrams of the beam for both $\alpha = 0.01$ and $\alpha = 0.25$ are shown in Figure 3.2.11a. The maximum dimensionless moment $(M_{max} / M_{max(Exact)})$ between the RSCM and exact solutions for different values of $\alpha$ are shown in Figure 3.2.11b. The agreement between RSCM and exact solutions becomes better as $\alpha$ is getting smaller because the shear force at the central knot $x_2$ is discontinuous due to the concentrated moment $M$. When $\alpha = 0.01$ and $\alpha = 0.25$

the maximum dimensionless shear are $1.00$ and $1.20$, respectively.
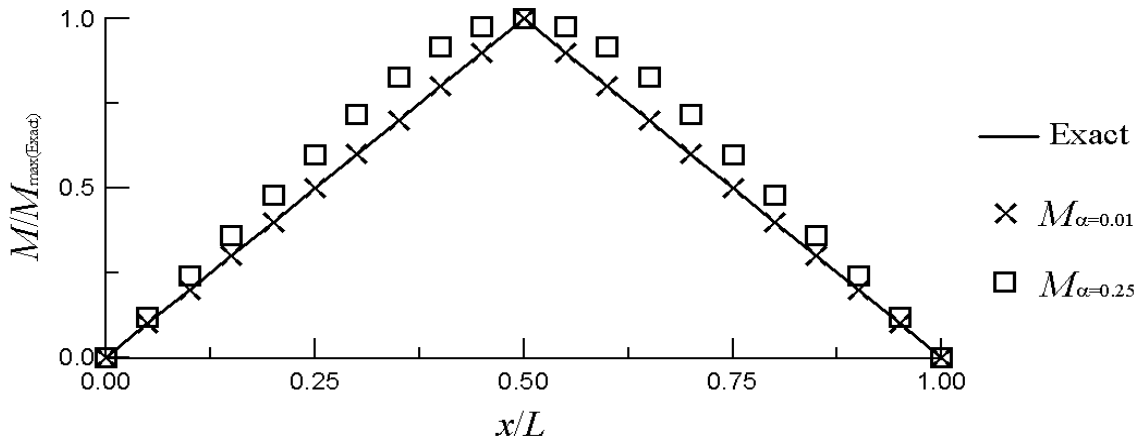


(a) dimensionless moment diagram
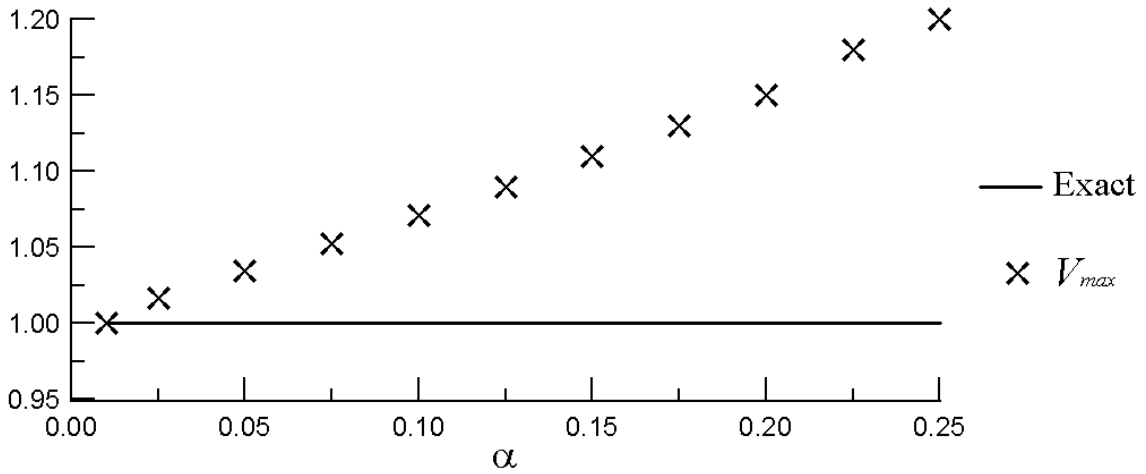


(b) maximum dimensionless shear force

**Figure 3.2.11 Radial Spline Collocation Method and exact solutions.**

Example 6: a continuous beam with four spans, each of length $L$, is subjected to three kinds of loading patterns including linear and nonlinear distributed loads, concentrated load $P$ and concentrated moment $M$ as shown in Figure 3.2.12.
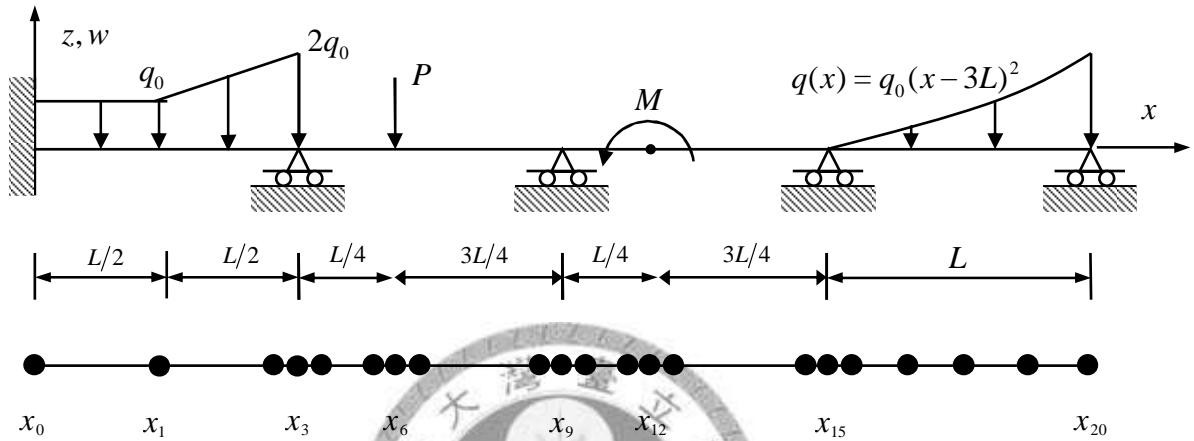


**Figure 3.2.12 Continuous beam.**

In this example, the application of RSCM is generalized to cover all the cases of example 1 to example 5 mentioned above. The deflection of the beam is represented by QRSF with 25 knots: 21 in the analyzed domain and four virtual ones beyond the analyzed domain. The spacing of any two consecutive knots varies form $0.01L$ to $0.73L$. The spacing is reduced to $0.01L$ in the location where loading is discontinuous. Figure 3.2.13 shows analysis results for dimensionless deflection, slope, shear force and bending moment, respectively. The results have good agreement with the corresponding exact solutions. It is shown in this example that RSCM can be applied to complicated beam problems.

118
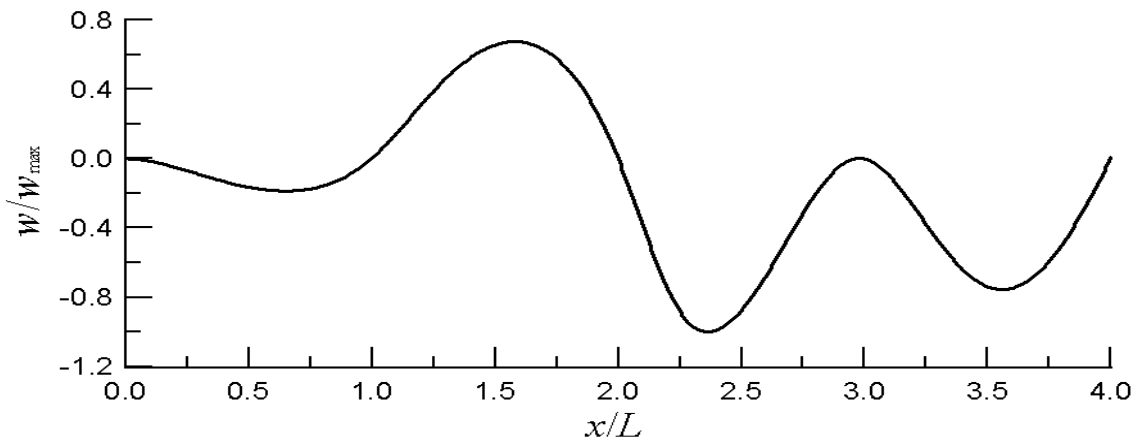
(a) dimensionless deflection
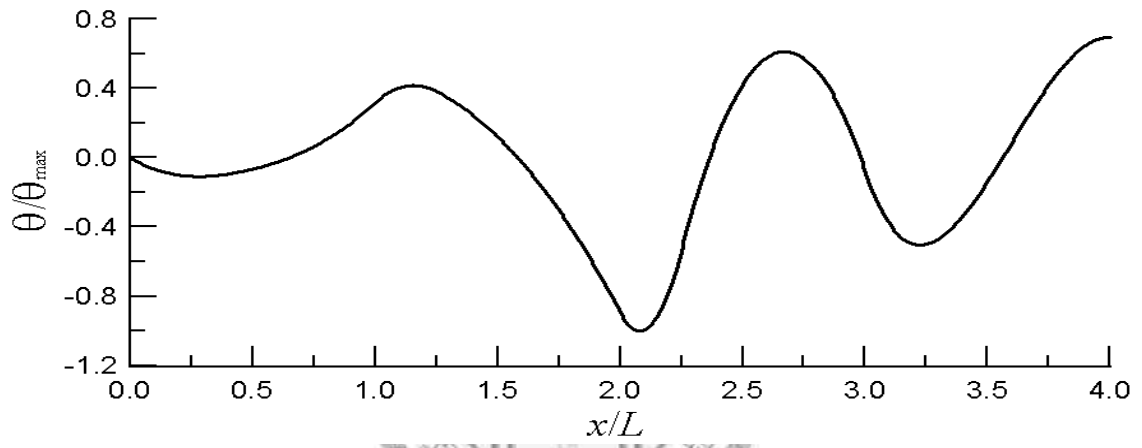


(b) dimensionless slope
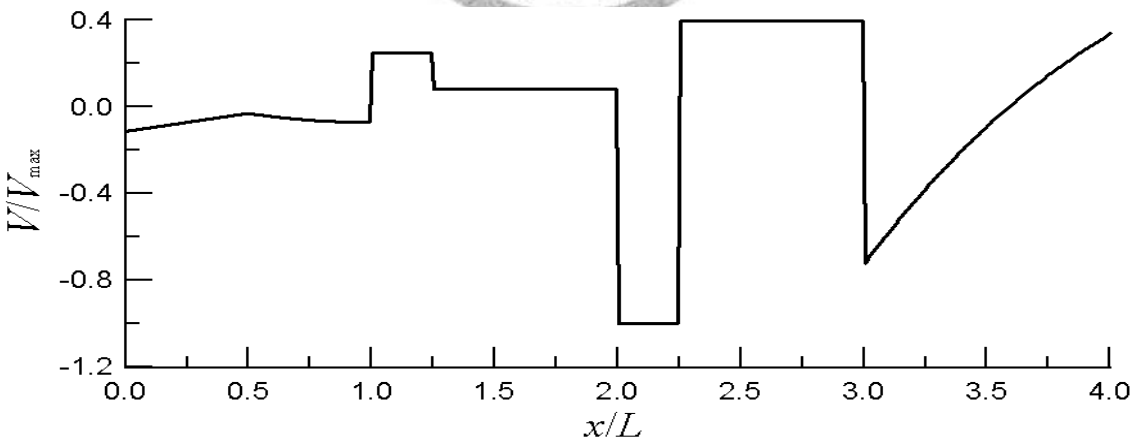


(c) dimensionless shear force

119
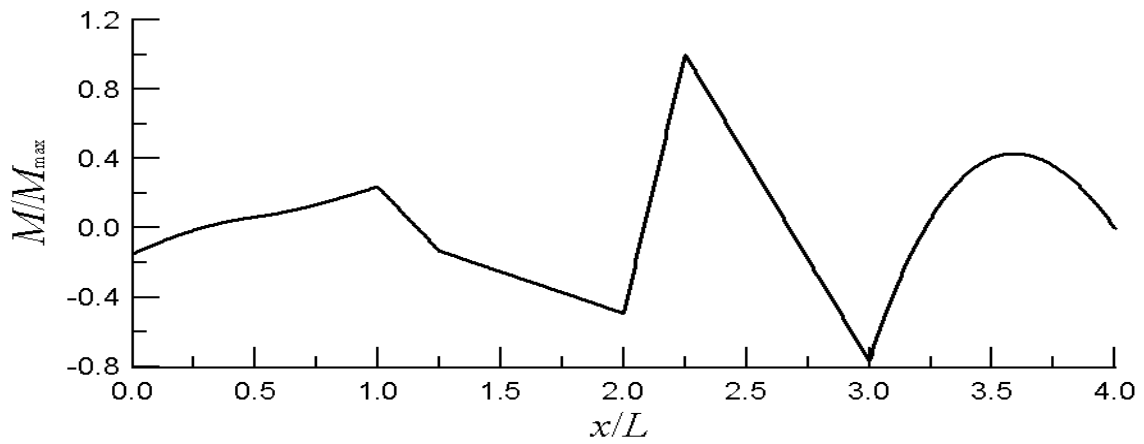
(d) dimensionless bending moment

**Figure 3.2.13 Radial Spline Collocation Method solutions for continuous beam.**

## 3.2.4 Nomenclature

| | |
|---|---|
| $a_i$ | unknown coefficients |
| $B_i(x)$ | Spline Function |
| $E$ | Young's modulus |
| $I$ | second moment of sectional area |
| $L$ | length |
| $M$ | concentrated moment |
| $P$ | concentrated load |
| $q$ | distributed load over the beam |
| $q_i = P/h$ | maximum intensity of distributed load |
| $V$ | shear force |
| $w$ | transverse deflection |
| $\Gamma_w$ | boundary regions of deflection |

120

$\Gamma_\theta$          boundary regions of slope

$\Gamma_M$          boundary regions of moment

$\Gamma_V$          boundary regions of shear force

## 3.3 Conclusions

In conventional SCM, the spacing of any two consecutive knots is kept constant to solve structural problems numerically. Incorporated with the concept of RBF, SCM is extended to RSCM where the spacing of any two consecutive knots may vary. In RSCM, the knots may be more densely spaced only in the location where discontinuity in loading, geometry and material is present. Therefore, the knots can be optimally allocated according to the variation in loading, geometry and material. Comparing with SCM, the number of knots used in the analyzed domain can be minimized and the efficiency of computation can be greatly enhanced. The feasibility of the proposed RSCM is illustrated through several numerical examples. The numerical results agree well with the corresponding exact ones. As a whole, the complicated beam problems with discontinuity characteristics can be solved accurately and efficiently by the proposed RSCM in the paper. The proposed RSCM also can be extended to solve the solutions of other structural problems such of frame, plate, shell, etc.

# Chapter 4 Spline collocation element method

## 4.1 Spline collocation Element method

Various numerical techniques have been developed for solving continuum mechanics problems. Among these techniques, the finite difference method was the first. This method uses divided difference expressions established from a local Taylor series to replace differential or partial differential operators appearing in a mathematical term in discretizing an engineering or scientific problem (Burden and Faires, 1985). Though the discretization is straight, it is difficult to deal with problems showing nonrectangular or complex curvilinear geometries using this method (Smith, 1978).

The finite element method can consistently discretize problems having arbitrary geometries since it uses interpolation and mapping techniques (Zienkiewicz, 1977). This method employs the variational calculus or weighted-residual along with the divergence theorem to carry out a weak formulation which results in an integral statement valid for a discretization. The discretization is performed on the domain of an element, which can have different shape configurations, to result in a computable algebraic form. This method has successfully been applied to the solution of various problems in many engineering or scientific areas.

The spline collocation method (SCM) uses an assumed function to approximate a variable function associated with the problem domain. Then spline function linear sums of the function values at all discrete points in the domain are used to approximate the derivatives in all mathematical terms, in discretizing the problem (Prenter, 1975). This method has been used to the solution of many different engineering and scientific problems ((Bert and Sheu, 1996; Wu, 2003a).

The author has proposed the spline collocation element method (SCEM) (Wu, 2003b). Like the finite-element method, in this method the domain of a problem is

separated into many sub-domains or elements. The SCM discretization is carried out on an element-basis. The governing differential or partial differential equations defined on the elements, the transition conditions on inter-element boundaries and the boundary conditions on the boundary of the problem domain are in computable algebraic forms after the SCM discretization. All discretized governing equations, transition conditions and boundary conditions are assembled to obtain a global algebraic equation system. The coefficient matrix of the algebraic equation system is generally non-symmetric. Therefore a direct non-symmetric or indirect iterative algorithm can be used to solve the problem. Since all relations governing a continuous problem are satisfied, the essence of this method is to find a rigorous solution numerically.

Due to the use of assumed variable functions to all elements, mapping technique can be used. Therefore this method has the same advantage as the finite element method of consistent boundary condition implementation and geometric flexibility. Hence a generic engineering or scientific problem can be converted into a numerical SCEM algorithm. And the related computer code can be systematically developed.

The gradient of a response function in the problem domain will depend on the distribution of external causes. Hence the adaptive concept is necessary in order to efficiently solve a generic engineering or scientific problem. The SCEM is suitable for adaptively discretizing a continuum problem in which various elements with differently assumed variable functions can be used simultaneously.

In treating a concentrated external cause existing in the problem domain, two approaches are available, one of which is to generate the mesh by locating the concentrated external cause on some inter-element boundaries and including it into the natural transition conditions. The second one is to locate the concentrated external cause in some element domains and use certain continuous functions defined over the element

domains to approximate it based on the rule of force equivalence.

## 4.2 Static Analysis of Two-dimensional Frame

### 4.2.1 Discrete Element Equation

Figure 2.2.1(a) shown an element placed in the global coordinates the differential equilibrium equation in the axial direction is

$$-\frac{d}{d\overline{x}^e}\left[EA(\overline{x}^e)\frac{d\overline{u}^e}{d\overline{x}^e}\right]=p(\overline{x}^e) \tag{4.2.1}$$

where $\overline{x}^e$ is the local physical coordinate, $\overline{u}^e$ the axial displacement, $E$ Young's modulus, $A(\overline{x}^e)$ the area of cross section and $p(\overline{x}^e)$ the distributed axial force.

According to SCM theorem assume axial displacement is

$$\overline{u}^e(\overline{x}^e)=\sum_{i=-1}^{m+1}B_i(\overline{x}^e)a_{u,i}^e \tag{4.2.2}$$

where $B_i(\overline{x}^e)$ using cubic spline function, $m$ is the number of knots and $a_{u,i}^e$ are unknown coefficients.

Employing Eq. (4.2.2) in Eq. (4.2.1) can be obtain

$$-\sum_{i=-1}^{m+1}\frac{d}{d\overline{x}^e}\left[EA(\overline{x}^e)B_i'\ (\overline{x}^e)\right]a_{u,i}^e=p(\overline{x}^e) \tag{4.2.3}$$

Therewithal, Figure 4.2.1(b) shown an element placed in the global coordinates The differential equilibrium equation in the lateral direction is

$$\frac{d^2}{d(\overline{x}^e)^2}\left[EI(\overline{x}^e)\frac{d^2\overline{v}^e}{d(\overline{x}^e)^2}\right]=q(\overline{x}^e) \tag{4.2.4}$$

where $\overline{x}^e$ is the local physical coordinate, $\overline{v}^e$ the lateral displacement, $E$ Young's modulus, $I(\overline{x}^e)$ the second moment of section area and $q(\overline{x}^e)$ the distributed lateral force.

According to SCM theorem assume lateral displacement is

$$\bar{v}^e(\bar{x}^e) = \sum_{i=-2}^{n+2} B_i(\bar{x}^e) a_{v,i}^e \qquad (4.2.5)$$

where $B_i(\bar{x}^e)$ using quintic spline function, $n$ is the number of knots, $a_{v,i}^e$ are unknown coefficients.

Employing Eq. (4.2.5) in Eq. (4.2.4) can be obtain

$$\sum_{i=-2}^{n+2} \frac{d^2}{d(\bar{x}^e)^2} \left[ EI(\bar{x}^e) B_i'' \ (\bar{x}^e) \right] a_{v,i}^e = q(\bar{x}^e) \qquad (4.2.6)$$

Attentively, axial and lateral unknown coefficients parting is $a_{u,i}^e$ and $a_{v,i}^e$, so axial and lateral can used difference number of knots.
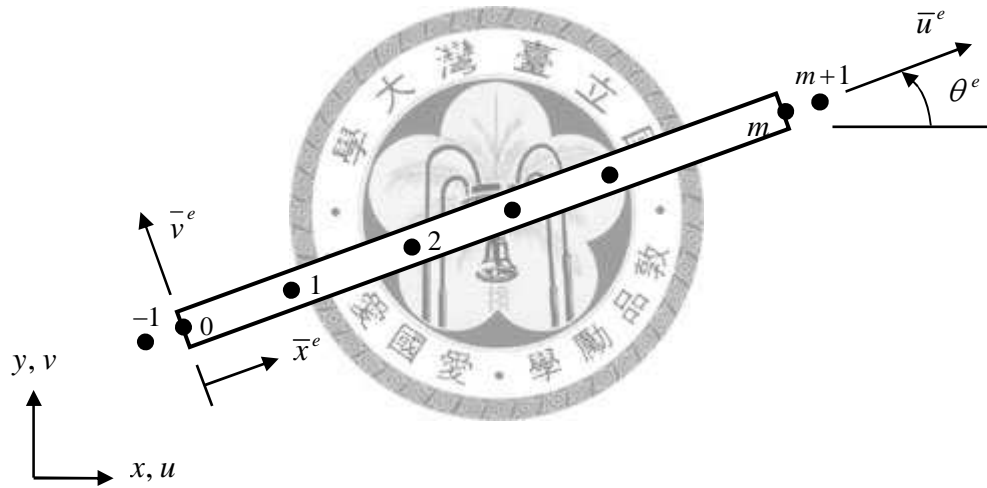


(a) knots for axial direction
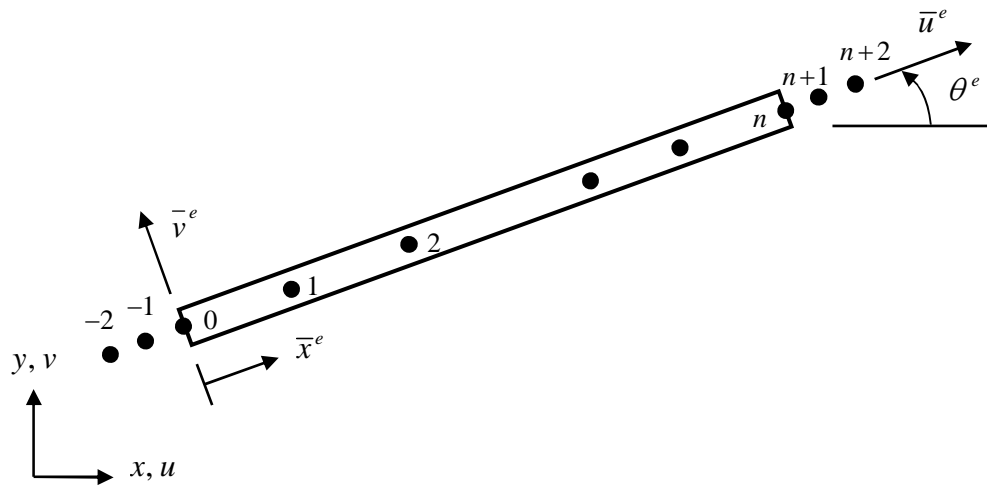


(b) knots for lateral direction

**Figure 4.2.1 Two-dimensional spline collection frame element.**

127

Each element connected joint must satisfy equilibrium and compatibility condition，so it will using transformation matrix in order to the local coordinates transformed into the global coordinates. The transformation matrix is defined as:

$$\mathbf{T}^e = \begin{pmatrix} \cos\theta^e & \sin\theta^e \\ -\sin\theta^e & \cos\theta^e \end{pmatrix} \tag{4.2.7}$$

where $\theta^e$ is direction angles between the local axes and the global axes. It defines same for structural matrix.

Denote $\overline{F}_e^x$ the axial force at an arbitrary point $\overline{x}^e$ in element. $\overline{F}_e^x$ is expressed as

$$\overline{F}_x^e = EA(\overline{x}^e)\frac{d\overline{u}^e}{d\overline{x}^e} \tag{4.2.8}$$

Using Eq. (4.2.2) in Eq. (4.2.8)

$$\overline{F}_x^e = EA(\overline{x}^e)\sum_{i=-1}^{m+1} B_i'(\overline{x}^e)a_{u,i}^e \tag{4.2.9}$$

The distribution of bending moment and shear force in element is

$$\overline{V}_y^e = -\frac{d}{d\overline{x}^e}\left[EI(\overline{x}^e)\frac{d^2\overline{V}^e}{d(\overline{x}^e)^2}\right] \tag{4.2.10}$$

$$\overline{M}_z^e = EI(\overline{x}^e)\frac{d^2\overline{v}^e}{d(\overline{x}^e)^2} \tag{4.2.11}$$

Using Eq. (4.2.5) in Eq. (4.2.10) and Eq. (4.2.11)

$$\overline{V}_y^e = -\sum_{i=-2}^{n+2}\frac{d}{d\overline{x}^e}\left[EI(\overline{x}^e)B_i^{(2)}(\overline{x}^e)\right]a_{v,i}^e \tag{4.2.12}$$

$$\overline{M}_z^e = \sum_{i=-2}^{n+2} EI(\overline{x}^e)B_i^{(2)}(\overline{x}^e)a_{v,i}^e \tag{4.2.13}$$

The deflection slop is

$$\theta_z(x) = \overline{\theta}_z(\overline{x}^e) = \frac{d\overline{v}^e}{d\overline{x}^e} \qquad (4.2.14)$$

Using Eq. (4.2.5) in Eq. (4.2.14)

$$\theta_z(x) = \overline{\theta}_z(\overline{x}^e) = \sum_{i=-2}^{n+2} B_i^{(1)}(\overline{x}^e) a_{v,i}^e \qquad (4.2.15)$$

## 4.2.2 Discrete Condition Equation of Joints

Let $M^j$ denote the number of elements connected to joint $j$. Also let $I^{e,\alpha^j}$ denote the element knot number of the $\alpha^j$th element connected to the joint. Then $I^{e,\alpha^j}$ is equal to 0 or $N^{e,\alpha^j}$, with $N^{e,\alpha^j}$ being the largest knot no. on the $\alpha^j$th element. With these in mind, the displacement compatibility conditions of a hinged or rigid joint, which are kinematic conditions of joint $j$ can be expressed as follows :

$$\begin{Bmatrix} u^{e,1^j} \\ v^{e,1^j} \end{Bmatrix} = \begin{Bmatrix} u^{e,2^j} \\ v^{e,2^j} \end{Bmatrix} = \cdots = \begin{Bmatrix} u^{e,\alpha^j} \\ v^{e,\alpha^j} \end{Bmatrix} = \cdots = \begin{Bmatrix} u^{e,M^j} \\ v^{e,M^j} \end{Bmatrix} = \begin{Bmatrix} U^j \\ V^j \end{Bmatrix} \qquad (4.2.16)$$

where $\begin{bmatrix} u^{e,\alpha^j} & v^{e,\alpha^j} \end{bmatrix}^T$ and $\begin{bmatrix} U^j & V^j \end{bmatrix}^T$ represent the global element displacement vector of the $\alpha^j$th element and the global displacement vector of joint $j$, respectively.

$\begin{bmatrix} u^{e,\alpha^j} & v^{e,\alpha^j} \end{bmatrix}^T$ can using Eq. (4.2.2) and Eq. (4.2.5) obtain

$$\begin{Bmatrix} u^{e,\alpha^j} \\ v^{e,\alpha^j} \end{Bmatrix} = \begin{bmatrix} \cos\theta^{e,\alpha^j} & -\sin\theta^{e,\alpha^j} \\ \sin\theta^{e,\alpha^j} & \cos\theta^{e,\alpha^j} \end{bmatrix} \begin{Bmatrix} \sum_{i=-1}^{m+1} a_{u,i}^{e,\alpha} B_i\left(\overline{x}^{e,\alpha^j}\right) \\ \sum_{i=-2}^{n+2} a_{v,i}^{e,\alpha} B_i\left(\overline{x}^{e,\alpha^j}\right) \end{Bmatrix} \qquad (4.2.17)$$

Slope compatibility conditions are also kinematic transition conditions of a rigid joint.

$$\theta^{e,1^j} = \theta^{e,2^j} = \cdots = \theta^{e,\alpha^j} = \cdots = \theta^{e,M^j} = \theta^j \qquad (4.2.18)$$

where $\theta^{e,\alpha^j}$ is slop deflection $\alpha^j$th element of joint $j$. $\theta^j$ is slop deflection of

joint $j$, $M^j$ is number of rigid joint in joint $j$. $\theta^{e,\alpha^j}$ can be obtain from Eq. (4.2.15).

The equilibrium conditions of external and internal forces at joints also have to be satisfied. Each equilibrium condition is either a natural transition condition or a natural boundary condition. Figure 4.2.2 shown a joint $j$ with external loads $P_x^j$, $P_y^j$ and $M_z^j$. Let $v^{e,m^j}$ denote an indicator defined by the local element node number of an element at the joint. $v^{e,m^j}$ is defined as :

$$v^{e,m^j} = \begin{cases} +1, & \text{if } I^{e,m^j} = N^{e,m^j} \\ -1, & \text{if } I^{e,m^j} = 0 \end{cases} \tag{4.2.19}$$

Then the two translational equilibrium conditions of joint $j$ can be expressed as the following matrix equation :

$$\sum_{\alpha=1}^{M^j} v^{e,m^j} \begin{bmatrix} \cos\theta^{e,\alpha^j} & \sin\theta^{e,\alpha^j} \\ \sin\theta^{e,\alpha^j} & \cos\theta^{e,\alpha^j} \end{bmatrix} \begin{Bmatrix} \overline{F}_x^{e,\alpha^j} \\ \overline{V}_y^{e,\alpha^j} \end{Bmatrix} = \begin{Bmatrix} P_x^j \\ P_y^j \end{Bmatrix} \tag{4.2.20}$$

where $\overline{F}_x^{e,\alpha^j}$ and $\overline{V}_y^{e,\alpha^j}$ can obtain by Eq. (4.2.9) and Eq. (4.2.12).

We might need one or two of two translational equilibrium equations for a hinged or rigid joint. We do also need a moment equilibrium condition for a rigid joint if the rotation is not prescribed. The equilibrium condition can be obtained

$$\sum_{\alpha=1}^{M^j} v^{e,m^j} M_z^{e,\alpha^j} = M_z^j \tag{4.2.21}$$

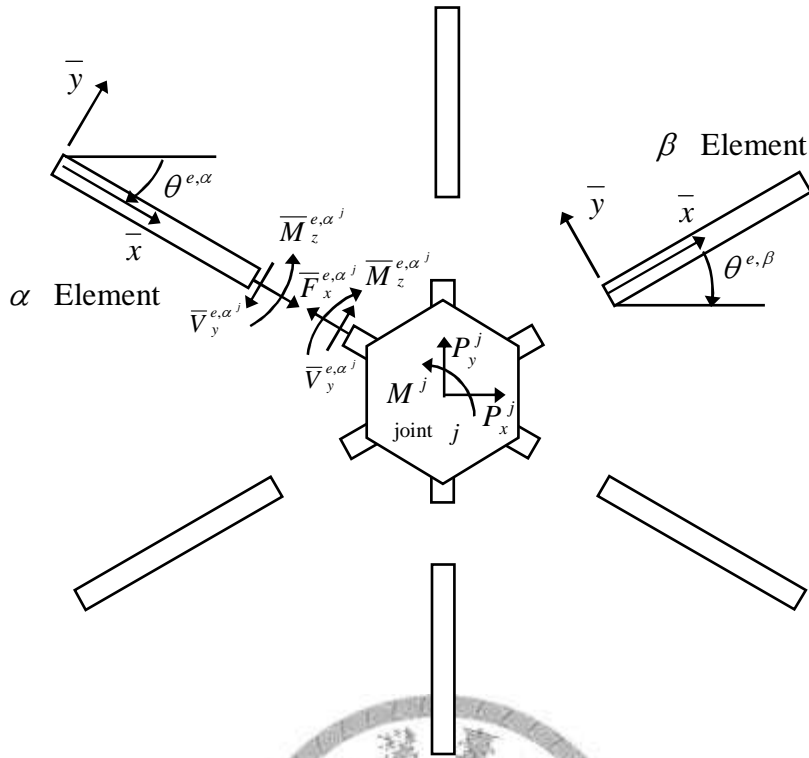where $M_z^{e,\alpha^j}$ can obtain by Eq. (4.2.13).

**Figure 4.2.2 Internal and external force at a joint.**

## 4.2.3 Numerical Algorithm

A computer program has written which implements the numerical procedures of the two-dimensional SCEM frame model. The SCM discretization is carried out on the natural coordinate system. Only elements with equally spaced knots are considered, unequally spaced knots will study next paper. The numerical procedures can be summarized and described as follows :

(a) The used elements are divided into various groups based on the number of axial and lateral knots of the element. Using $m+1$ axial knots and $n+1$ lateral knots on element parting into Eq. (4.2.4) and Eq. (4.2.6) can obtain $m+n+2$ equations.

(b) Calculate element transformation matrix of Eq. (4.2.7), using for next step.

(c) In order to obtain unique solution, each element must have another six equation, include three unknown (one of $a_{u,i}^e$ and two of $a_{v,i}^e$) for each element external endpoint. These equations can be obtain form equilibrium and compatibility conditions, that is Eqs. (4.2.16) to (4.2.21). It need to using element transformation

matrix from step b.

(d) Using a solver to solve the algebraic equation system, unknown $a_{u,i}^e$ and $a_{v,i}^e$ can be otained.

(e) The axial displacement, lateral displacement, slope deflection, axial force, bending moment and shear force can be calculated using Eq. (4.2.2), Eq. (4.2.5), Eq. (4.2.15), Eq. (4.2.13) and Eq. (4.2.12), respectively. SCM (or SCEM) be different than matrix structural analysis or Finite Element Method, element don't need through transformation matrix obtain displacement or internal force; even can calculate arbitrary location on element.

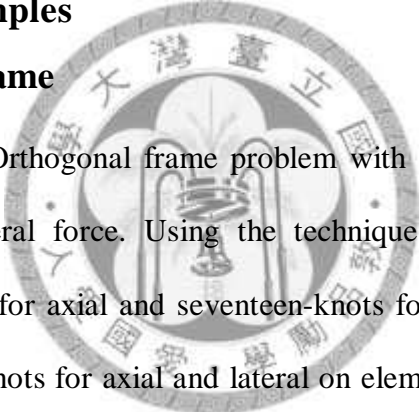## 4.2.4 Numerical Examples
## 4.2.4.1 Orthogonal Frame

Figure 4.2.3 shown a Orthogonal frame problem with member AB subjected to a aquatically distributed lateral force. Using the technique of adaptive discretization element 1 is a three-knots for axial and seventeen-knots for lateral on element, which element2 and 3 are three-knots for axial and lateral on elements. Figure 4.2.4 to Figure 4.2.6 represent the displacement, bending moment and shear force diagrams, respectively. Although only three elements are used, the SCEM result are excellent.

The problem was also solved by using the MSC/NASTRAN finite element problem. The lateral displacement at point B, obtained by gradually increasing the number of finite elements up to 128 to model member AB, converged to the fifth digit accuracy as compared to the SCEM result. This result has confirmed that the developed two-dimensional SCEM frame model is efficient for accurately solving problem with highly nonlinear distributed loads.
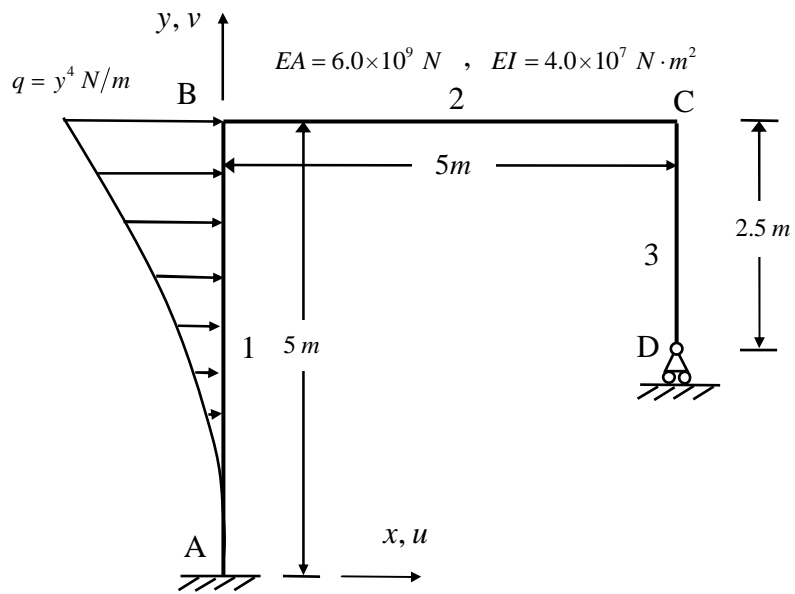
**Figure 4.2.3 Orthogonal frame.**



Displacement : └────┘ 0.1 mm
Dimension : └────┘ 0.5 m
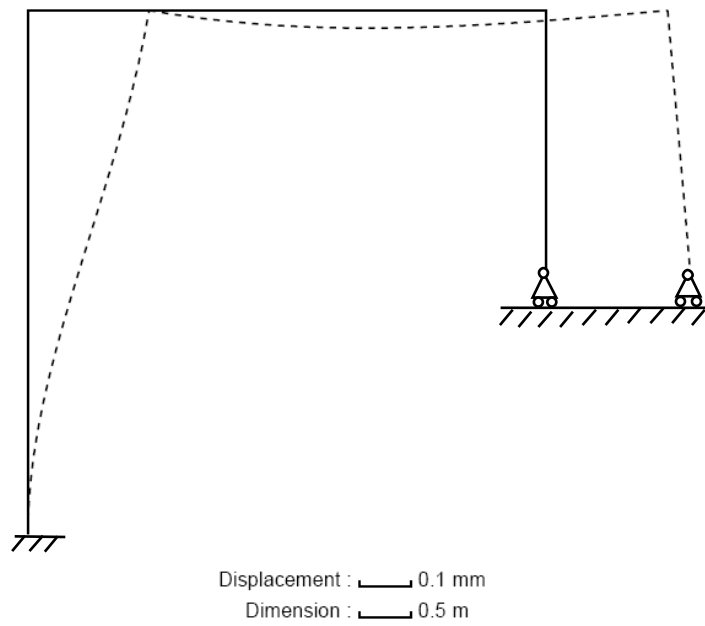
**Figure 4.2.4 Displacement diagram for orthogonal frame.**

$8.41 \times 10^2$

$8.41 \times 10^2$

0.

0.

$1.77 \times 10^3$

Bending moment : ⊢——⊣ 5.E+02N-m
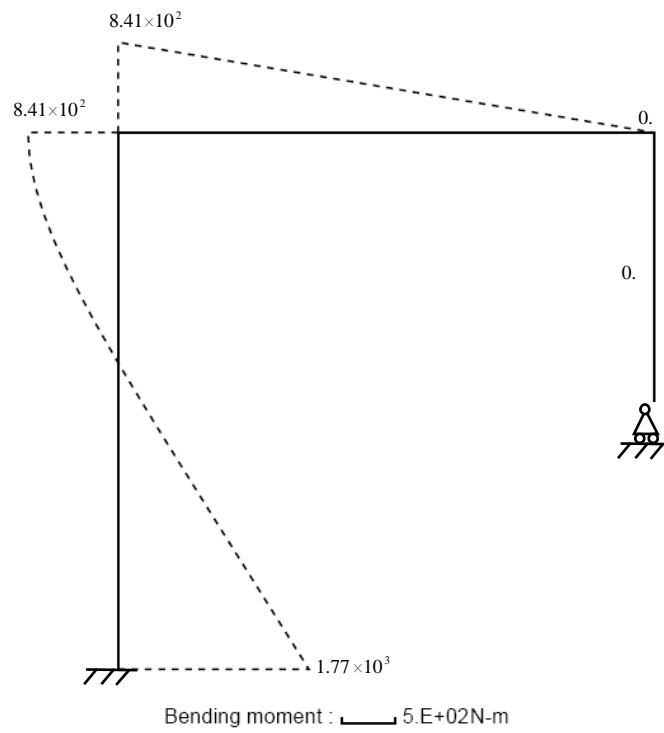
**Figure 4.2.5 Bending moment diagram for orthogonal frame.**



0.

$-1.67 \times 10^2$

0.

$6.25 \times 10^2$

Shear force : ⊢——⊣ 5.E+02N

**Figure 4.2.6 Shear force diagram for orthogonal frame.**

### 4.2.4.2 Two-bay Two-span Orthogonal Frame

The frame structure shown Figure 4.2.7 has two hinged joints and is subjected to highly nonlinear distributed loads. In the SCEM analysis, 15 elements were used to model the structure. Element 3, which is subjected to a quadratically distributed load, is a eleven-knots for lateral and three-knots for axial on elements, and element 4, which is subjected to a cubically distributed load, number of knots is same as element 3. All other elements are three-knots for axial and lateral on element. The 15 elements are divided into two groups based on their axial and flexural rigidities.

Element 7~12 : $EA = 4.0 \times 10^9 \ N$ ; $EI = 4.0 \times 10^7 \ N \cdot m^2$
14~15 :
Element 1~6 : $EA = 1.4 \times 10^{10} \ N$ ; $EI = 4.0 \times 10^7 \ N \cdot m^2$
13 :
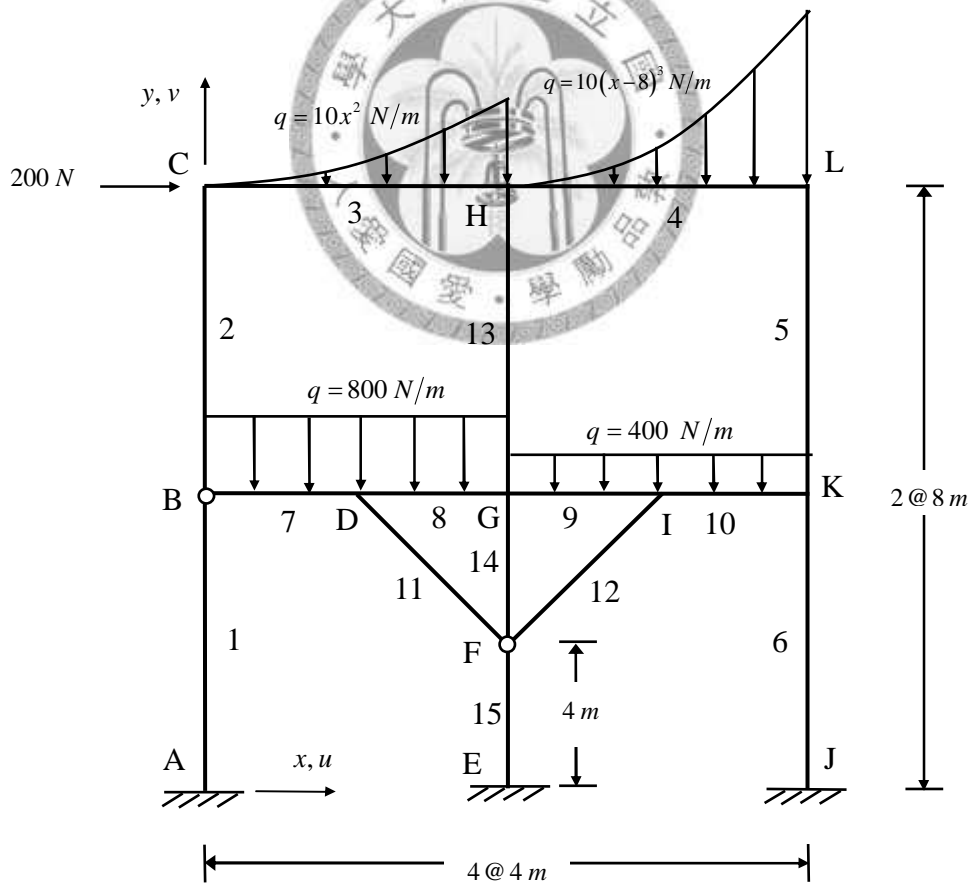


**Figure 4.2.7 Two-bay two-span orthogonal frame.**

The results of displacement, bending moment, and shear force were plotted, and are shown in Figure 4.2.8 to Figure 4.2.10, respectively. Highly nonlinear distributions

of internal forces which represent excellent global and local accuracy were obtained.



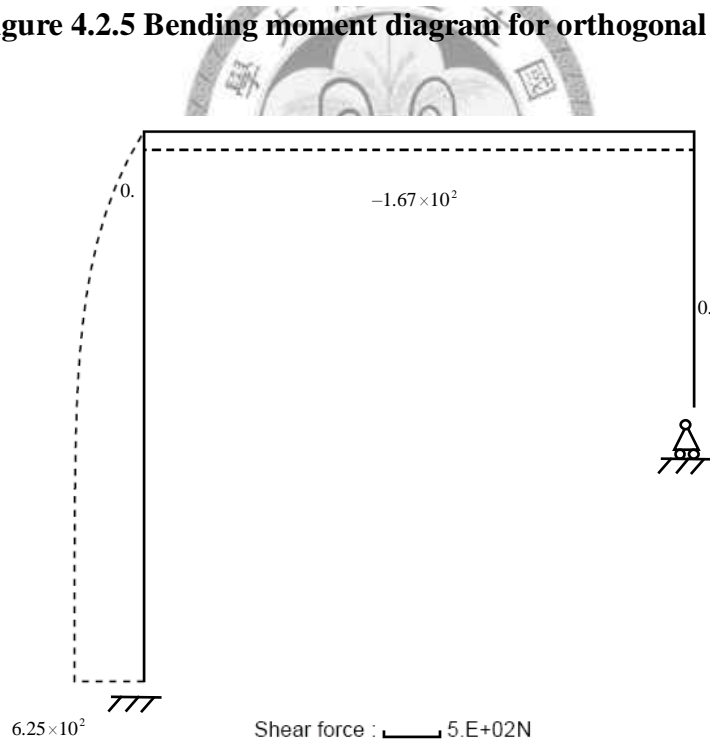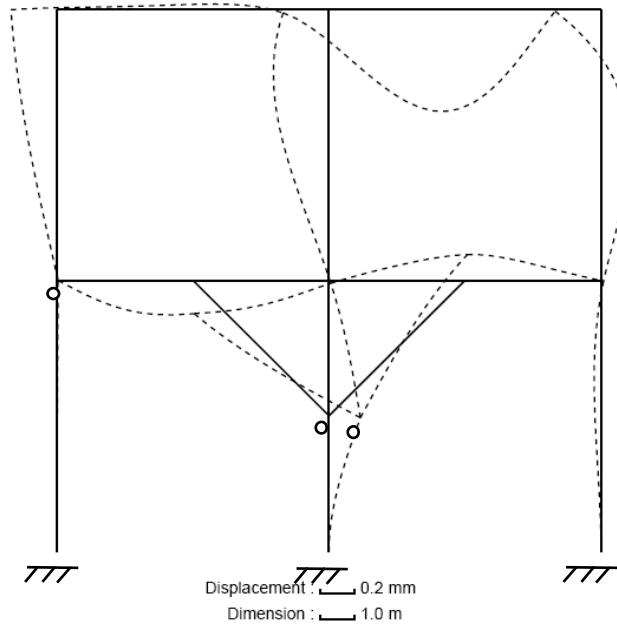**Figure 4.2.8 Displacement diagram for two-bay two-span orthogonal frame.**
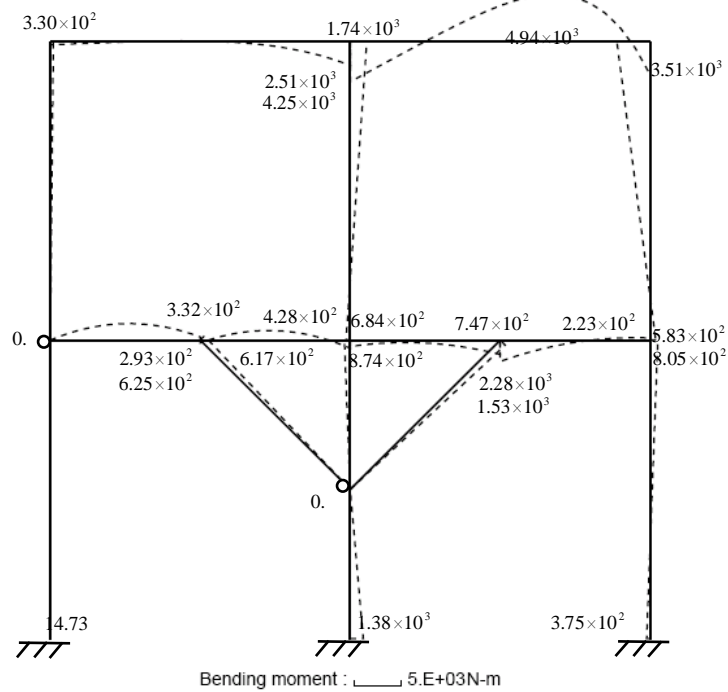


**Figure 4.2.9 Bending moment diagram for two-bay two-span orthogonal frame.**
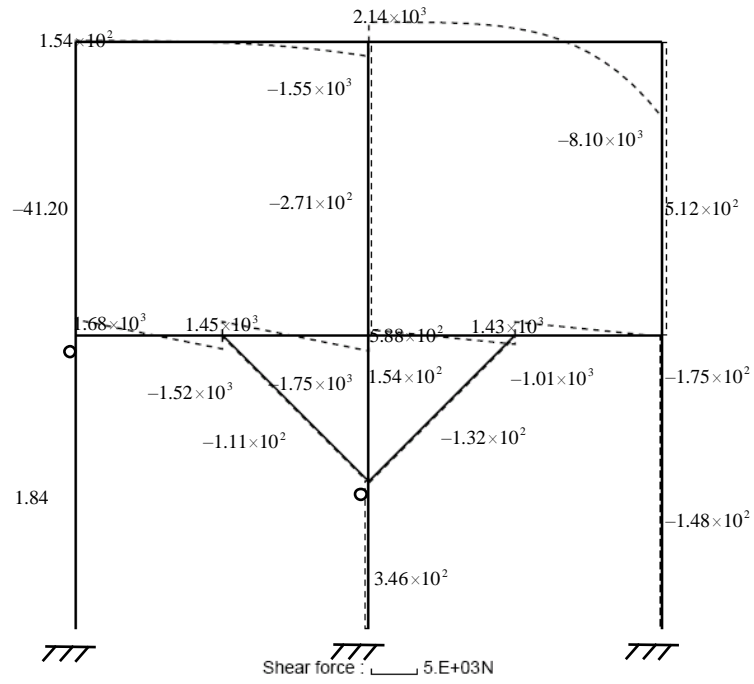
**Figure 4.2.10 Shear force diagram for two-bay two-span orthogonal frame.**

## 4.2.4.3 Non-orthogonal Frame

Figure 4.2.11 shown a non-orthogonal frame subjected to two uniformly distributed forces and a support settlement. In the SCEM analysis, 10 three-knots for axial and lateral elements were used to model the structure. The results of displacement, bending moment and shear force were plotted, and are shown in Figure 4.2.12 to Figure 4.2.14.

$$EA = 2.0 \times 10^{10} \ N \ \ ; \ \ EI = 4.0 \times 10^{7} \ N \cdot m^{2}$$
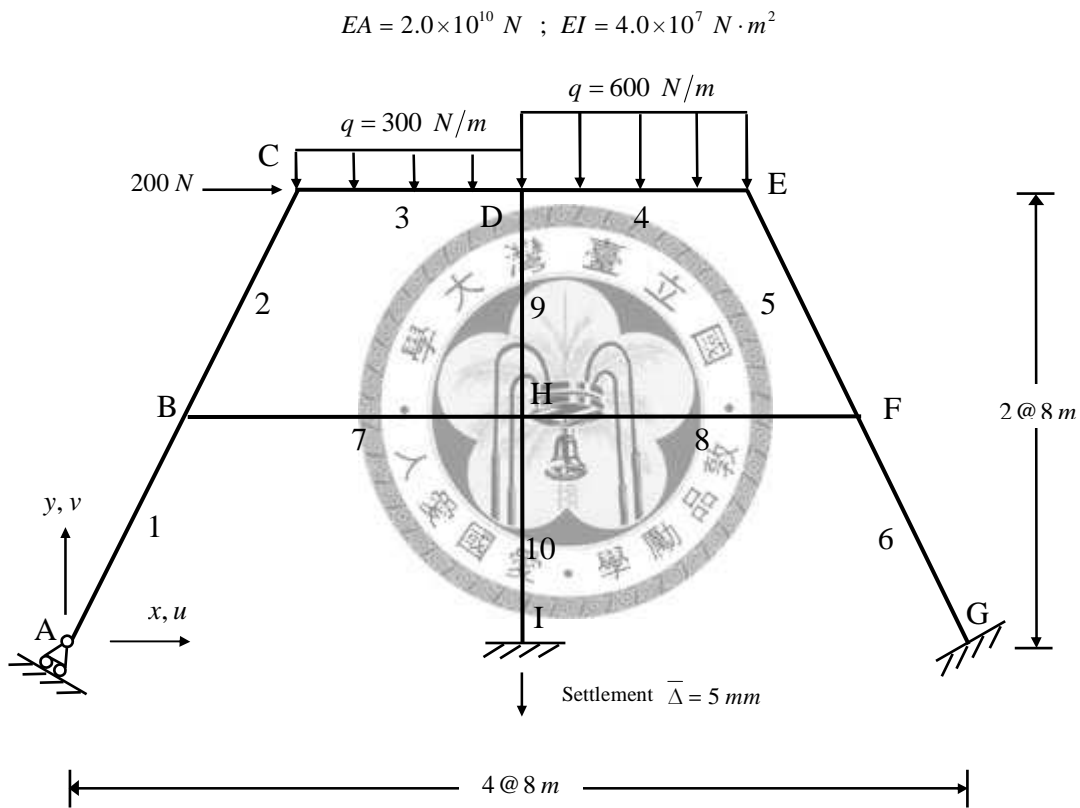


**Figure 4.2.11 Non-orthogonal frame.**
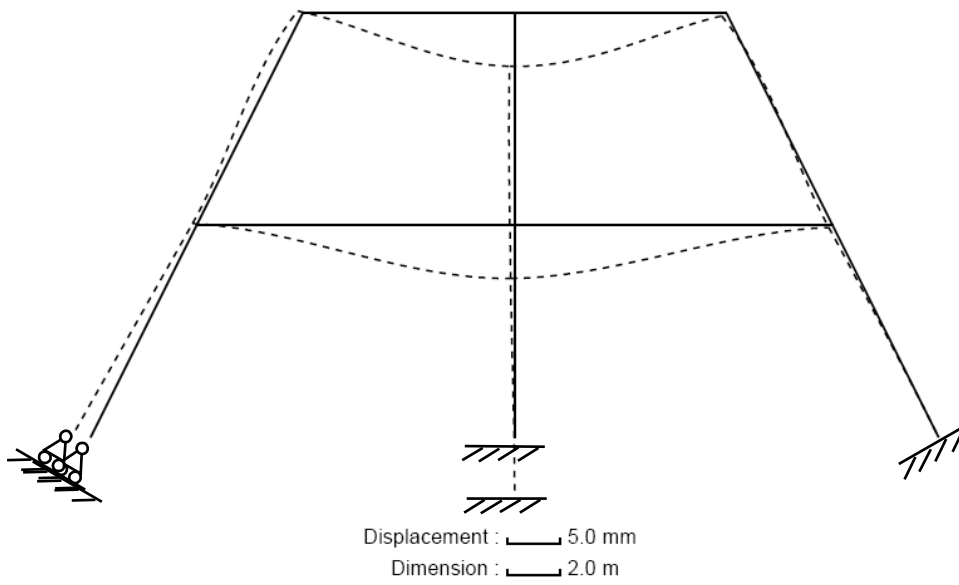
**Figure 4.2.12 Displacement diagram for Non-orthogonal frame.**
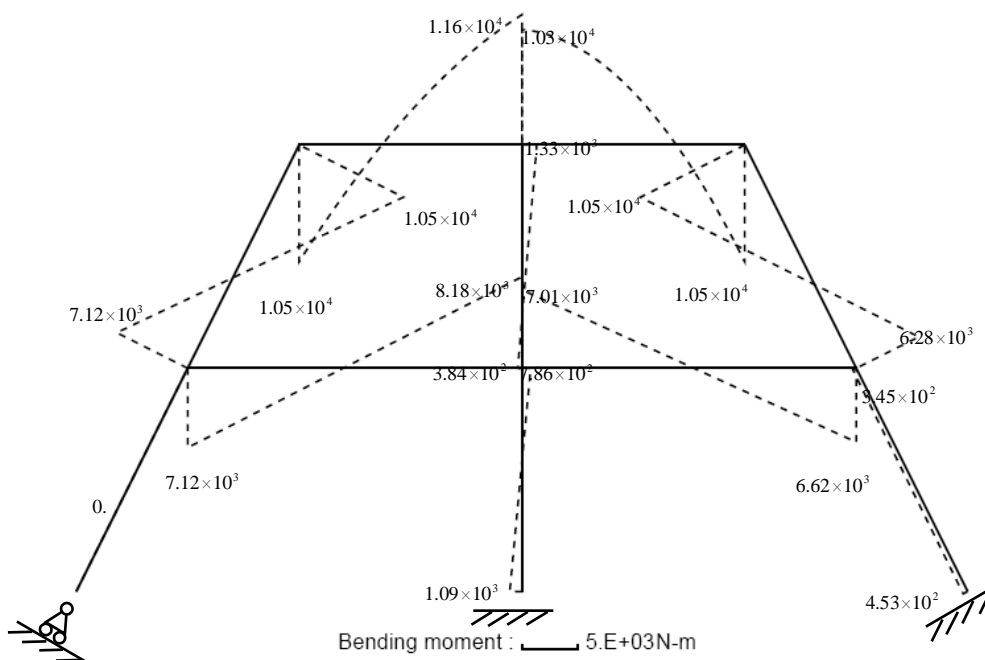


**Figure 4.2.13 Bending moment diagram for Non-orthogonal frame.**

139
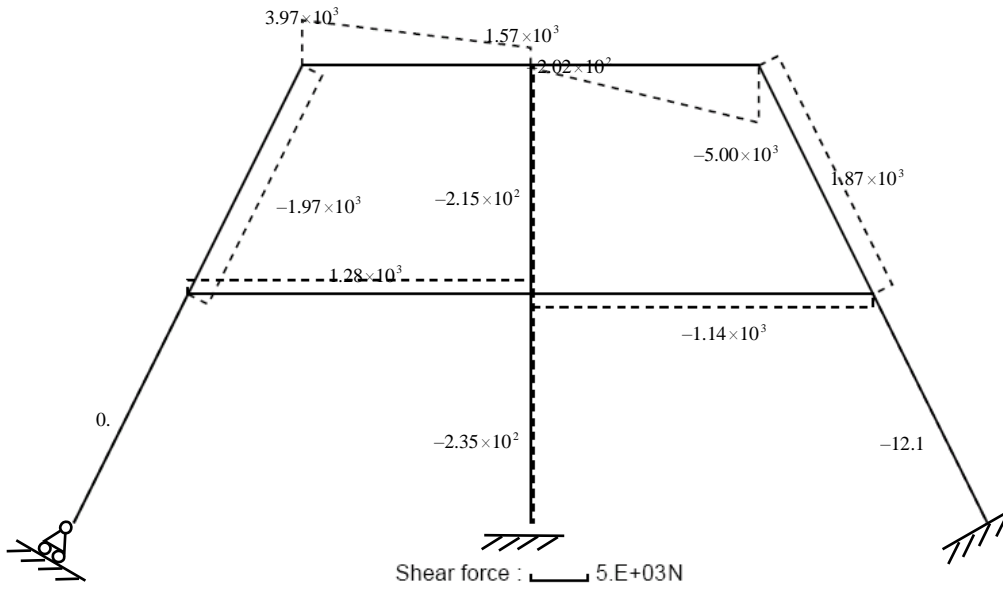
**Figure 4.2.14 Shear force diagram for Non-orthogonal frame.**

## 4.2.4.4 Four-bay Eight-span Orthogonal Frame

Figure 4.2.15 shows a four-bay eight-span orthogonal frame. The left column and all beams are subjected to uniform loads. The discrete SCEM structural model is composed of 68 three knots for axial and lateral on elements of which beam elements and column elements have different structural rigidities. The results of displacement, bending moment and shear force are plotted, and are shown in Figure 4.2.16 to Figure 4.2.18.



Beams : $EA = 2.0 \times 10^{11}\ N$ ; $EI = 4.0 \times 10^{7}\ N \cdot m^{2}$
Column : $EA = 4.0 \times 10^{10}\ N$ ; $EI = 1.0 \times 10^{7}\ N \cdot m^{2}$
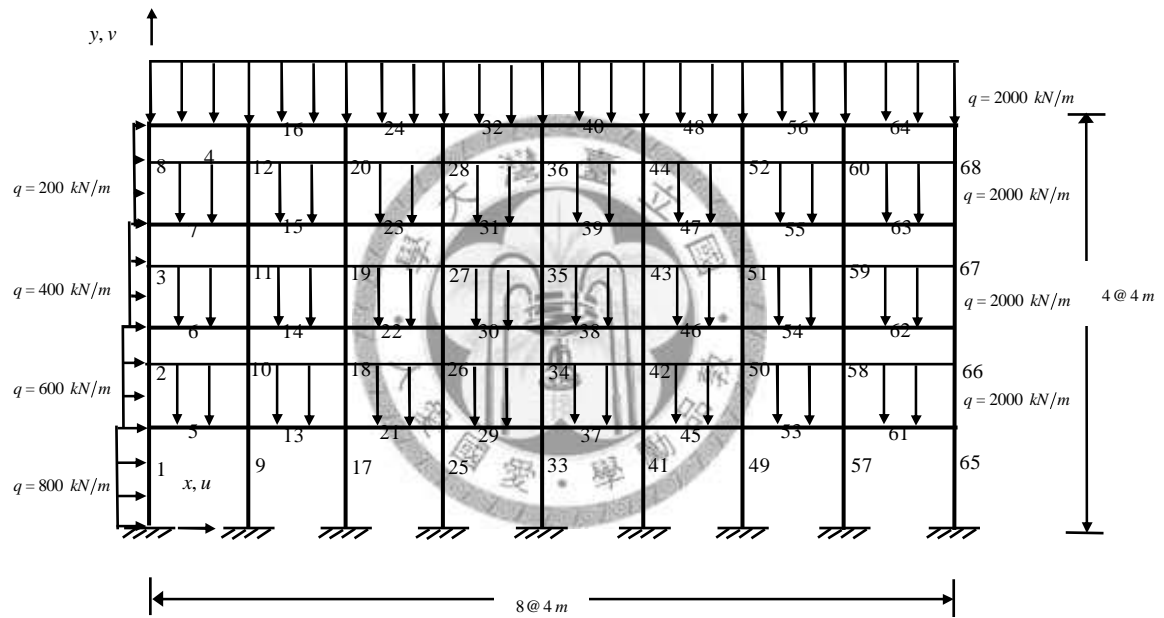
**Figure 4.2.15 Four-bay eight-span orthogonal frame.**

Displacement : |____| 1.0 m
Dimension : |____| 2.0 m
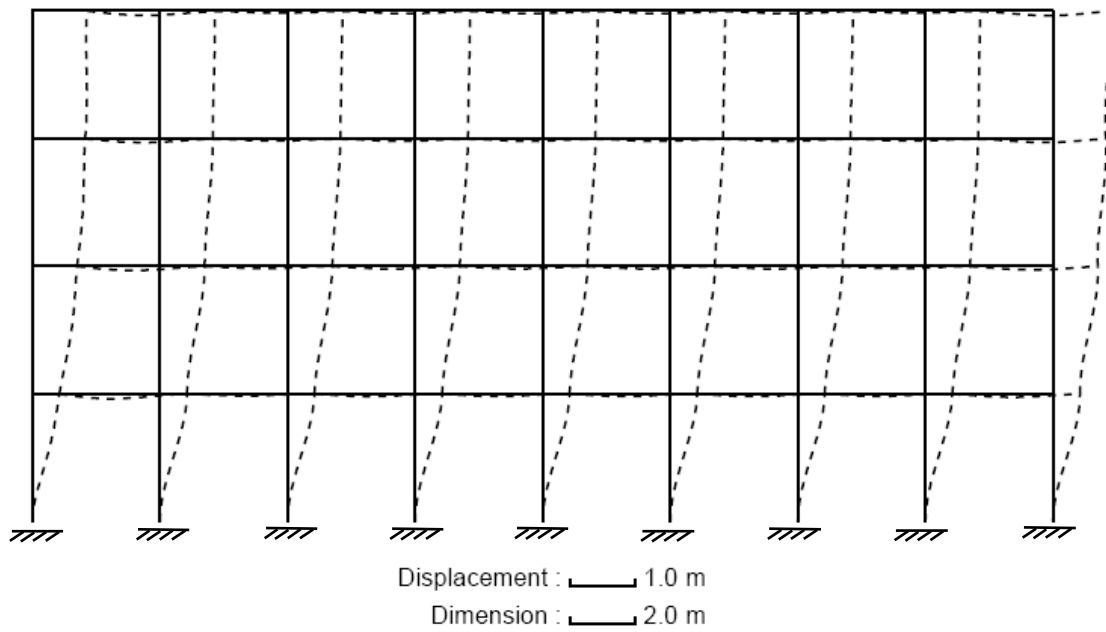
**Figure 4.2.16 Displacement diagram for four-bay eight-span orthogonal frame.**



$1.95 \times 10^6$        $1.33 \times 10^6$      $1.36 \times 10^6$       $2.00 \times 10^6$

$8.76 \times 10^5$                             $8.27 \times 10^5$

$2.26 \times 10^6$      $1.48 \times 10^6$     $1.50 \times 10^6$       $1.50 \times 10^6$     $1.60 \times 10^6$

Bending moment : |____| 3.E+06N-m
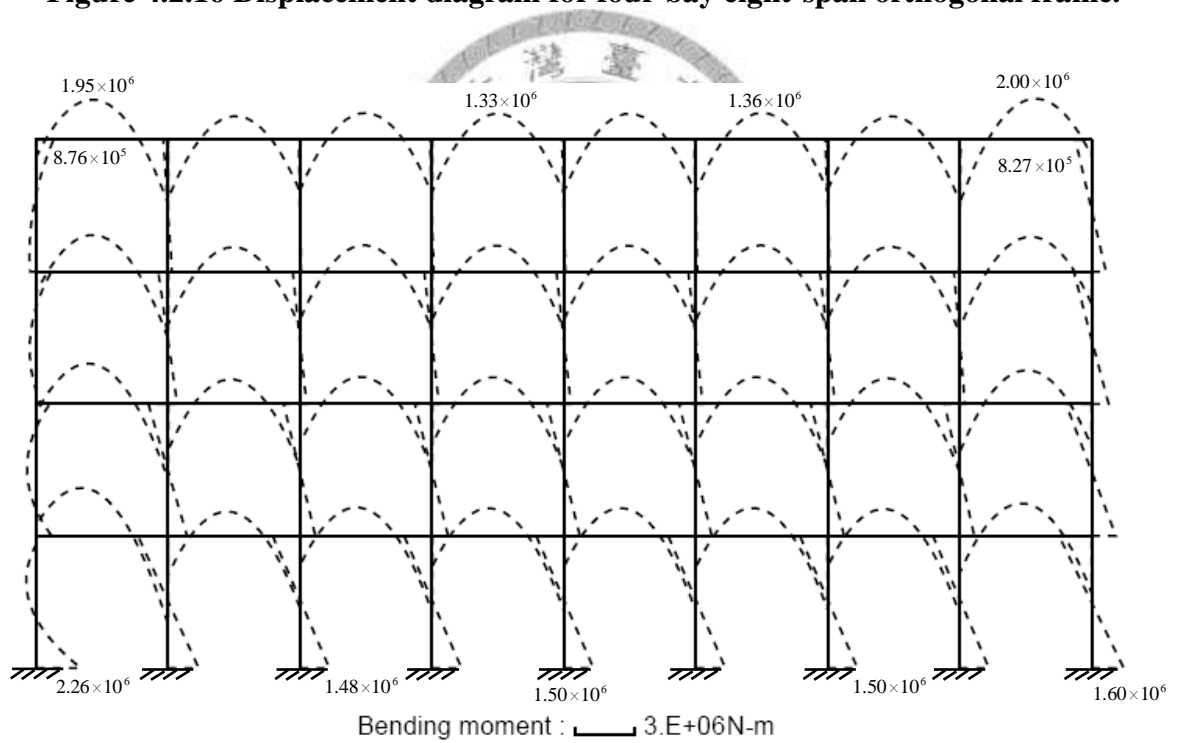
**Figure 4.2.17 Bending moment diagram for four-bay eight-span orthogonal frame.**

142
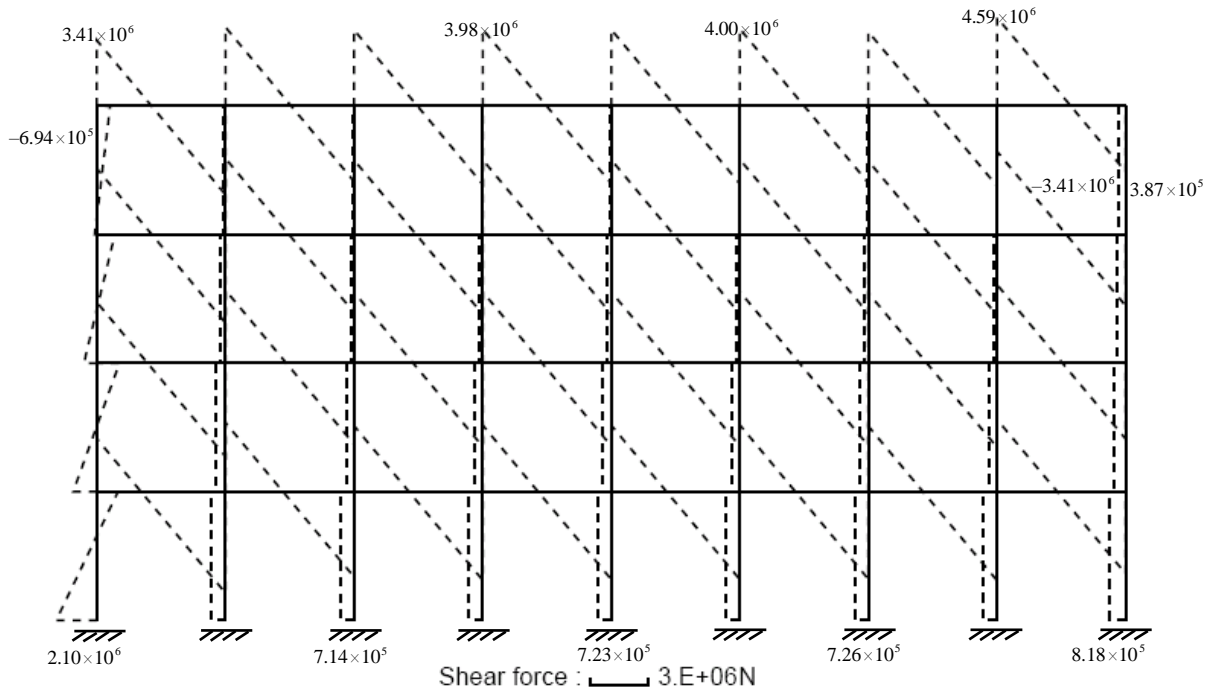
**Figure 4.2.18 Shear force diagram for four-bay eight-span orthogonal frame.**

## 4.2.5 Nomenclature

| | |
|---|---|
| $a_{u,i}^e$ | unknown coefficients. |
| $a_{v,i}^e$ | unknown coefficients |
| $A(\overline{x}^e)$ | area of cross section |
| $B_i(\overline{x}^e)$ | cubic spline function |
| $E$ | Young's modulus |
| $\overline{F}_e^x$ | axial force at an arbitrary point $\overline{x}^e$ in element |
| $I(\overline{x}^e)$ | second moment of section area |
| $I^{e,\alpha^j}$ | element knot number of the $\alpha^j$ th element connected to the joint |
| $m$ | number of knots |
| $M^j$ | number of elements connected to joint $j$ |
| $\overline{M}_z^e$ | distribution of bending moment in element |
| $n$ | number of knots, |

143

$p(\overline{x}^e)$    distributed axial force

$q(\overline{x}^e)$    distributed lateral force

$\overline{u}^e$    local axial displacement

$\overline{v}^e$    lateral displacement

$\overline{V}_y^e$    distribution of shear force in element

$v^{e,m^j}$    indicator defined by the local element node number of an element at the joint

$\overline{x}^e$    local physical coordinate

$\theta^e$    direction angles between the local axes and the global axes

$\theta^j$    slop deflection of joint $j$

$\theta^{e,\alpha^j}$    slop deflection $\alpha^j$ th element of joint $j$

## 4.3 Conclusions

Mathematical formulations for the two-dimensional SCEM frame model were carried out. The related numerical procedures were implemented into a computed code. The capability of the program was demonstrated by solving various frame problems having complex geometrical properties. This SCEM frame model has the same advantage as the finite element method of being able to solve generic problems. Due to the availability of adaptive discretization and the inclusion of all mechanics relations to from the algebraic equation system, accurate results can efficiently be obtained by using this method. Numerical results proved it. The developed computer code can also be used to solve two-dimensional truss problems of which all joints are hinged and only concentrated joint loads and distributed axial loads can be applied.
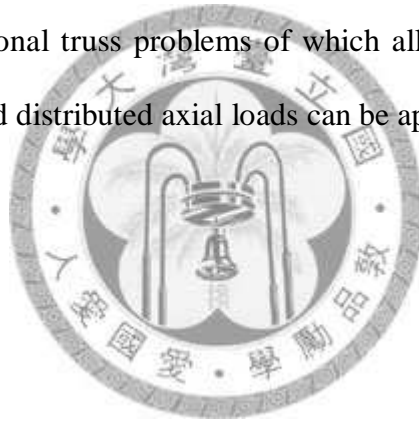
# Reference

[1] Abdulloev Kh.O., Bogalubsky H., Markhankov V.G., (1976), One more example of inelastic solution interaction, Phys. Lett. **56**A 427-428.

[2] Aircraft design manual (Vol 9: Loading, strength and rigidity). Aviation Industry Book Company, Beijing, China, 2001.

[3] Ali A.H.A., Gardner L.R.T. and Gardner G.A., (1990), A Galerkin Approach to the Solution of Burgers' Equation, Maths Preprint Series, No. 90. 04, University College of North Wales, Bangor.

[4] Ali A.H.A, Gardner G.A. and Gardner L.R.T., (1992), A collocation solution for Burgers' equation using cubic B-spline finite elements, *Comput. Method Appl.* M. **100**(3) 325–337.

[5] Archer J.S., (1965), Consistent matrix formulations for structural analysis using finite-element techniques. *AIAA J.* **3**, 191-1918.

[6] Atluri S.N., Kim H.G. et al., (1999), A critical assessment f the truly Meshless Local Petrov-Galerkin (MLPG), and Local Boundary Integral Equation (LBIE) methods, *Comput. Mech.* **24** 348-372.

[7] Atluri S.N., and Zhu T., (1998), A new Meshless Local Petrov-Galerkin (MLPG) approach in computational mechanics, *Comput. Mech.* **22** 117-127.

[8] Atluri S.N., and Zhu T.L., (2000a), The meshless local Petrov-Galerkin (MLPG) approach for solving problem in elasto-statics **25** 169-179.

[9] Atluri S.N., and Zhu T.L., (2000b), New concepts in meshless methods, *Int. J. Numer. Math. Engrg.* **47** 537-556.Atluri SN, Sladek J et al. (2000), The Local Boundary Integral Equation (LBIE) and it's meshless implementation for linear elasticity, *Comput. Mech.* **25** 180-198.

[10] Bateman H., (1915), Some recent researches on the motion of fluids, *Monthly Weather Rec.* **43** (4) 163–170.

[11] Batdorf S.B. and Stein M., (1947), *Critical combinations of shear and direct stress for simply supported rectangular plates*, Washington: NACA TN-1223.

[12] Bateman H, (1915), Bateman, Some recent researches on the motion of fluids, *Monthly Weather Rec*. **43**(4) 163–170.

[13] Bathe K.J., (9182), *Finite Elemhnr Procedures in Engineering Analysis*. Prentice-Hall, Englewood Cliffs, NJ.

[14] Belytschko T., Lu Y., and Gu L., (1994), Element free Galrkin methods, *Int. J. Number Methods Engrg*. **37** 229-256.

[15] Bellman R.E. and Casti J., (1971), Differential Quadrature and Long-term Integration, *J. Math. Anal. Appl*. **34** 235-238.

[16] Benoy M.B., (1969), An energy solution for the buckling of rectangular plates under non-uniform in-plane loading, *Aeronaut J* **73** 974-977.

[17] Benton E., and Platzman G.W., (1972), A table of solutions of the one-dimensional Burgers' equations, *Quart. Appl. Math*. **30** 195–212.

[18] Bert C.W., Devarakonda K.K., (2003), Buckling of rectangular plates subjected to nonlinearly distributed in-plane loading, *Int. J. Solids Struct*. **40** 4097-106.

[19] Bert C.W. and Sheu Y., (1996), Static analysis of beams and plates by spline collocation method, *J. Eng. Mech*. **122**(4) 375-378.

[20] Bhashyam G.R. and Prathap G., (1980), Galerkin finite element method for non-linear beam vibration, *J. Sound Vibr*. **72** 191-203.

[21] Bokaian A., (1988), Natural frequencies of beams under compressive axial loads. *J. Sound Vibr*. **126**, 49-65.

[22] Botella O., (2002), On a collocation B-spline method for the solution of the Navier-Stokes equations, *Comput. Fluids* **31** 397-420.

[23] Boor C. De, Schwartz B., (1973), Collocation at Gaussian points. *SIAM J. Numer. Anal*. **10** 582-606.

[24] Budiansky B. and Connor R.W., (1948), *Buckling stresses of clamped rectangular flat plates in shear*, Washington: NACA TN-1559.

[25] Burden R.L. and Faires. J.D., (1985), *Numerical Analysis*. Prindle, Weber & Schmidt, Boston, MA.

[26] Burgers J.M., (1939), Mathematical examples illustrating relations occurring in the theory of turbulent fluid motion, *Trans. Roy. Neth. Acad. Sci. Amsterdam* **17** 1–53.

[27] Burgers J.M., (1948), A mathematical model illustrating the theory of turbulence, *Adv. Appl. Mech., Academic Press*, New York, 171–199.

[28] Caldwell J., Wanless P., Cook A.E., (1981), A finite element approach to Burgers' equation, *Appl. Math. Modelling* **5** 189–193.

[29] Caldwell J., Smith P., (1982), Solution of Burger's equation with large Reynold's number, *Appl. Math. Modelling* **6** 381–385.

[30] Caoron M.D. and Williams F.W., (1988), Exact dynamic stiff nesses for an axially loaded uniform Timoihenko member embedded in an elastic medium. *J. Sound Vibr.* **124**, 453-466.

[31] Cheng F.Y. and Pantelides C.P., (1988), Dynamic Timoshenko beam-columns on elastic media. *ASCE J. Srrucr. Engng* **114**(ST7), 1524-1550.

[32] Christie I., Griffiths D.F., Mitchell A.R., Sanz-Serna J.M., (1981), Product approximation for non- linear problems in the finite element method, IMA, *J. Num. Anal.* **1** 253–266.

[33] Cole J. D., (1915), On a quasi-linear parabolic equation occurring in aerodynamics, *Q. Appl. Math.* **9** 225–236.

[34] Cowper G.R., (1966), The shear coefficient in Timoshenko's beam theory. *ASME J. Appt. Mech.* **33**,335-340.

[35] Column Research Committee of Japan, (1971), *Handbook of Structural Stability*, Tokyo : Corona Publishing Company Ltd..

[36] Davies A.M., (1978), Application of the Galerkin method to the solution of the Burgers' equation, *Comput. Method Appl. M.* **14** 305–321.

[37] Dagˇ I., Irk D., and Saka B., (2005a), A numerical solution of the Burgers's equation using cubic B-splines, *Appl. Math. Comput.* **163** 199–211.

[38] Dag I., Irk D., and Sahin A., (2005b), B-spline collocation methods for numerical solutions of the Burgers' equation, *Math. Prob. Eng.* **5** 521-538.

[39] Dag I., Irk D., and Sahin A., (2005c), B-spline collocation methods for numerical solutions of the Burgers' equation, *Math. Prob. Eng.* **5** 521-538.

[40] Chia M., (1980), *Nonlinear analysis of plates*, New York: McGraw-Hill.

[41] Davies A.M., (1978), Application of the Galerkin method to the solution of the Burgers' equation, *Comput. Method Appl. M.* **14** 305–321.

[42] De Rosa M.A., (1989), Stability and dynamics of beams on Winkler elastic foundations. *Earthquake Engng Srruct. Dyn.* **18**, 377-388.

[43] De Rosa M.A., (1993), Stability and dynamic analysis of two-parameter foundation beams. *Comput. Srrucr.* **49**, 341-349.

[44] Djodjo B.A., (1969), Transfer matrices for beams loaded axially and laid on an elastic foundation. *Aeronaut. Q.* **20**, 281-306.

[45] Doyle P.F. and Pavlovic M.N., (1982), Vibration of beams on partial elastic foundations. *Earthquake Engng Srruct. Dyn.* **10**, 663-674.

[46] Elibeck J.C., and McGuire G.R., (1977), Numerical study of the RLW equation II: Interaction of solitary waves, *J. Comp. Phys.* **23** 63-73.

[47] Eringen A.C., (1972), Nonlocal polar elastic continua, *Int. J. Eng.*, **10** 1–16.

[48] Eringen A.C., and Edelen D.G.B., (1972), On nonlocal elasticity, *Int. J. Eng.*, **10** 233–248 .

[49] Eringen A.C., (1983), On differential equations of nonlocal elasticity and solutions of screw dislocation and surface waves, *J. Appl. Phys.*, **54** 4703-4710.

[50] Eisenberger M. and Alexandrov A., (2003), Buckling loads of variable thickness thin isotropic plates, *Thin Wall. Struct.*, **41** 871-889.

[51] Eisenberger M. and Clastornik J., (1987), Beams on variable two-parameter elastic foundation. *ASCE J. Engng Mech.* **113**(EMlO), 1454-1466.

[52] Eisenberger M. and Clastornik J., (1980), Vibrations and foundation: *ASME J. Appl. Mech.* **47**, 139-144.

[53] Eisenberger M., Yankelevsky D.Z. and Adin M.A., (1985), Vibrations of beams fully or partially supported on elastic foundations. *Earthquake Engng Struct. Dyn.* **13**, 651-660.

[54] Evensen D.A., (1968), Nonlinear vibrations of beams with various boundary conditions, *Am. Inst. Aeronaut. Astronaut. J.* **6** 370-372.

[55] Feng Y. and Bert C.W., (1992), Application of the quadrature method to flexural vibration analysis of a geometrically nonlinear beam, *Nonlinear Dyn.* **3** 13-18.

[56] Ferguson N.B., and Finlayson B.A., (1970), Transient chemical reaction analysis by orthogonal collocation, *Chem. Eng. J.* **1** 327-336.

[57] Ferguson H.B., (1971), *Orthogonal collocation as a method of analysis in chemical engineering*. Ph.D. Thesis, University of Washington, Seattle.

[58] Filipich C.P., Laura P.A.A., Sonenblum M. and Gil E., (1988), Transverse vibrations of a stepped beam subjected to an axial force and embedded in a non-homogeneous Winkler foundation. *J. Sound Vibr.* **126**(l), 1-8.

[59] Filipich C.P. and Rosales M.B., (1988), A variant of Rayleigh's method applied to Timoshenko beams embedded in a Winkler-Pasternak medium. *J. Sound Vibr.* **124**, 443-451.

[60] Finlayson B.A., (1971), Packed bed reactor analysis by orthogonal collocation, *Chem. Eng. Sci.* **26** 1081-1091.

[61] Fletcher D.Q. and Hermann L.R., (1971), Elastic foundation representation of continuum. *ASCE J. Engng Mech.* **97**(EMI), 95-107.

[62] Franciosi C. and Masi A., (1993), Free vibrations of foundation beams on two parameter elastic *soil. Comput. Strucr.* **47** 419-426.

[63] Frank R., (1972), Scattered data interpolation: tests of some methods, *Math. Comput.* **38** 181-199.

[64] Franke C, and Schaback R. (1998), Solving partial differential equations by collocation using

radial basis functions, *Appl. Math. Comput.* **93** 73-82.

[65] Gardner L.R.T., Gardner G.A. and Ali A.H.A., (1991), A method of lines solutions for Burgers' equation, *Proceeding of the Asian Pacific Conference on Computational Mechanics*, A.A. Balkema/Rotterdam/Brookfield, Hong Kong.

[66] Gardner L.R.T., and Gardner G.A., (1992), Solitary waves of the equal width waves equation, *J. Comp. Phys.* 218-223.

[67] Gardner L.R.T., Gardner G.A., Zaki S.I., and Sahrawi Z. El, (1993), B-spline finite element studies of the non-linear Schrodinger equation, *Comput. Meth. Appl. Mech. Eng.* **108** 303-318.

[68] Gardner L.R.T., Gardner G.A., Ayoub F.A., Amein.N.K., (1997), Simulations of the EW undular bore, *Comm. Numer. Methods Engrg.* **13** (7) 583-592.

[69] Gardner L.R.T., and Gargner G.A., (1999), Solitary waves of RLW equation, *J. Comp. Phys.* **91** (2) 441-459.

[70] Guo Q. and Zhong H., (2004), Non-linear vibration analysis of beams by a spline-based differential quadrature method, *J. Sound Vibr.* **269** 413-420.

[71] Gupta A., Kiusalas J., and Saraph, M., (1991), Cubic B-spline for finite element analysis of axisymmetric shells, *Comput. Struct* **38** 463-469.

[72] Gingold R.A., and Moraghan J.J., (1977), Smoothed particle hydrodynamic : theory and applications to non-spherical stars, *Man Not Astrou Soc* **181** 375-389.

[73] Gosz J., and Liu W.K., (1996), Admissible approximations for essential boundary conditions in the reproducing kernel particle method, *Comput. Mech.* **19** 120-135.

[74] Gupta A., Kiusalas J., and Saraph M., (1991), Cubic B-spline for finite element analysis of axisymmetric shells, *Comp. Struct.* **38** 463-469.

[75] Hardy R.L., (1971), Multiquadric equations of topography and other irregular surfaces, *J. Geophys. Res.* **76** 1905-1915.

[76] Horvay G., and Spiess F.N., (1954), Orthogonal edge polynomial in the solution of boundary value problems, *Quant. Appl. Math.* **12** 57-65.

[77] Hopf E., (1950), The partial differential equation $u_t + uu_x = \mu u_{xx}$, *Commun. Pur. Appl. Math.* **3** 201–230.

[78] Huang T.C., (1961), The effect of rotatory inertia and of shear deformation on the frequency and normal mode equations of uniform beams with simple end conditions. *J. Appl. Mech.* **28**, 579-584.

[79] Iskander L., and Mohamedein M.Sh. El-Decn, (1992), Solitary waves interaction foe the BBM equation, *Comput. Meth. Appl. Mech. Eng.* **96** 361-372.

[80] Issa M.S., (1988), Natural frequencies of continuous curved beams on Winkler-type foundation. *J. Sound Vibr.* **127**, 291-301.

[81] Jain P.C. and Holla D.N., (1978), Numerical solutions of coupled Burgers' equations, *Int. J. Nonlinear Mech.* **13** 213–222.

[82] Jain P.C. and Lohar B.L., (1979), Cubic spline technique for coupled nonlinear parabolic equations, *Comput. Math. Appl.* **5**(3) 179–185.

[83] Jain P.C., Shankar R. and Singh T.V., (1995), Numerical technique for solving convective-reaction diffusion equation, *Math. Comput. Model* **22**(9) 113–125.

[84] Jones R. and Xenophontos J., (1977), The Elastic foundation model. *Inc. J. Mech. Sci.* **19**, 317-323.

[85] Kakuda K., and Tosaka N., (1990), The generalised boundary element approach to Burgers' equation, *Int. J. Numer. Meth. Eng.* **29** 245–261.

[86] Kansa E.J., (1990), Multiquadrics – a scattered data approximation scheme with applications to computational fluid dynamics – I. Surface approximations and partial derivative estimates, *Comput. Math. Appl.* **19**(8/9) 127-145.

[87] Kansa E.J., (1990), Multiquadrics – a scattered data approximation scheme with applications to computational fluid dynamics – II. Solutions to hyperbolic, parabolic, and elliptic partical differential equations, *Comput. Math. Appl.* **19**(8/9) 147-161.

[88] Karamanlidis D. and Prakash V., (1988), Buckling and vibration analysis of flexible beams resting on an elastic half-space. *Earthquake Engng Srruct. Dyn.* **16**, 1103-1144.

[89] Karamanlidis D. and Prakash V., (1989), Exact transfer and stiffness matrices for a beam-column resting on a two-parameter foundation. *Compur. Merh.* **72**, 77-89.

[90] Kanaka Raju K., Sastry B.P. and Venkateswara Rao G., (1976), A finite element formulation for the large amplitude vibration of tapered beams, *J. Sound and Vibr.* **47** 595-598.

[91] Kerr A.D., (1964), Elastic and visco-elastic foundation models. *ASME J. Appl. Mech.* **31**, 491-498.

[92] Khalifa A.K., Ali A.H., and Raslan K.R., (1999), Numerical study foe the equal width wave (EWE) equation, *J. Memoirs of the Faculty of Science, Kochi, Japan, Series A* **20** 47-55.

[93] Khalifa A.K., and Raslan K.R., (1999), Finite difference methods for the equal width wave equation, *J. Egypt. Math. Soc.* **7** (2) 47-55.

[94] Krongauz Y., and Belytschko T., (1996), Enforcement of essential boundary conditions in meshless approximations using finite elements, *Comput. Methods Appl. Mech. Engrg.* **131** 133-145.

[95] Kukla S., (1991), Free vibration of a beam supported on a stepped elastic foundation. J. *Sound Vibr.* **149**,259-265.

[96] Kutluay S., Bahadır A.R., and zdes's A. O¨, (1999), Numerical solution of one-dimensional Burgers's equation: explicit and exact-explicit finite difference methods, *J. Comput. Appl. Math.* **103** 251–261.

[97] Kutluay S., and Esen A., (2004), A linearized numerical scheme for Burgers-like equations, *Appl. Math. Comput.* **156** 295–305.

[98] Kutluay S., Esen A., and Dagˇ I., (2004), Numerical solutions of the Burgers's equation by the least-squares quadratic B-spline finite element method, *J. Comput. Appl. Math.* **167** 21–33.

[99] Lanczos C., (1938), Trigonometric interpolation of empirical and analytical functions, *J. Math. Phys.* **17** 123-199.

[100] Lanczos C., (1956), *Applied analysis, Prentice Hall*, New Jersey.

[101] Laura P.A.A. and Cortinez V.H., (1987), Vibrating beam partially embedded in Winkler-type foundation. *AXE J. Engng Mech.* **113**(EMl), 143-147.

[102] Lee S.Y. and Ke H.Y., (1990), Free vibrations of non-uniform beams resting on non-uniform elastic foundation with general elastic end restraints. *Compur. Srruct.* **34**, 421-429.

[103] Lighthill M. J., (1956), Viscosity effects in sound waves of finite amplitude, *Surveys in Mechanics* 250–351.

[104] Liu W.K., Jun S., and Zhang Y.F., (1995), Reproducing kernel particle methods, *Int. J. Number Methods Fluids* **20** 1081-1106.

[105] Liszka T.J., Duarte C.A.M., and Tworzydlo W.W., (1996), hp-meshless cloud method, *Comput. Methods Appl. Mech.* **139** 263-288.

[106] Lohar B.L. and Jain P.C., (1981), Variable mesh cubic spline technique for N-wave solution of Burgers' equation, *J. Comput. Phys.* **39**(2) 433–442.

[107] Lu P., Lee H.P., Lu C., and Zhang P.Q., (2006), Dynamic properties of flexural beams using a nonlocal elasticity model, *J. Appl. Phys.*, **99** 073510.

[108] Mei C., (1972), Finite element displacement method for large amplitude free oscillations of beams and plates, *Comp. Struct.* **3** 163-174.

[109] Mei C., (1973a), Finite element analysis of nonlinear vibrations of beam columns, *Am. Inst. Aeronaut. Astronaut. J.* **11** 115-117.

[110] Mei C., (1973b), Finite element displacement method for large amplitude free flexural vibrations, *Comput. Struct.* **3** 163-174.

[111] Mei C., (1973c), Nonlinear vibrations of beams by matrix displacement method, *Am. Inst. Aeronaut. Astronaut. J.* **10** 355-357.

[112] Miller E.L., (1966), *Predictor–Corrector studies of Burger's model of turbulent flow*, M.S. Thesis, University of Delaware, Newark, Deleware.

[113] Mittal R.C., and Singhal P., (1993), Numerical solution of Burgers's equation, Commun.

*Numer. Meth. Eng.* **9** 397–406.

[114] Mittal R.C., and Singhal P., (1996), Numerical solution of periodic Burgers's equation, *Indian J. Pure Appl. Math.* **27** 689–700.

[115] Mizusawa T., Kajita T., and Narouka, M., (1979), Vibration of skew plates by using B-spline functions, *J. Sound Vibr.* 301-308

[116] Mukherjee Y.X., and Mukherjee S., (1997), On boundary conditions in the element free Galerkin method, *Comput. Mech.* **19** 267-270.

[117] Morrison P.J., Meiss J.D., Cary J.R., (1981), Scattering of RLW solitary waves, Physical **11**D 324-336.

[118] Mohamed A.R., Talaat S.E., and Faisal E.I., (2005), A numerical solution of the Burgers's equation using septic B-splines, Chaos, *Solitons and Fractals* **26** 795–804.

[119] Nayfeh A.H. and Mook D.T., (1979), *Nonlinear oscillations*, New York: John Wiley.

[120] Onate E., Idelsohn S., Zienkiewicz O.C., and Taylor R.L., (1996), A finite point method in computational mechanics : Applications to convective transport and fluid flow, *Int J. Number Methods Engrg.* **39** 3839-3866.

[121] Panayotounakos D.E. and Theocaris P.S., (1980), The dynamically loaded circular beam on an elastic foundation: *ASME J. Appl. Mech.* **47**, 139-144.

[122] Pasternak P.L., (1954), *On a new method of analysis of an elastic foundation by means of two foundation constants*. Gos. Izd. Lip. po Strait i Arkh, Moscow (in Russian).

[123] Pavlovic M.N. and Wylie G.B., (1983), Vibration of beams on non-homogeneous elastic foundations. *Earthquake Engng Struct. Dyn.* **11**, 797-808.

[124] Peddieson J., Buchanan G.R., and McNitt R.P., (2003), Application of nonlocal continuum models to nanotechnology, *Int. J. Eng.*, **41** (2003) 305-312.

[125] Peregrine D.H., (1996), Calculations of the development of an undular bore, *J. Fluid Mech.* **25** 321-330.

[126] Prathap G. and Varadan T.K., (1978a), The large amplitude vibration of hinged beams, *J. Comput. Struct.* **9** 219-222.

[127] Prathap G. and Varadan T.K.,(1978b), The large amplitude vibration of tapered clamped beams, *J. Comput. Struct.* **58** 87-94.

[128] Prenter P.M., (1975), *Splines and Variational Methods*, New York: John Wiley & Sons.

[129] Pol B. van der, (1915), On a non-linear partial differential equation satisfied by the logarithm of the Jaco-bian theta-functions, with arithmetical applications, Proc. Acad. Sci. Amsterdam **013** 261–271.

[130] Pospelov L. A., (1966), Propagation of finite-amplitude elastic waves, *Soviet Phys. Acoust.* **11** 302–304.

[131] Raslan K.R., (1999), *Numerical Methods for Partial Differential Equations*, Ph.D. Thesis, Al-Azhar University, Cairo.

[132] Raslan K.R., (2000), Collocation method using cubic spline for the regularized long wave equation, *Int. Conference on Appl. Comput. Fluid Dynam.*, October 17-20, Beijing China, pp. 567-574.

[133] Raslan K.R., (2005), Collocation method using quartic B-spline for the equal width (EW) equation, *Appl. Math. Comp.* **168** 795-805.

[134] Ray J.D. and Bert C.W., (1969), Nonlinear vibrations of beams with pinned ends, *J. Eng. Ind.* **9** 977-1004.

[135] Reddy J.N., (1999), *Theory and Analysis of Elastic Plates*, Taylor and Francis, Philadelphia, PA.

[136] Richart F.E., Hall J.R. and Woods R.D., (1970), *Vibrations of Soils and Foundations*. Prentice-Hall, Englewood Cliffs, NJ.

[137] Roark R.J. and Young W.C., (1975), *Formulas for Stress and Strain*, New York: McGraw-Hill, 5th edn.

[138] Rubin S.G. and Graves R.A., (1975), Cubic spline approximation for problems influid mechanics, Nasa TRR-436, District of Columbia.

[139] Rubin S.G. and Khosla P.K., (1976), Higher-order numerical solutions using cubic splines, AIAA J. **14**(7) 851–858.

[140] Sathyamoorthy M., (1982a), Nonlinear analysis of beams part I: a survey of recent advances, *Shock Vibr. Dig.* **14**(17) 19-35.

[141] Sathyamoorthy M., (1982b), Nonlinear analysis of beams part II: finite element methods, *Shock Vibr. Dig.* **14**(18) 7-18.

[142] Sarma B.S., (1983), Large-type formulation for finite element analysis of non-linear beam vibrations, *J. Sound Vibr.* **86** 61-70.

[143] Schoenberg I.J., (1946), Contributions to the problem of approximation of equidistant data by analytic functions, *J. Appl. Math.* **4**(45-99) 112-114

[144] Shames I.H., and Dym C.L., (1985), *Energy and Finite Element Methods in Structural Mechanics*, McGraw-Hill Publ., New York.

[145] Sharan M., Kansa E.J., and Gupta S., (1997), Applications of the multiquadric method for the solution of elliptic partial differential equations, *Appl. Math. Comput.* **84** 275-302.

[146] Shen P.C., and Wang JC., (1987), Static analysis of cylindrical shells by using B-spline functions, *Comp. Struct.* **25** 809-816.

[147] Shufrin I. and Eisenberger M., (2005), Stability and vibration of shear deformable plates –first order and higher order analyses, *Int. J. Solids & Struct.*, **42**(3-4)  1225-1251.

[148] Shufrin I. and Eisenberger M., (2007), Shear buckling of thin plates with constant in-plane stresses, *Int. J. Struct. Stabil. & Dyn.*, **7**(2) 179-192.

[149] Singh G., Sharma A.K. and Rao G.V., (1990), Large-amplitude free vibration of beams – a discussion on various formulations and assumptions, *J. Sound Vibr.* **142** 77-85.

[150] Smith G.D., (1978), Numerical Solution of Partial Differential Equations: Finite Difference Methods. Oxford University Press, Oxford.

[151] Smith J.P., (1995), Buckling of shears deformable plates using the p-version of the finite element method, *Comput. & Struct.*, **57**(3) 527-532.

[152] Soliman A.A., and Raslan K.R., (2001), Collocation method using quadratic B-spline for the regularized long wave equation, *Int. J. Comput. Math.* **78** 399-412.

[153] Sudak L.J., (2003), Column buckling of multiwalled carbon nanotubes using nonlocal continuum mechanics, *J. Appl. Phys.*, **94** 7281-7287.

[154] Srinivasan A.V., (1965), Large amplitude free oscillations of beams and plates, *Am. Inst. Aeronaut. Astronaut. J.* **3** 1951-1953.

[155] Stein M. and Neff J., (1947), *Buckling stresses of simply supported rectangular flat plates in shear*, Washington : NACA TN-1222.

[156] Striz A.G., Chen W. and Bert C.W., (1994), Static Analysis of Structures by the Quadrature Element Method (QEM), *Int. J. Solids Struct.* **31**(20) 2807-2818.

[157] Tauchert T. R., (1974), *Energy Principles in Srrucrural Mechanics*. McGraw-Hill. New York.

[158] Timoshenko S.P. and Woinowsky-Krieger S., (1959), *Theory of Plates and Shells*. Second Edition, McGraw-Hill.

[159] Timoshenko S.P. and Gere J.M., (1961), *Theory of elastic stability*, New York: McGraw-Hill.

[160] Timoshenko S.P., Young D.H. and Weaver Jr. W., (1947), *Vibration Problem in Engineering*, 4th Edition, Wiley, New York.

[161] Valsangkar A.J.and Pradhanang R.B., (1987), Free vibration of partially supported piles. *AXE J. Engng Mech.* **113**(EM8), 1244-1247.

[162] Valsangkar A.J.and Pradhanang R., (1988), Vibrations of beam-columns on two-parameter elastic foundations. *Earthquake Engng Srrucr. Dyn.* **16**, 217-225.

[163] Van der Neut A., (1958), Buckling caused by thermal stresses, High temperature effects in aircraft structures AGAR Dograph **28** 215-47.

[164] Varogˇlu E., and Finn W.D., (1980), Space–time finite element incorporating characteristics

for the Burgers' equation, *Int. J. Numer. Methods Eng.* **16** 171–184.

[165] Villadsen J.V., Stewart W.E., (1967), Solution of boundary value problems by orthogonal collocation, *Chem. Eng. Sci.* **22** 1483-1501.

[166] Wang C.M., Reddy J.N., and Lee K.H., (2000), Shear Deformable Beams and Plates: Relationships with Classical Solutions, (Oxford: Elsevier) M (2000).

[167] Wang C.M., Zhang Y.Y., and He X.Q., (2007), Vibration of nonlocal Timoshenko beams, Nanotechnology, *Inst. Phys. Publish.*,**18** (10) 105401.

[168] Wang L.F., and Hu H.Y., (2005), Flexural wave propagation in single-walled carbon nanotubes, *Phys. Rev. B*, **71** 195412.

[169] Wang Q., (2005), Wave propagation in carbon nanotubes via nonlocal continuum mechanics, *J. Appl. Phys.*, **98** 124301.

[170] Wang Q., and Varadan V.K., (2006), Vibration of carbon nanotubes studied using nonlocal continuum mechanics Smart Mater, *Struct.*, **15** 659-666.

[171] Wang J., (1991), Vibration of stepped beams on elastic foundations. *J. Sound Vibr.* **149**, 315-322.

[172] Wang T.M. and Stephens J.E., (1977), Natural frequencies of Timoshenko beams on Pasternak foundations. *J. Sound Vibr.* **51**, 149-155.

[173] Wang T.M. and Gagnon L.W., (1978), Vibrations of continuous Timoshenko beams on Winkler-Pasternak foundations. *J. Sound Vibr.* **59**, 211-220.

[174] Wang X., Wang X. and Shi X., (2006), Differential quadrature buckling analyses of rectangular plates subjected to non-uniform distributed in-plane loadings, *Thin-Walled Struct.* **44** 837-843.

[175] Weller T., and Patlashenko I., (1993), Postbuckling of infinite length cylindrical panels under combined thermal and mechanical loading, *J. Soilds Struct.* **30** 1649-1662.

[176] Weller T., Patlashenko I., (1993), Cubic B-spline collocation method for nonlinear static analysis of panels under mechanical and thermal loadings, *Comp. Struct.* **49** 89-96.

[177] Woinowsky-Krieger S., (1950), The effect of an axial force on the vibration of hinged bars, *J. Appl. Mech.* **17** 35-36.

[178] Wright K., (1964), Chebychev collocation methods for ordinary differential equations, *Cpmp. J.* **16** 358-365.

[179] Wu L.Y. and Chen Y.T., (2003a), Application of spline collocation method in analysis of beam and continuous beam, *Chin. J. Mech.-Series A* **19**(2) 319-326.

[180] Wu L.Y. and Chen Y.T., (2003b), Analysis of rigid frame by spline collocation method, *J. Chin. Inst. Eng.* **26**(5) 619-634.

[181] Wu Z., and Schaback R., (1993), Local error estimates for radial basis function interpolation of scattered data, *IMA J. Numer. Anal.* **13** 13-27.

[182] Weller T. and Patlashenko I., (1993a), Postbuckling of infinite length cylindrical panels under combined thermal and mechanical loading, *J. Soilds Struct.* **30** 1649-1662.

[183] Weller T. and Patlashenko I., (1993b), Cubic B-spline collocation method for nonlinear static analysis of panels under mechanical and thermal loadings. *Comput. Struct.* **49** 89-96.

[184] Winkler E., (1867), *Die Lehre Von der Elasticitaet und Festigkeir*. Dominicus, Prague.

[185] Williams F.W. and Kennedy D., (1987), Exact dynamic member stiffnesses for a beam on an elastic foundation. *Earthquake Engng Strucr. Dyn.* **15**, 133-136.

[186] Yakobson B.I., Brabec C.J., and Bernholc J., (1996), Nanomechanics of carbon tubes: instabilities beyond linear range, *Phys. Rev.Lett.*, **76** 2511-2514 J.

[187] Yuan S. and Jin Y., (1998), Computation of elastic buckling loads of rectangular thin plates using the extended Kantorovich method, *Comput. & Struct.*, **6** 861-867.

[188] Yokoyama T., (9187), Vibrations and transient responses of Timoshenko beams on elastic foundations. *Ing.-Arch.* **57**, 81-90.

[189] Yokoyama T., (1991), Vibrations of Timoshenko beam-columns on two-parameter elastic foundations. *Earrhquake Engng Srrucr. Dyn.* **20**, 355-370.

[190] Yokoyamat T., (1996), Vibration analysis of Timoshenko beam-column on two-parameter elastic foundation. *Comput. Struct.* **61**(6), 995-1007.

[191] Young W.C. and Budynas R.G., (2002), *Roark's formulas for stress & strain*, 7th ed. New York, USA: McGraw-Hill.

[192] Zhou D., (1993), A general solution to vibrations of beams on variable Winkler elastic foundation. *Comput. Struct.* **47**, 83-90.

[193] Zaki S.I., (2000), A least-squares finite element scheme for the EW equation, *Comput. Methods Appl. Mech. Engrg.* **189** 587-594.

[194] Zaki S.I., (2001), Solitary waves induced by the boundary forced EW equation, *Comput. Methods Appl. Mech. Engrg.* **190** 4881-4887.

[195] Zhang Y.Q., Liu G.R., and Xie X.Y., (2005), Free transverse vibrations of double-walled carbon nanotubes using a theory of nonlocal elasticity, *Phys. Rev. B*, **71** 195-404.

[196] Zhu T., and Atluri S.N., (1998), Modified collocation method and a penalty formulation for enforcing the essential boundary conditions in the element free Galerkin method, *Comput. Mech.* **21** 211-222.

[197] Zhu T., Zhang J.D., and Atluri S.N., (1998), A Local Boundary Integral Equation (LBIE) method in computational mechanics and a meshless discretization approach, *Comp. Mech.* **21** 223-235.

[198] Zienkiewicz O.C., (1977), *The Finite Element Method*. McGraw-Hill, New York.

[199] zis T. O¨, and zdes A. O¨, (1996), A direct variational methods applied to Burgers's equation, *J. Comput. Appl. Math.* **71** 163–175.

[200] zis T. O¨, Aksan E.N., and zdes A. O¨, (2003), A finite element approach for solution of Burgers' equation, *Appl. Math. Comput.* **139** 417–428.

# Appendix A Derivation of Cubic B-spline Function

The $k$ th forward difference $f(\xi_0)$ of a given function $f(\xi)$ at $\xi_0$ is defined recursively by

$$\Delta f(\xi_0) = f(\xi_1) - f(\xi_0), \quad \Delta^{k+1} f(\xi_0) = \Delta^k f(\xi_1) - \Delta^k f(\xi_0) \tag{A.1}$$

In particular

$$\Delta^2 f(\xi_0) = f(\xi_2) - 2f(\xi_1) + f(\xi_0) \tag{A.2}$$

$$\Delta^3 f(\xi_0) = f(\xi_3) - 3f(\xi_2) + 3f(\xi_1) + f(\xi_0) \tag{A.3}$$

$$\Delta^4 f(\xi_0) = f(\xi_4) - 4f(\xi_3) + 6f(\xi_2) - 4f(\xi_1) + f(\xi_0) \tag{A.4}$$

And so forth. The coefficient of $f(\xi_k)$ in $\Delta^n f(\xi_0)$ is simply the binomial coefficient $(-1)^k \binom{n}{k}$. It is well known that with evenly spaced knots, $\Delta^n$ annihilates all polynomials of degree $n-1$.

In order to device the cubic B-splines, ones compute

$$\begin{aligned} K(t) &= \Delta^4 F_t(\xi_0) \\ &= F_t(\xi_4) - 4F_t(\xi_3) + 6F_t(\xi_2) - 4F_t(\xi_1) + F_t(\xi_0) \end{aligned} \tag{A.5}$$

where $\Delta^4 F_t(\xi_0)$ is fourth forward difference $\Delta^4 f(\xi_0)$.

The $F_t(\xi)$ for each fixed $t$ have

$$F_t(\xi) = (\xi - t)_+^3 \tag{A.6}$$

where the function $(\xi - t)_+^3$ is defined by,

$$(\xi - t)_+^3 = \begin{cases} (\xi - t)^3 & \text{when } t \le \xi \\ 0 & \text{when } t > \xi \end{cases} \tag{A.7}$$

Then, Eq. (A.7) substituting into Eq. (A.5), obtained as

$$K(t) = (\xi_4 - t)_+^3 - 4(\xi_3 - t)_+^3 + 6(\xi_2 - t)_+^3 - 4(\xi_1 - t)_+^3 + (\xi_0 - t)_+^3 \tag{A.8}$$

It is clear form the definition Eq. (A.5) of $(\xi - t)_+^3$ that $K(t) \equiv 0$ for all $t \geq \xi_4$. Moreover, for fixed $t$ and $\xi < t$, $F_t(\xi) = (\xi - t)^3$ is a polynomial of degree six. Thus any sixth forward difference $\Delta^4 F_t(\xi_0)$ with evenly spaced knots vanishes identically when $\xi_0 \geq t$. That is

$$K(t) \equiv 0 \quad \text{when} \quad t \geq \xi_4 \text{ and } t \leq \xi_0 \tag{A.9}$$

A sum of cubic B-splines $(\xi - t)_+^3$, $K(t)$ becomes

$$K(t) = \begin{cases} (\xi_4 - t)^3, & \xi_3 \leq t \leq \xi_4 \\ (\xi_4 - t)^3 - 4(\xi_3 - t)^3, & \xi_2 \leq t \leq \xi_3 \\ (\xi_4 - t)^3 - 4(\xi_3 - t)^3 + 6(\xi_2 - t)^3, & \xi_1 \leq t \leq \xi_2 \\ (\xi_4 - t)^3 - 4(\xi_3 - t)^3 + 6(\xi_2 - t)^3 - 4(\xi_1 - t)^3, & \xi_0 \leq t \leq \xi_1 \\ 0, & \text{otherwise} \end{cases} \tag{A.10}$$

To generalize, one can transform the independent variables $\xi_0$, ... $\xi_4$ into $\xi_{i-2}$, ..., $\xi_{i+2}$ by setting $\xi_i = \xi_2$, so the above expression $K(t)$ can be reduced to

$$K(t) = \begin{cases} (\xi_{i+2} - t)^3, & \xi_{i+1} \leq t \leq \xi_{i+2} \\ (\xi_{i+2} - t)^3 - 4(\xi_{i+2} - t)^3, & \xi_i \leq t \leq \xi_{i+1} \\ (\xi_{i+2} - t)^3 - 4(\xi_{i+2} - t)^3 + 6(\xi_{i+1} - t)^3, & \xi_{i-1} \leq t \leq \xi_i \\ (\xi_{i+2} - t)^3 - 4(\xi_{i+2} - t)^3 + 6(\xi_{i+1} - t)^3 - 4(\xi_i - t)^3, & \xi_{i-2} \leq t \leq \xi_{i-1} \\ 0, & \text{otherwise} \end{cases} \tag{A.11}$$

For evenly spaced partitions, $\xi_{j+1} - \xi_j = h$, $j = i+1, ..., i-3$, $K(t)$ can be reduced further to

$$B_i(t) = \frac{1}{h^3} \begin{cases} (\xi_{i+2} - t)^3 - 4(\xi_{i+2} - t)^5 + 6(\xi_{i+1} - t)^5 - 4(\xi_i - t)^5, & \xi_{i+1} \leq t \leq \xi_{i+2} \\ (\xi_{i+2} - t)^3 - 4(\xi_{i+2} - t)^3 + 6(\xi_{i+1} - t)^3, & \xi_i \leq t \leq \xi_{i+1} \\ (\xi_{i+2} - t)^3 - 4(\xi_{i+2} - t)^3, & \xi_{i-1} \leq t \leq \xi_i \\ (\xi_{i+2} - t)^3, & \xi_{i-2} \leq t \leq \xi_{i-1} \\ 0, & \text{otherwise} \end{cases} \tag{A.12}$$

and the above $B_i(t) = K(t)/h^3$ are the required quintic B-splines (Prenter, 1975).

# Appendix B Derivation of Quintic B-spline Function

The $k$ th forward difference $f(\xi_0)$ of a given function $f(\xi)$ at $\xi_0$ is defined recursively by

$$\Delta f(\xi_0) = f(\xi_1) - f(\xi_0), \quad \Delta^{k+1} f(\xi_0) = \Delta^k f(\xi_1) - \Delta^k f(\xi_0) \tag{B.1}$$

In particular

$$\Delta^2 f(\xi_0) = f(\xi_2) - 2f(\xi_1) + f(\xi_0) \tag{B.2}$$

$$\Delta^3 f(\xi_0) = f(\xi_3) - 3f(\xi_2) + 3f(\xi_1) + f(\xi_0) \tag{B.3}$$

$$\Delta^4 f(\xi_0) = f(\xi_4) - 4f(\xi_3) + 6f(\xi_2) - 4f(\xi_1) + f(\xi_0) \tag{B.4}$$

$$\Delta^5 f(\xi_0) = f(\xi_5) - 5f(\xi_4) + 10f(\xi_3) + 10f(\xi_2) - 5f(\xi_1) + f(\xi_0) \tag{B.5}$$

$$\Delta^6 f(\xi_0) = f(\xi_6) - 6f(\xi_5) + 15f(\xi_4) - 20f(\xi_3) + 15f(\xi_2) - 6f(\xi_1) + f(\xi_0) \tag{B.6}$$

And so forth. The coefficient of $f(\xi_k)$ in $\Delta^n f(\xi_0)$ is simply the binomial coefficient $(-1)^k \begin{pmatrix} n \\ k \end{pmatrix}$. It is well known that with evenly spaced knots, $\Delta^n$ annihialates all polynomials of degree $n-1$.

In order to device the quintic B-splines, ones compute

$$\begin{aligned}
K(t) &= \Delta^6 F_t(\xi_0) \\
&= F_t(\xi_6) - 6F_t(\xi_5) + 15F_t(\xi_4) - 20F_t(\xi_3) + 15F_t(\xi_2) - 6F_t(\xi_1) + F_t(\xi_0)
\end{aligned} \tag{B.7}$$

where $\Delta^6 F_t(\xi_0)$ is sixth forward difference $f(\xi_0)$, see Appendix B.

The $F_t(\xi)$ for each fixed $t$ have

$$F_t(\xi) = (\xi - t)_+^5 \tag{B.8}$$

where the function $(\xi - t)_+^5$ is defined by,

$$(\xi - t)_+^5 = \begin{cases} (\xi - t)^5 & \text{when } t \le \xi \\ 0 & \text{when } t > \xi \end{cases} \tag{B.9}$$

Then, Eq. (B.8) substituting into Eq. (B.7), obtained as

$$
\begin{aligned}
K(t) = (\xi_6 - t)_+^5 - 6(\xi_5 - t)_+^5 + 15(\xi_4 - t)_+^5 - 20(\xi_3 - t)_+^5 \\
+ 15(\xi_2 - t)_+^5 - 6(\xi_1 - t)_+^5 + (\xi_0 - t)_+^5
\end{aligned}
\tag{B.10}
$$

It is clear form the definition Eq. (B.7) of $(\xi - t)_+^5$ that $K(t) \equiv 0$ for all $t \geq \xi_6$. Moreover, for fixed $t$ and $\xi < t$, $F_t(\xi) = (\xi - t)^5$ is a polynomial of degree six. Thus any sixth forward difference $\Delta^6 F_t(\xi_0)$ with evenly spaced knots vanishes identically when $\xi_0 \geq t$. That is

$$
K(t) \equiv 0 \quad \text{when} \quad t \geq \xi_6 \quad \text{and} \quad t \leq \xi_0
\tag{B.11}
$$

A sum of quintic B-splines $(\xi - t)_+^5$, $K(t)$ becomes

$$
K(t) = \begin{cases}
(\xi_6 - t)^5, & \xi_5 \leq t \leq \xi_6 \\
(\xi_6 - t)^5 - 6(\xi_5 - t)^5, & \xi_4 \leq t \leq \xi_5 \\
(\xi_6 - t)^5 - 6(\xi_5 - t)^5 + 15(\xi_4 - t)^5, & \xi_3 \leq t \leq \xi_4 \\
(\xi_6 - t)^5 - 6(\xi_5 - t)^5 + 15(\xi_4 - t)^5 - 20(\xi_3 - t)^5, & \xi_2 \leq t \leq \xi_3 \\
(\xi_6 - t)^5 - 6(\xi_5 - t)^5 + 15(\xi_4 - t)^5 - 20(\xi_3 - t)^5 + 15(\xi_2 - t)^5, & \xi_1 \leq t \leq \xi_2 \\
(\xi_6 - t)^5 - 6(\xi_5 - t)^5 + 15(\xi_4 - t)^5 - 20(\xi_3 - t)^5 + 15(\xi_2 - t)^5 - 6(\xi_1 - t)^5, & \xi_0 \leq t \leq \xi_1 \\
0, & \text{otherwise}
\end{cases}
\tag{B.12}
$$

To generalize, one can transform the independent variables $\xi_0$, ... $\xi_6$ into $\xi_{i-3}$, ..., $\xi_{i+3}$ by setting $\xi_i = \xi_3$, so the above expression $K(t)$ can be reduced to

$$
K(t) = \begin{cases}
(\xi_{i+3} - t)^5, & \xi_{i+2} \leq t \leq \xi_{i+3} \\
(\xi_{i+3} - t)^5 - 6(\xi_{i+2} - t)^5, & \xi_{i+1} \leq t \leq \xi_{i+2} \\
(\xi_{i+3} - t)^5 - 6(\xi_{i+2} - t)^5 + 15(\xi_{i+1} - t)^5, & \xi_i \leq t \leq \xi_{i+1} \\
(\xi_{i+3} - t)^5 - 6(\xi_{i+2} - t)^5 + 15(\xi_{i+1} - t)^5 - 20(\xi_i - t)^5, & \xi_{i-1} \leq t \leq \xi_i \\
(\xi_{i+3} - t)^5 - 6(\xi_{i+2} - t)^5 + 15(\xi_{i+1} - t)^5 - 20(\xi_i - t)^5 + 15(\xi_{i-1} - t)^5, & \xi_{i-2} \leq t \leq \xi_{i-1} \\
(\xi_{i+3} - t)^5 - 6(\xi_{i+2} - t)^5 + 15(\xi_{i+1} - t)^5 - 20(\xi_i - t)^5 + 15(\xi_{i-1} - t)^5 - 6(\xi_{i-2} - t)^5, & \xi_{i-3} \leq t \leq \xi_{i-2} \\
0, & \text{otherwise}
\end{cases}
\tag{B.13}
$$

For evenly spaced partitions, $\xi_{j+1} - \xi_j = h$, $j = i+2, ..., i-4$, $K(t)$ can be reduced further to

$$B_i(t) = \frac{1}{h^5} \begin{cases} (\xi_{i+3}-t)^5 - 6(\xi_{i+2}-t)^5 + 15(\xi_{i+1}-t)^5 - 20(\xi_i-t)^5 + 15(\xi_{i-1}-t)^5 - 6(\xi_{i-2}-t)^5, & \xi_{i+2} \le t \le \xi_{i+3} \\ (\xi_{i+3}-t)^5 - 6(\xi_{i+2}-t)^5 + 15(\xi_{i+1}-t)^5 - 20(\xi_i-t)^5 + 15(\xi_{i-1}-t)^5, & \xi_{i+1} \le t \le \xi_{i+2} \\ (\xi_{i+3}-t)^5 - 6(\xi_{i+2}-t)^5 + 15(\xi_{i+1}-t)^5 - 20(\xi_i-t)^5, & \xi_i \le t \le \xi_{i+1} \\ (\xi_{i+3}-t)^5 - 6(\xi_{i+2}-t)^5 + 15(\xi_{i+1}-t)^5, & \xi_{i-1} \le t \le \xi_i \\ (\xi_{i+3}-t)^5 - 6(\xi_{i+2}-t)^5, & \xi_{i-2} \le t \le \xi_{i-1} \\ (\xi_{i+3}-t)^5, & \xi_{i-3} \le t \le \xi_{i-2} \\ 0, & \text{otherwise} \end{cases} \tag{B.14}$$

and the above $B_i(t) = K(t)/h^5$ are the required quintic B-splines (Bert and Sheu, 1996).